GEOMORPHOLOGICAL RELATIONSHIPS THROUGH THE USE OF 2-D SEISMIC REFLECTION DATA, LIDAR, AND AERIAL IMAGERY

by

MEGHAN ELIZABETH ALESCE

ANDREW M. GOODLIFFE, COMMITTEE CHAIR

C. FRED T. ANDRUS
RYAN C. EWING
STEPHEN C. JONES

A THESIS

Submitted in partial fulfillment of the requirements
for the degree of Master of Arts
in the Department of Geological Sciences
in the Graduate School of
The University of Alabama

TUSCALOOSA, ALABAMA

2014

Copyright Meghan Elizabeth Alesce 2014
ALL RIGHTS RESERVED

ABSTRACT

Barrier Islands are crucial in protecting coastal environments. This study focuses on Dauphin Island, Alabama, located within the Northern Gulf of Mexico (NGOM) Barrier Island complex. It is one of many islands serving as natural protection for NGOM ecosystems and coastal cities. The NGOM barrier islands formed at 4 kya in response to a decrease in rate of sea level rise. The morphology of these islands changes with hurricanes, anthropogenic activity, and tidal and wave action. This study focuses on ancient incised valleys and and the impact on island morphology on hurricane breaches.

Using high frequency 2-D seismic reflection data four horizons, including the present seafloor, were interpreted. Subaerial portions of Dauphin Island were imaged using Lidar data and aerial imagery over a ten-year time span, as well as historical maps. Historical shorelines of Dauphin Island were extracted from aerial imagery and historical maps, and were compared to the location of incised valleys seen within the 2-D seismic reflection data. Erosion and deposition volumes of Dauphin Island from 1998 to 2010 (the time span covering hurricanes Ivan and Katrina) in the vicinity of Katrina Cut and Pelican Island were quantified using Lidar data.

For the time period prior to Hurricane Ivan an erosional volume of 46,382,552 m^3 and depositional volume of 16,113.6 m^3 were quantified from Lidar data. The effects of Hurricane Ivan produced a total erosion volume of 4,076,041.5 m^3. The erosional and depositional volumes of Katrina Cut being were 7,562,068.5 m^3 and 510,936.7 m^3, respectively. More volume change

was found within Pelican Pass. For the period between hurricanes Ivan and Katrina the erosion volume was 595,713.8 m^3. This was mostly located within Katrina Cut. Total deposition for the same period, including in Pelican Pass, was 15,353,961 m^3.

Hurricane breaches were compared to ancient incised valleys seen within the 2-D seismic reflection results. Breaches from hurricanes from 1849, 1916, and 2005 all correlated with incised valley. Interpretations from horizons A and P correlated well with the 1849 shoreline, while Horizon B correlated best with the 1916 and 2005 hurricane breaches.

The correlation of incised valleys and breaches provides a probable causation of breach locations. With further investigations, determination of the impacts of these relict valleys can be validated and established. Preferential subsidence within the relict incised valleys would account for the lower elevations on the island surface. Very fine to fine grained sediment deposits from the Mobile Bay would contribute to preferential subsidence. The lower elevations are more likely to erode from overwash and surges during strong storm systems.

DEDICATION

This thesis is dedicated to God, each member of my family, my fiancée, and every friend who helped me through this process in writing my manuscript. Without their constant support, faith, time, encouragement and guidance throughout this process I would not have met my goal of completion. Thank you for always believing in me when I did not.

LIST OF ABBREVIATIONS AND SYMBOLS

NGOM	Northern Gulf of Mexico
msl	Mean sea level
m	meters
yr.	year
CHIRP	Compressed High Intensity Radar Pulse
Lidar	Light Detection and Range
USGS	United States Geological Society
NOAA	National Oceanic and Atmospheric Administration
USACE	United States Army Corps of Engineers

ACKNOWLEDGMENTS

I would like to acknowledge my colleagues, friends, and faculty who helped me to complete this thesis. I am grateful to my thesis committee chair, Andrew Goodliffe, for his expertise and knowledge in the geophysics and direction throughout the many phases of my project. I would also like to acknowledge and thank my committee members Dr. Ryan Ewing, Dr. Fred Andrus, and Steve Jones. Thank you for your direction and expertise in the completion of this thesis.

I would like to thank the United States Geological Survey for the data used in this project. I would also like to thank the U.S. Army Corps of Engineers for the experience that led to my research topic as well as direction and support in continuing my education and completing my thesis.

I would like to thank my friends and colleagues for guidance assistance with software and geophysical interpretations. I would also like to acknowledge the University of Alabama Department of Geological Sciences for the use of their resources and for financial support in the form of teaching and research assistantships.

This completed project would not have been possible without my family, fiancée, friends and co-workers who have consistently supported me throughout the entire process. Thank you for believing in me when I did not, and the constant motivation, patience, and support needed to reach my goal.

CONTENTS

LIST OF FIGURES

1.0 INTRODUCTION

Coastlines are very susceptible to natural and anthropogenic factors that can result in erosion, migration, and morphologic changes. Barrier islands serve as a first line of defense for many mainland coastlines and also for the fragile ecosystems within the lagoonal areas between the islands and the mainland. The preservation of these barrier islands is vital to these fragile ecosystems and mainland coastal cities.

Barrier Island chains are found throughout the world (Matias et al., 2008; Cooper et al., 2012). In North America, an extensive line of barrier islands is found along the East Coast and along the northern coast of the Gulf of Mexico (Field and Duane, 1976). Although the origin of these islands varies, a common factor is the progradation of a loose sediment spit. These systems serve as a vital defense to coastlines, especially the delicate wetland areas found in the Mississippi Sound (Figure 1.1). Wave action and currents are less intense in the Gulf of Mexico than in many other places, resulting in differences in the amount of deposition, erosion, and morphology of the islands. Islands along the North American Atlantic coast are subjected to intense wave and tidal action. For example, areas along the Atlantic coast will experience tidal changes of up to four foot difference between low and high tide in the month of May, while the NGOM around Dauphin Island will be under one foot (http://tidesandcurrents.noaa.gov/map/).

There are multiple hypotheses for the formation of barrier islands (Schwartz, 1971) including nucleation as a result of relict land structures, drowned dunes, shoal emergence, and spit accretion (Otvos, 1977; Morton et al., 2004). The evolution of barrier islands is influenced by a number of variables including sea level rise, sediment supply, littoral drift, wave and tidal

actions, and hurricane and storm systems (Otvos, 1977; Morton et al., 2004; Byrnes et al., 2010). All of the above contribute to erosion and deposition and influence the morphology and sustainability of a barrier island.

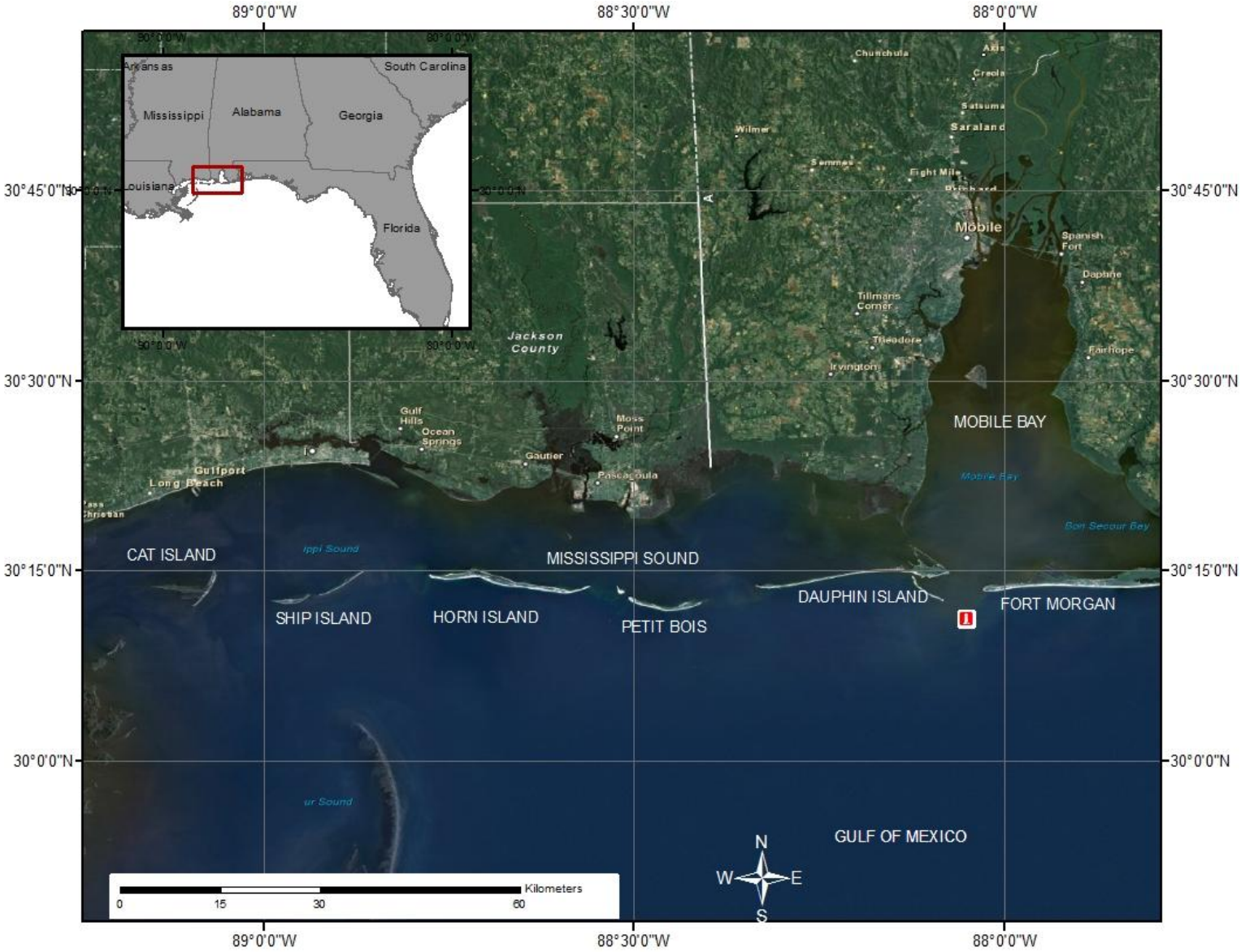

Figure 1.1 Location map of the Northern Gulf of Mexico Barrier Island chain system. The 105 km Mississippi-Alabama barrier chain, comprising Cat, West Ship, East Ship, Horn, Petit Bois, and Dauphin islands, is separated by inlets and bounded to the north by Mississippi Sound, a 4-20 km wide and 1-4 m deep lagoon.

This thesis explores the hypothesis that relict features, including incised valleys, affect the island's susceptibility to intense wave or storm action. It is hypothesized that incised valley infill, typically very fine to fine grained sediments from Mobile Bay, and fine to medium grained sands, may result in preferential subsidence and hence greater susceptibility to overwash and breaches. If this is the case, focused coastal engineering projects, including geotubes and sand renourishments, offer a solution.

1.1 Northern Gulf of Mexico

The constantly evolving Northern Gulf of Mexico (NGOM) barrier island chain, formed during the Late Holocene (Figure 1.1) stretches from the Florida panhandle to the Chandeleur Islands off the eastern coast of Louisiana (Otvos, 2001; Morton et al., 2004). The NGOM island chain is a result of progradating and aggradating sands during the Early and Late Holocene sea level oscillations (Otvos 1985; Rosati and Stone, 2009; Byrnes et al., 2010; Otvos and Giardino, 2004). Littoral transport, wave and tidal action, and currents in the NGOM are vital in the formation of the islands (Otvos, 1970; 1981; 1985; 2001; Schwartz, 1971; Otvos and Giardino, 2004; Rosati and Stone, 2009).

During the Late Pleistocene (~18 ka; Kindinger, 1988; Kindinger et al., 1994) the NGOM island chain was in a fluvial and deltaic environment. As sea level rose rapidly, river valleys were infilled with estuarine deposits and relict barrier deposits (Flocks et al., 2010; Figure 1.2). Due to a decrease in rate of sea level rise at approximately 4 ka (Flocks et al., 2010), the present-day NGOM barrier chain began to form.

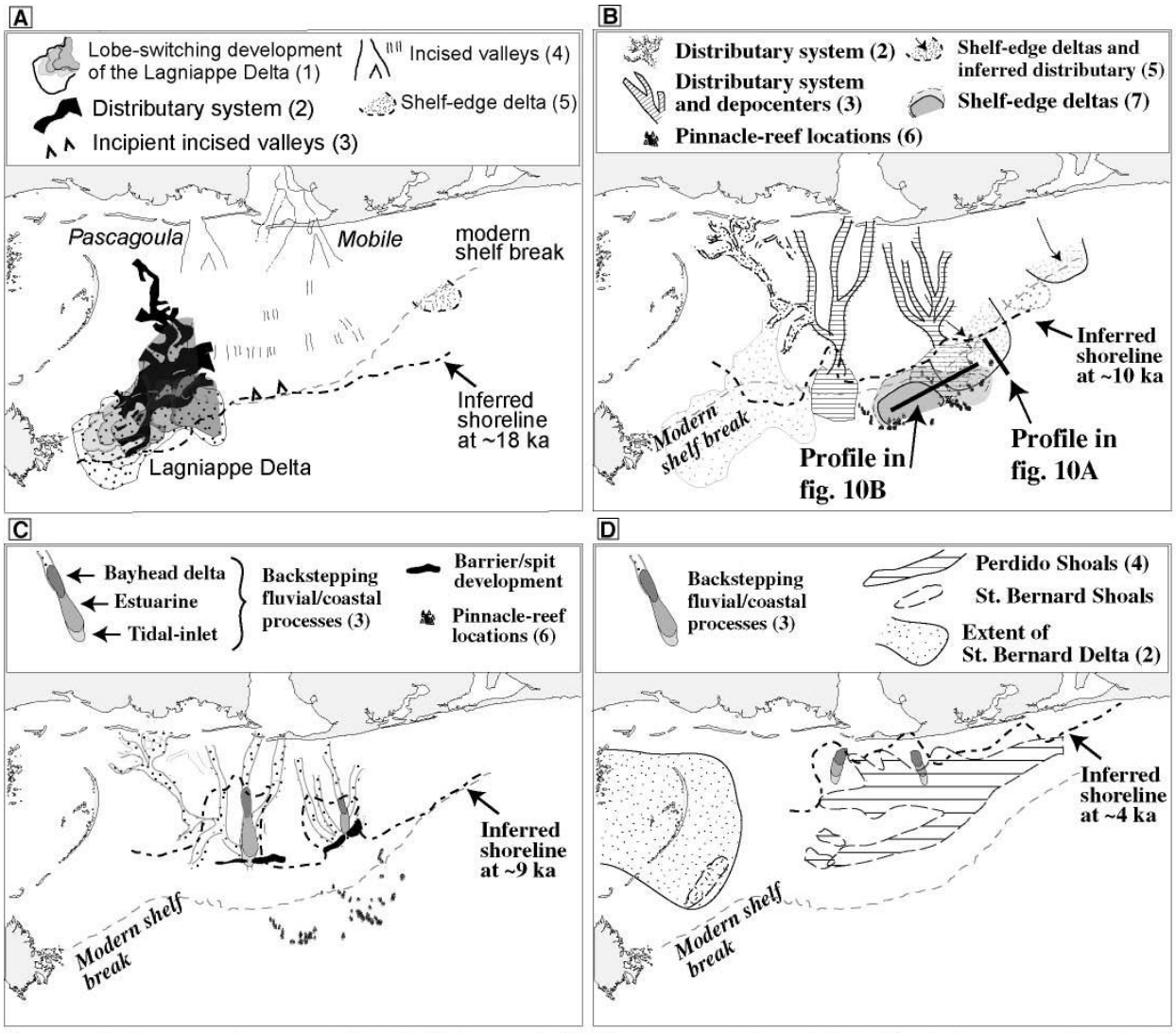

Figure 1.2 Sea level transgression to present-day from a compilation of studies. Adapted from Flocks et al. (2009).

1.2 Incised River Valleys

Drowned incised river valley systems are found throughout the NGOM shelf (Kindinger, 1988; Kindinger et al., 1994; Flocks et al., 2009; Donoghue, 2011; Twichell et al., 2011). These river systems developed during the Wisconsin glaciation when sea level was approximately 120 m below present day sea level (see Appendix A for more on Wisconsin Glaciation; Kindinger et al., 1994; Donoghue, 2011). As ice sheets began melting at around 18 kya creating rapid transgression, the incised valleys were infilled with estuarine, fluvial and marine deposits. Along

the continental shelf Kindinger et al. (1994) found drowned sand ridges that are believed to be relict barrier islands formed as a response to the oscillating sea level during the Early Holocene. The Mobile River incised valley of the Mississippi-Alabama shelf is a conduit for drainage from the Mobile River catchment (Kindinger et al., 1994). This catchment, the fourth largest in the United States, ends at the Mobile Bay delta head northeast of Dauphin Island (Figure 1.1). The Pascagoula incised valley system lies west of Dauphin Island.

1.3 Dauphin Island

Until a hurricane in the 19th century, Dauphin Island was the largest island within the NGOM (Byrnes et al., 2010). As a result of this storm event, the island split into Dauphin Island and Petit Bois (Figure 1.1). A 1716 hand-drawn map shows the ephemeral Pelican Island, until recently a separate island, accreted onto central Dauphin Island (Figure 1.3) as is once again the case today.

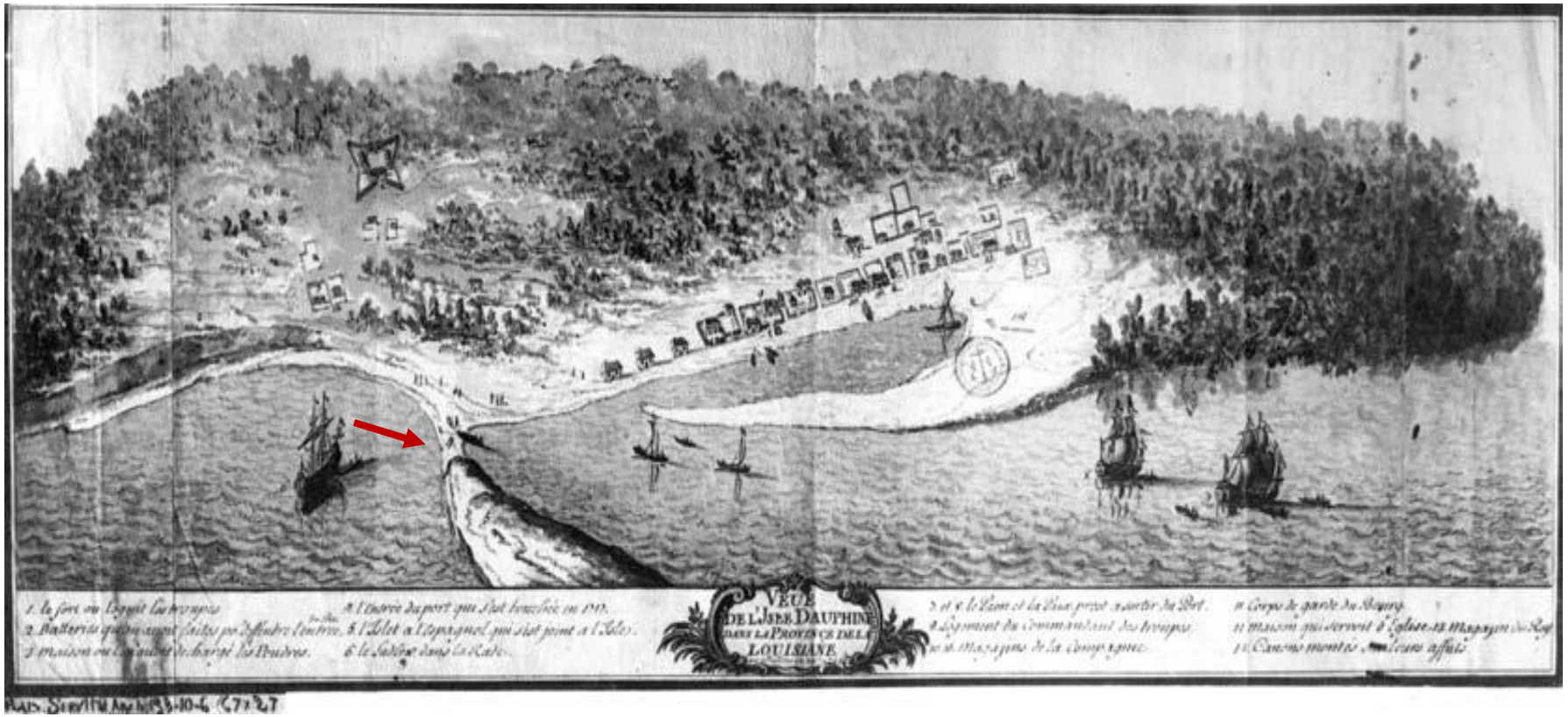

Figure 1.3 A hand-drawn illustration of east Dauphin Island (known as Massacre Island in the 18th century) from 1718. A thin sand bridge (red arrow) connects Pelican and Dauphin Islands. A lagoonal area created as a result of the sand bridge was used as a shipping port for the Louisiana Province (National Library of France; Byrnes et al., 2010).

Dauphin Island originally formed as a westward progradating spit around a previous island core (Morton et al., 2004; Figure 1.4). The island is described as a complex platform (Otvos, 1984) with a stable eastern core (Rosati and Stone, 2009; Byrnes et al., 2010). The eastern 5 km of Dauphin Island comprises compacted Pleistocene deposits with dense vegetation and dunes with relief of approximately 14 m above msl (mean sea level; Byrnes, et al., 2010). The lower relief western spit has a maximum relief of approximately 2 m above msl (Byrnes et al., 2010) and comprises loose Holocene deposits. It is more susceptible to over-wash, island breaches from hurricane systems, and barrier rollover. The different features found in high-relief barrier island systems provide stability and resistance to erosion (Figure 1.5). In contrast, low-profile systems are more susceptible to morphologic change.

Figure 1.4 Location map of Dauphin Island, Alabama. Key features include Mississippi Sound, Mobile Bay, and the ephemeral Pelican/Sand Island.

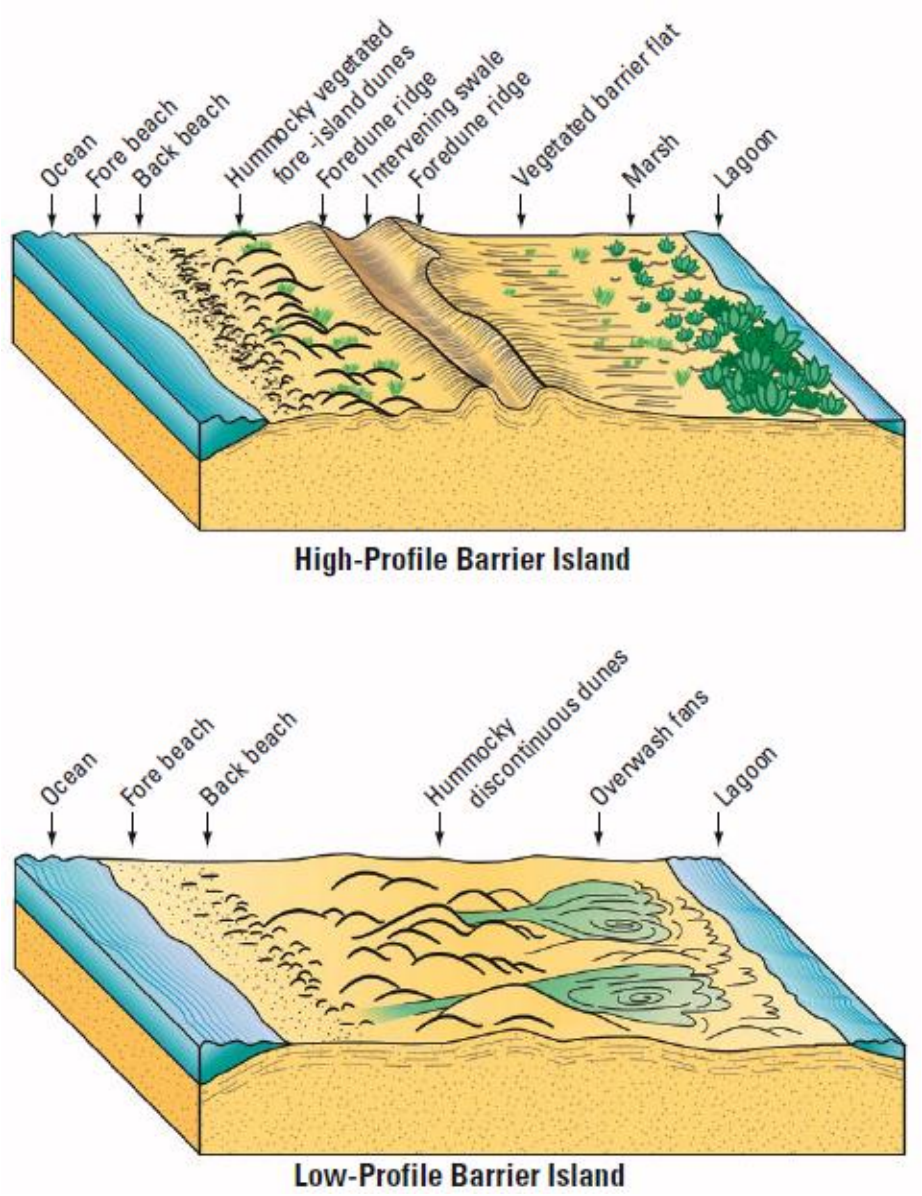

Figure 1.5 Morphological features of high- (similar to eastern Dauphin Island) and low-relief (or profile) barrier islands. From Morton et al. (2004)

The western spit of Dauphin Island has experienced many hurricane breaches that were subsequently infilled as a result of abundant sediment supply (Byrnes et al., 2010). Sediment sources for the NGOM comprise shoals along the continental shelf, river deposits, ebb-tidal shoals, and island erosion. Littoral transport and longshore drift move from the eastern NGOM islands and the Florida shelf in an east-west direction (Rosati and Stone, 2009; Byrnes et al.,

2010), transporting and depositing sediment from the Florida panhandle along the NGOM coastline to the western Chandeleur and Texas islands. Mobile Bay, the ebb shoal within Mobile Bay Pass, and the ephemeral Pelican and Sand islands also serve as sediment sources for Dauphin Island. Cipriani and Stone (2001) proposed a reversal drift just west of Pelican Island. This drift current aids in transporting eroded beach sand deposits back onto Dauphin Island and the ephemeral islands.

As a result of the limitation of sediment transport in modern times by dams there is a smaller littoral drift sediment supply. As a result, barrier islands do not rebound from rapid erosional events as quickly and are more susceptible to storm overwash (Byrnes et al., 2010).

The direction of the east-west littoral transport, longshore drift, and the southeast-northwest wave direction, result in westward propagation of the elongated, low-relief spit of Dauphin Island and the remaining Mississippi islands' shorelines. Over-wash and barrier rollover are pushing the western spit of Dauphin Island northward toward the mainland coastline. This is facilitated by the shallow, gently sloping platform of the Mississippi Sound (Otvos, 1981; Byrnes et al., 2010).

1.4 Hurricane History

Storm surges result in increased wave and tidal action and can result in overwash. Prior to modern times, damage to barrier islands from large storm systems has been largely healed by ongoing littoral drift. More recently, anthropogenic effects have reduced the sediment supply and decreased the time it takes to naturally heal the islands.

In 1852 a hurricane separated "Massacre Island" (a.k.a Dauphin Island) into two islands: Petit Bois and Dauphin Island. An inlet formed between the two islands, and the islands and inlet migrated westward never closing the gap. In 1916, an unnamed hurricane breached the island once again. This breach infilled naturally. In September 2004, Hurricane Ivan (Category 3) made landfall just west of Gulf Shores, Alabama, causing extensive damage to the northwest Florida and Alabama coastlines. Although the damage was not as extensive on the western Alabama coast, there were areas within the study area that were weakened (i.e., lower elevations) due to storm surges and intense wave action. In August 2005 Hurricane Katrina made landfall near Buras, Louisiana. Known as one of the deadliest hurricane systems within the NGOM, Hurricane Katrina sustained category 5 winds at landfall (National Hurricane Center, 2013). The majority of the NGOM was affected, with areas just east of the point of landfall devastated. Dauphin Island spit was breached, creating an approximately 2500 m gap known as Katrina Cut (Figure 1.6). Katrina Cut has yet to naturally close. In the summer of 2010 boulders were used to connect the two edges of Katrina Cut to lessen the threat from oil plumes from the 2010 Deep Horizon oil spill.

Figure 1.6 Google Earth satellite imagery of Dauphin Island. The red polygon shows the location of Katrina Cut, a breach created during Hurricane Katrina.

2.0 DATA AND METHODS

Datasets used in this study include Compressed High Intensity Radar Pulse (CHIRP) 2-D seismic reflection, satellite and aerial imagery, and Lidar. 2-D Seismic reflection data were collected during a United States Geological Survey (USGS) sand resource investigation along the NGOM barrier islands. Lidar data, including a compilation of data from NOAA, USGS, and the United States Army Corps of Engineers (USACE), were downloaded from the National Oceanic and Atmospheric Association (NOAA) Coastal Service Center. Aerial and historical imagery data were gathered from The University of Alabama library, the USGS, NOAA, the Geological Survey of Alabama, USACE, and Google Earth imagery.

2.1 CHIRP

CHIRP 2-D seismic reflection systems employ a high frequency source, making them ideal for shallow water subbottom profiling (e.g. Twichell et al., 2011; Pendleton et al., 2011; Forde et al., 2011). The swept-frequency signal covers a range of frequencies, creating a distinct source signal (Figures 2.1, 2.2). The source signal reflects off boundaries with an acoustic impedance contrast (e.g. the seafloor and geological layers), returning to the receiver (Figure 2.1). Cross-correlation between the original source signal and the received signal results in a seismic section that reveals reflectors in the subsurface. The frequency of the system used in this study limits penetration depths to approximately 30 to 50 m. Data were recorded to a depth of approximately 40 meters (0.05 sec).

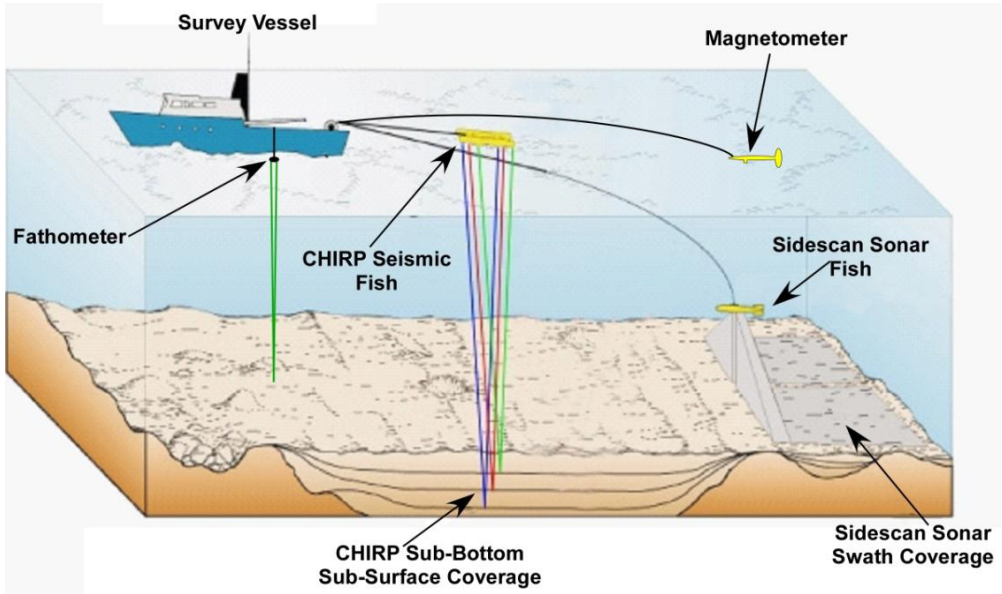

Figure 2.1 Marine geophysical data methods typically used at sea. CHIRP serves as the source and the receiver for the 2-D seismic reflection data. For this study, the system was towed 6 m behind the vessel. Adapted from Forrest-Vandera et al. (2011).

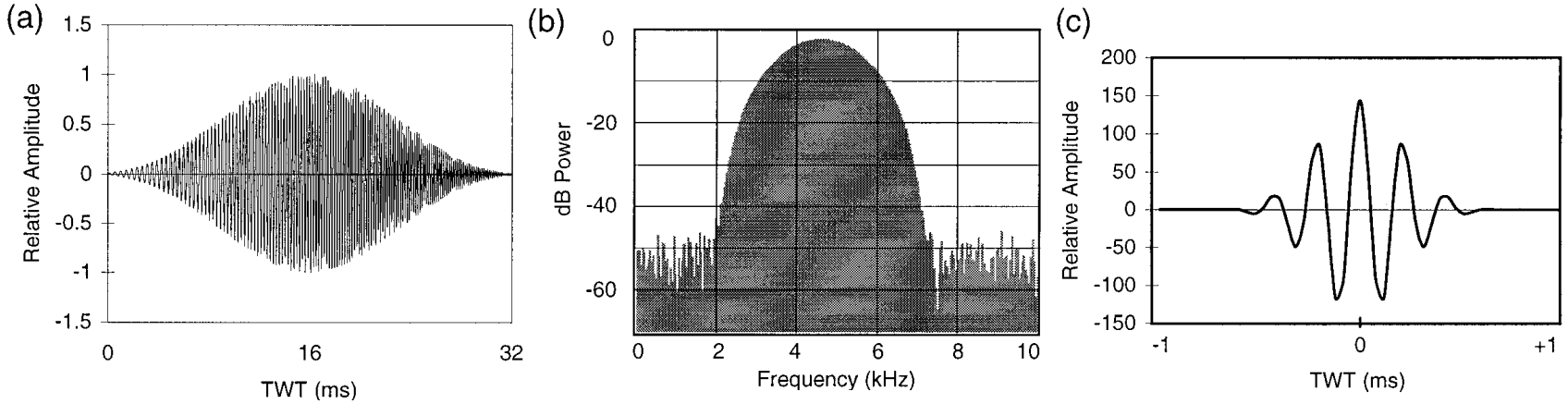

Figure 2.2 A linear 32 ms frequency-modulated CHIRP pulse sweeping from 2-8 kHz (a), the power spectrum of the CHIRP pulse (b), Klauder wavelet autocorrelation of the CHIRP pulse. From Quinn et al. (1998)

The 2-D seismic reflection data were collected during April and March of 2010 (Twichell et al., 2011). The survey covered 40 nautical miles (nm) of the inner continental shelf offshore of the Mississippi-Alabama barrier island shorelines (Figure 2.3). Only the easternmost 8 nm of the survey was used for this study. Data acquisition used an EdgeTech SB-512i towfish that was towed at 1.5 - 2.5 m/s 6 m behind the S/V *Irvington*. The source signal comprised a 0.5 to 8-kHz frequency sweep. The received signal was sampled at 43 kHz with a 75 ms record length. Data were recorded in SEG-Y format. Navigation used differential Global Positioning System (GPS). Navigation data were edited and static corrections for fish depth were applied (Twichell et al., 2011).

A total of eighteen lines of processed 2-D seismic reflection data were interpreted in Kingdom Suite. Horizons were picked along peaks. Units were identified based on the depth of Pleistocene deposits identified at approximately 16-30 m depth in the study area (Flocks et al., 2010). This corresponds to 25-320 ms in two-way travel time assuming a velocity of 1600 m/s (Figure 2.4). Interpreted horizons were gridded using a 6m by 6m flex grid interpolation.

2.2 Aerial Imagery

Aerial imagery was used to analyze geomorphologic changes. Images were georeferenced using the georeference tool in ArcGIS and added to shape files obtained from USGS, NOAA, and data from Byrnes et al. (2010; Figure 2.5). Coastlines from Google Earth, NOAA, and the USGS were used and imported in ArcGIS and georeferenced. Hand-drawn maps from 1718 and 1756 from the National Library of France were used as visual and relative comparisons to the modern data due to distortion during the georeference process.

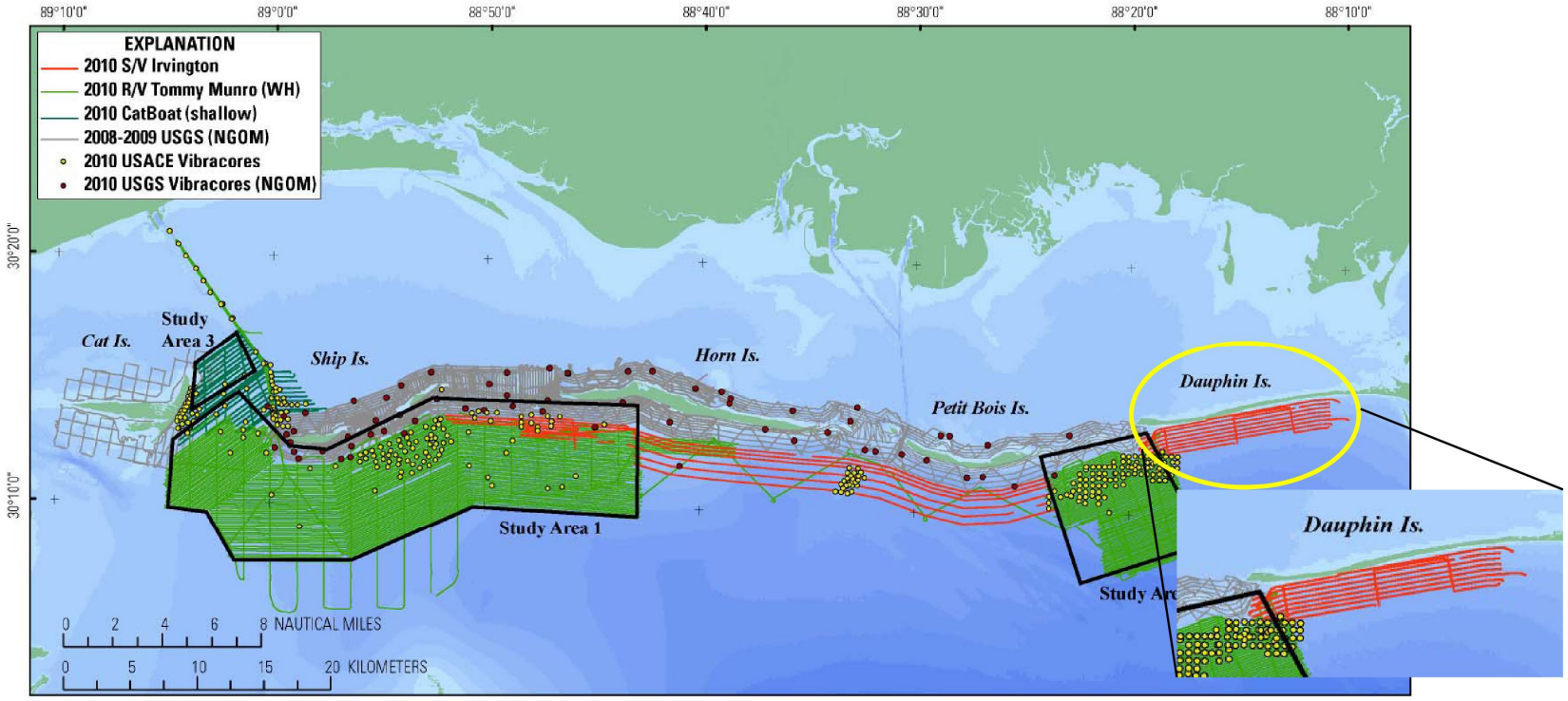

Figure 2.3 2010 CHIRP survey of the inner continental shelf offshore of the Mississippi-Alabama barrier island. The inset shows the location of the data used for this study. Modified from Twichell et al. (2011).

(a).

(b).

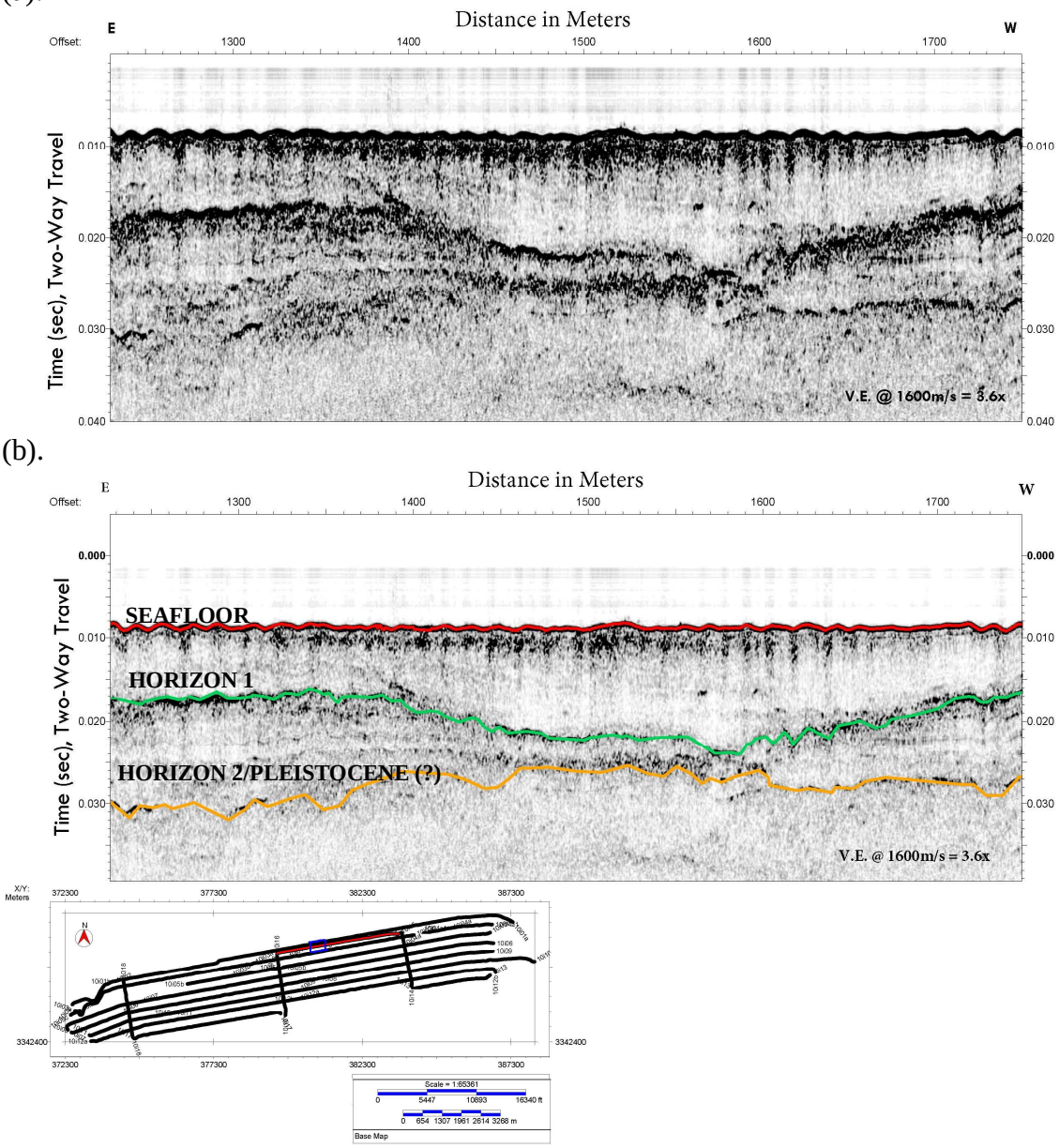

Figure 2.4 Original 2-D seismic reflection Line 10i15 (a) and interpreted line (b). Three horizons were identified: red = seafloor, green = horizon 1, orange = horizon 2 (interpreted as Pleistocene deposits). A channel feature, interpreted as a relict river channel or a former island breach, is seen along horizon 1.

2.3 Lidar

Lidar data are collected by measuring the time for a light pulses to reflect from georeferenced targets (Figure 2.5).

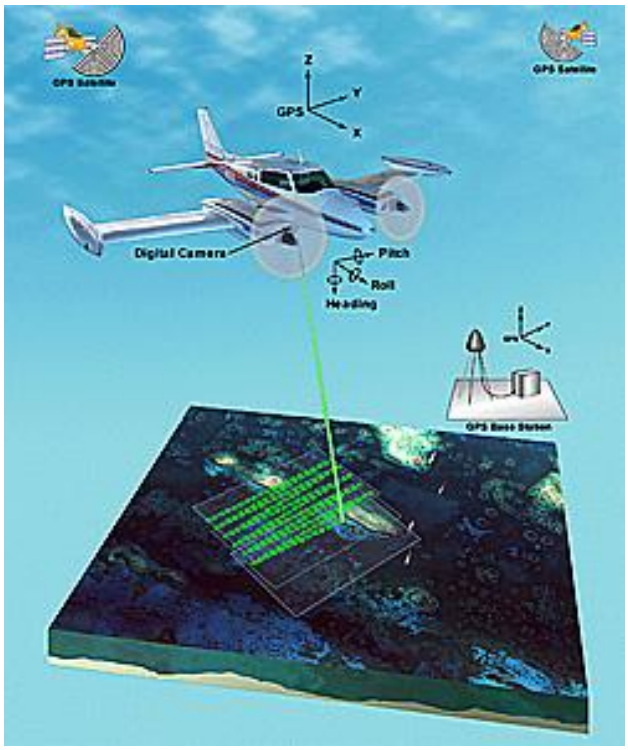

Figure 2.5 Lidar data are usually collected from an airplane traveling at a constant speed and elevation. A signal from a laser mounted on the airplane reflects off the ground surface and returns to the receiver. Adapted from http://ngom.usgs.gov/task4_2/index.php.

The Lidar data used in this study included fine-scale topography and nearshore bathymetry. By comparing data sets collected at different times, Lidar data were used to quantify geomorphologic changes due to storms and long-term morphologic changes, including erosion and deposition. The X,Y,Z LiDAR data were imported into ArcGIS using the "File to Point" tool. The points generated produced point clouds that were interpolated using the "Natural

Neighbor" method to create a grid file. The raster calculator tool was used to extract integer values from the grids. Following this step, the "Extract Attributes" tool was used to extract elevations above 4 m to eliminate buildings and trees and to achieve a closer bare earth interpolation. A polygon was created from the raster produced by the "Extract Attributes" tool and was used to distinguish dunes from buildings and trees (Figure 2.6). Areas of the polygon that represented dunes or areas of natural elevation (meaning no man-made structures or trees) were edited out of the polygon so the resulting polygon best represented buildings and tree elevations. The resulting polygon was applied to the point cloud of the associated time period to eliminate elevations that did not best represent bare earth elevations on the island.

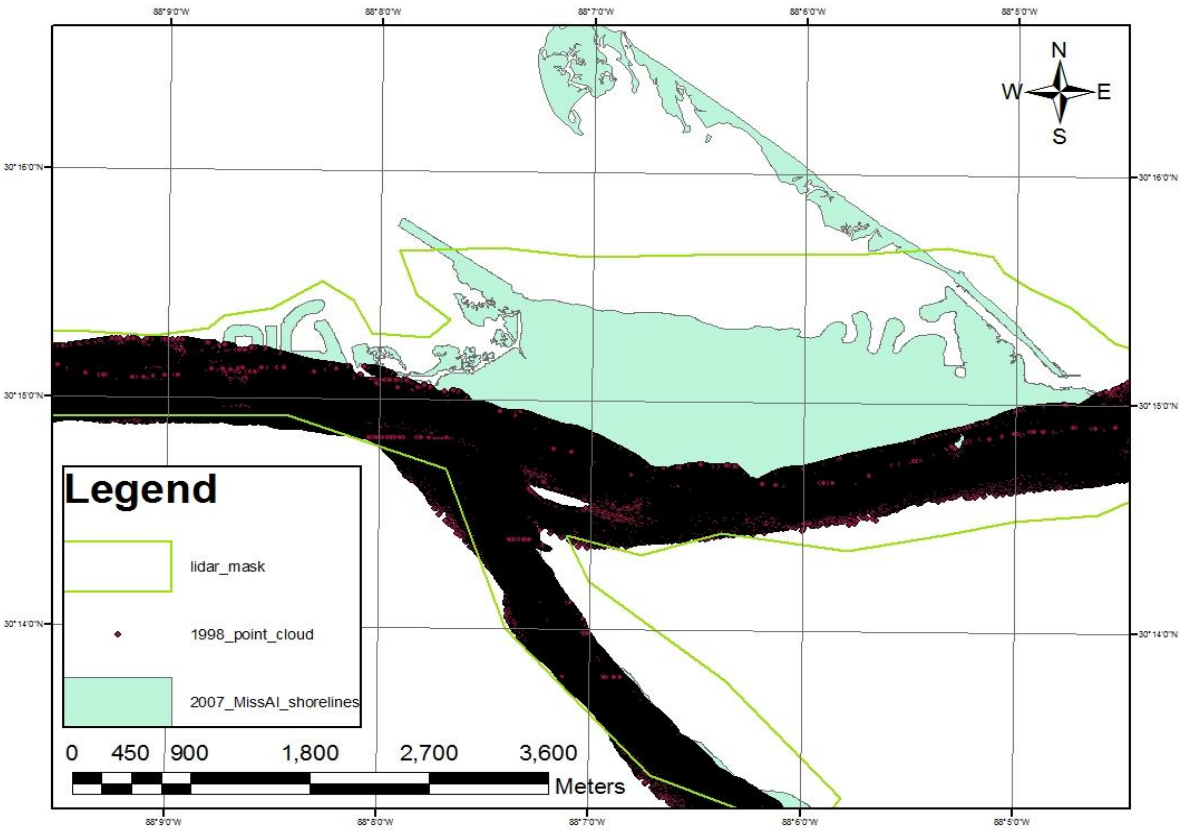

Figure 2.6 The eastern portion of Dauphin Island displayed with the 1998 Lidar point cloud dataset. The associated polygon for the 1998 data set is used to eliminate elevations that do not best represent bare earth elevations. This process helped to minimize error introduction for elevations. Once the interpolation was completed, a mask (green outline) was applied to eliminate areas extrapolated beyond the data boundaries. The data are overlain on a 2007 shoreline, showing that the data do not cover the entire island.

The altered point cloud was interpolated using natural neighbor then used for calculating volumes. These steps were applied to each time period. The interpolated models (Digital Elevation Models, DEM) were used to calculate volumes of erosion and deposition between certain time periods used for this study (Figure 2.7). Error is introduced when the point cloud is not as dense in certain areas (introducing the need for greater interpolation) or when vegetation or building extensions (i.e. awnings and covered walkways) disrupt the pulse (Pe'eri and Long, 2011).

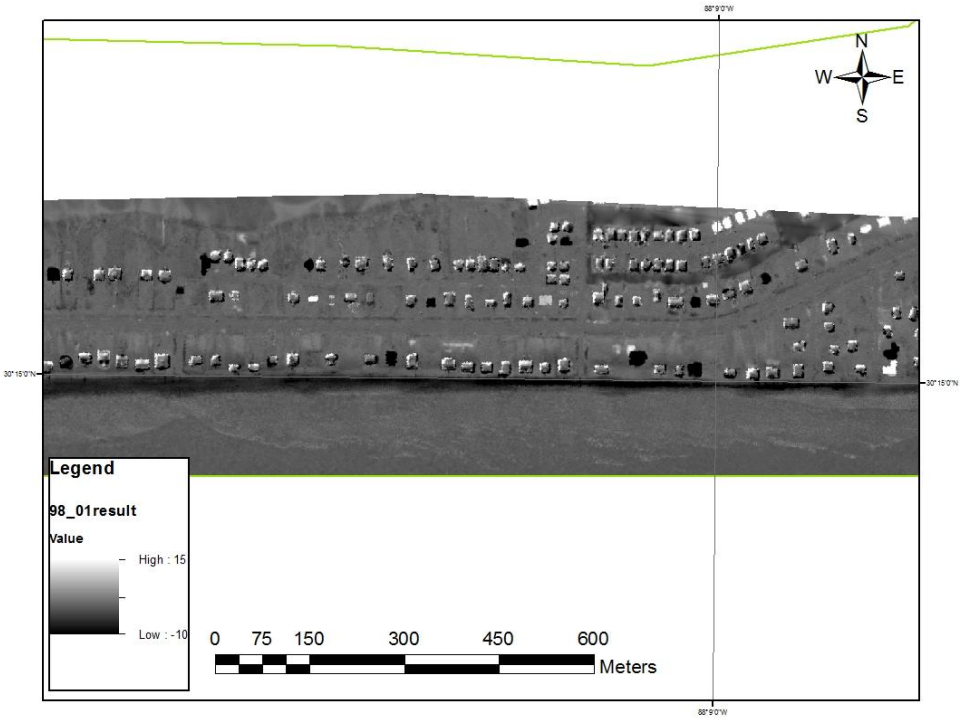

Figure 2.7 DEM created from the 1998 and 2001 datasets. Erosion, or negative difference is seen in black and deposition or a positive difference is seen in the lighter shades and white. No storm systems had a large effect on Dauphin Island during this time period, but it is apparent that some houses were built or knocked down.

The Lidar data used in this study were downloaded from NOAA's Coastal Services Center. The datasets used were collected in 1998, 2000, 2001, 2004, 2005, 2007, and 2010. A 1m by 1m grid was generated using natural neighbor interpolation and distance weighting (Figure 2.8). Grids from different time periods were compared and residual datasets derived. A mask was created to eliminate areas that did not contain data. To account for error between datasets, a set of seventy-five random points were added to each gridset (Figure 2.8). These points were selected on permanent structures, including roads and Fort Gaines. These points are constant in location with minimal lateral movement and elevation change over the period of this study.

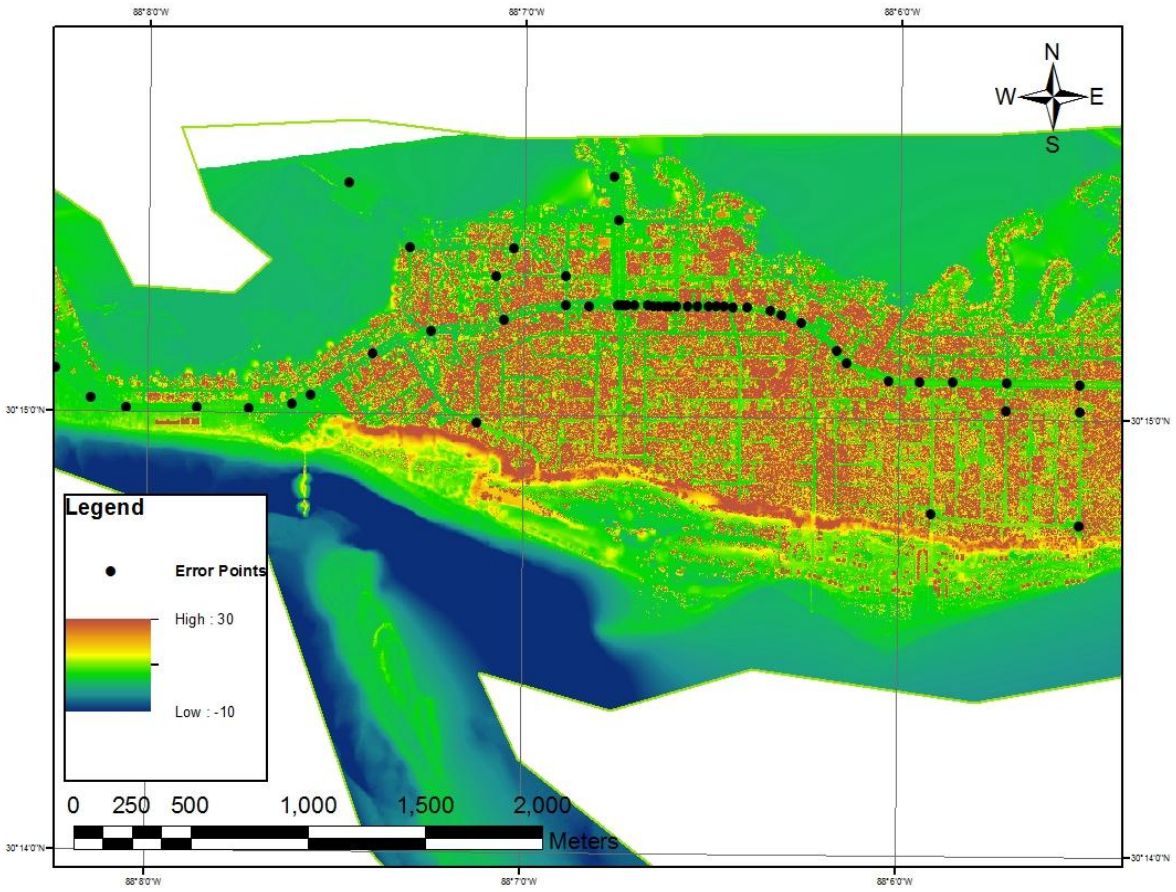

Figure 2.8 Error points were placed along the main road of Dauphin Island, the airstrip, and connecting roads for consistency throughout all datasets. The error points are displayed on a pre-Hurricane Ivan DEM.

The values for these points were extracted from the interpolated rasters for each time period dataset and the residual calculated. For example, if a residual was calculated between the 1998 and 2004 pre-Hurricane Ivan rasters, then the values of the seventy-five error points were taken from both raster datasets and compared. If the difference between the points extracted from each data set at the same location was less than or approaching zero (1^{-10}) then no further calculations were applied. However, if the difference was much greater than zero (greater than 1^{-10}), then the difference was subtracted from the 2004 pre-Hurricane Ivan raster error values. Using the corrected 2004 pre-Hurricane Ivan dataset, the differences between 2004 and 1998

error values were calculated resulting in a difference approaching zero. After the error values were calculated, the resulting difference was applied to the interpolated pre-Hurricane Ivan grid raster. The resulting grid of the difference between the corrected 2004 pre-Hurricane Ivan and 1998 raster were calculated using the raster calculator in ArcGIS program. The resulting difference rasters were used to calculate the amount of erosion or deposition. This error and difference-grid process was completed for each time period combination of near-hit hurricane systems (2004 and 2006) and intervals between storms (1998 to 2004, 2006 to 2010).

3.0 RESULTS

3.1 CHIRP 2-D Seismic Reflection Data

The eighteen survey tracks conducted by the USGS were located approximately two miles from the southern shoreline of Dauphin Island. Segments that were interpreted as channel structures within these eighteen profiles are seen in Figures 3.1 through 3.70. Complete 2-D seismic reflection profiles of this survey can be found in the USGS database (Forde et al., 2011). Each line was interpreted using four easily identified horizons. The depth of each corrected for towfish depth. The four interpreted horizons are seafloor (red), Horizon A (yellow), Horizon P (purple, interpreted as the top of Pleistocene deposits), and Horizon B (blue). Horizon A is the most prominent horizon between the seafloor and Horizon P. Horizon B is interpreted as acoustic "basement". Channel-like structures were annotated on the profiles. The profiles parallel to the shoreline are displayed west to east, and the profiles perpendicular to the shoreline (10i14, 10i16, and 10i18) are displayed south to north.

Figure 3.1 includes a segment of line 10i01a interpreted with an approximately 200 m wide channel structure that is 8 m deep. The channel has been infilled with deposits occurring

between the time periods of Horizon A and Horizon P. The majority of the channel structures seen throughout line 10i01a (Figures 3.1 through 3.4) are interpreted to lie along Horizons A and B. Line 10i01b (Figures 3.5 through 3.11) includes channel structures primarily along Horizon P. Line 10i02 does not include prominent structures. Line 10i03a (Figures 3.12 through 3.16) includes wide and deep channels along Horizons A and P. For these lines Horizon B was not interpretable. Horizon B is interpreted in line 10i03b (Figure 3.17) as sloping upward to the east from a depth of approximately 40 m (0.05 sec). Channel structures are seen along Horizons A and P in line 10i03b (Figures 3.17 thru 3.19). In Figure 3.20, Horizon B is interpreted as being truncated by Horizon P in line 10i04a. Line 10i05a (Figures 3.21 through 3.22) includes a wide and relatively shallow channel structure along Horizon A and Horizon B. Line 10i05b (Figures 3.23 through 3.25) shows intermittent channel structures within close proximity of each other in Horizon P. Line 10i06 (Figures 3.26 through 3.33) is the longest profile and includes features interpreted as channel structures along Horizons A, P, and B. Line 10i07 (Figures 3.34 through 3.35) includes a prominent channel structure along Horizon B. Horizons P and B dip to the east. Line 10i08 (Figures 3.36 through 3.41) includes channel structures along Horizons A, P and B. Horizons along line 10i09 (Figures 3.42 thru 3.44) dip generally to the west. Small channel are seen along Horizons P and B. Line 10i10 (Figures 3.45 through 3.51) includes Horizons A and P in the western portion of the line. Horizon B is interpreted within the remaining portion of the line. Channel structures are interpreted along Horizons A and B. Line 10i11 (Figures 3.52 through 3.53) does not include interpretable channel structures, but is interpreted to show a 0.5^{o} slope change between Horizons P and B. The interpretation of line 10i12a (Figures 3.54 through 3.57) includes channel structures at the eastern end of the line in horizons A, P, and B. Line 10i12b (Figures 3.58 through 3.60) includes a deep and relatively wide channel structure

(478.4m by 9.9m) in Horizon B that extends to line 10i12a. No significant structures are interpreted along line 10i13 (Figure 3.61) undulating relief along the three Horizons A, P and B. Line 10i14 (Figure 3.62) runs north towards the Dauphin Island shoreline. The seafloor and Horizon B shallow towards the shoreline. Horizons A and P are horizontal. The interpretation of line 10i15 (Figures 3.63 through 3.64) includes shallow valleys (1.4m to 4.5m depths) with 200 to 300m wide channels interpreted along Horizons A, P and B. Line 10i16 (Figures 3.65 through 3.67) is perpendicular to the shoreline. Horizons A and B are interpreted to dip at 3.3^{o} to the south with Horizon B terminating at Horizon P. A 450m by 10m channel is interpreted along Horizon B. Line 10i17 (Figure 3.68) is interpreted as including a horizontal Horizon P and a small channel structure in Horizon B. Line 10i18 (Figures 3.69 thru 3.70) is perpendicular to the shoreline and the horizons are interpreted as having dips of 1.2^{o} to5.2^{o} towards the shoreline in the southern portion of the line changing to a northerly dip at the northern end of the line.

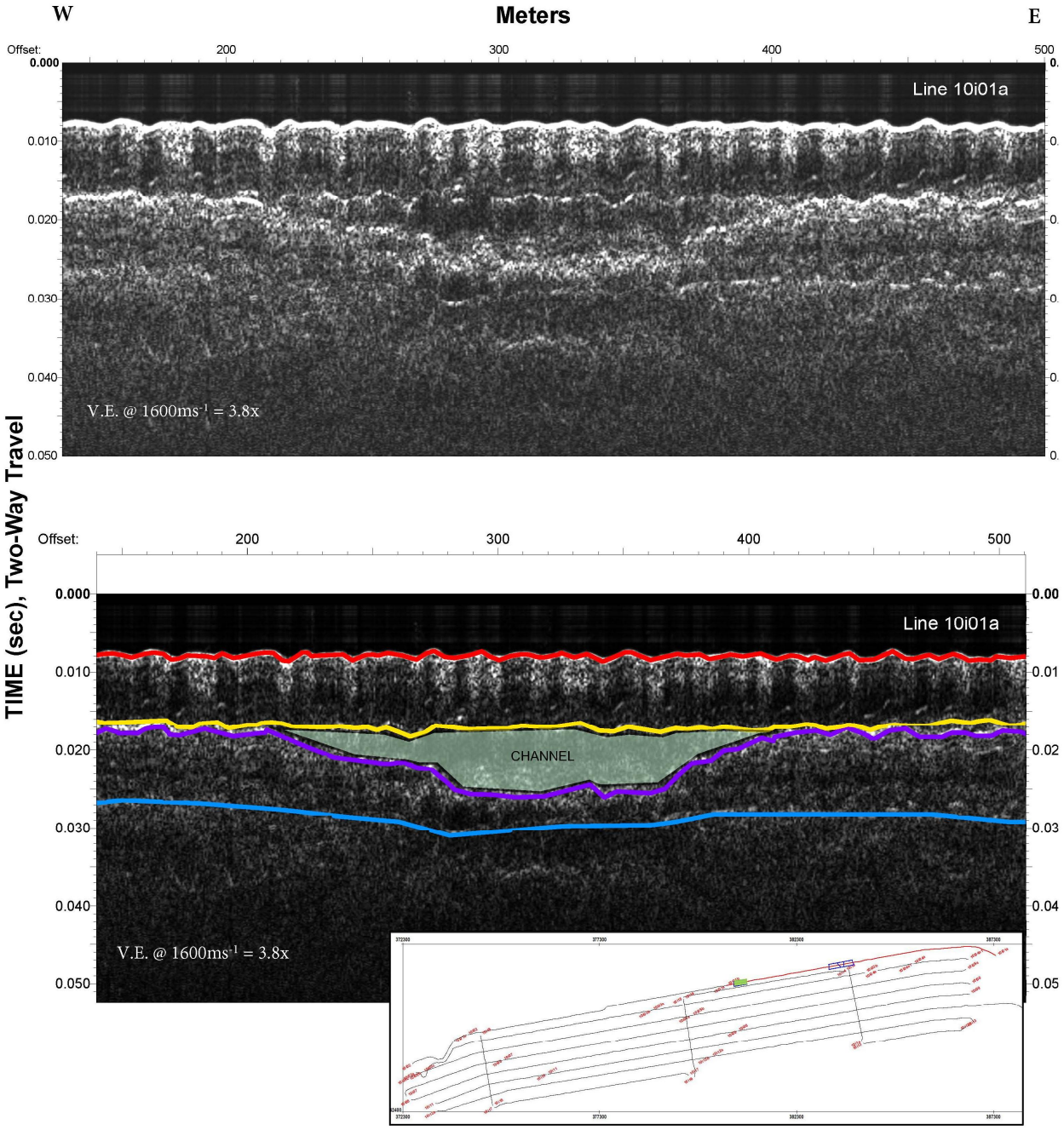

Figure 3.1 A channel-like structure is seen along Horizon P (purple) that is 6.4 m deep by 223.7 m wide with a 5.2° western slope and a 7.8° eastern slope in this segment of line10i01a. Deposits directly below Horizon A (yellow) have infilled the channel structure. A structure seen along Horizon B (blue) mimics the deepest point seen in Horizon P. The inset shows the location of this line as a green box.

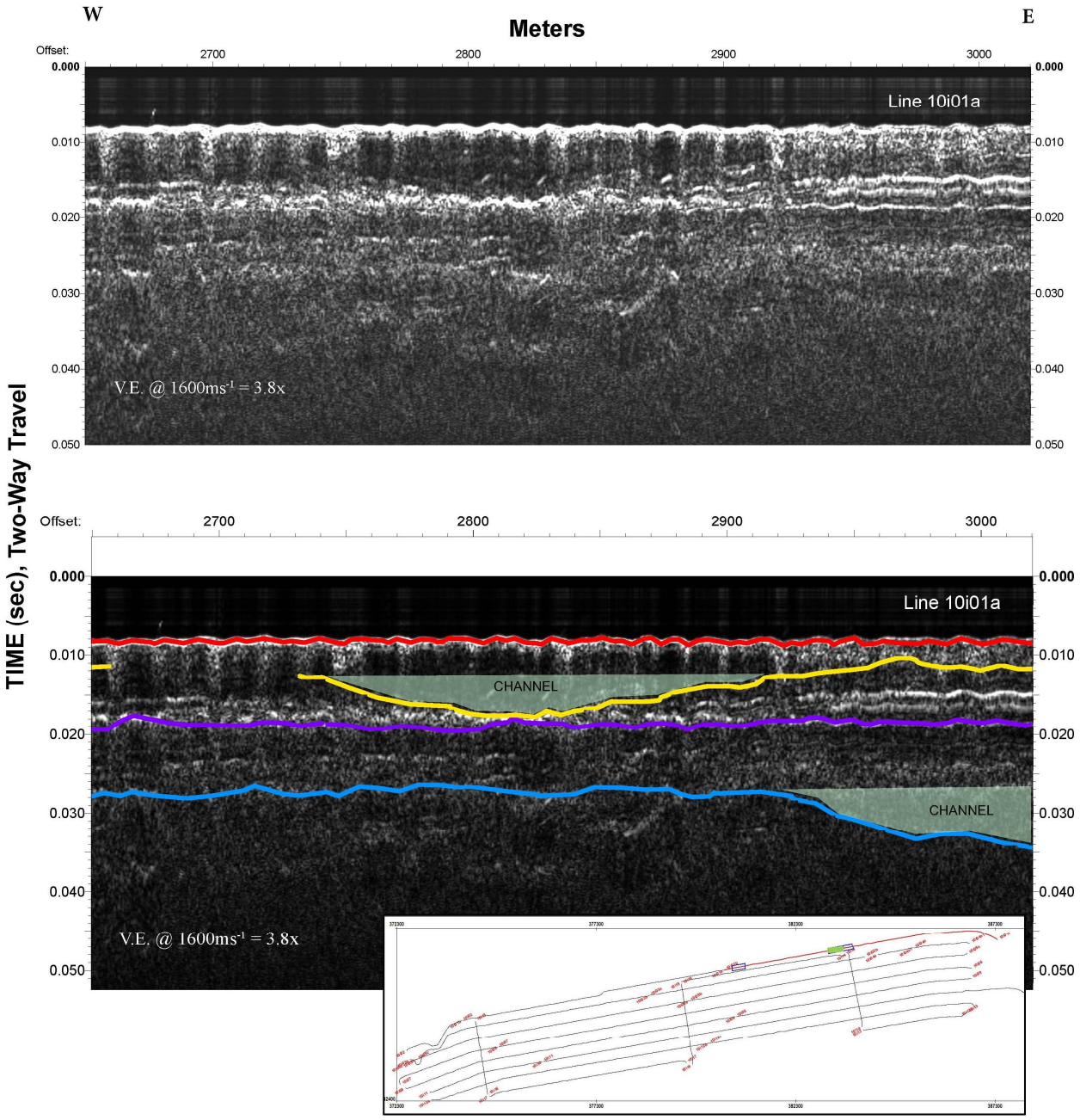

Figure 3.2 Two channel structures are seen in Horizons A and B in this segment of line 10i01a. Horizon The top structure has a relief of 4.5 m and is 206.2 m wide with a 4.4° western slope and a 2.7° eastern slope. The deeper structure seen in Horizon B overlaps onto the following profile segment (see Figure 3.3).

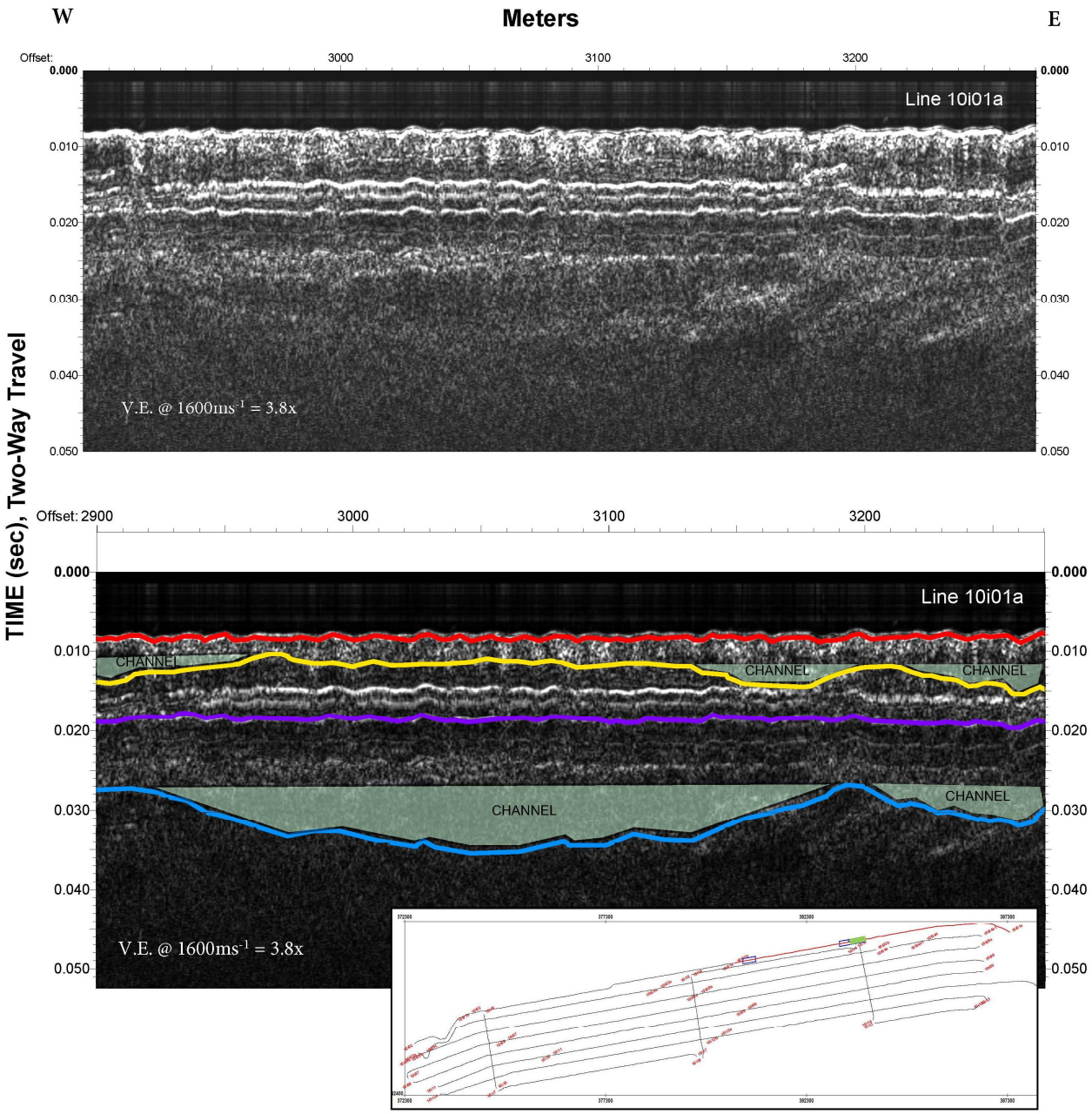

Figure 3.3 Multiple channels structures are seen in this segment of line 10i01a in both Horizons A and B. The dominant channel feature is within Horizon B. The channel is 6.5 m deep, 292 m wide, and 3.2° western and eastern slopes.

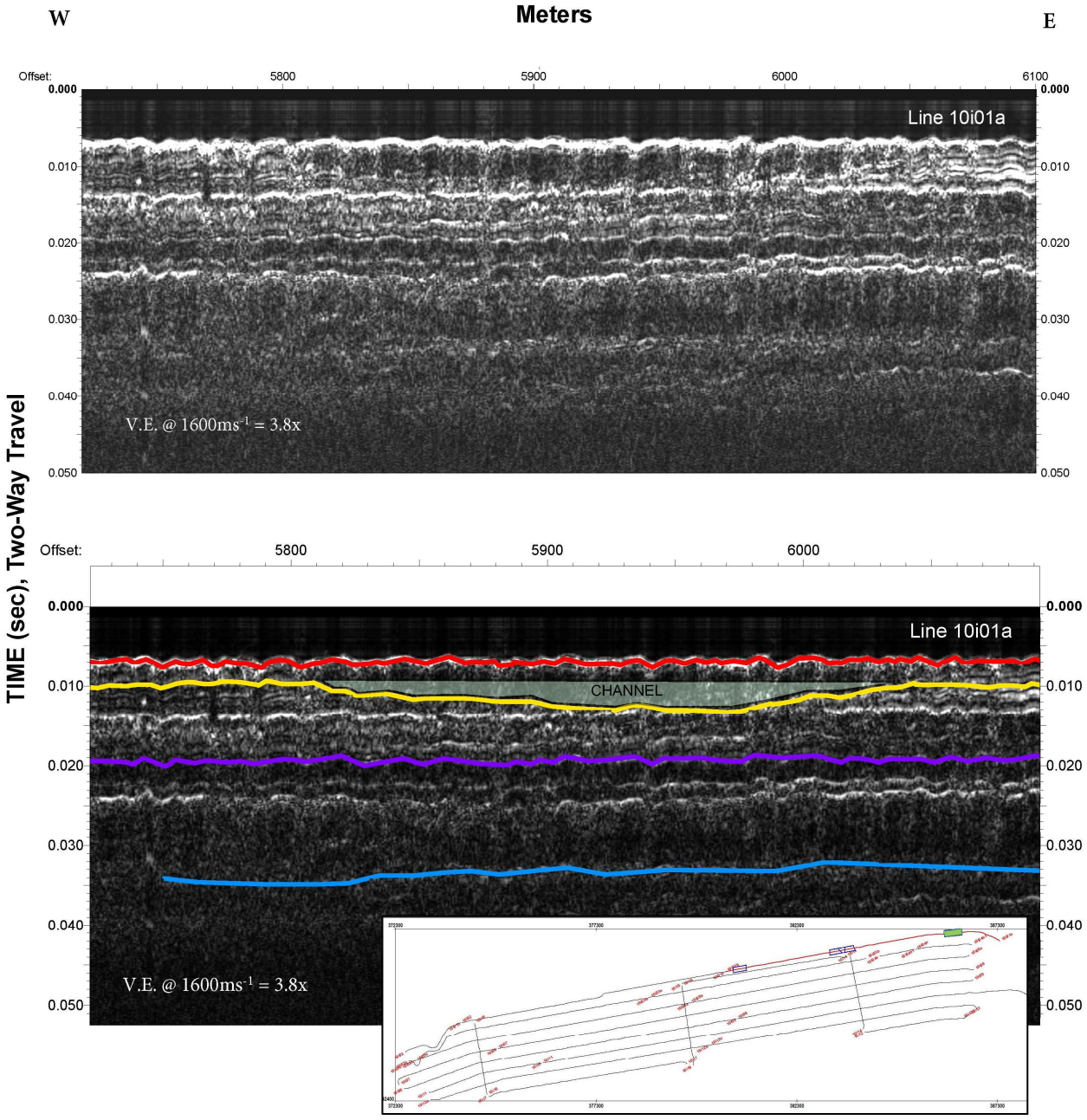

Figure 3.4 The interpretation of Horizon A includes a shallow (2.7 m) structure, 225.1 m wide, with a western 1.1° slope and eastern 2.4° slope. The location of this line segment of 10i01 is shown as a green box in the inset map.

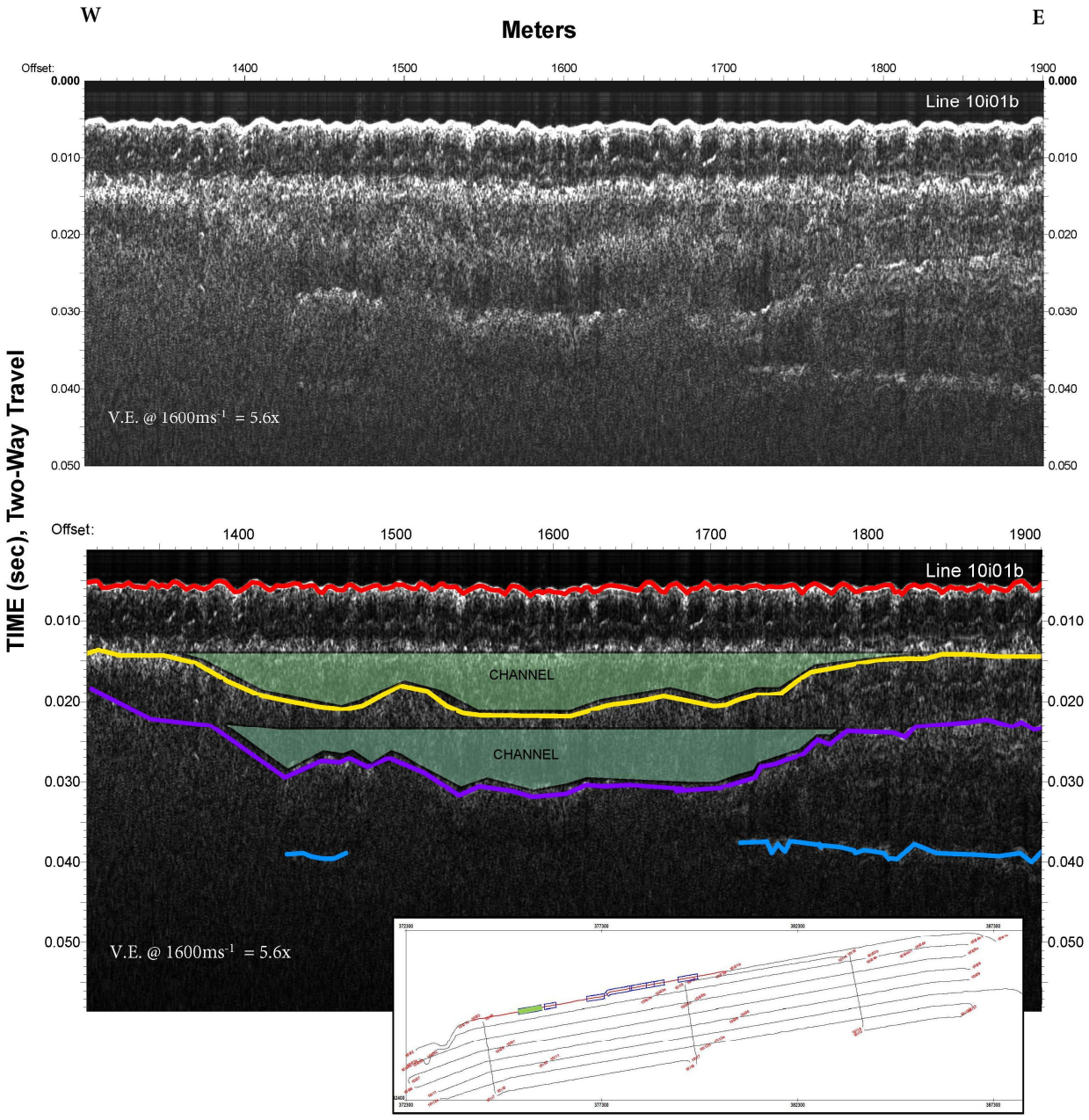

Figure 3.5 A channel structure is seen in each of Horizons A and P. The channel in Horizon A is 6.4 m deep by 504.7m wide with a western 3.2° slope and eastern 1.6° slope. The channel structure in Horizon P is 6.4 m by 395.7 m with a western 2.5° slope and eastern 4.5° slope in this segment of line10i01b.

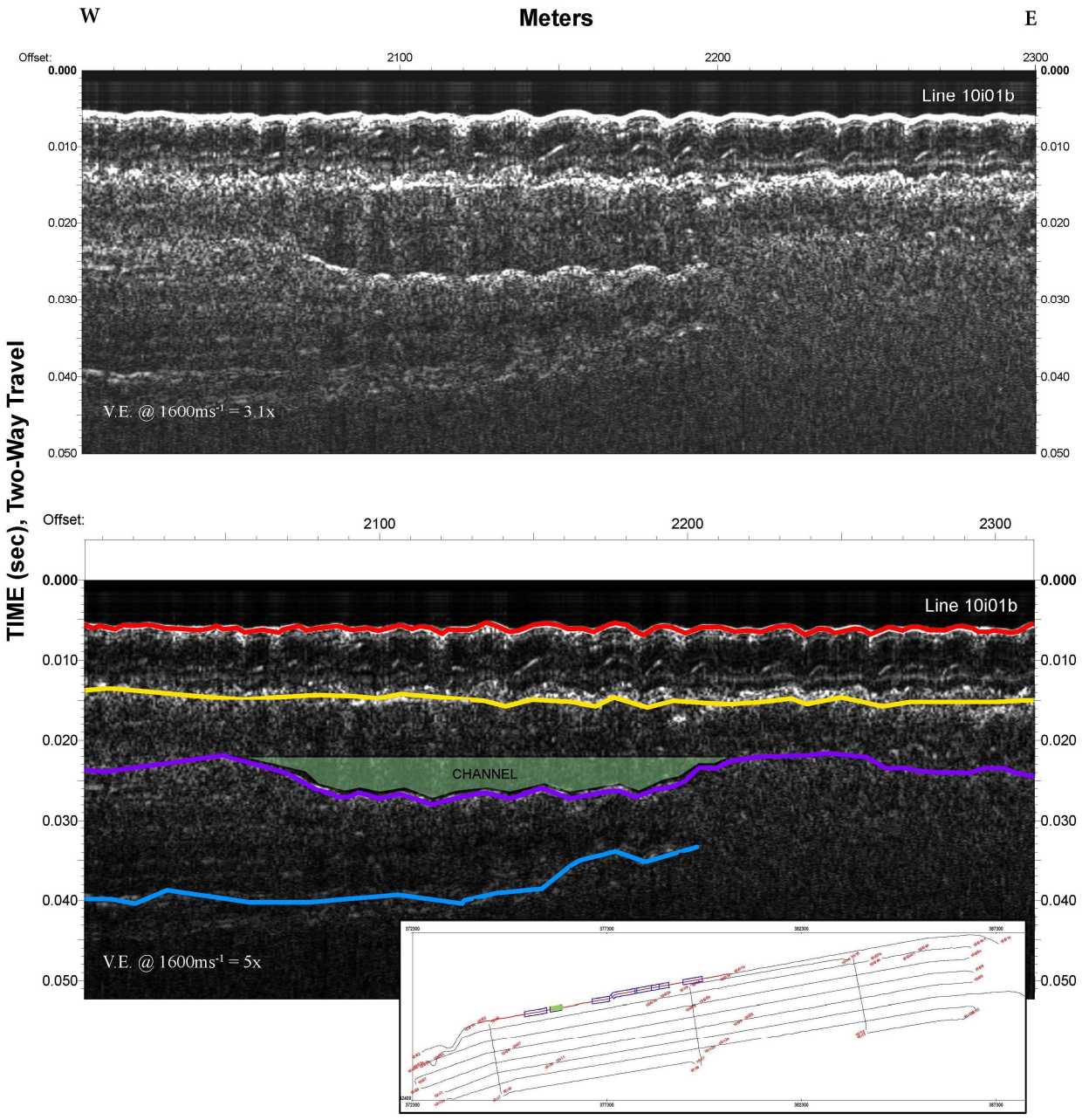

Figure 3.6 In this segment of line 10i01b a single channel is seen along Horizon P. The channel is 5 m deep by 175.2 m wide with a western 7.5° slope and an eastern 3.0° slope. Horizon B slopes westward at 5° degrees.

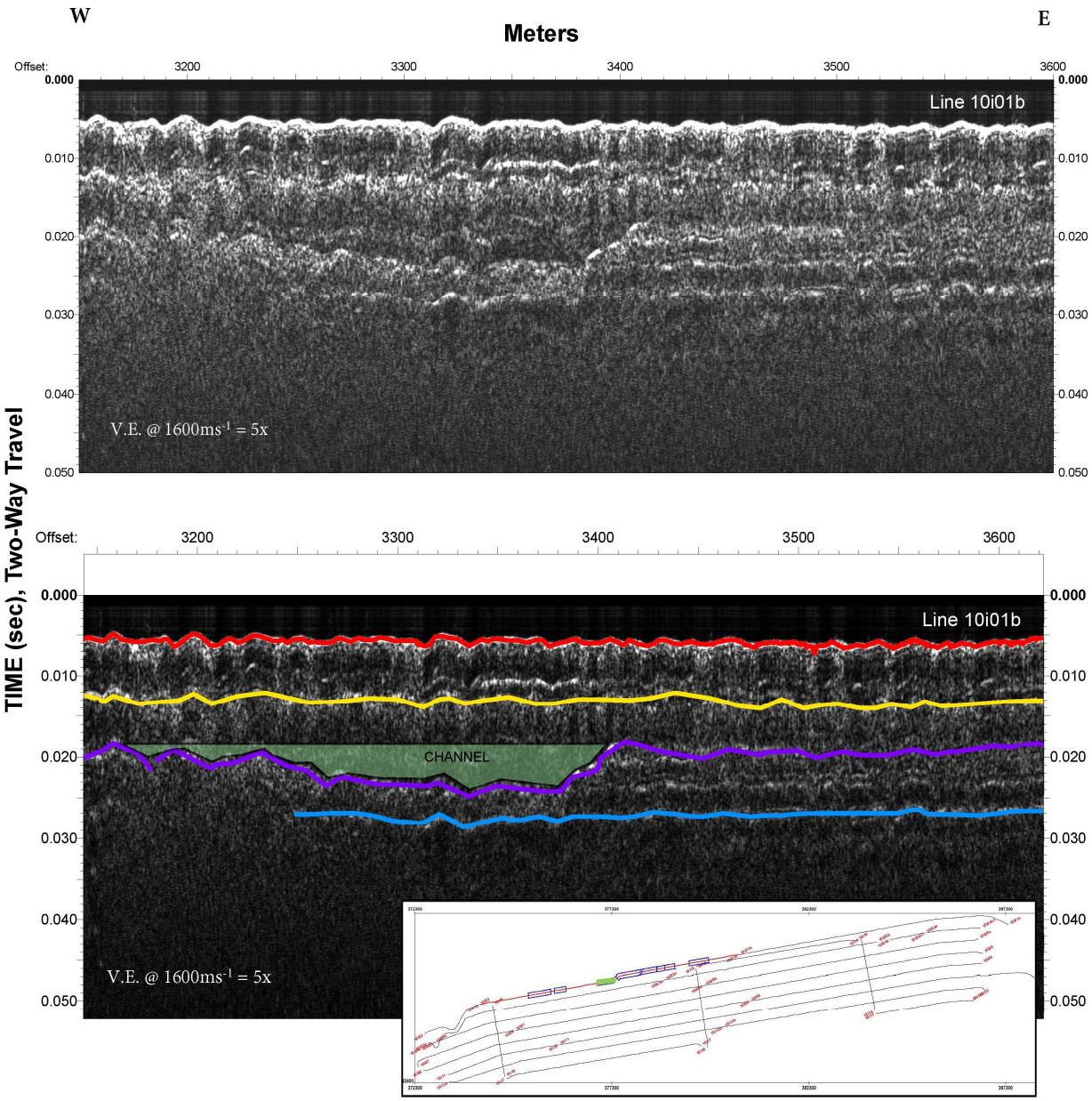

Figure 3.7 Horizon P includes a channel in this segment of line 10i01b. The channel is 4.8 m at its deepest and 230 m wide. The western 1.6° degree slope contrasts with the eastern 8.8° slope.

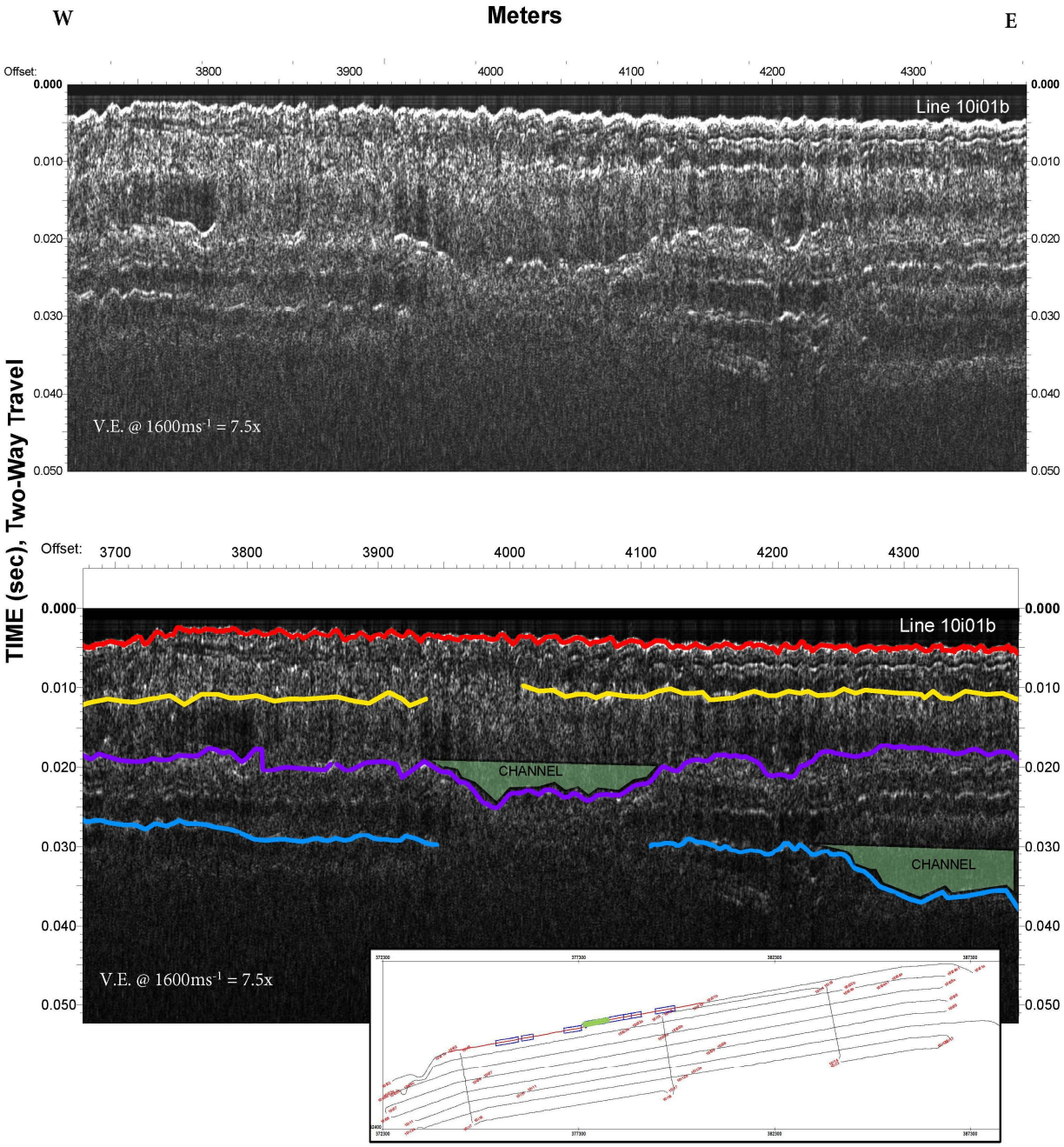

Figure 3.8 The interpretation of this line segment of 10i01b includes the seafloor horizon having an eastern dip, and channel structures seen in both Horizons P and B. Horizon P includes a structure that is 3.6 m deep and 230 m wide with a western 44.7° slope and an eastern 1.9° slope. Horizon B includes a channel structure that continues into the segment profile in Figure 3.9. This portion of the channel has a western 2.3° slope (the total depth and width of this channel structure is in Figure 3.9 caption).

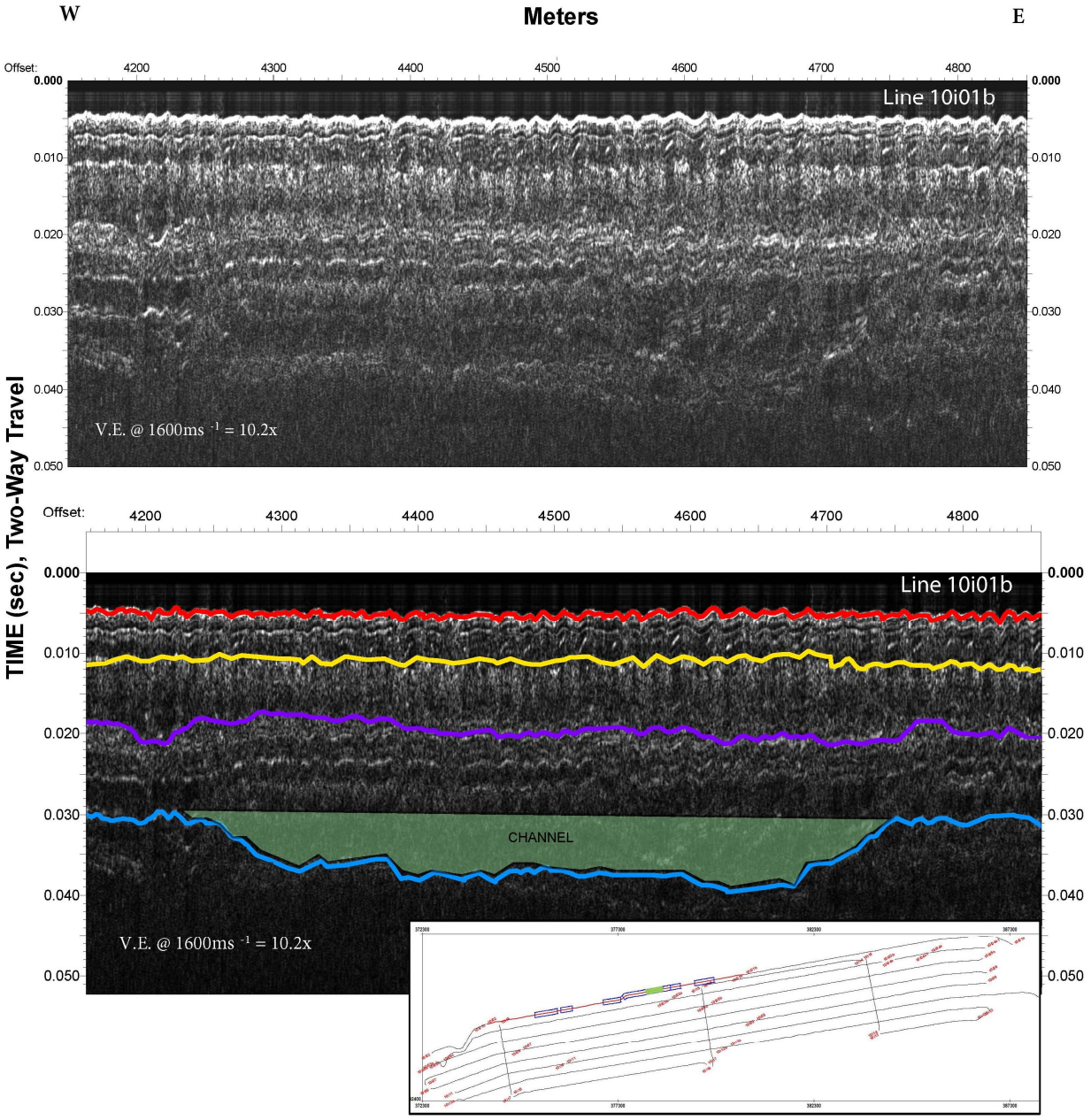

Figure 3.9 A channel structure is seen along Horizon B in this segment of line 10i01b that is 6.4 m by 543.9 m channel with a western 2.3° slope and eastern 5.5° slope. The western portion of this channel is seen in the line segment of 10i01b in Figure 3.8.

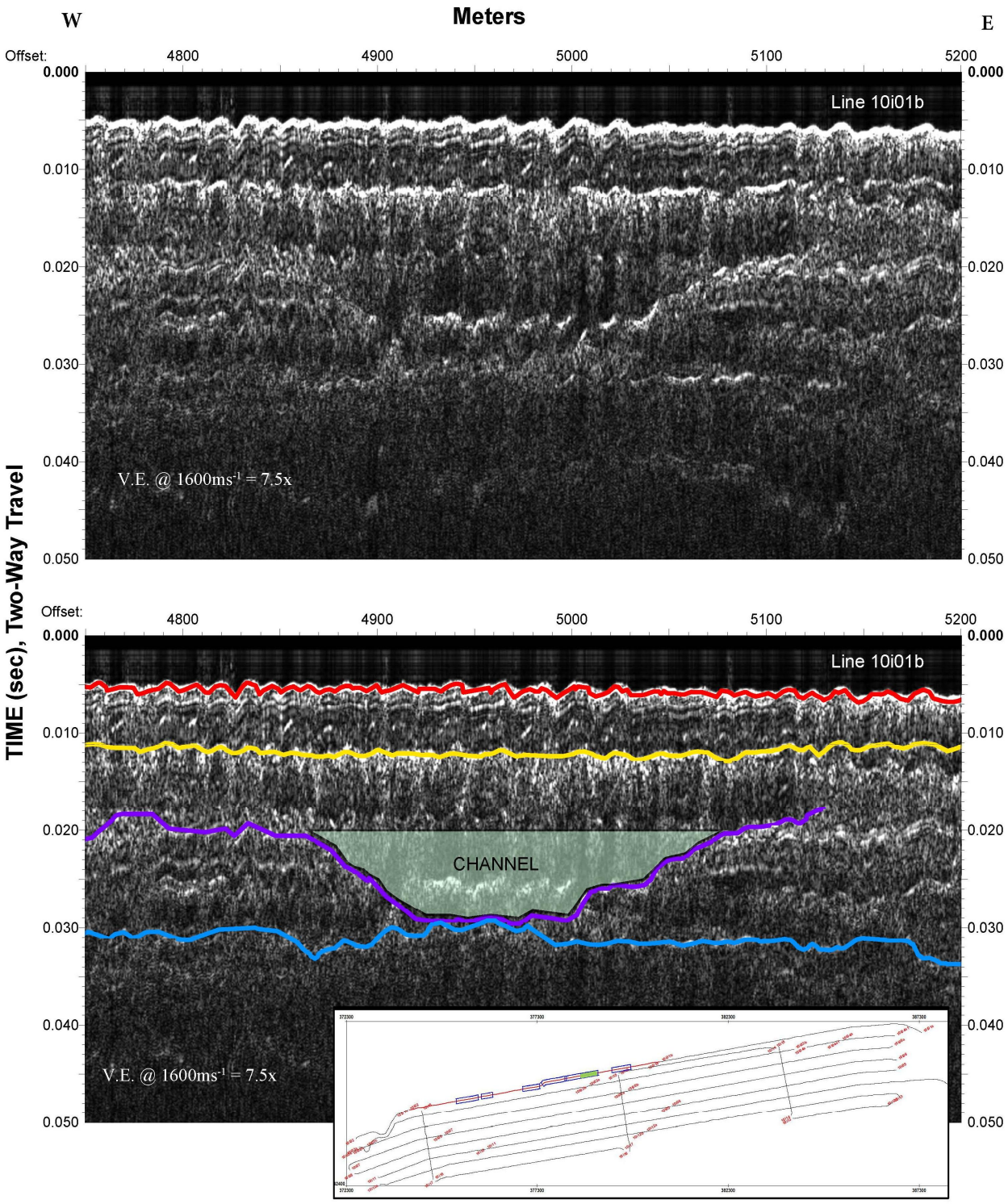

Figure 3.10 A channel is seen along Horizon P in this line segment of 10i01b that is 7.2 m deep and 249.1 m wide with a 7.2° western slope and a 5.2° eastern slope.

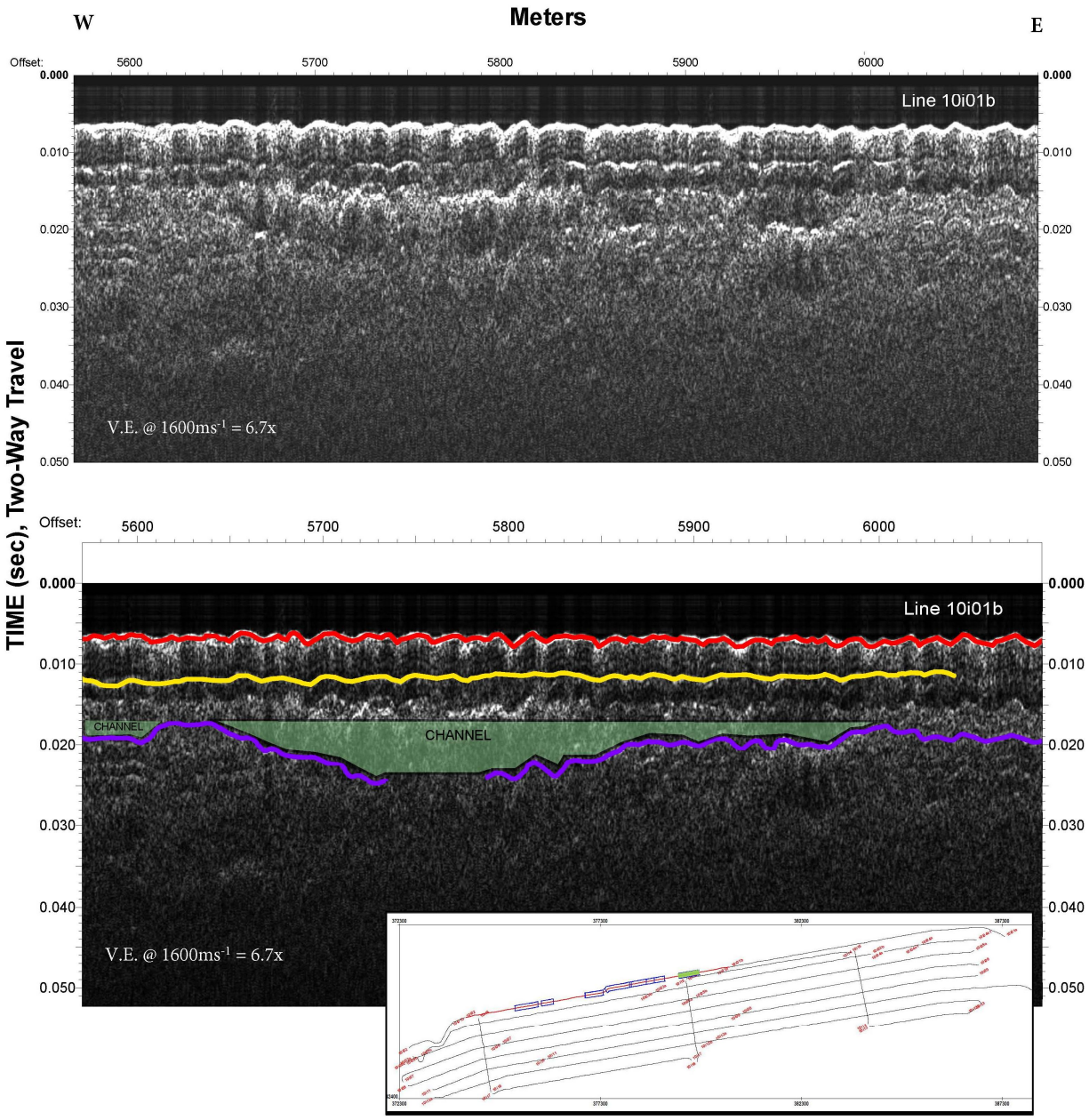

Figure 3.11 The interpretation of Horizon P in this segment of line 10i01b includes a channel structure that is 5.6 m deep and 386.1 m wide with a western 3.5° slope and an eastern1.8° slope.

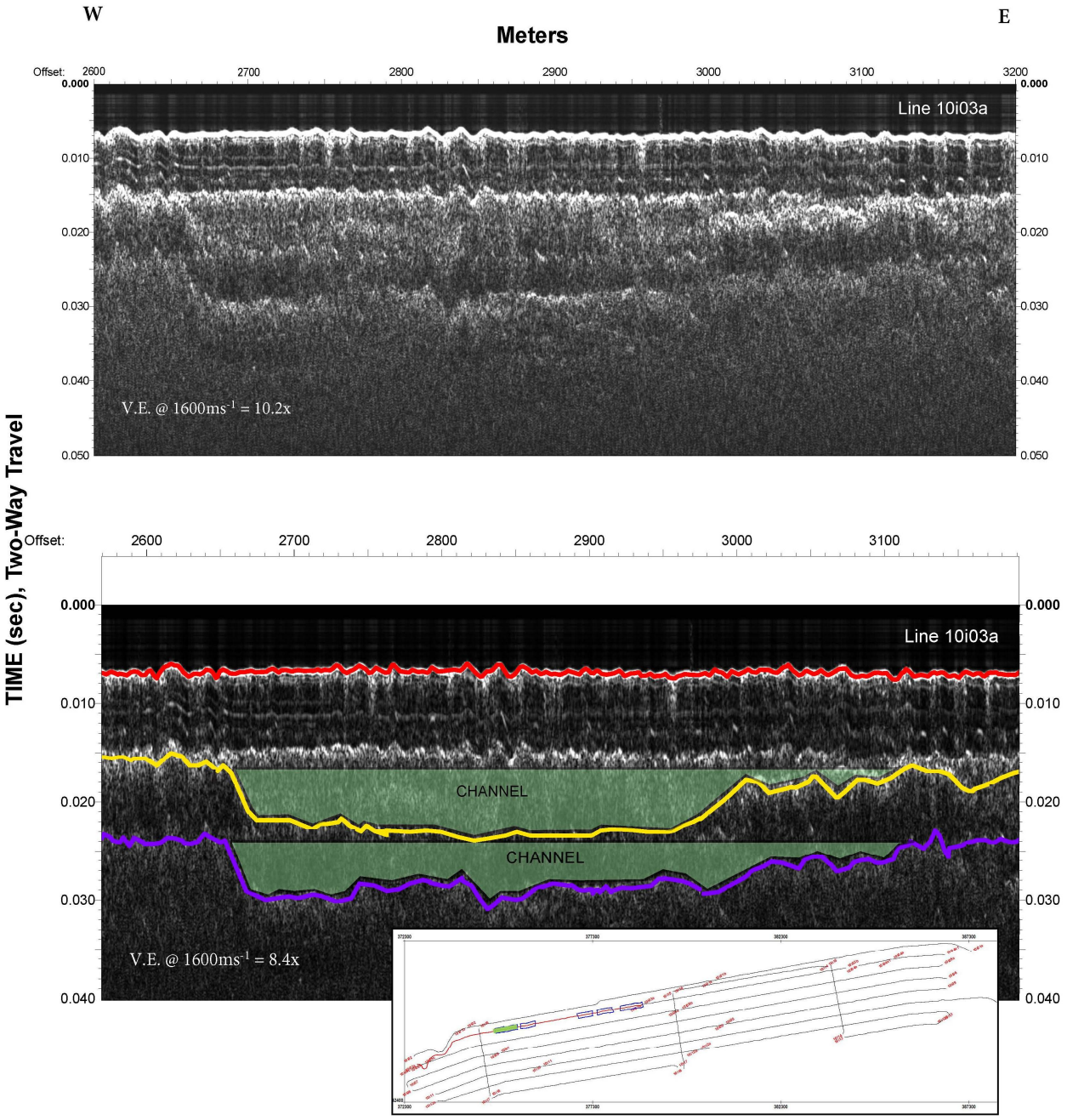

Figure 3.12 This western segment of line 10i03a is interpreted with channel structures in each of horizons A and P. Horizon A consists of a structure that is 4.6 m deep and 479.3 m wide with a 2.9° western slope and a 1.8° eastern slope. A similar channel structure is seen along Horizon P and is a 5.8 m deep by 456.1 m wide channel with a 10.9° western slope and 1.2° eastern slope.

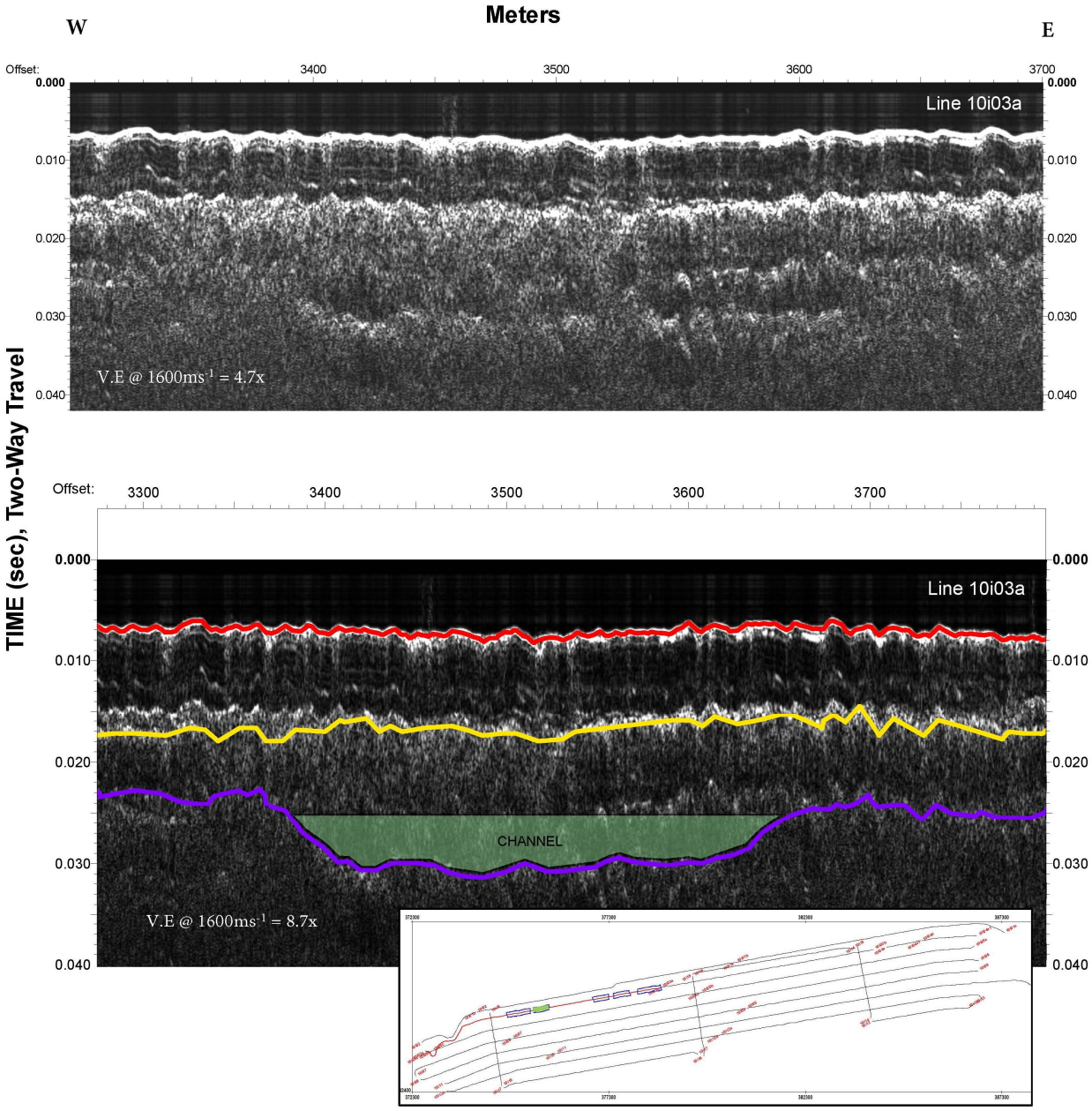

Figure 3.13 The interpretation of Horizon P in this segment of line 10i03a includes a channel that is 4.8 m deep by 337 m wide with a 6.5° western slope and 1.6° eastern slope.

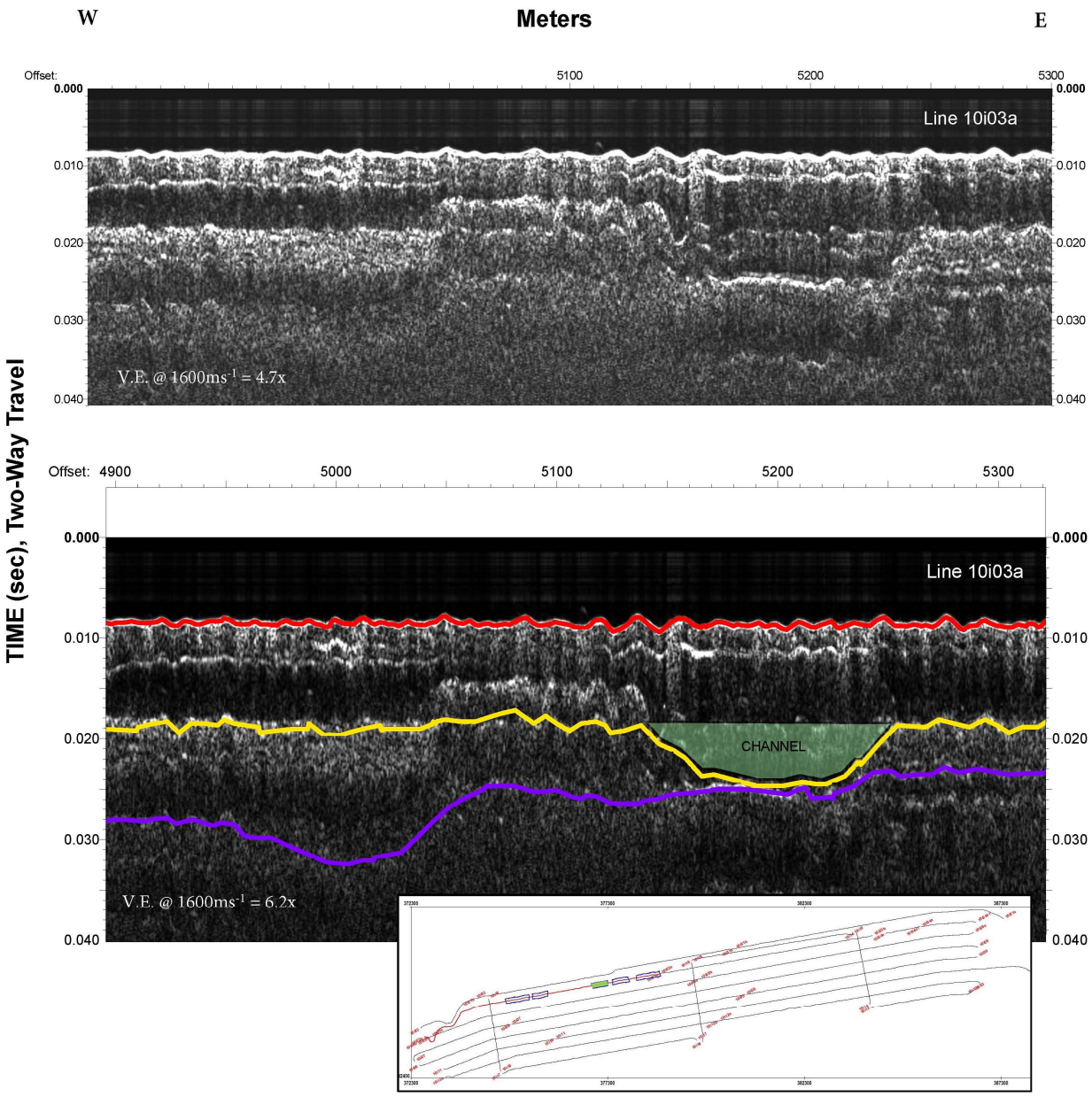

Figure 3.14 A wide channel is seen along Horizon A in this line segment of 10i03a. The channel is 4.4 m deep by 128.4 m wide with a 5.3° western slope and a 9.3° eastern slope.

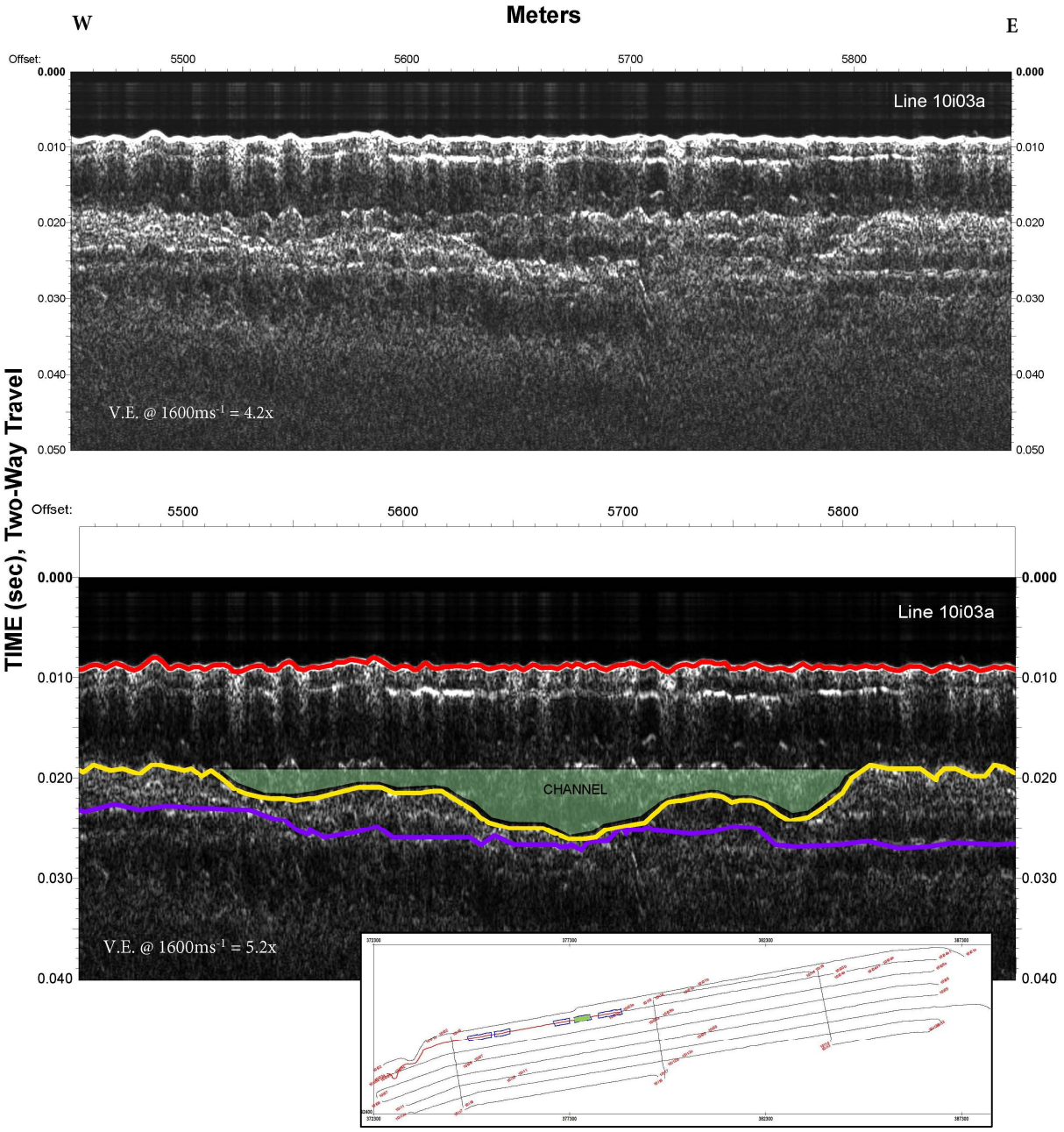

Figure 3.15 This line segment of 10i03a shows the Horizon A interpretation to consist of a channel structure with varying depths, the deepest point at 4.8 m, and total width 323.5 m with a 1.8° western slope and an eastern 2.3° slope.

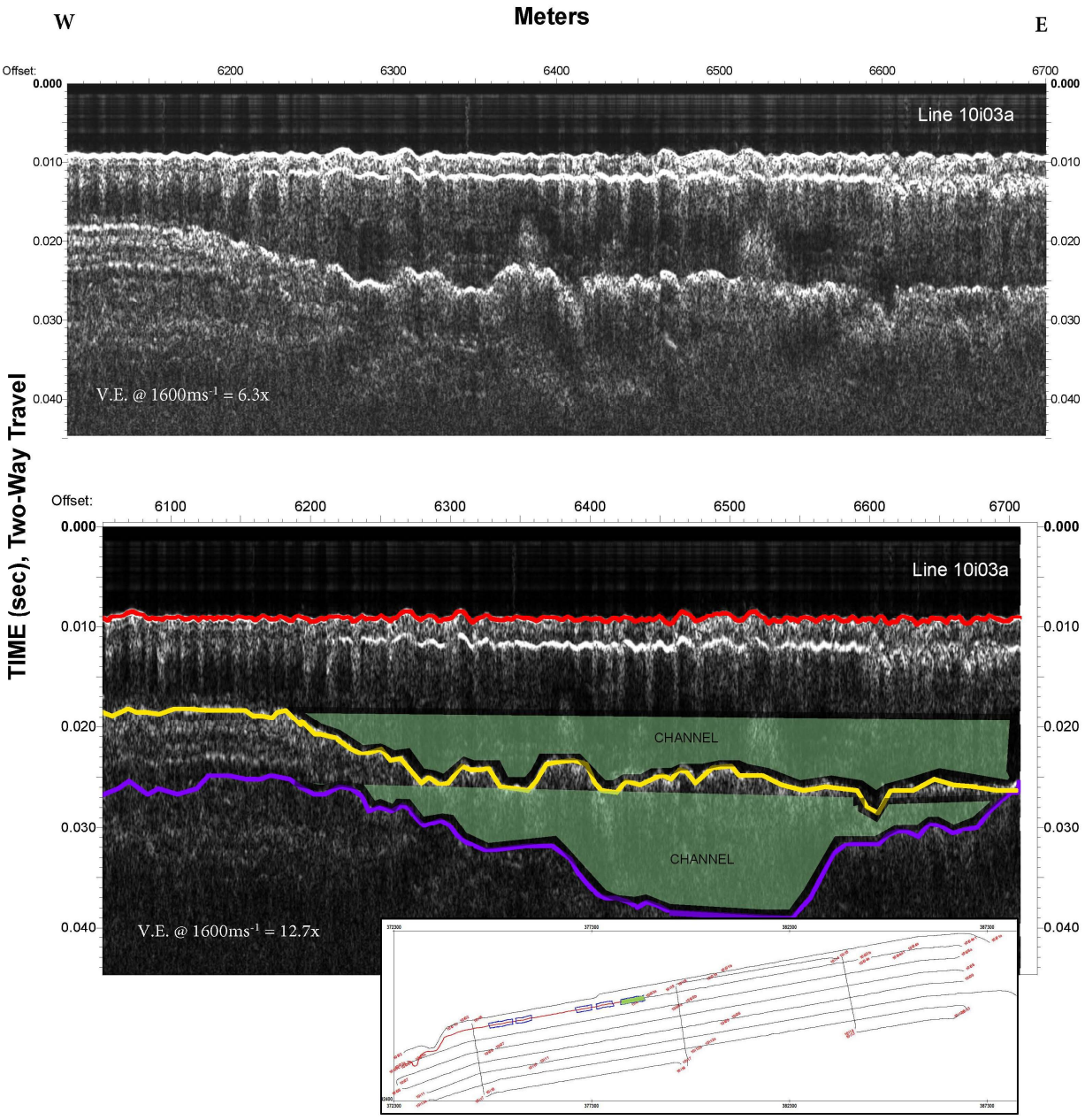

Figure 3.16 A channel is seen along Horizons A and P in this segment of line 10i03a. The interpretation of Horizon A includes a channel that is 5.6 m deep and 771.7 m wide with a 2.9° western slope (this channel structure continues into Figure 3.17). A channel-like structure seen along Horizon P is 9.6 m deep by 467.7 m wide with an average western 2.8° slope and an average 5.8° eastern slope.

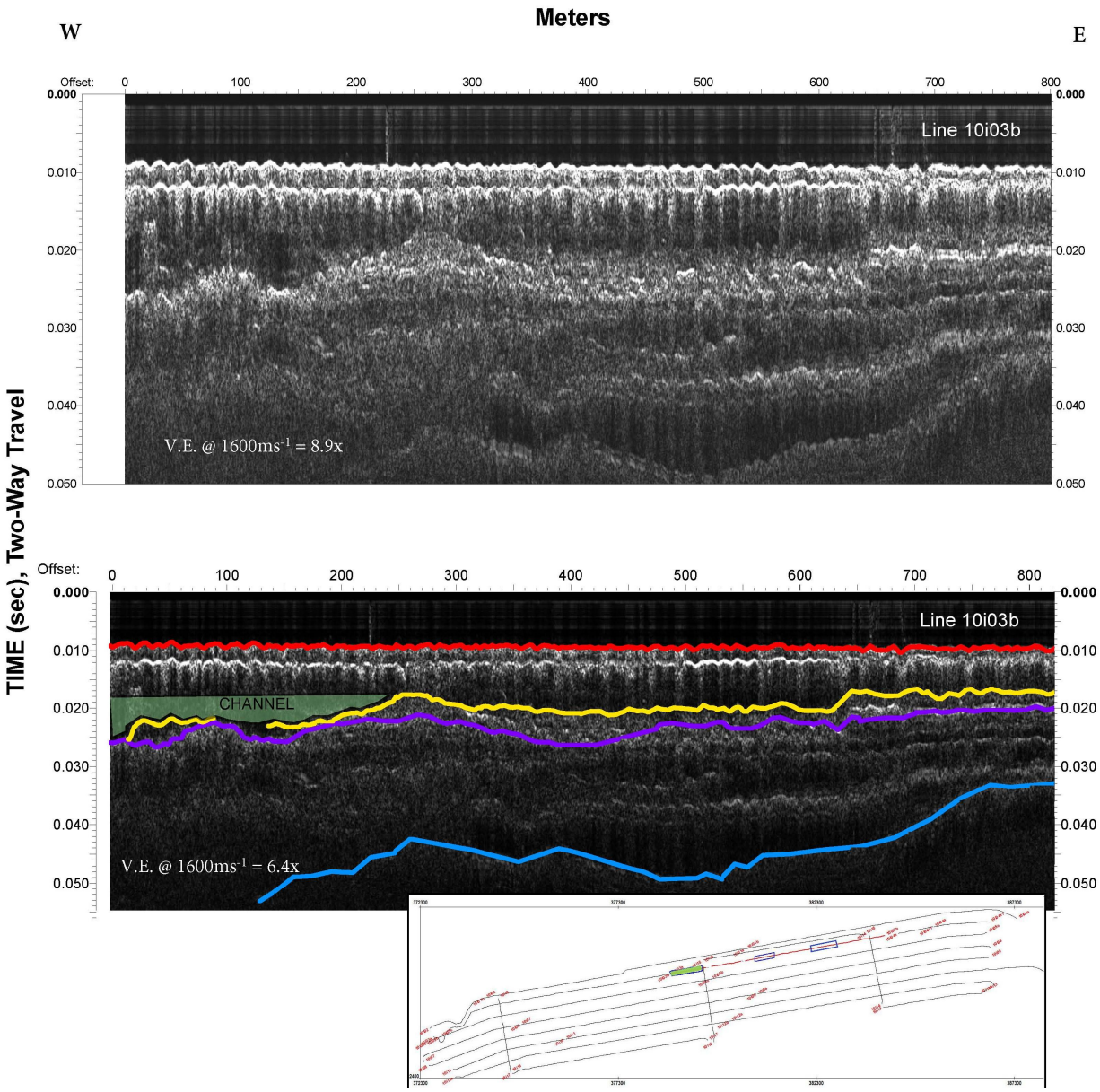

Figure 3.17 The structures seen in this line segment of 10i03b are continued from the structures seen in figure 3.16. Horizon A interpretation includes a 2.7° eastern slope, and Horizon B consists of a structure sloping to the east with an 2.8° slope.

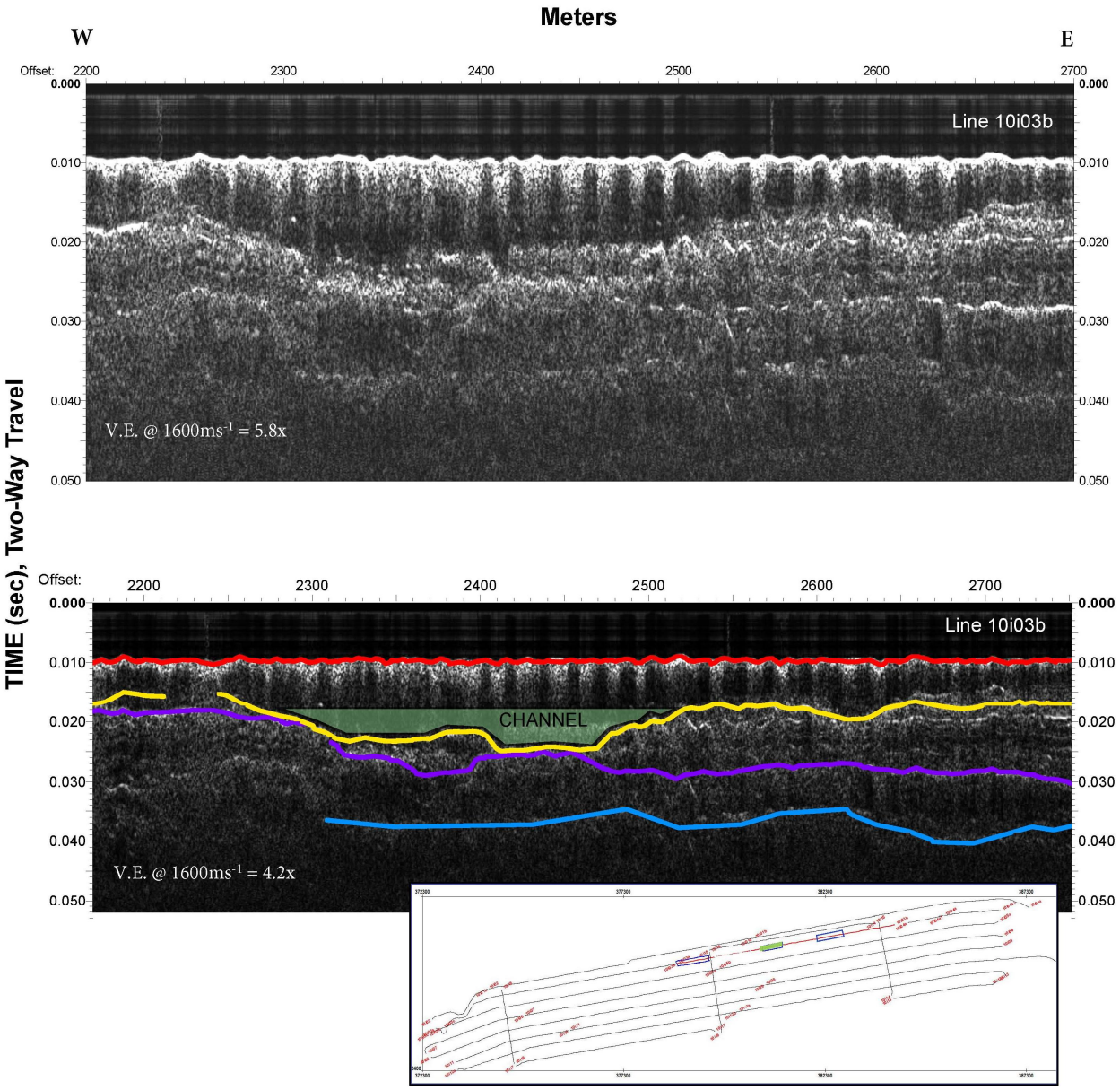

Figure 3.18 A channel structure is seen along Horizon A in this segment of line 10i03b. The channel is 4.8 m deep by 274.5 m wide with a 2.2° western slope and a 5.0° eastern slope.

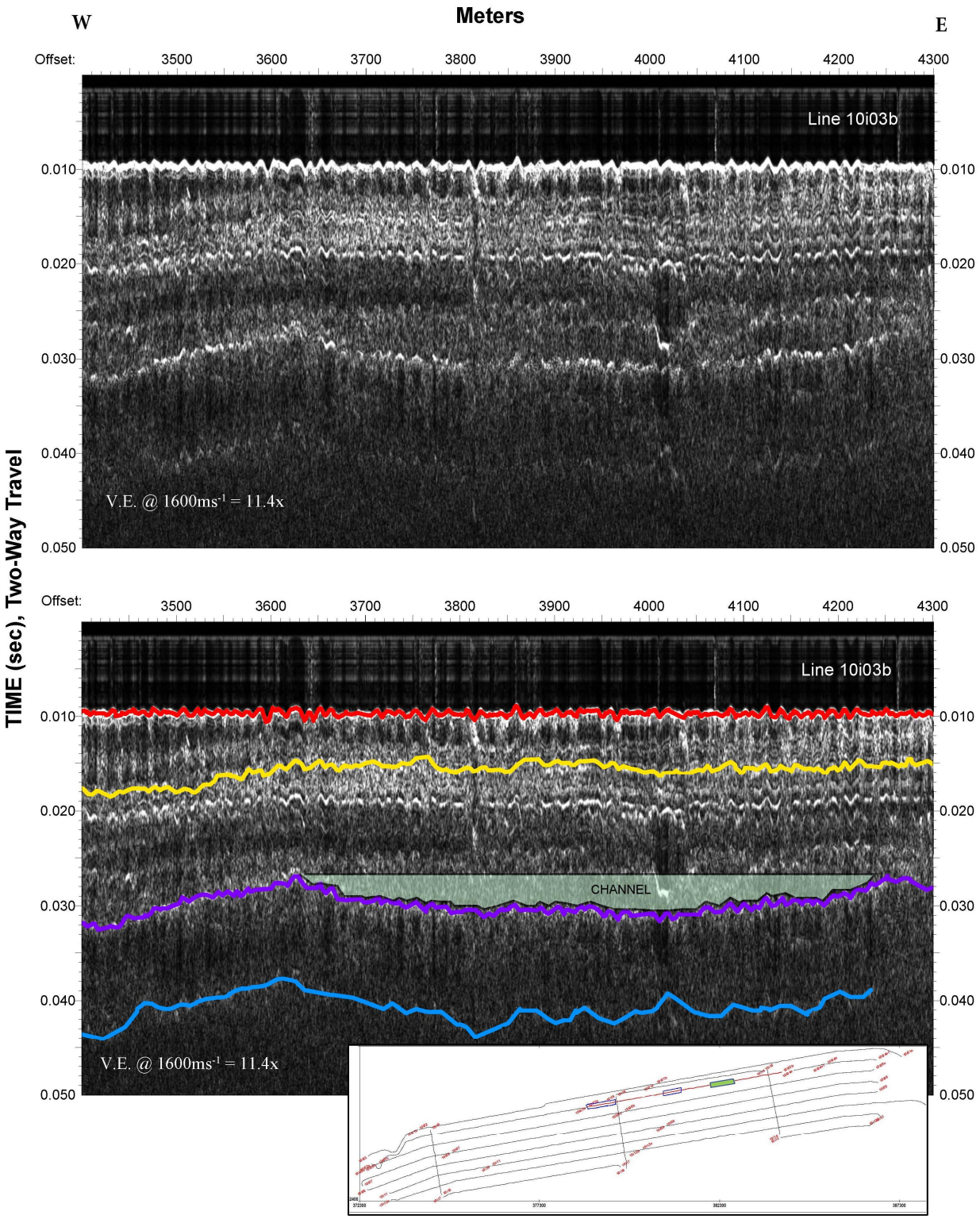

Figure 3.19 A channel is seen along Horizon P in this line segment of 10i03b. The channel is 2.3 m deep and 616.9 m wide with a 0.7° western and eastern slope.

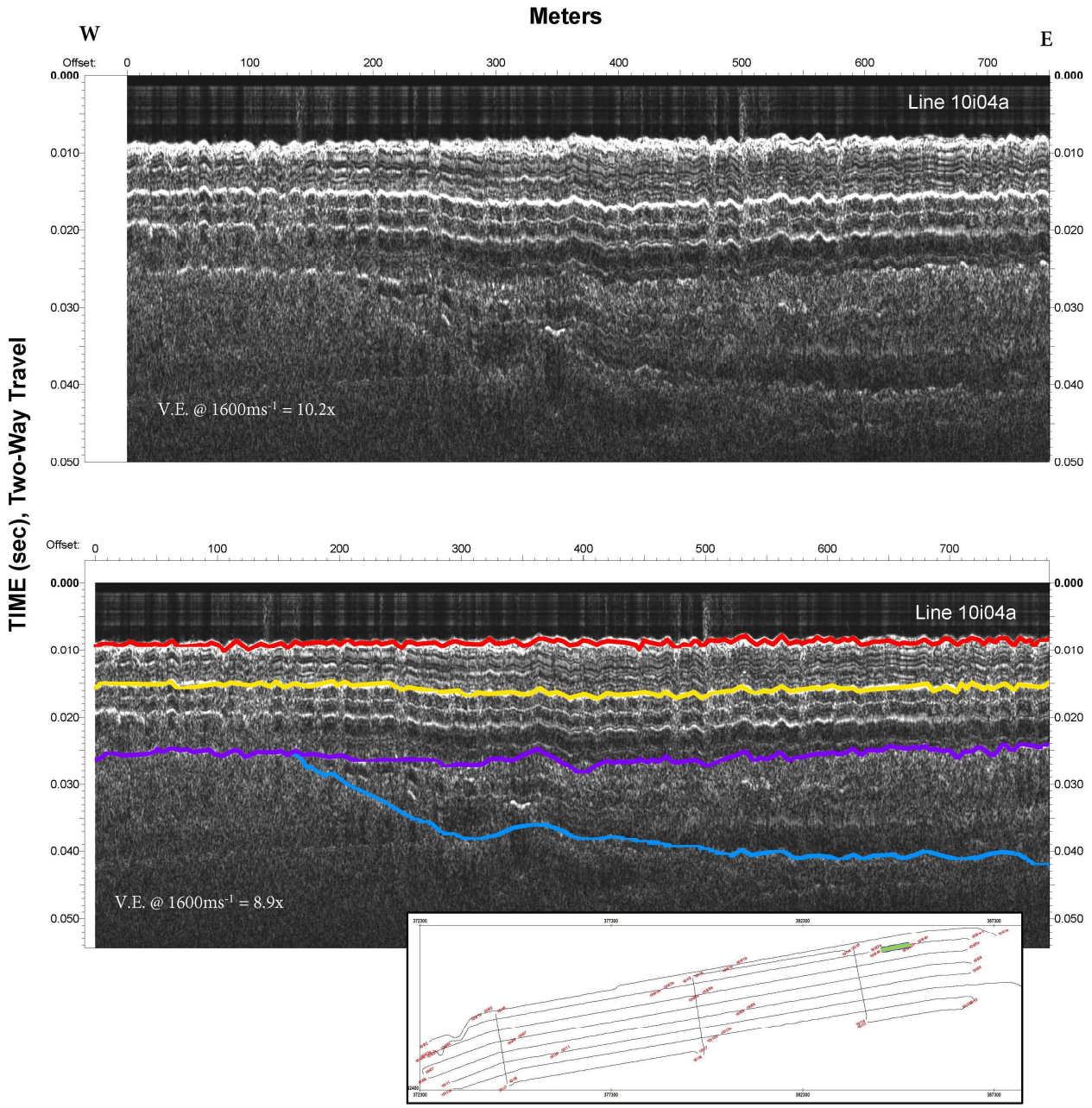

Figure 3.20 No channel structures were interpreted in this segment of line 10i04a. The interpretation of Horizon B consists of the horizon truncating into Horizon P with a 3.1° western slope.

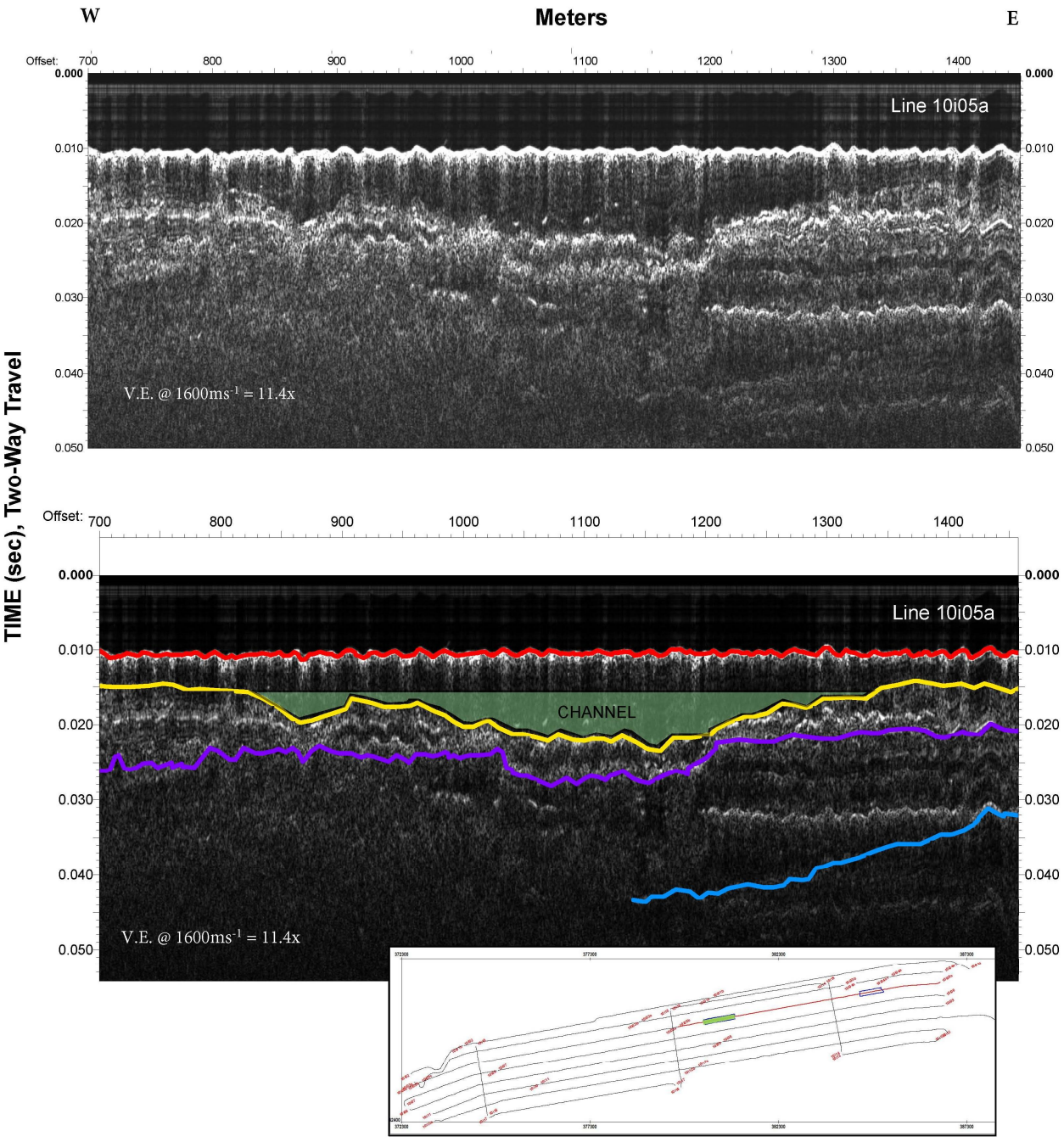

Figure 3.21 Channel structures are seen along Horizons A and P in this segment of line 10i05a. Horizon A includes a 4.8 m deep by 592.0 m wide channel with a 1.7° western slope and a 1.6° eastern slope. Horizon P consists of a channel-like structure beneath the deepest point of Horizon A. The Horizon B interpretation includes a 2.1° eastern slope.

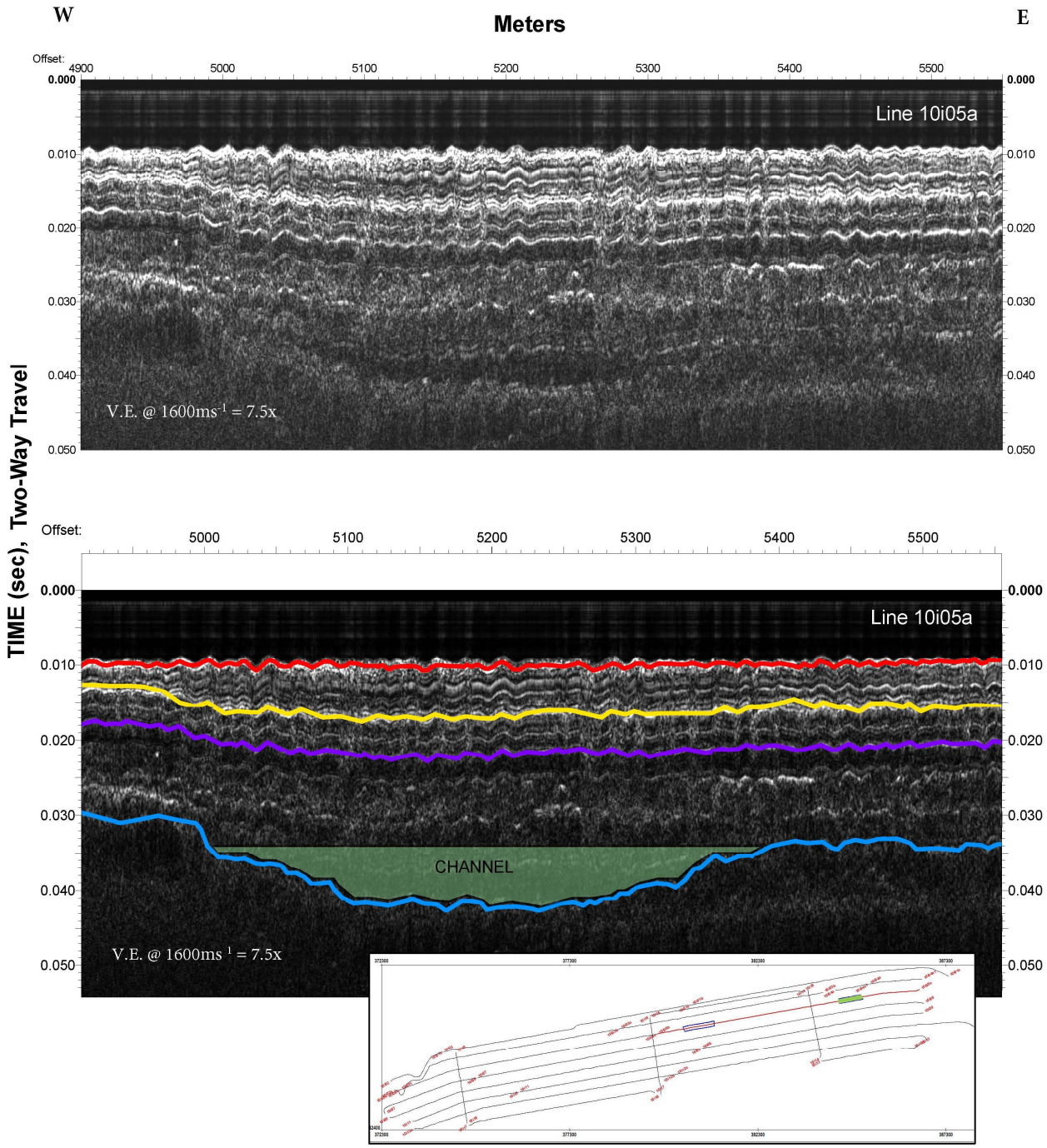

Figure 3.22 A channel structure is seen along Horizon B in this line segment of line 10i05a. The channel is 6.4 m deep and 400.2 m wide with a 3.7° western slope and a 2.4° eastern slope.

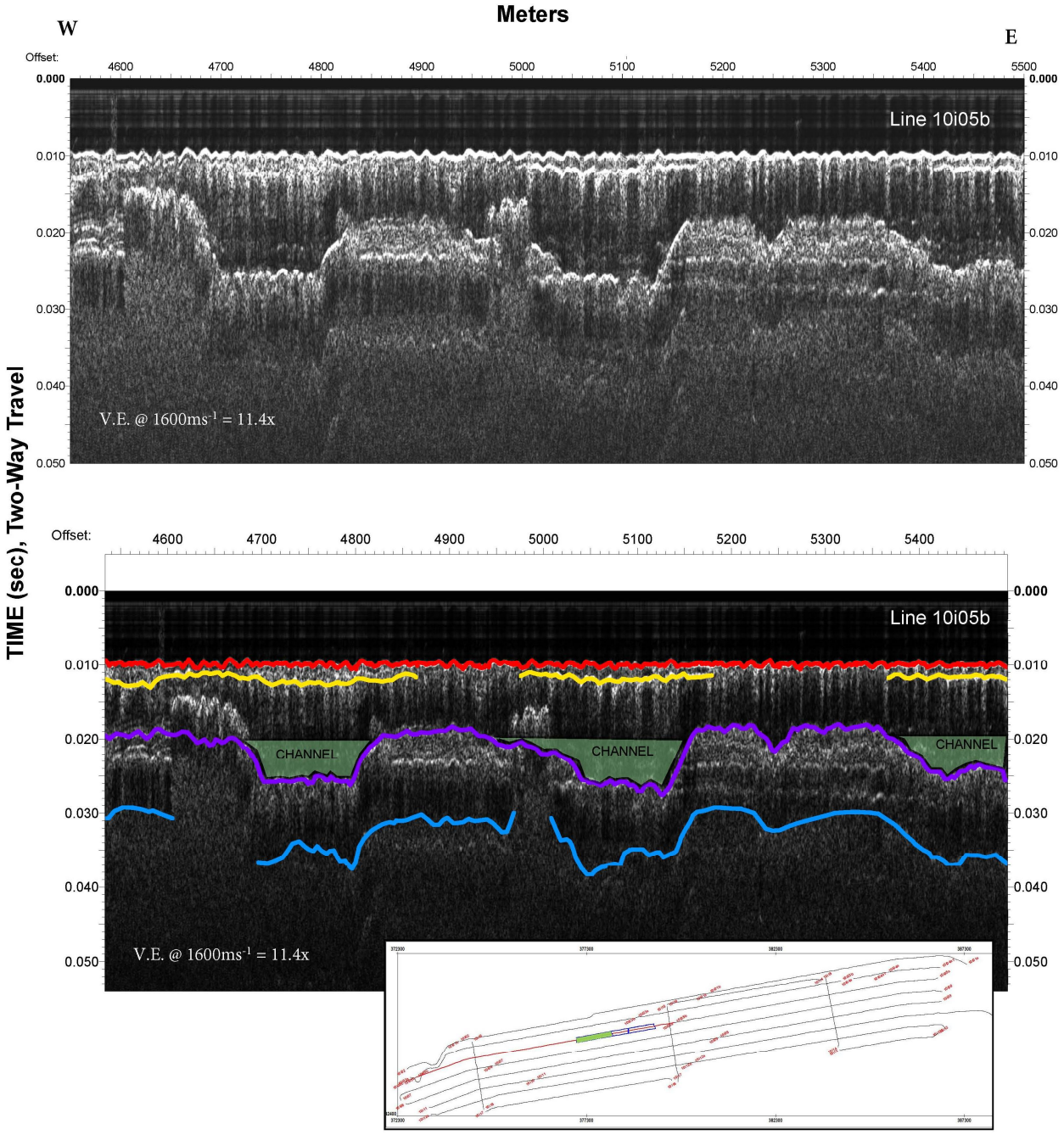

Figure 3.23 Multiple channel-like structures are interpreted within Horizon P in this line segment of 10i05b. Looking west to east, the first channel is 4 m deep by 177.2 m wide with 15.9° western and eastern slopes. The second channel is 4.8 m deep by 196.4 m wide with a 2.7° western slope and a 9.4° eastern slope. The third (far east) channel (continues into Figure 3.24) is 4 m deep with a western 4.0° slope in this profile segment.

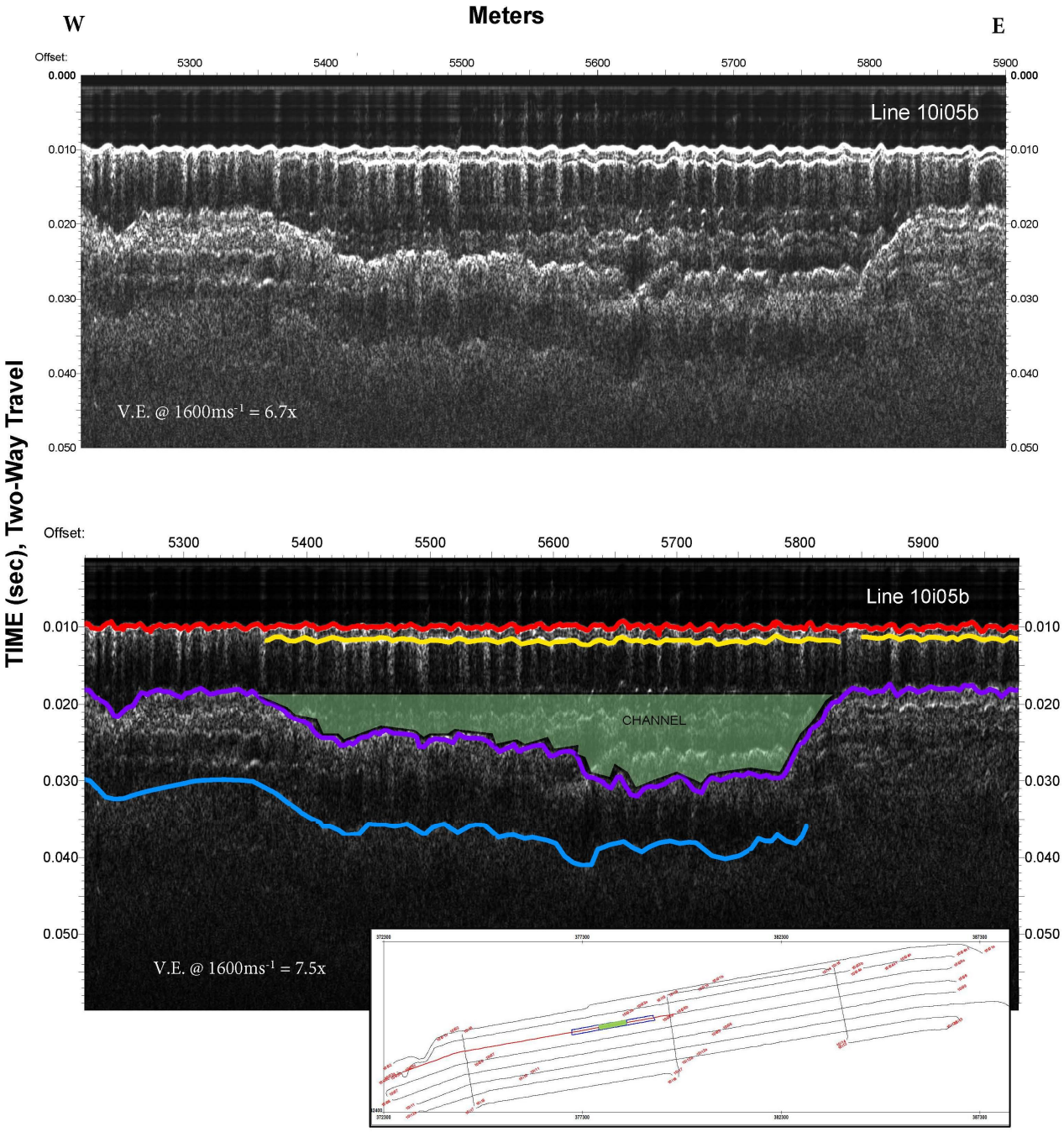

Figure 3.24 The channel structure seen in this line segment of line 10i05b extends from Figure 3.23. The Horizon P interpretation consists of a structure that is 9.9 m deep by 500.6 m wide with a western 2.1° slope and a 12.7° eastern slope.

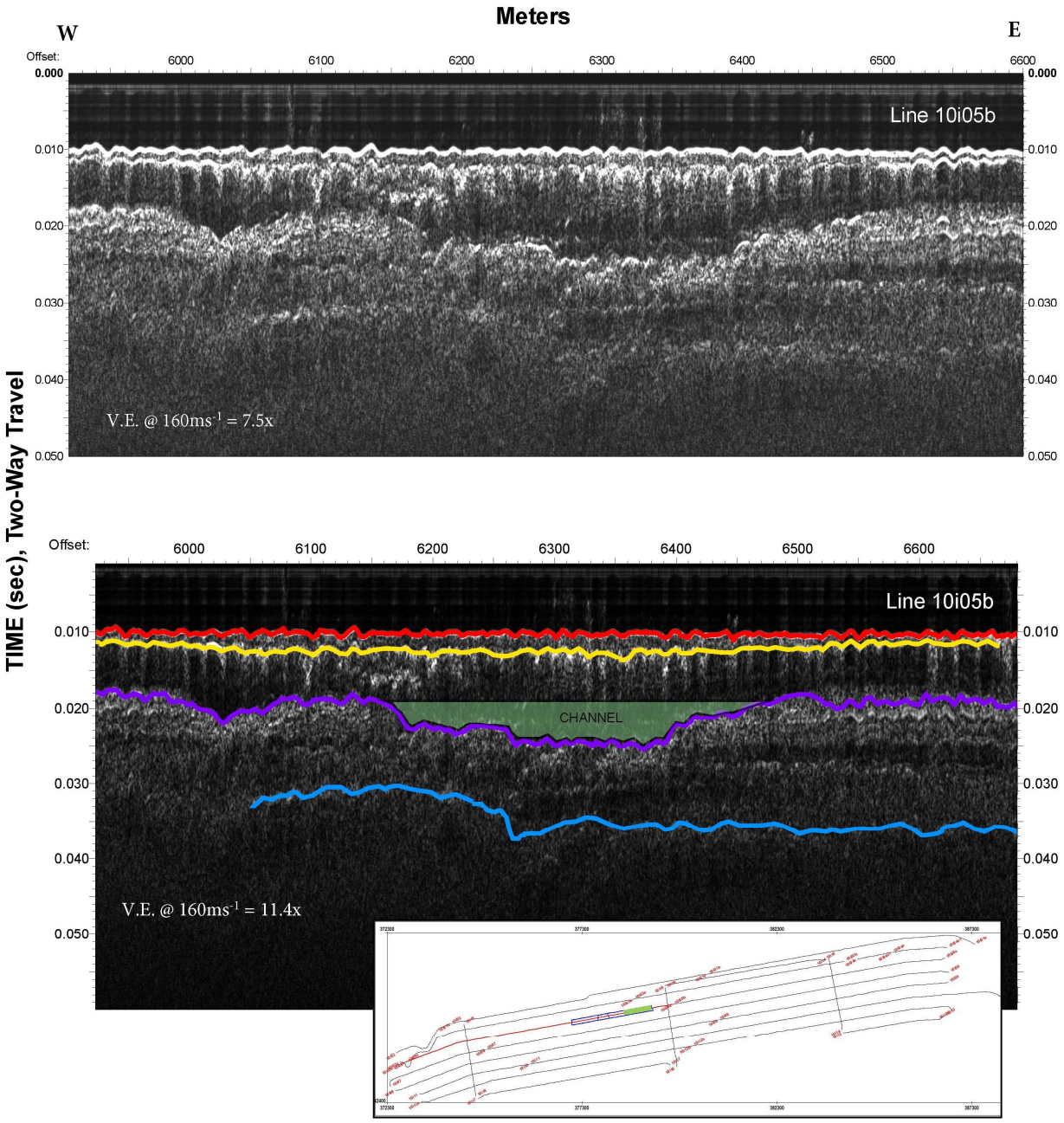

Figure 3.25 This interpretation of Horizon P, in this line segment of 10i05b, includes a 4 m deep by 370.0 m wide channel-like structure with a 1.8° western and a 2.3° eastern slope in this most eastern section of line 10i05b.

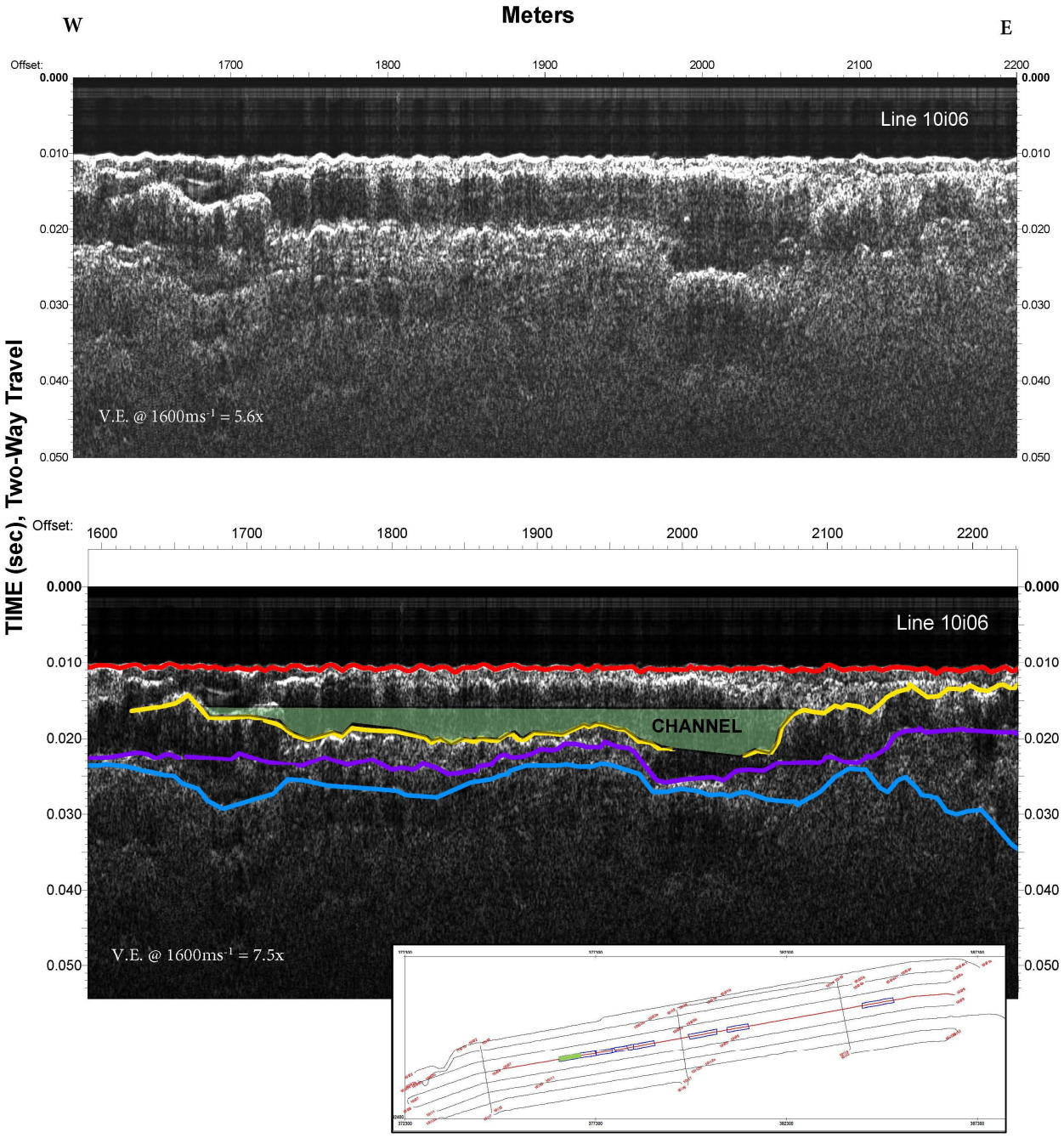

Figure 3.26 In this line segment of line 10i06, the interpretation of Horizon A is a channel-like structure that ranges from 3.2 m to 4.8 m in depth and is 411.8 m wide with a 1.2° western and 13.5° eastern slope.

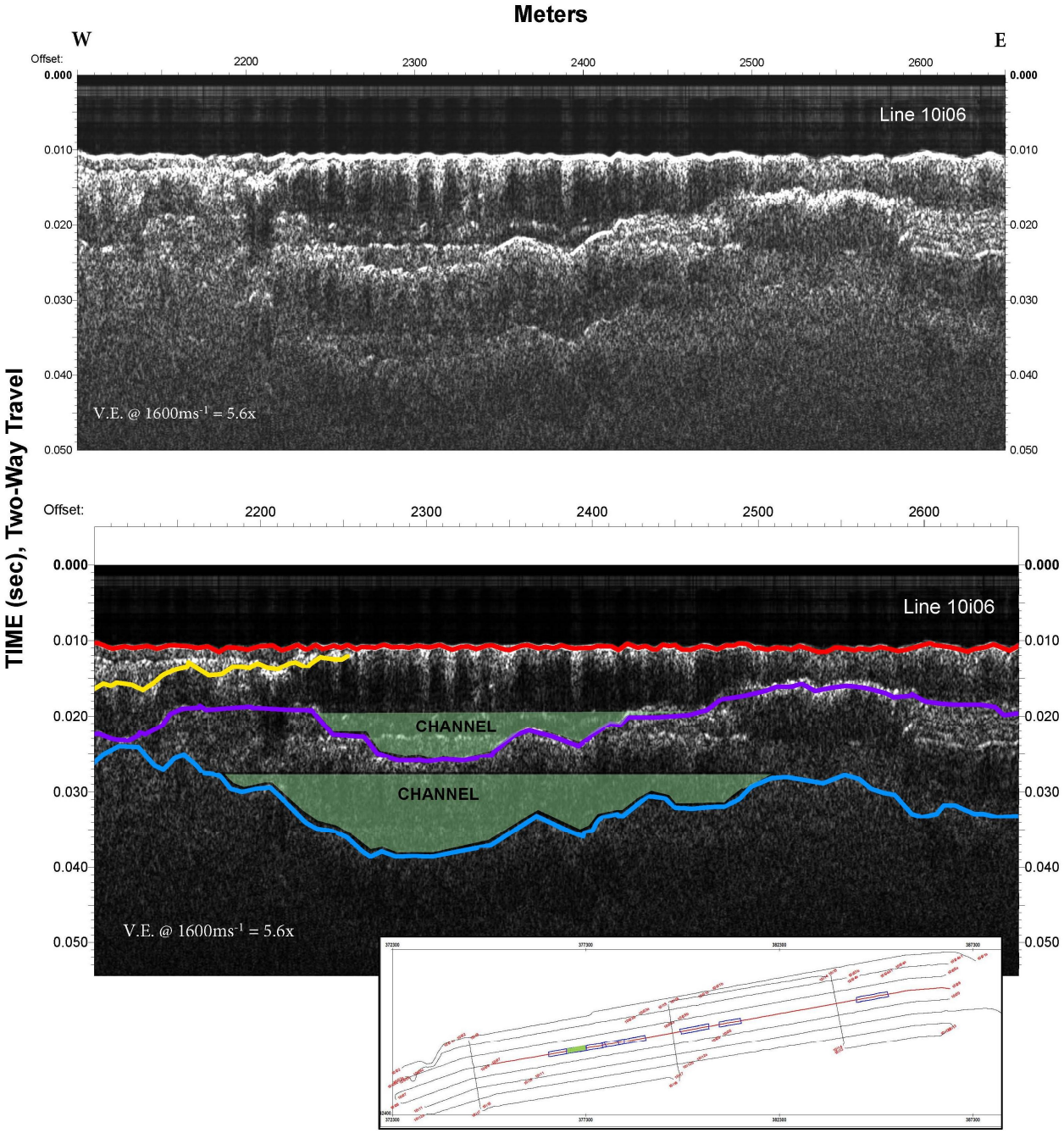

Figure 3.27 Channel structures were interpreted along Horizons P and B in this segment of line 10i06. Horizon P includes a 5.4 m deep by 241.8 m wide channel-like structure with a 7.3° western slope and an eastern 2.5° slope. Horizon B includes a 9 m deep by 280.3 m wide channel-like structure with a 6.2° western slope and a 2.6° eastern slope.

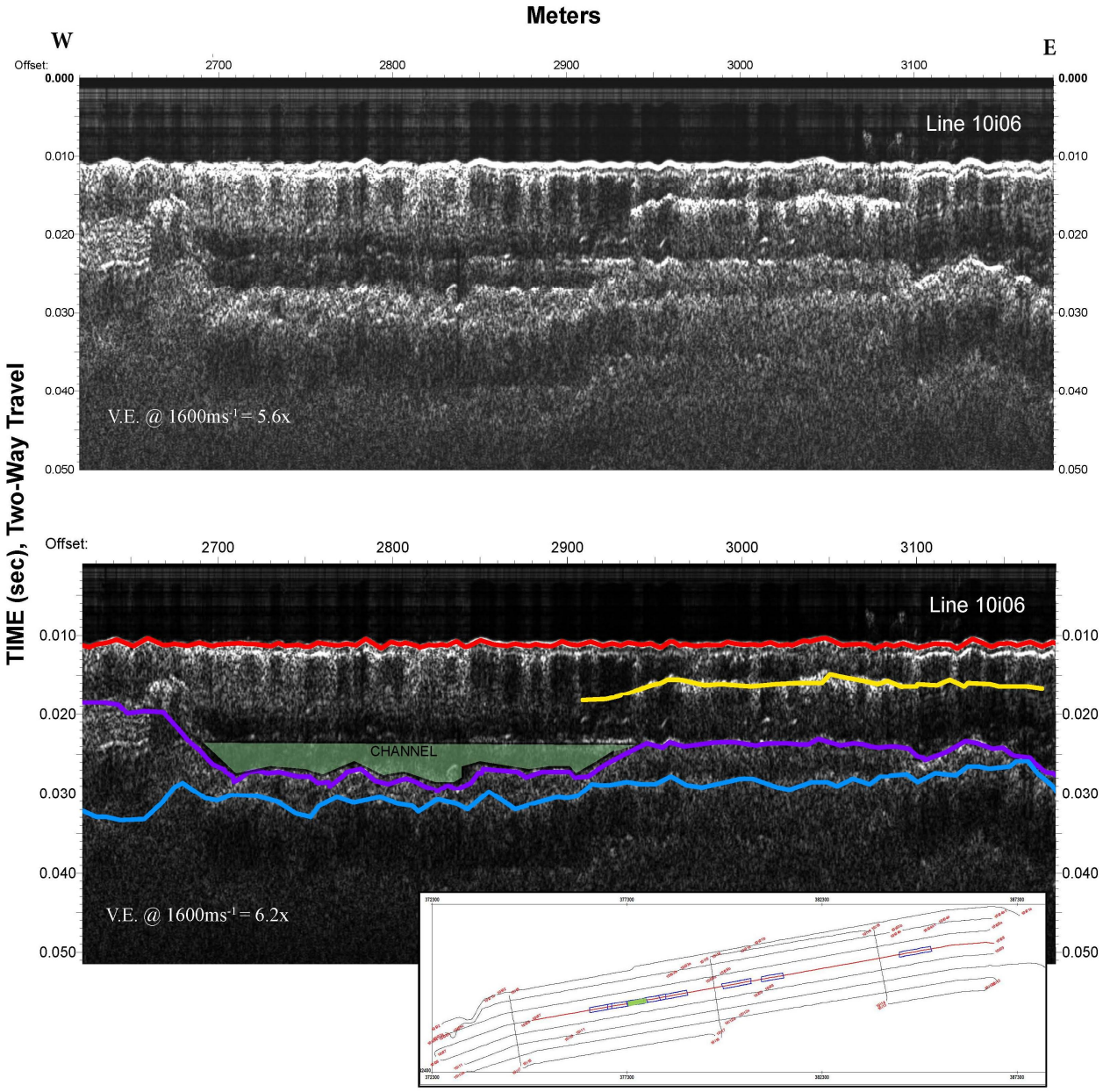

Figure 3.28 This segment of line 10i06 displays a channel structure along Horizon P. The structure is interpreted as a 4 m deep by 267.0 m wide channel structure with a 13.2° western and a 2.3° eastern slope.

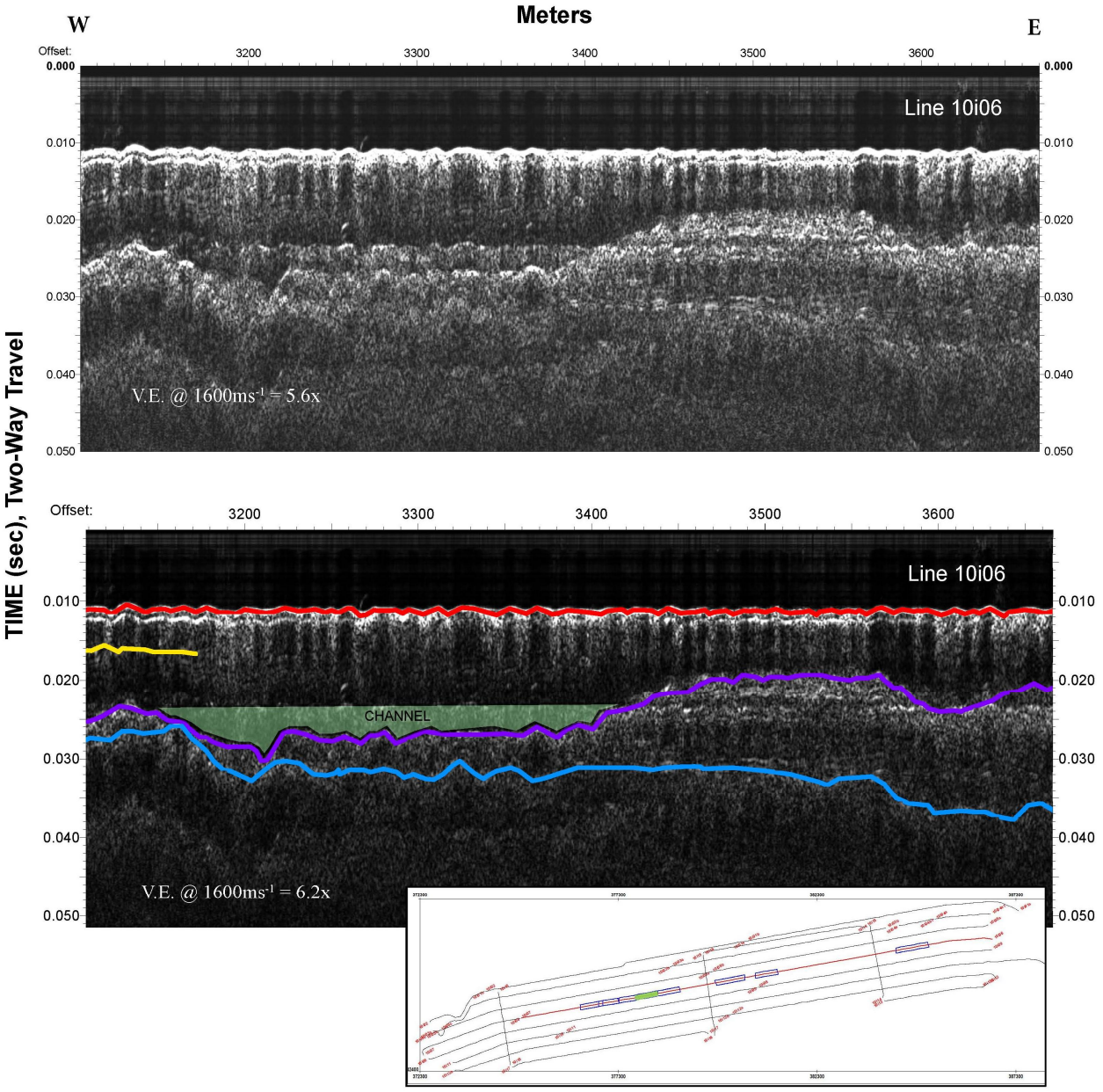

Figure 3.29 A channel structure is seen along Horizon P in this line segment of line 10i06. The structure is a 3.6 m deep by 297.9 m wide channel with a western 3.6° slope and an eastern 4.9° slope.

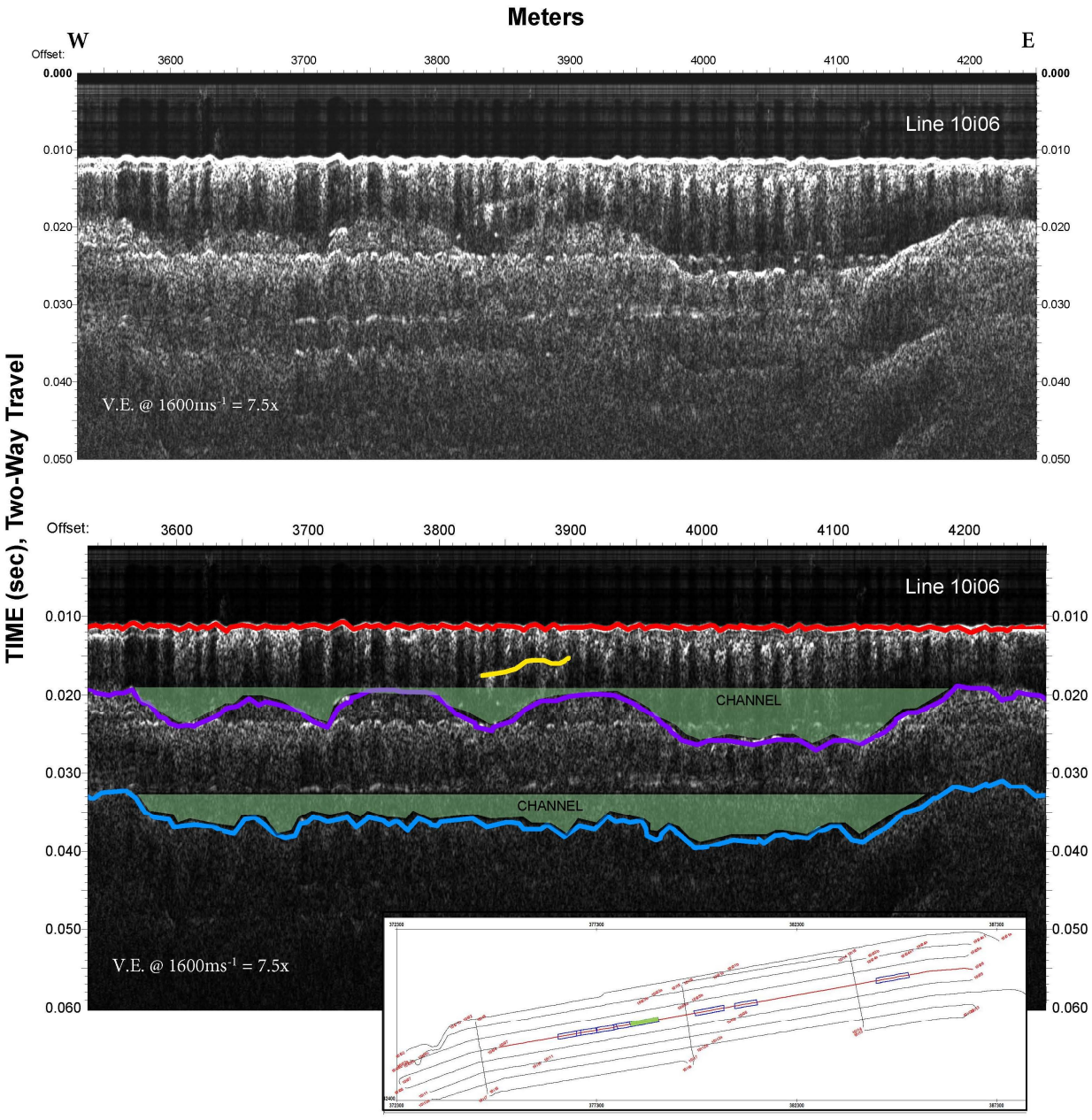

Figure 3.30 Channel structures are seen along each of Horizon P and B in this line segment of line 10i06. Horizon P includes multiple channel structures that range from 3.2 m to 4.8 m deep in total are 628.4 m wide. The largest channel (farthest east) has a 5.0° western and a 3.6° eastern slope. Horizon B consists of a channel-like structure that ranges from 2.4 m to 4 m in depth and is 628.4 m wide with a western 1.2° and a 4.2° eastern slope.

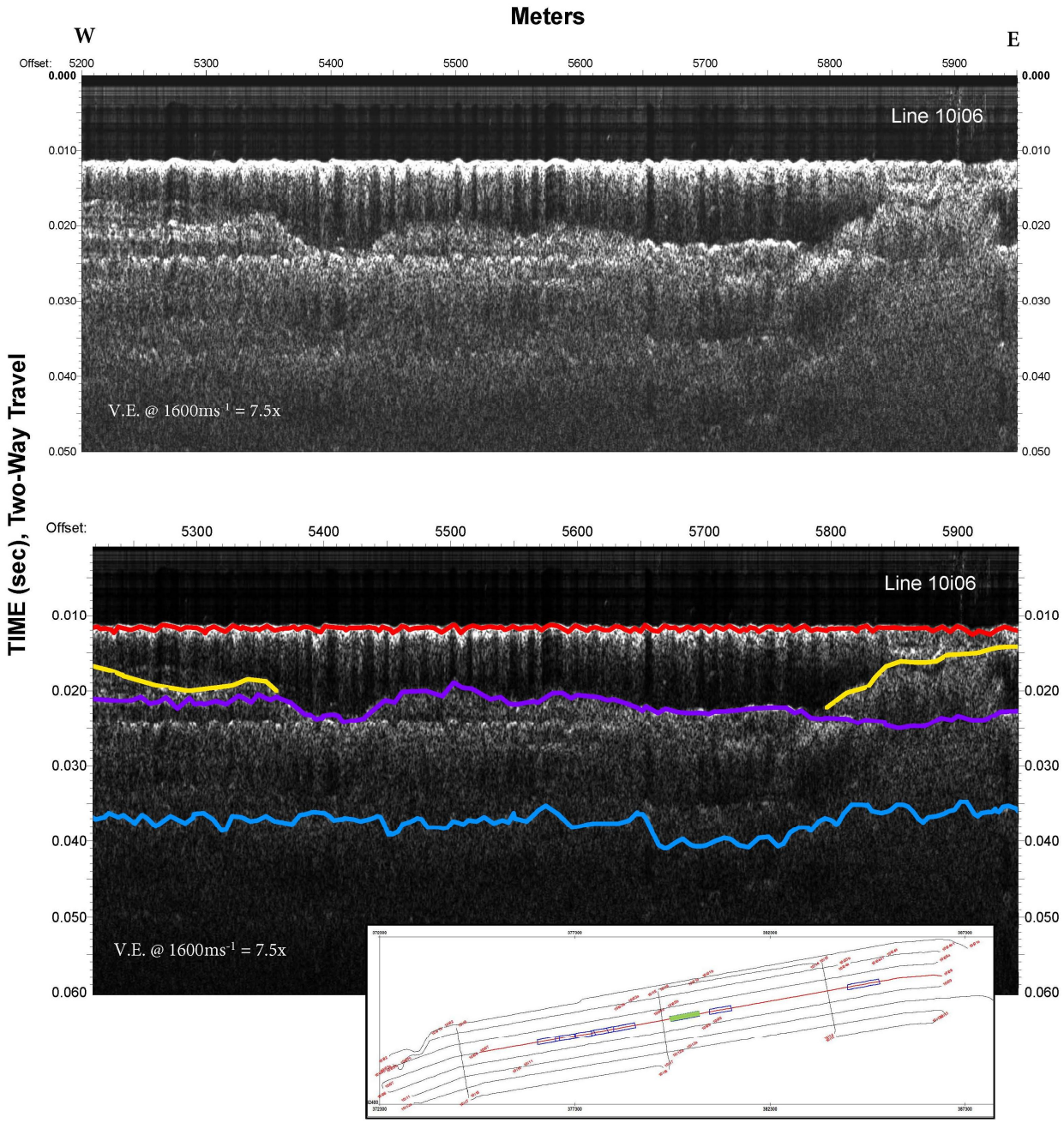

Figure 3.31 No channel structures were seen in this section of line 10i06, except a structure along Horizon A. This interpretation of Horizon A shows that it truncates southward into Horizon P. It has a western 2.4° slope and an eastern 3.8° slope. The truncation creates a feature that is 517.6 m wide.

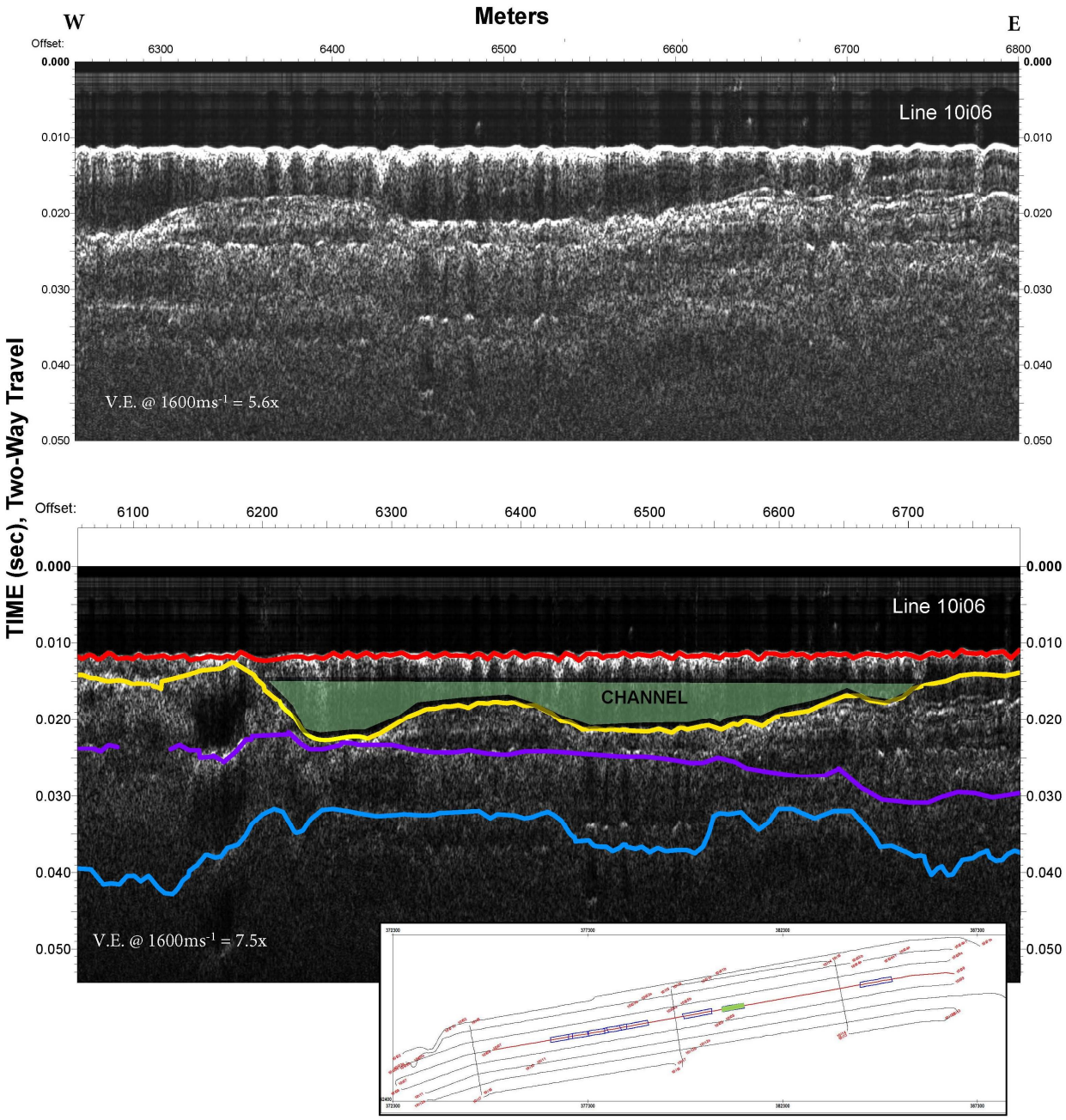

Figure 3.32 This segment of line 10i06 shows an interpretation of Horizon A consisting of a channel-like structure ranging from 5.6 m to 4.4 m deep and 512.1 m wide. The Horizon B interpretation includes a western dip of 7.1°.

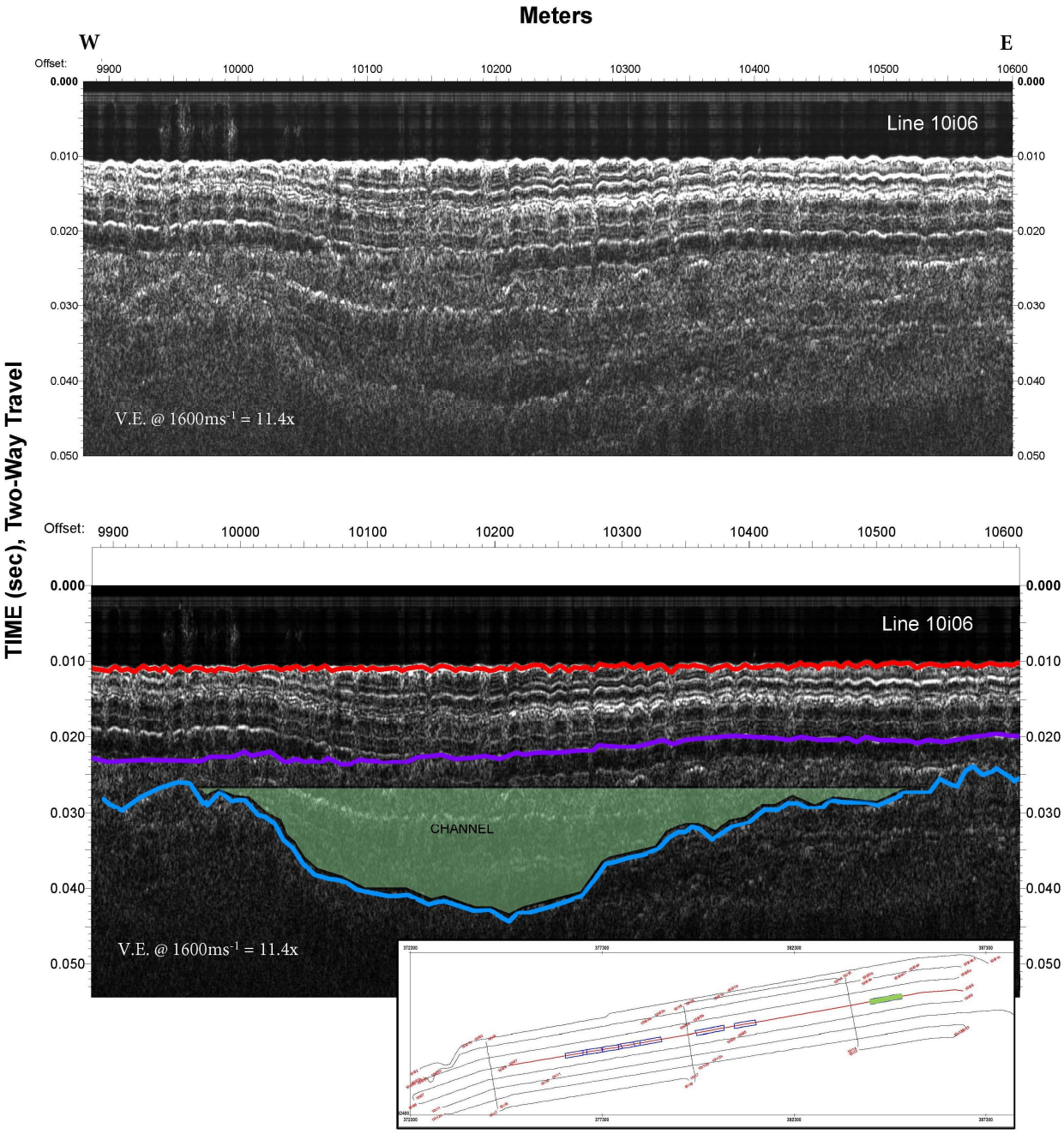

Figure 3.33 The Horizon B interpretation has a deep (12.8 m) channel-like structure that is 587.1 m wide in this eastern segment of line 10i06. The channel has a 3.5° western and a 2.6° eastern slope. Multiple stacked strata are seen between the seafloor horizon and Horizon P. The interpretation of the strata consists of a slight dip above the channel in Horizon B.

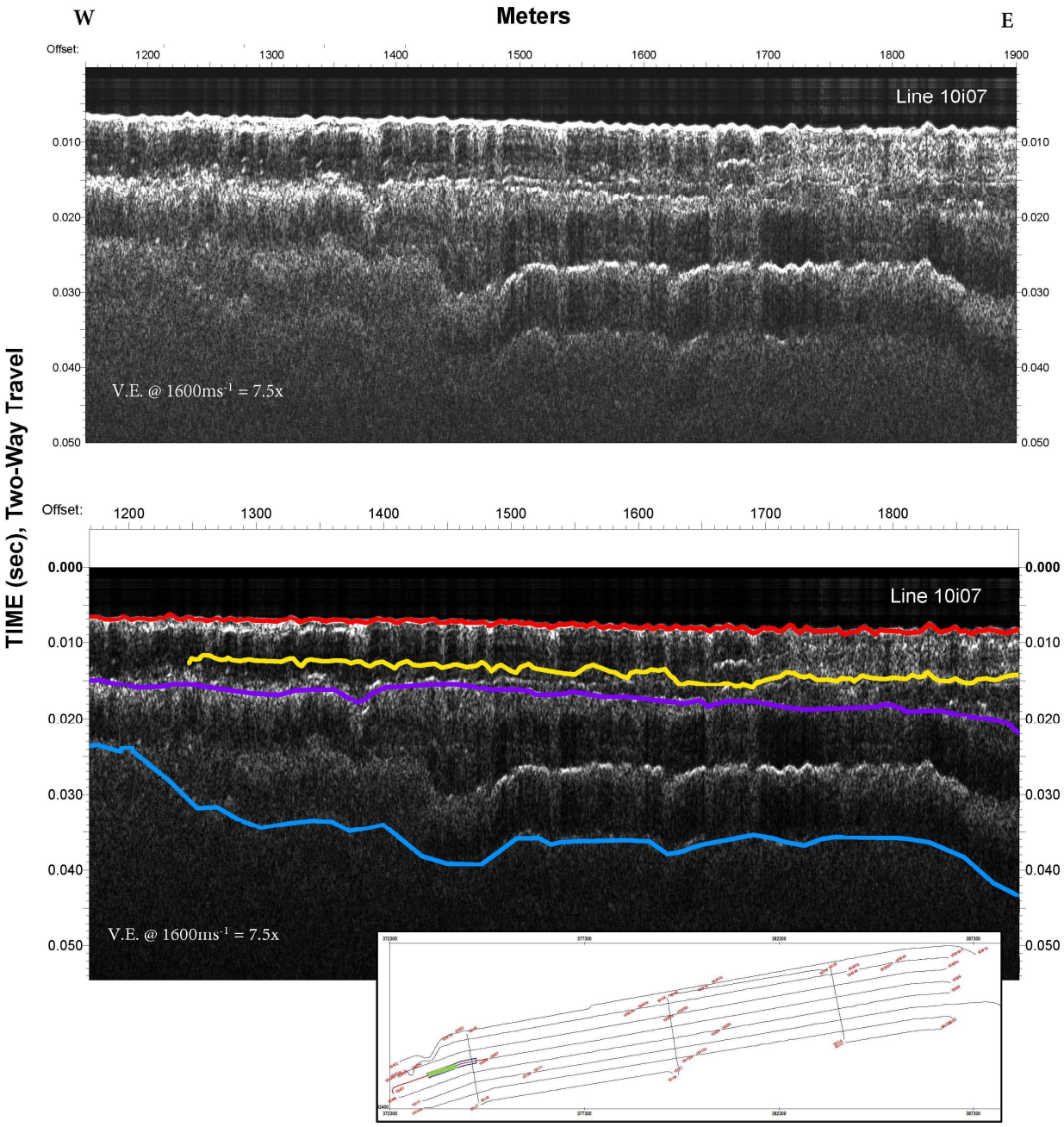

Figure 3.34 The interpretation of Horizon B in this segment of line 10i07 includes a decrease in elevation from the west to the east with a dip of 3.2°.

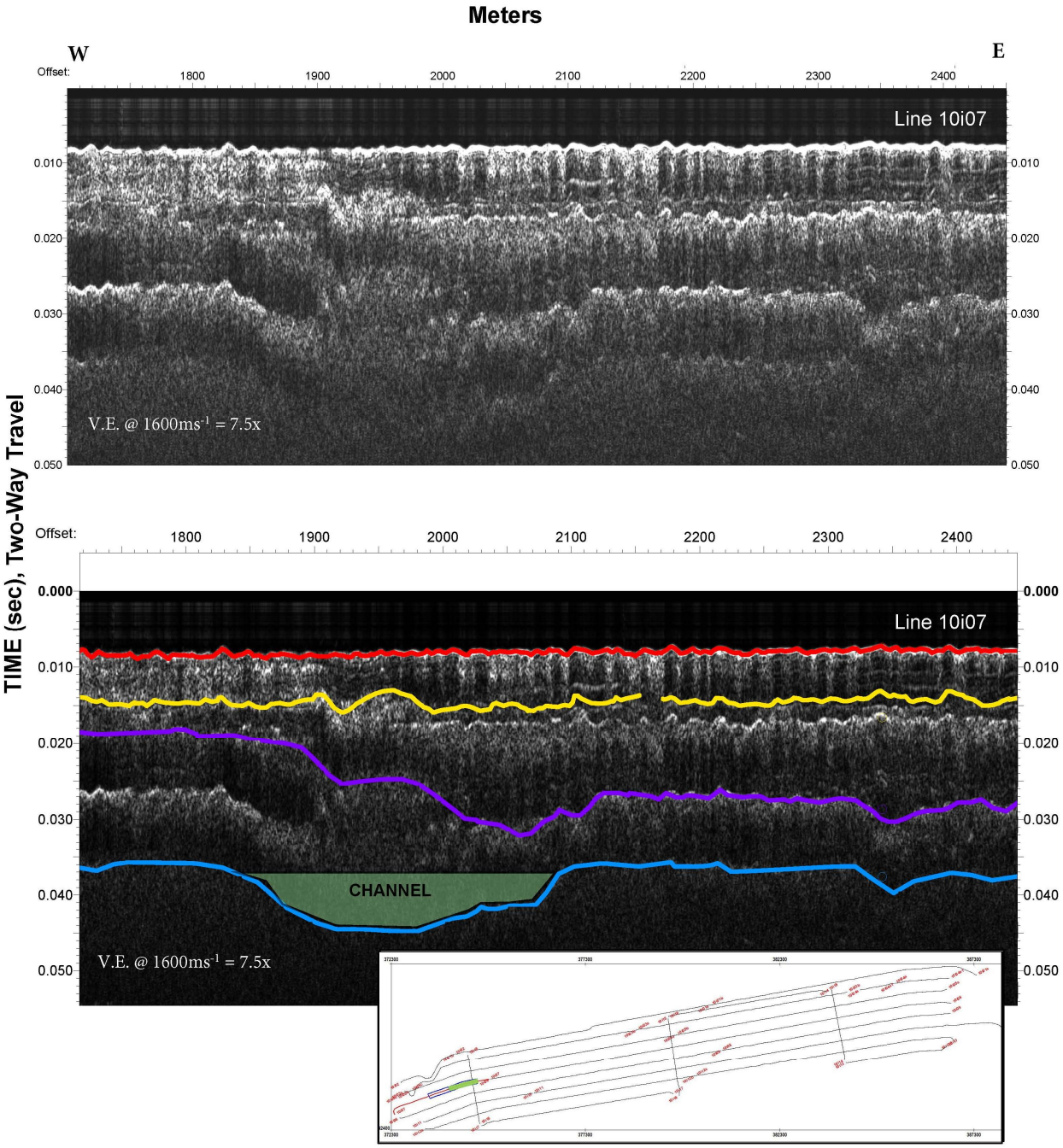

Figure 3.35 In this portion of line 10i07, the Horizon P interpretation includes an eastern dip with a slope of 3.1°. Horizon B consists of a 5.2 m deep by 267.9 m wide channel-like structure with a western 4.5° and an eastern 2.7° slope.

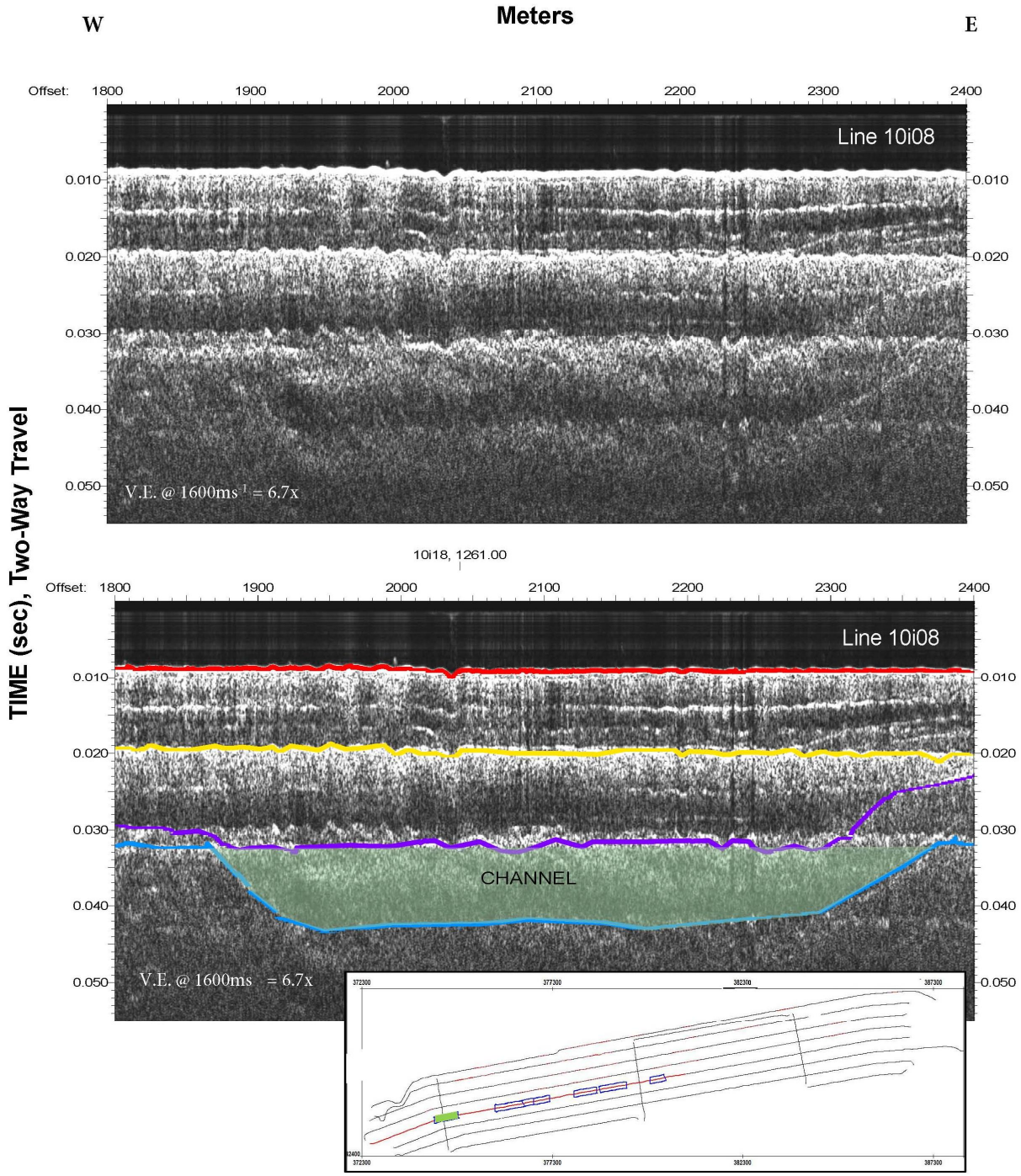

Figure 3.36 A channel-like structure is seen along Horizon B that is 513.2 m wide by 8.8 m deep with a 6.3 ° western slope and 3.1° eastern slope in this portion of line 10i08.

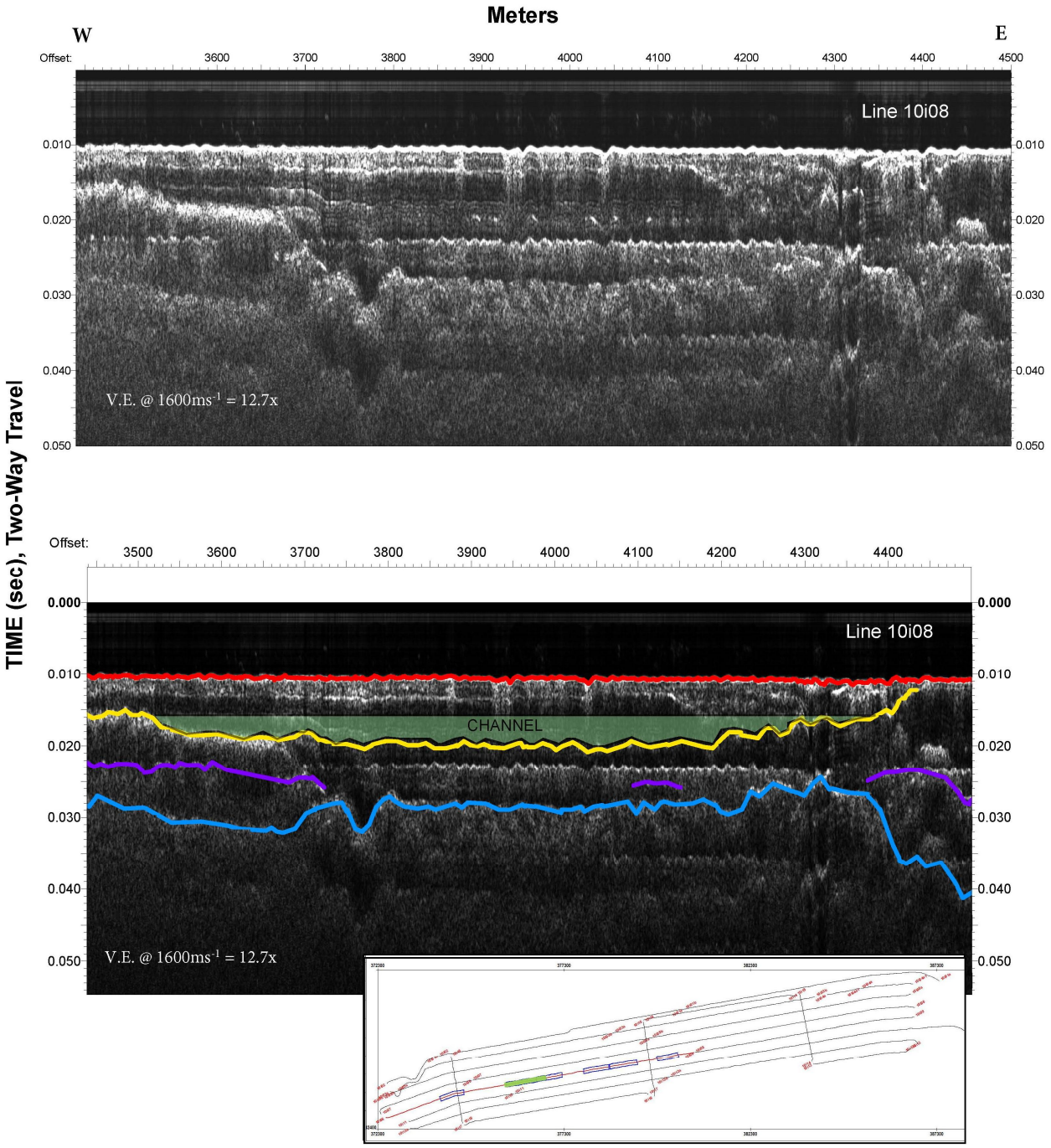

Figure 3.37 Horizon A in this segment of line 10i08 is interpreted to have a shallow (3.2 m) and wide (901.7 m) channel-like structure with a 0.8° western and 0.9° eastern slopes. Horizon B includes a steep 7.3° dip to the east.

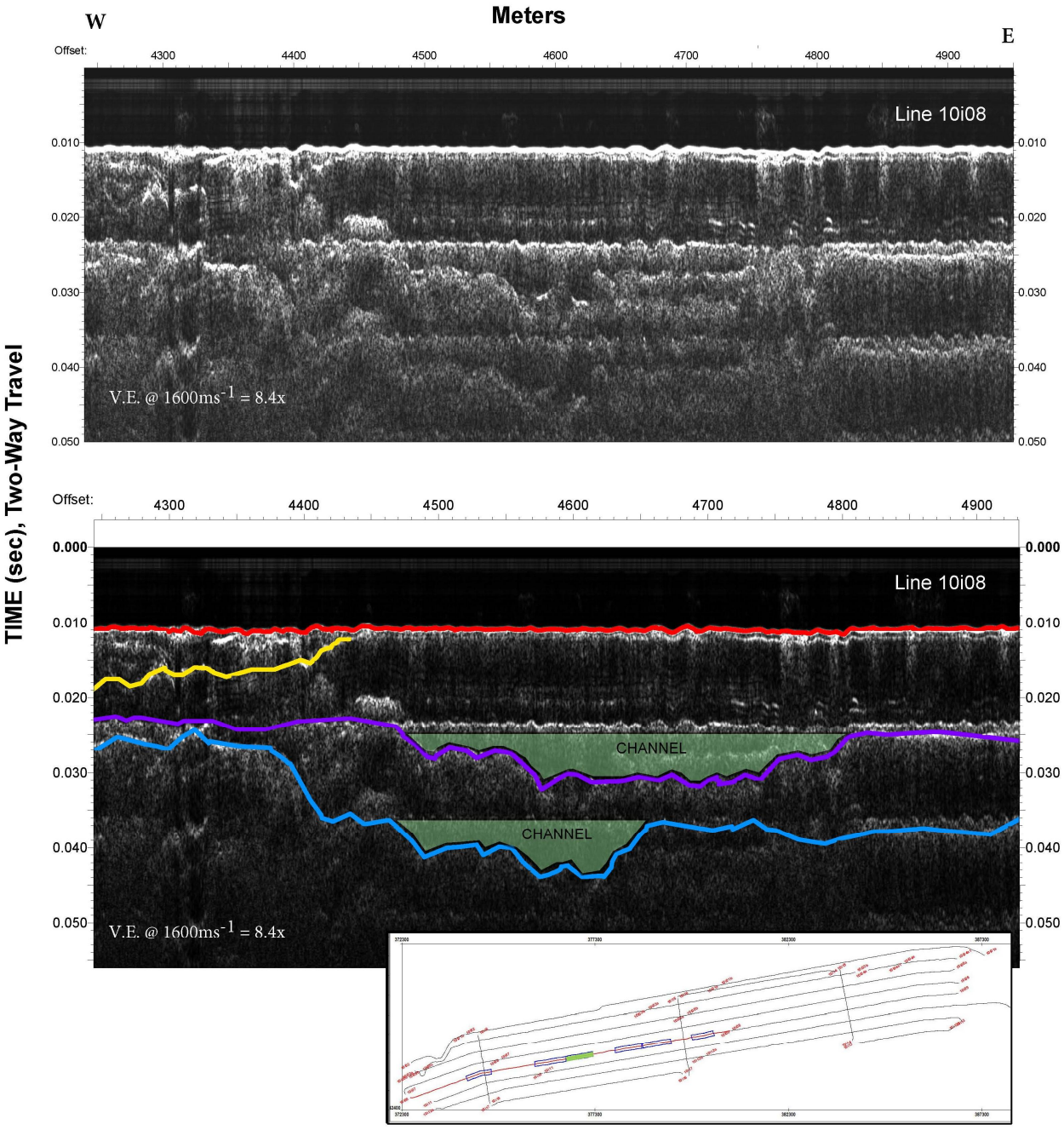

Figure 3.38 Two channel structures are seen along this segment of line 10i08 in each of Horizon P and B. Horizon P includes a 4.0 m deep by 351.1 m wide channel-like structure with a 2.3° western and 3.5° eastern slope. Horizon B includes of a channel-like structure that is 5.6 m deep by 212.8 m wide with a 3.2° western and a 9.6° eastern slope.

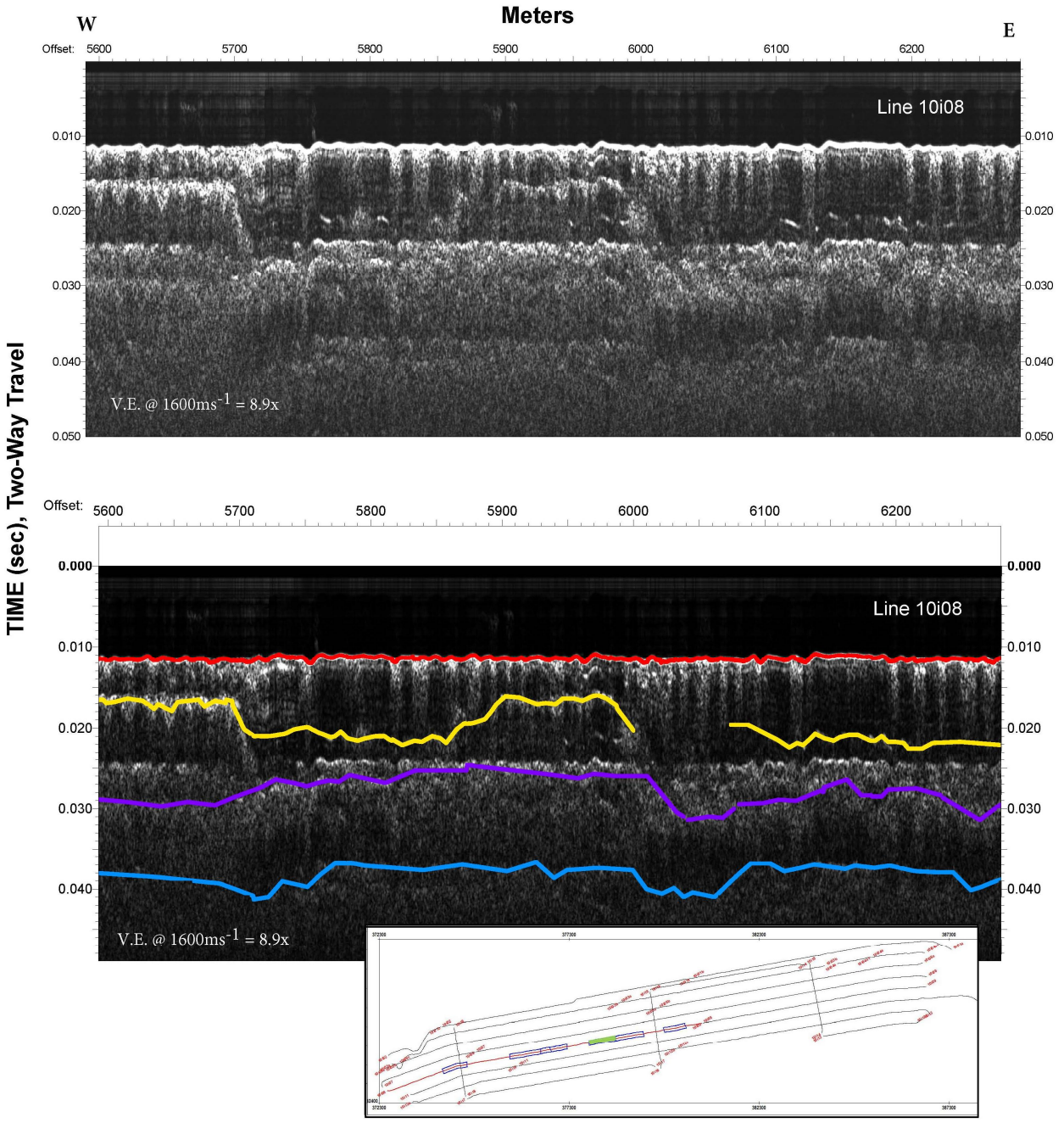

Figure 3.39 The Horizon A interpretation includes a channel-like structure that is 3.6 m deep by 372.4 m wide in this segment of line 10i8. Horizon P and B mimic one another as horizontal surfaces with minimal dips.

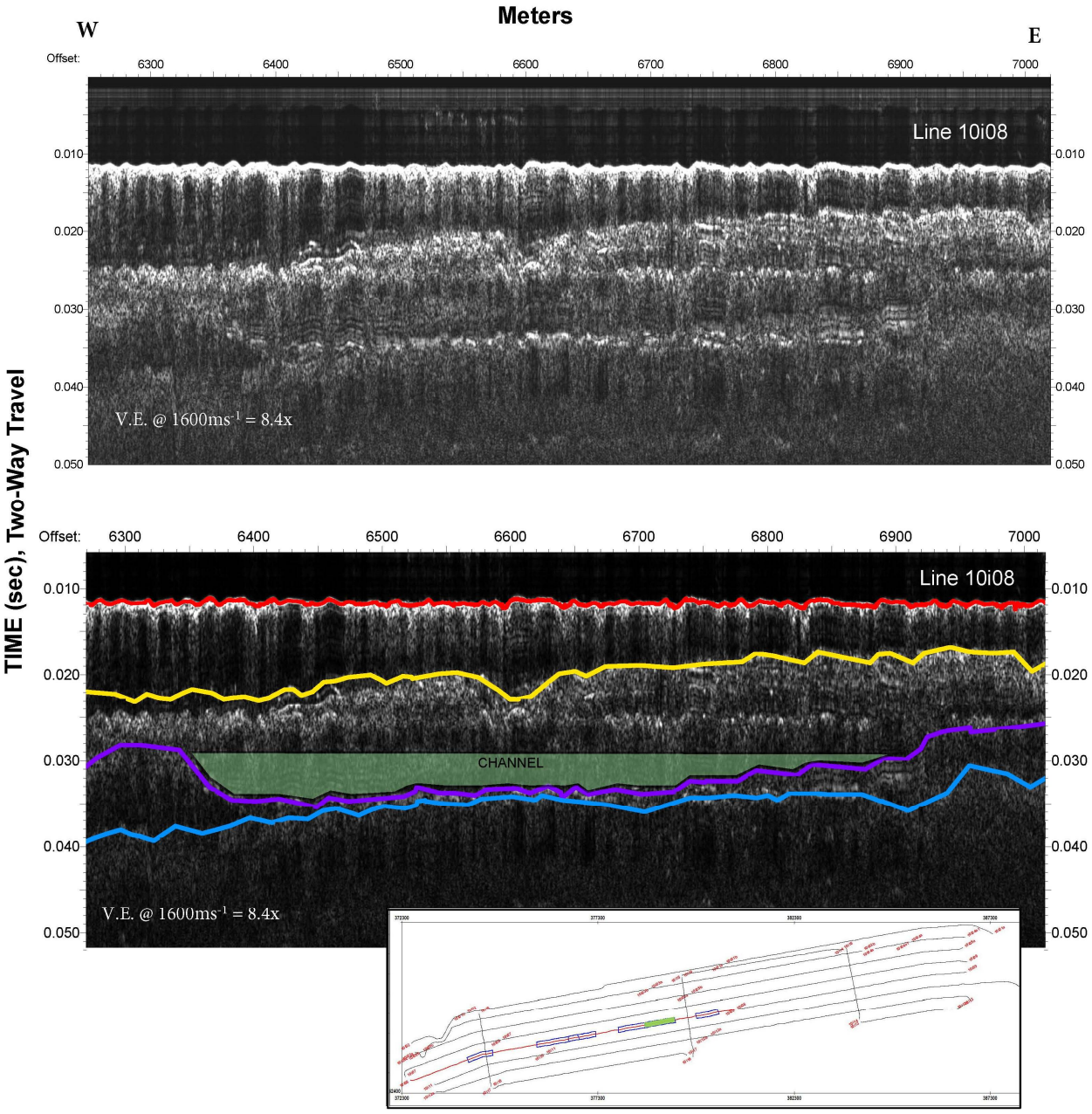

Figure 3.40 The interpretation of this segment of line 10i08 Horizons A and B includes a slope upwards to the east. Horizon A and B consist of a 0.7° eastern slope. Horizon P interpretation includes a channel-like structure that varies in depth from 4.4 m to 0.8 m and is 584.3 m wide. The channel structure has a 7.6° western and a 1.4° eastern slope.

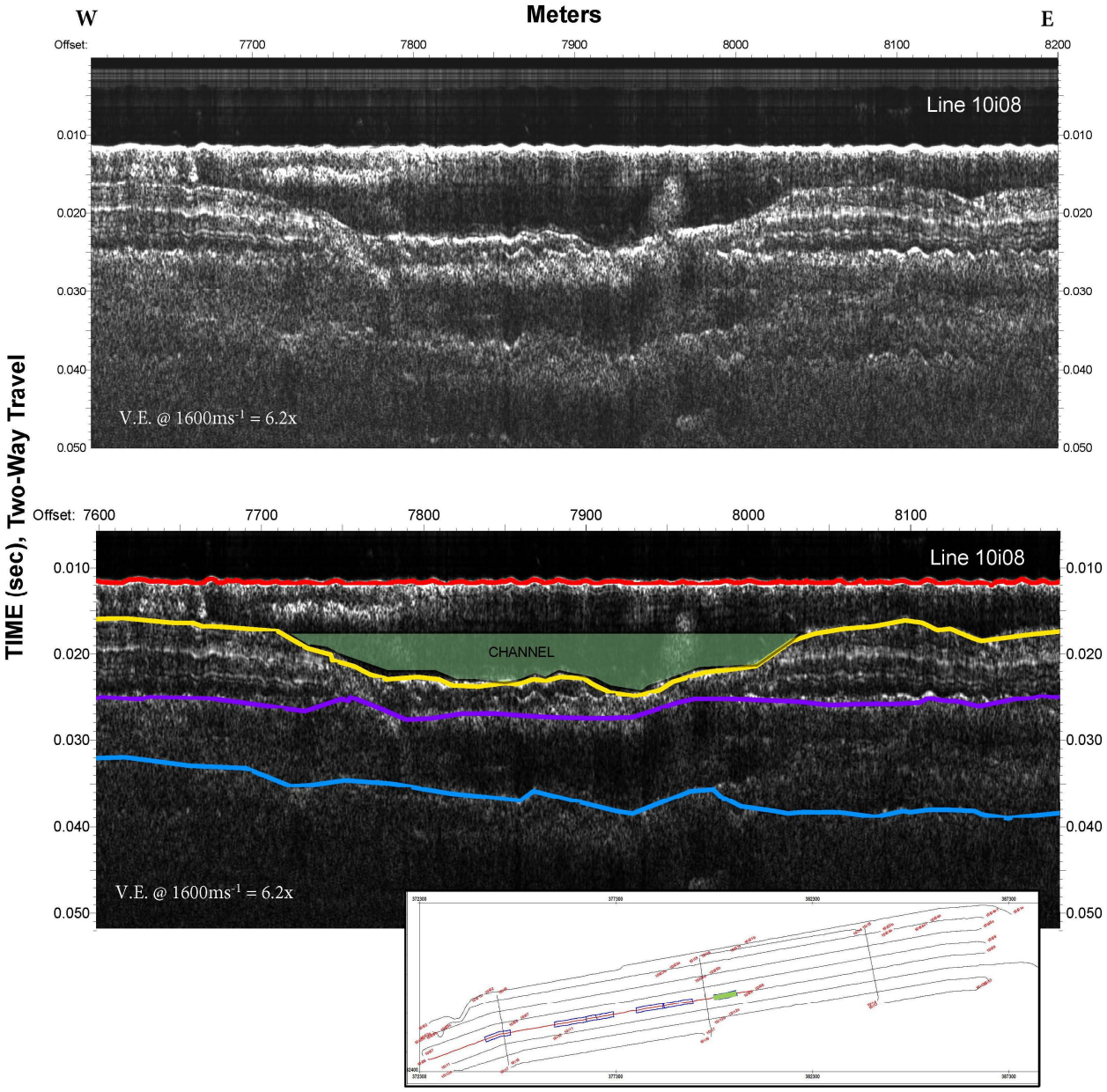

Figure 3.41 A structure is seen along Horizon A of this segment of line 10i08 that is a 4.5 m deep by 317.8 m wide channel-like structure with a western a 2.6° slope and an eastern slope of 2.8° .

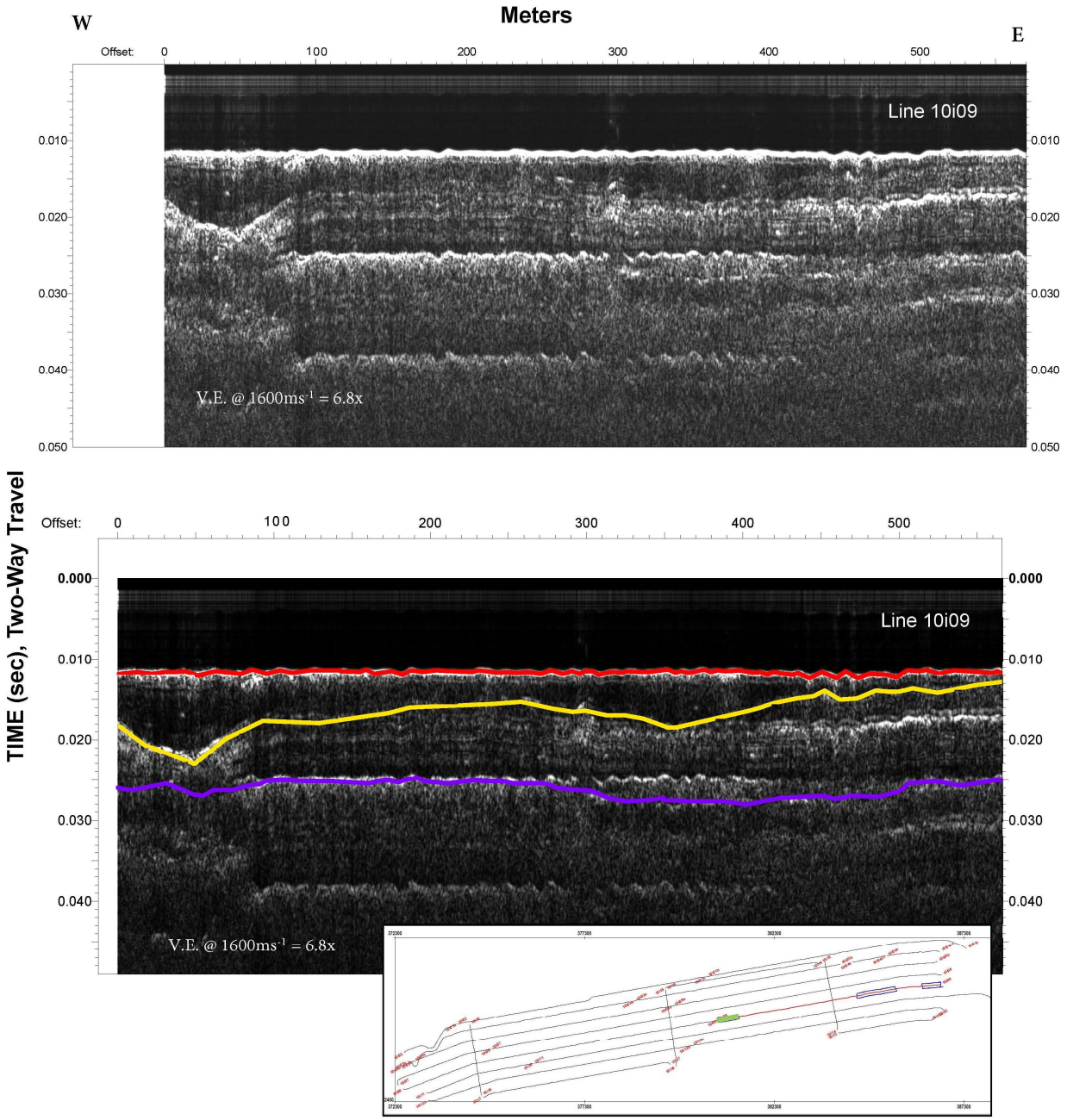

Figure 3.42 The Horizon A interpretation consists of a potential channel-like structure with an eastern slope of 1.5° in this western segment of line 10i09.

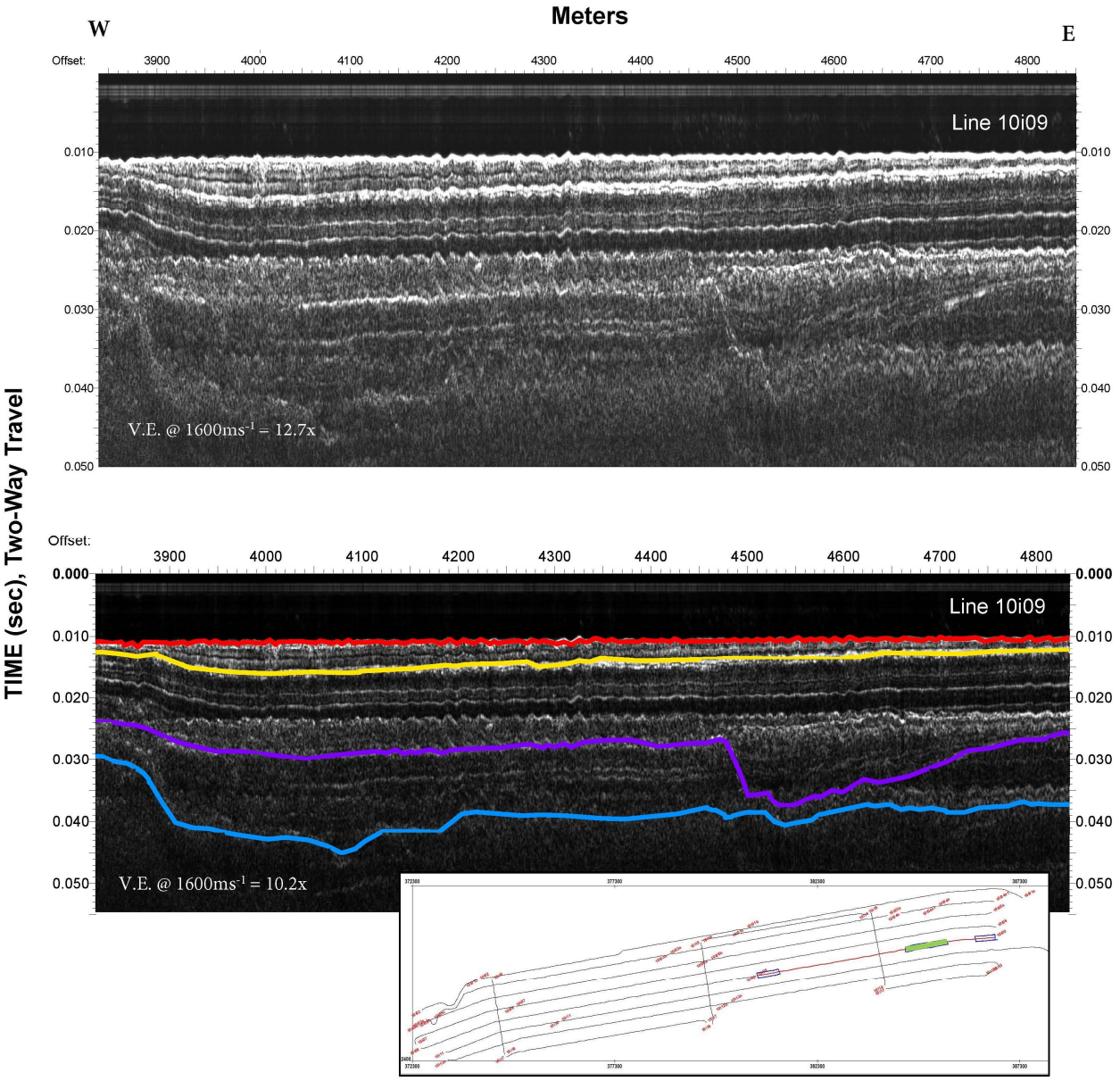

Figure 3.43 The interpretation of this segment of line 10i09 shows a western slope of 10.6° along Horizon A. Horizon P includes a western slope of 1.9° and a channel-like structure that is 8 m deep by 573 m wide with a western 6.8° slope and an eastern 1.6° slope. Along Horizon B a 6.8° western slope is seen.

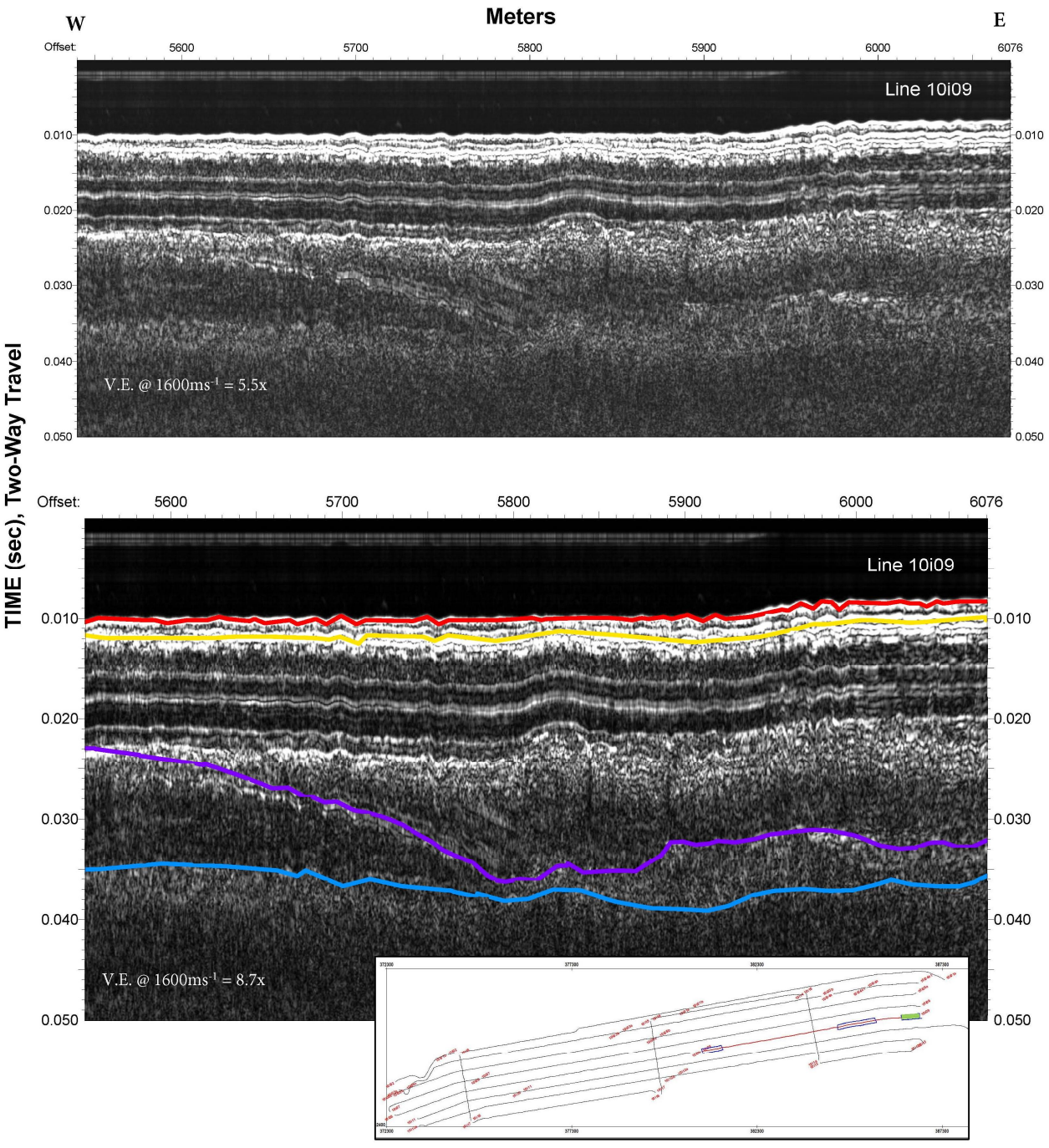

Figure 3.44 A 2.4° western slope is seen along Horizon P in this eastern segment of line 10i09.

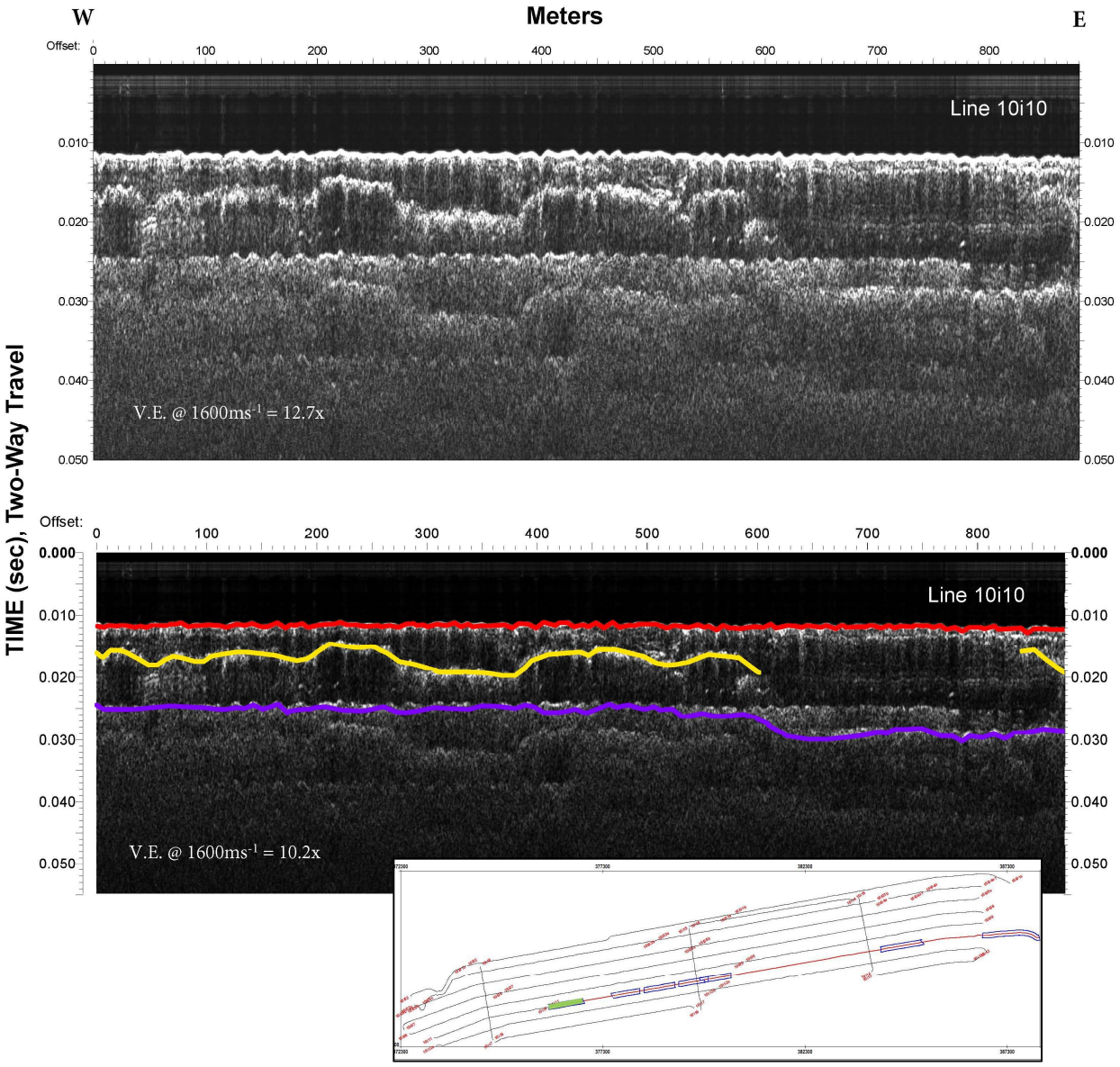

Figure 3.45 Intermittent high and low elevations are seen along Horizon A in this portion of line 10i10.

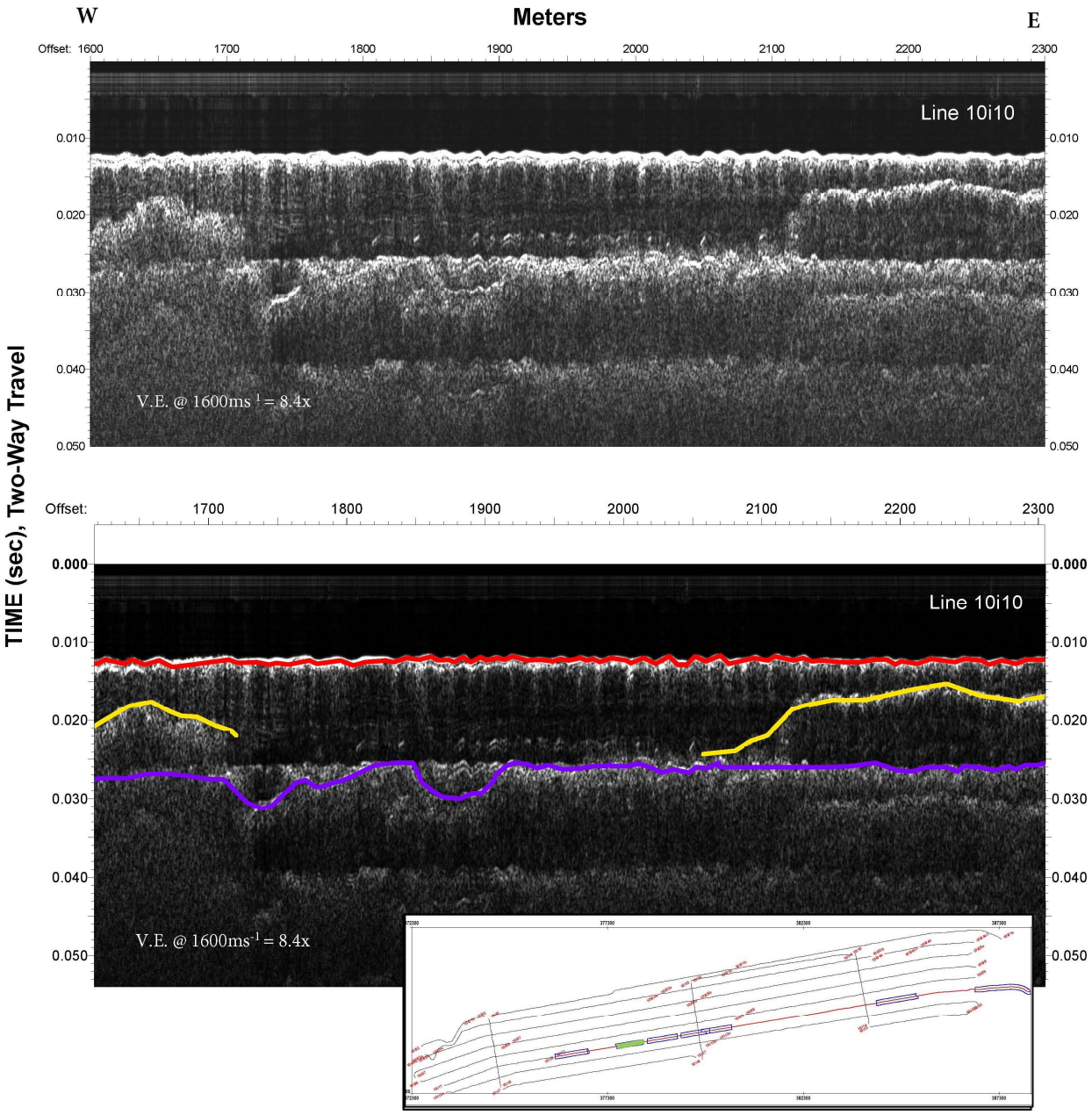

Figure 3.46 The interpretation of Horizon A in this segment of line 10i10 includes a dip on both the west (4.2°) and east (3.3°) sides that have potential to be a channel structure. Horizon P consists of two channel-like structures.

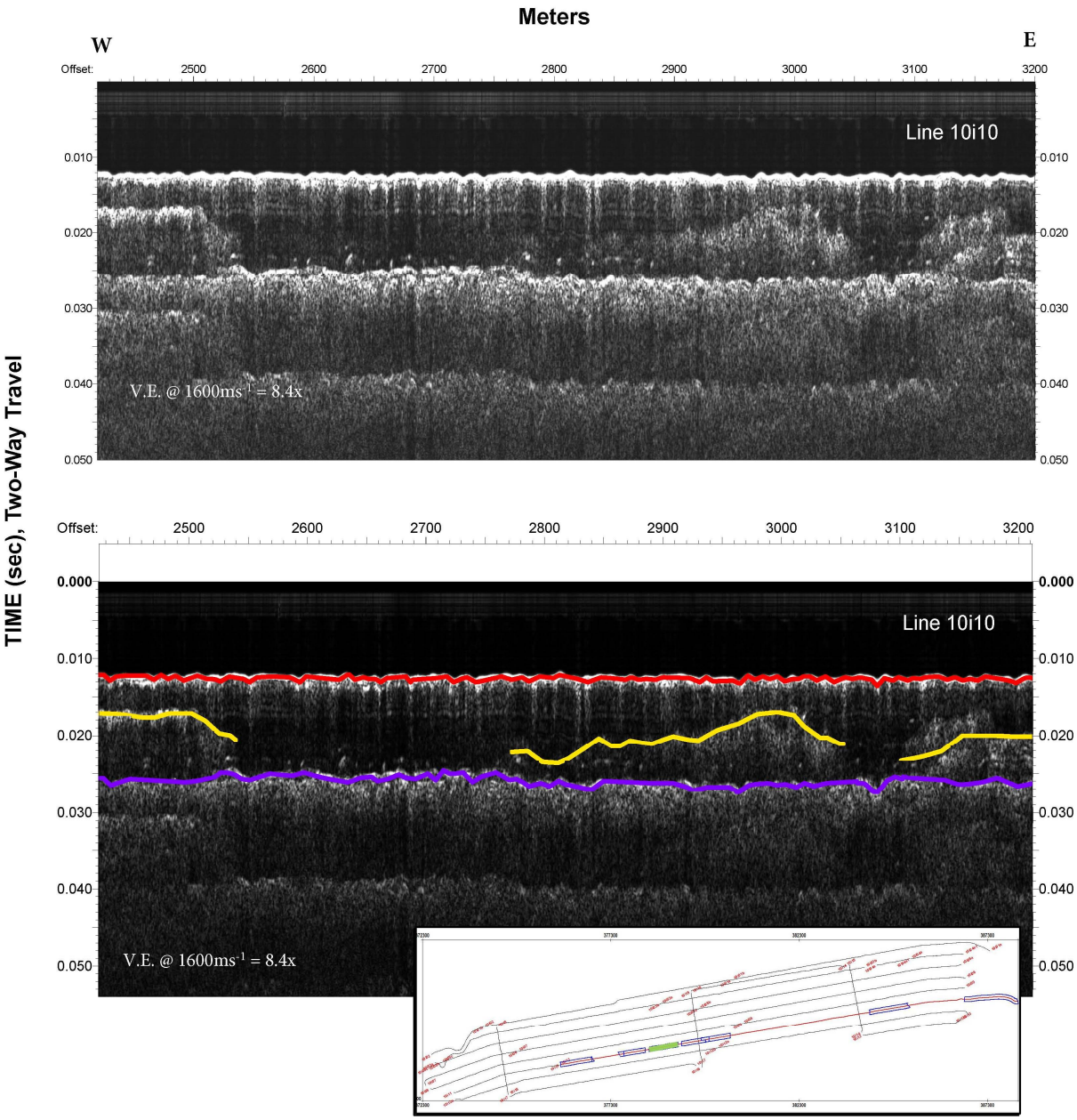

Figure 3.47 Poor imaging in this segment of line 10i10 limits the interpretation of Horizon A. No structures are seen along Horizon P.

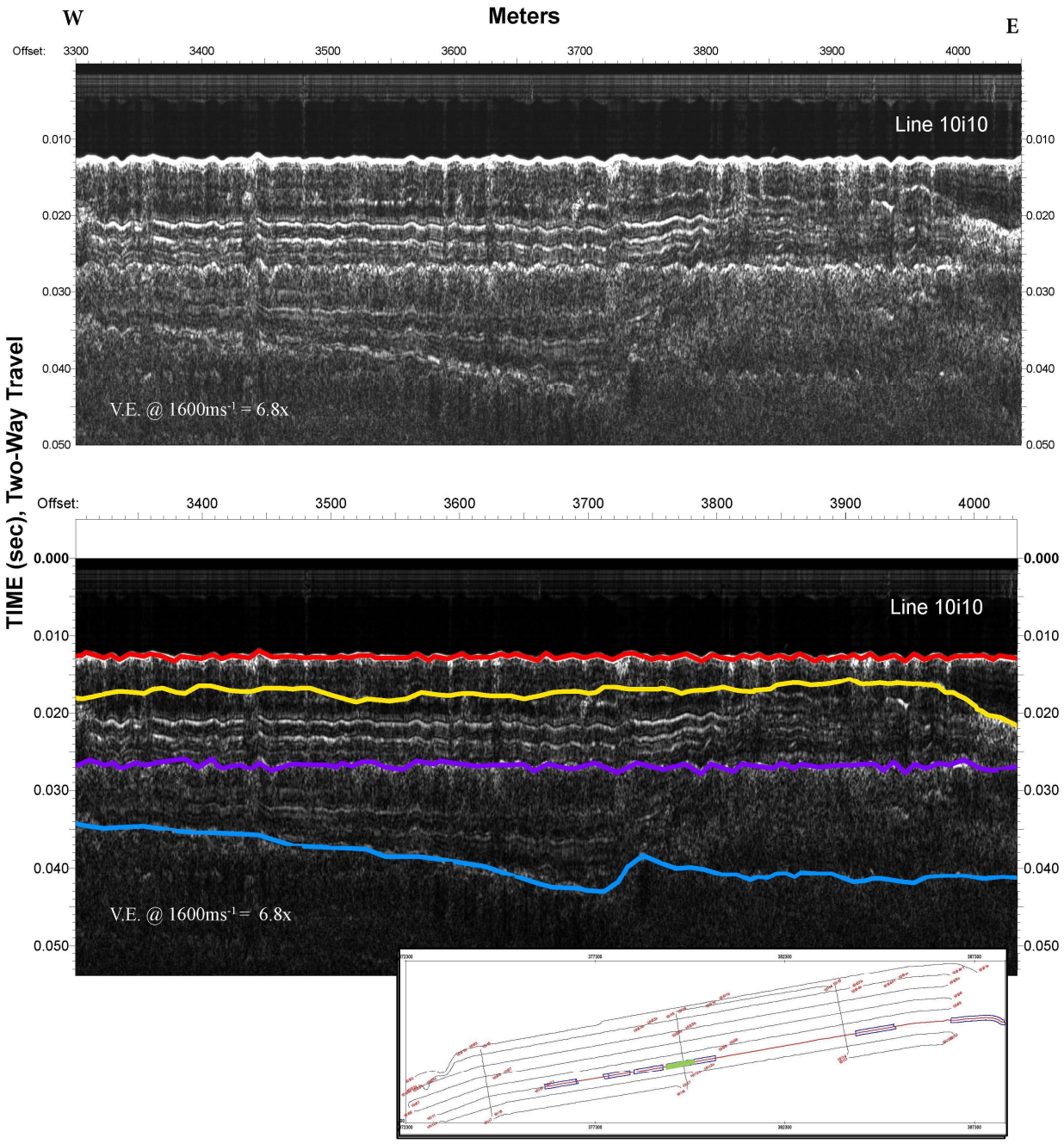

Figure 3.48 The interpretation of Horizon A in this segment of line 10i10 includes slope upward to the east and then a dip to the east. The Horizon B interpretation consists of a 1.4° eastern dip in the central portion of this segment.

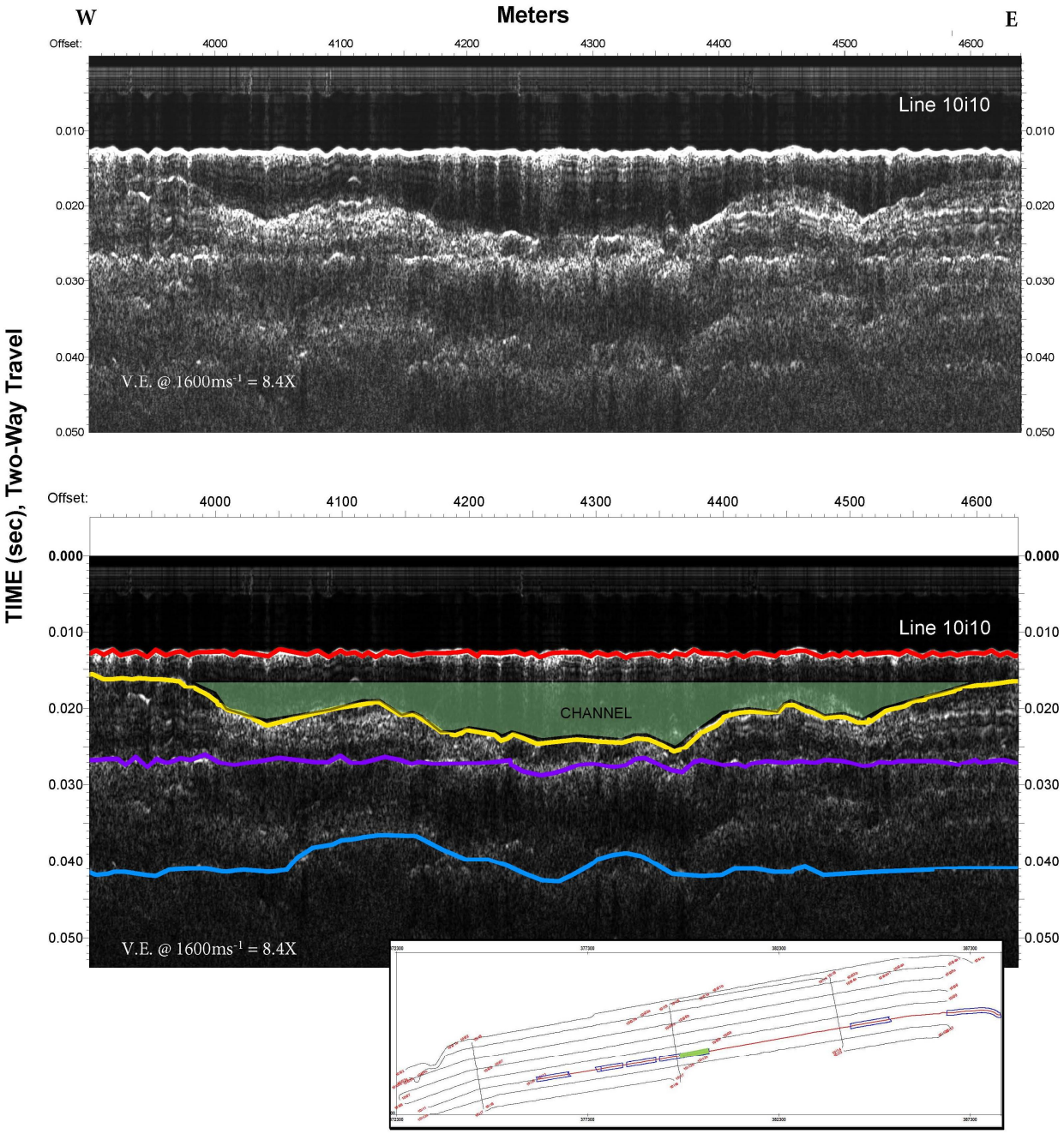

Figure 3.49 The Horizon A interpretation includes a structure that is 6.3 m deep by 612.8 m wide with a western 1.4° and an eastern 1.7° slope. Horizon B consists of intermittent high and low elevations along this segment of line 10i10.

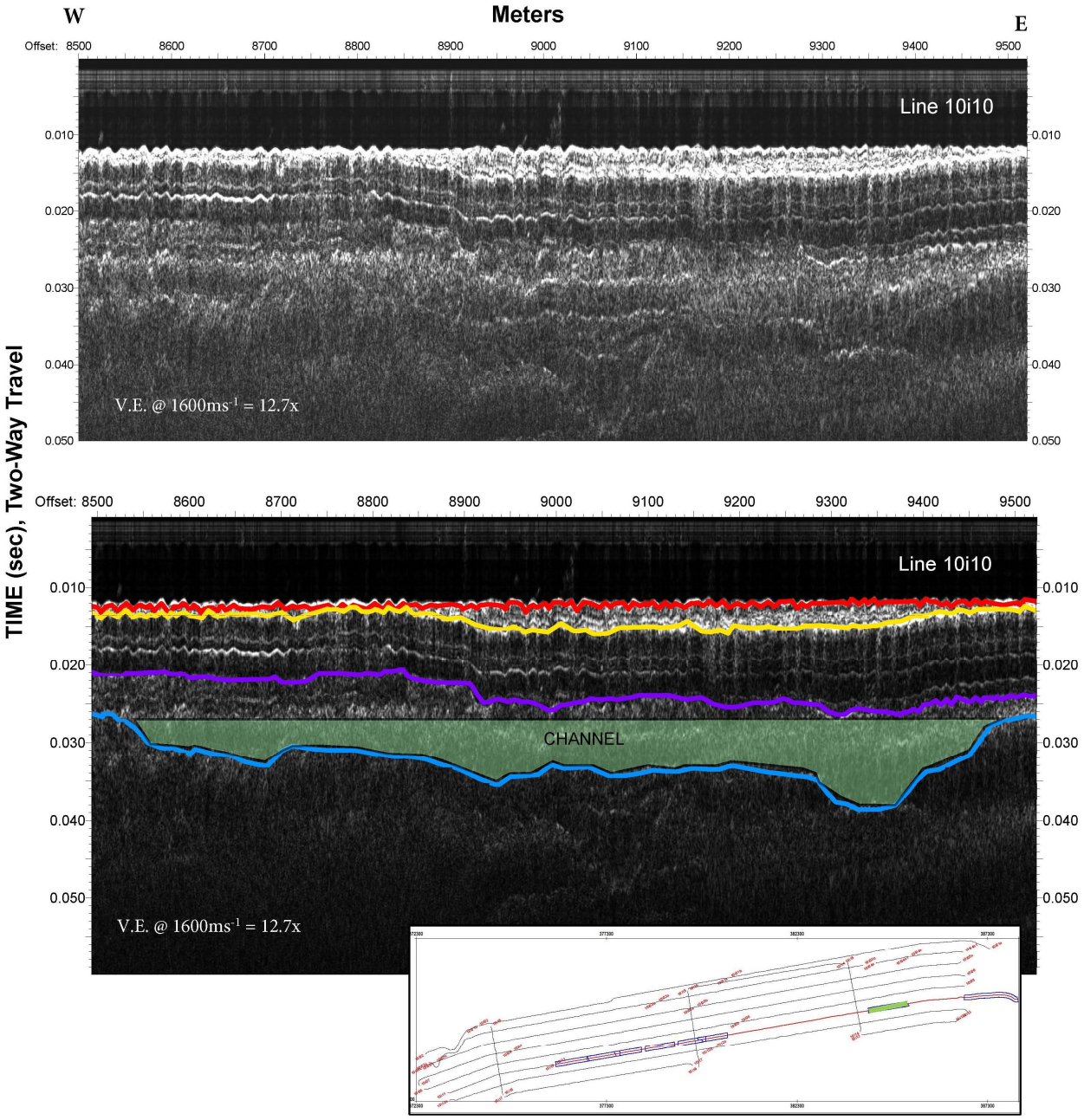

Figure 3.50 A channel structure is seen along Horizon B in this segment of line 10i10. The structure has varying depths of 3.1 m to 9.3 m and a total width of 1,038.5 m. The slopes for this channel structure are a 1.0° western slope and a 4.0° eastern slope.

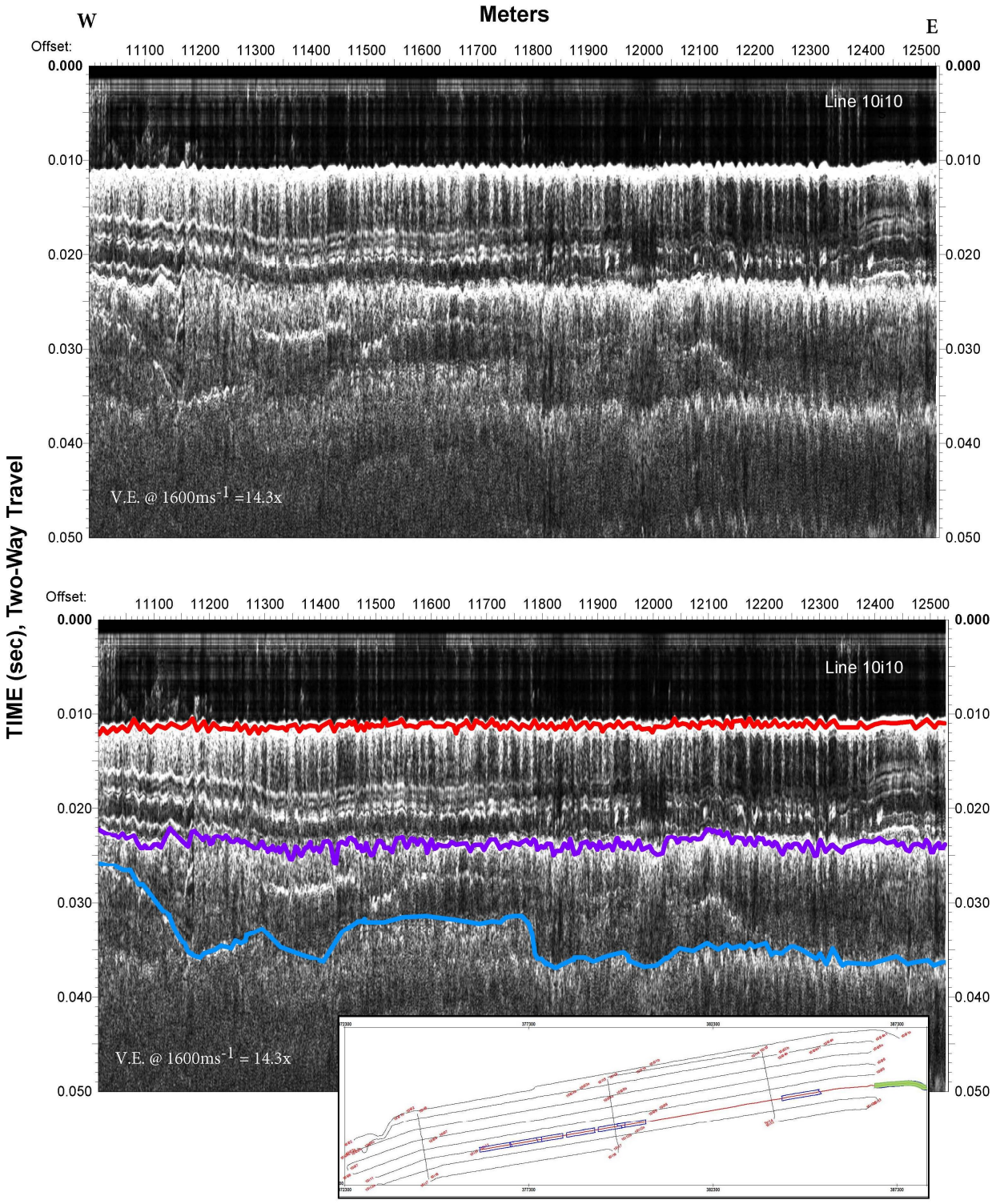

Figure 3.51 The interpretation of this segment of line 10i10 consists of Horizon B having a 2.6° dip to the east with high and low elevations along this portion of the profile.

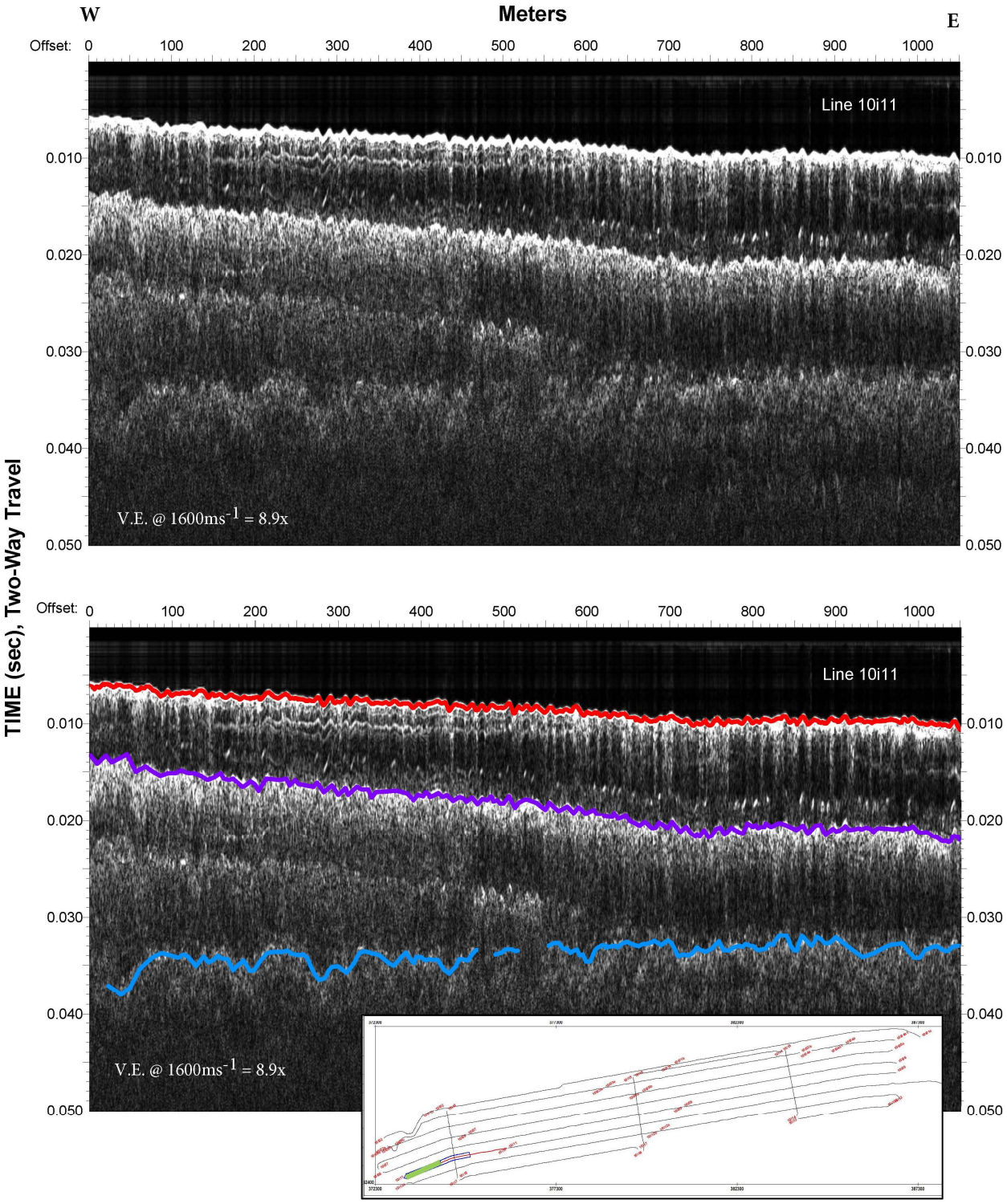

Figure 3.52 The interpretation of Horizon P is seen to mimic the seafloor with a 0.5° slope to the west while Horizon B remains horizontal in this section of line 10i11.

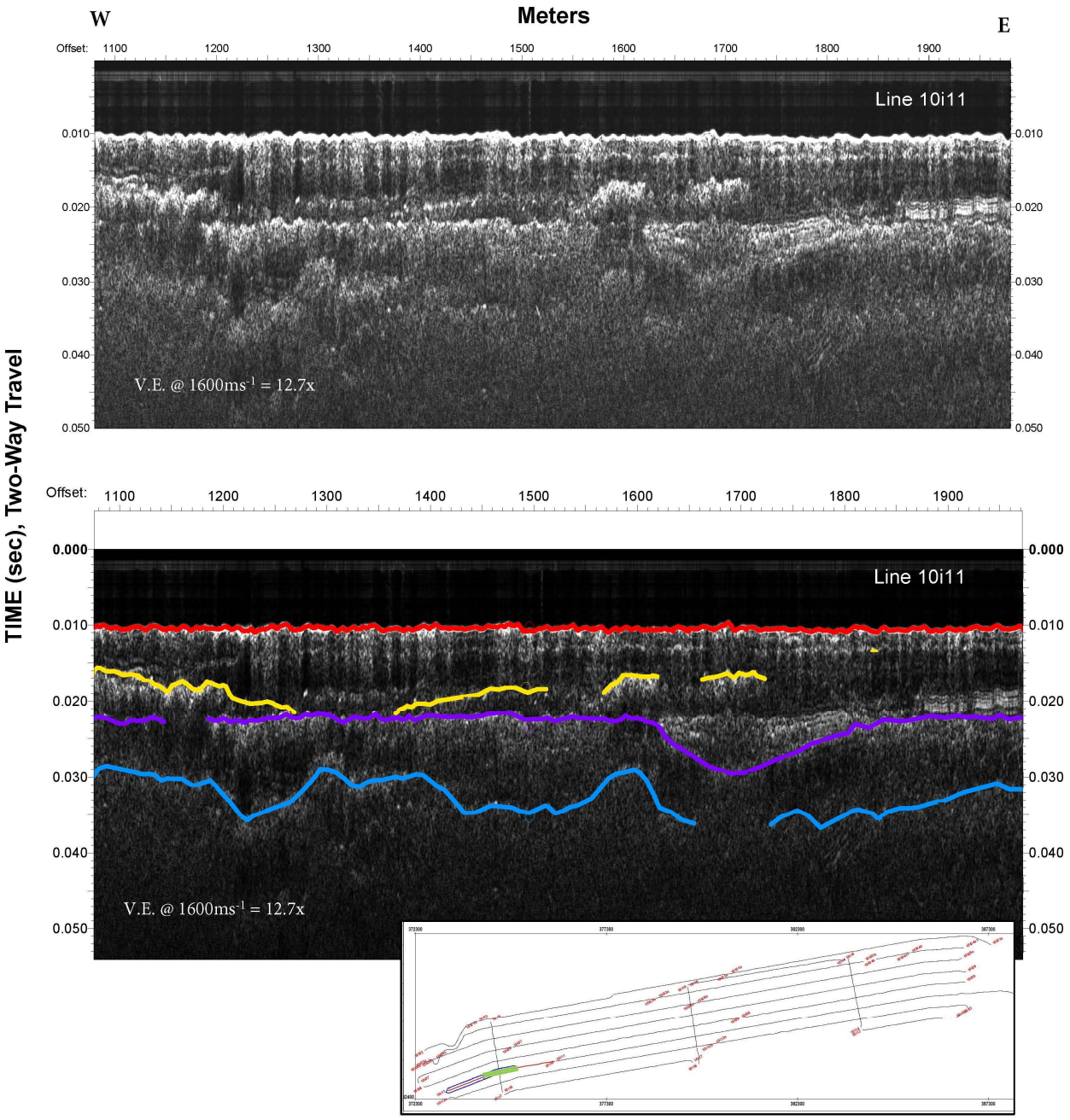

Figure 3.53 The interpretations of Horizons A and B consist of high and low elevations across the profile segment of line 10i11. Horizon P includes a 5.4 m deep by 211.1 m wide channel-like structure with 4.3° western and 2.4° eastern slope.

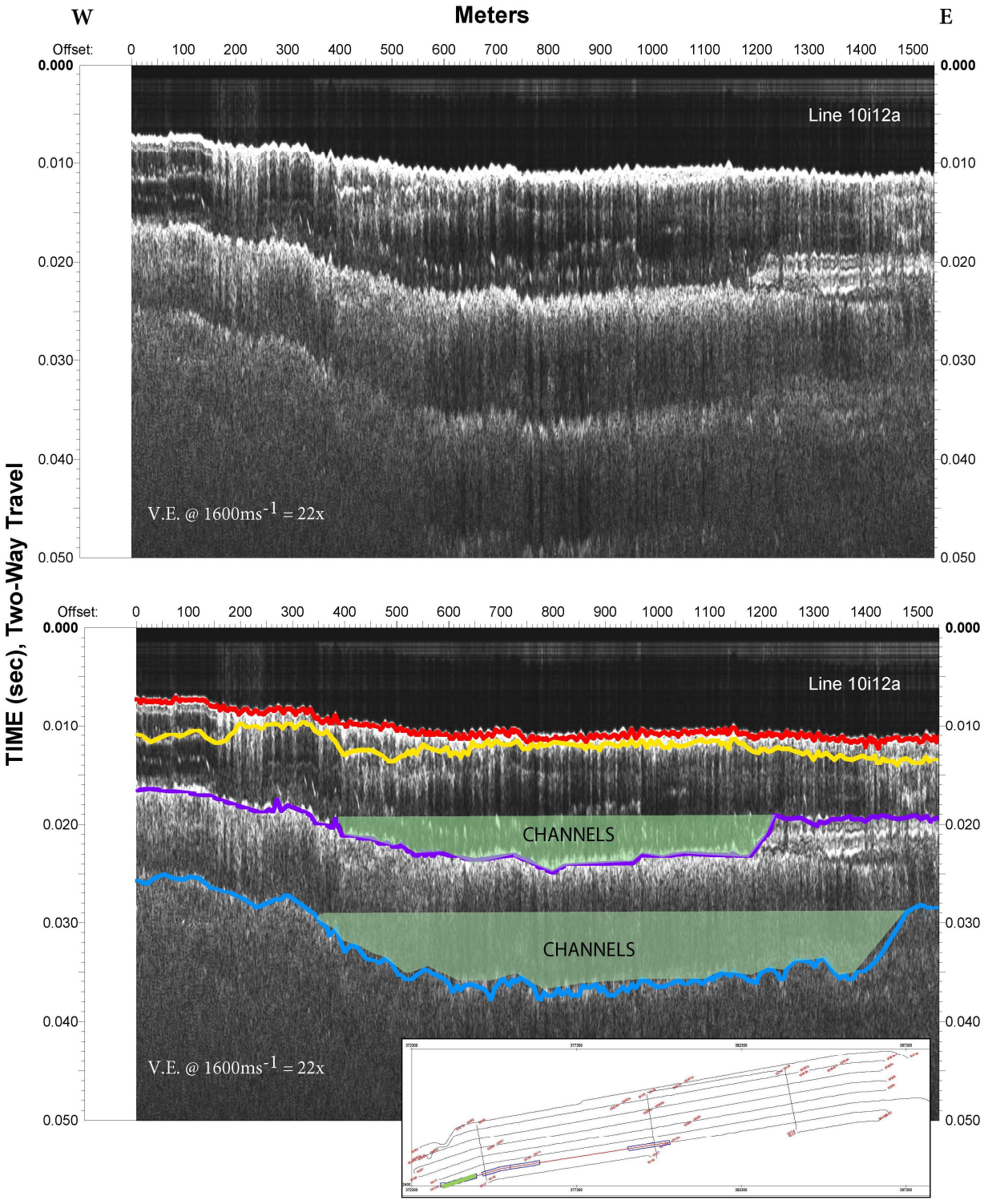

Figure 3.54 The interpretation of Horizons P and B includes channel-like structures in this segment of line 10i12a. Horizon P is a 4.8 m deep by 782 m wide channel-like structure with a western 0.7° and an eastern 5.5° slope. Horizon B is a 6.4 m deep by 1,071 m wide channel structure with a western 1.5° and an eastern 2.9° slope.

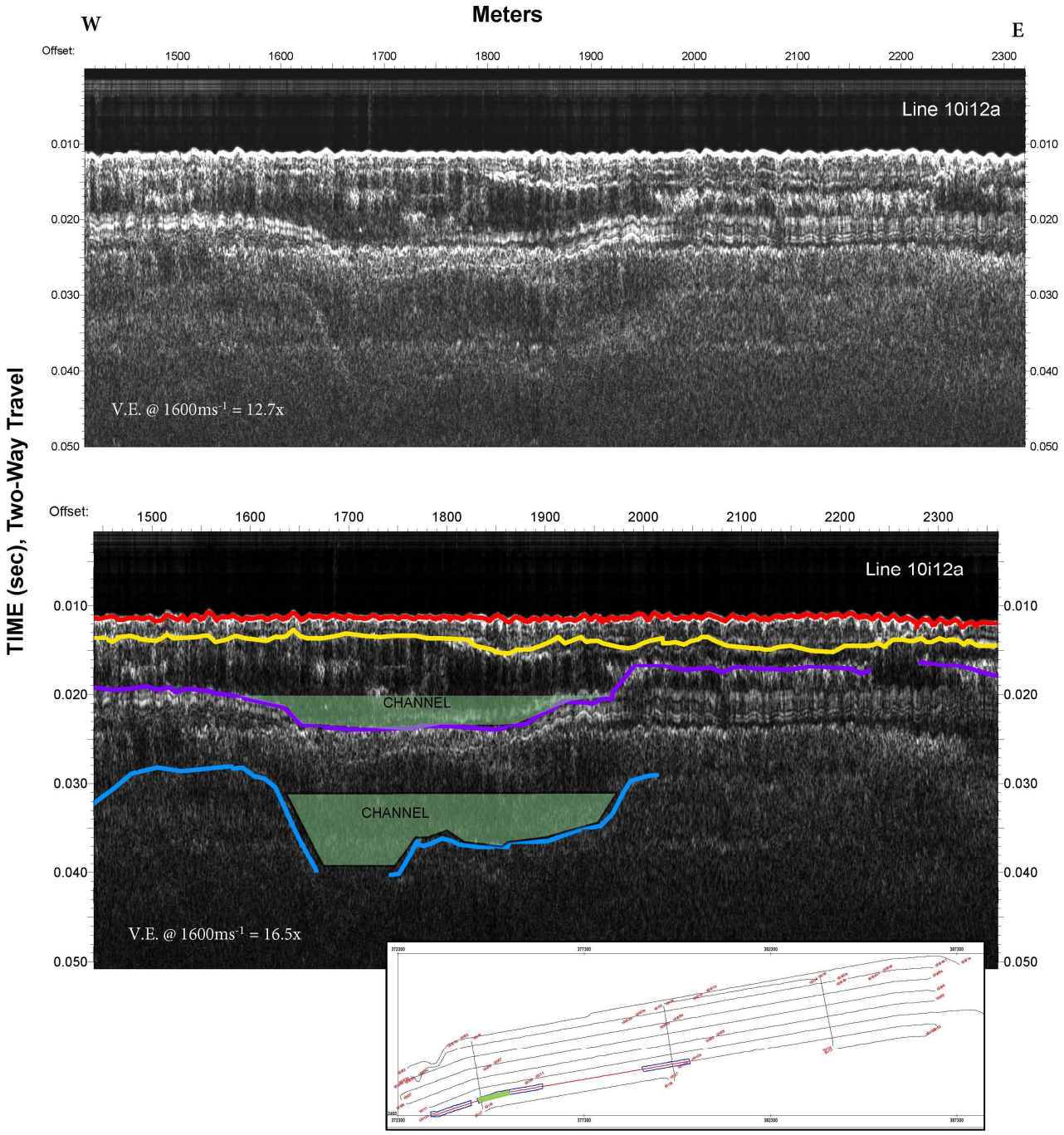

Figure 3.55 Channel structures are seen along Horizons P and B in this segment of line 10i12a. Horizon P includes a 2.8 m deep by 332.7 m wide channel-like structure with a western 2.8° slope and an eastern 1.9° slope. The Horizon B channel varies in depth from 4.4 m to 6.8 m and is 370.8 m wide. It has a western 9.0° and an eastern 2.2° slope.

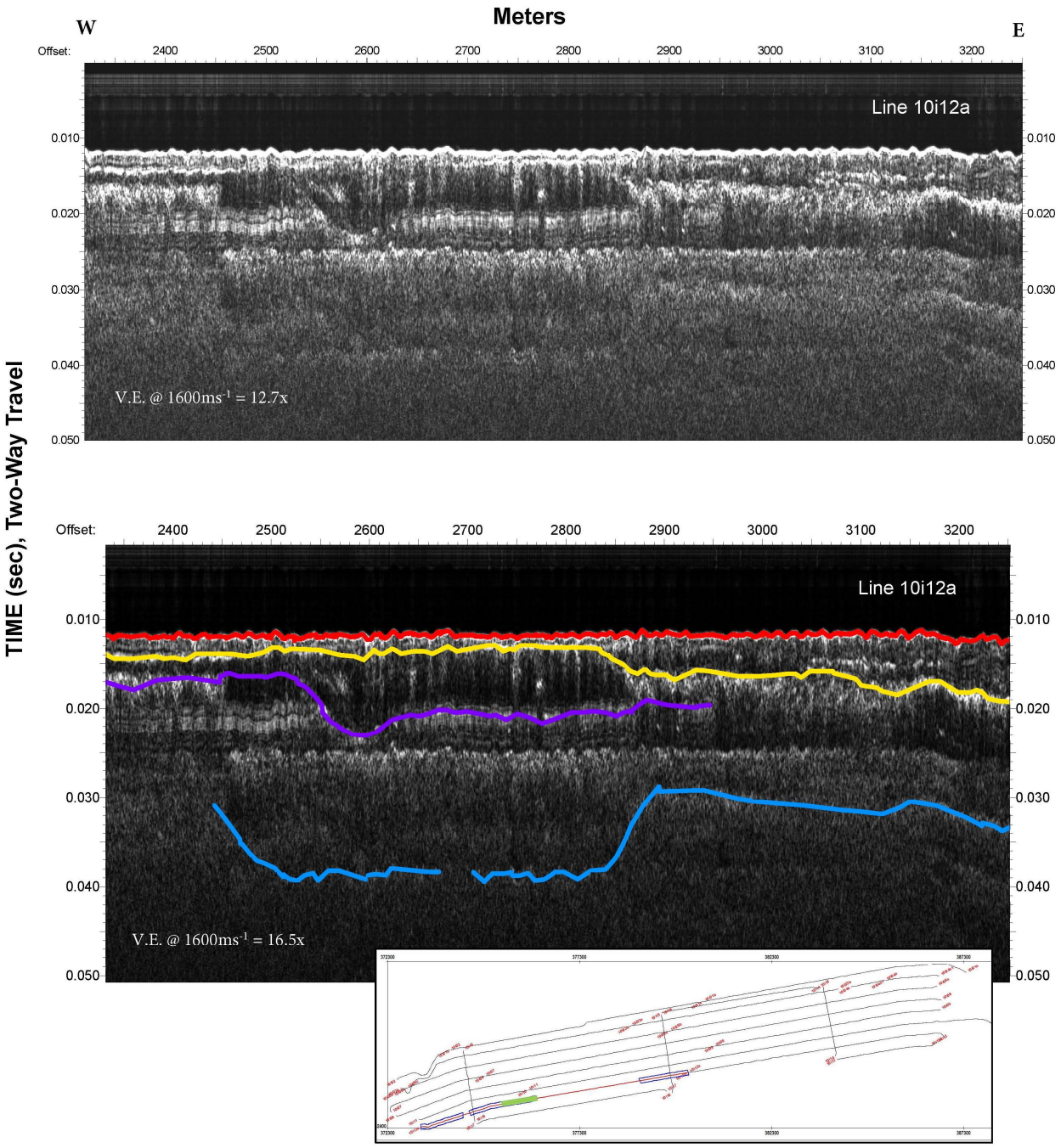

Figure 3.56 This interpretation of Horizons A and P include dips to the east and Horizon B with a channel-like structure that is 7.2 m deep by 448.6 m wide with a 5.8° western and a 9.5° eastern slope in this section of line 10i12a.

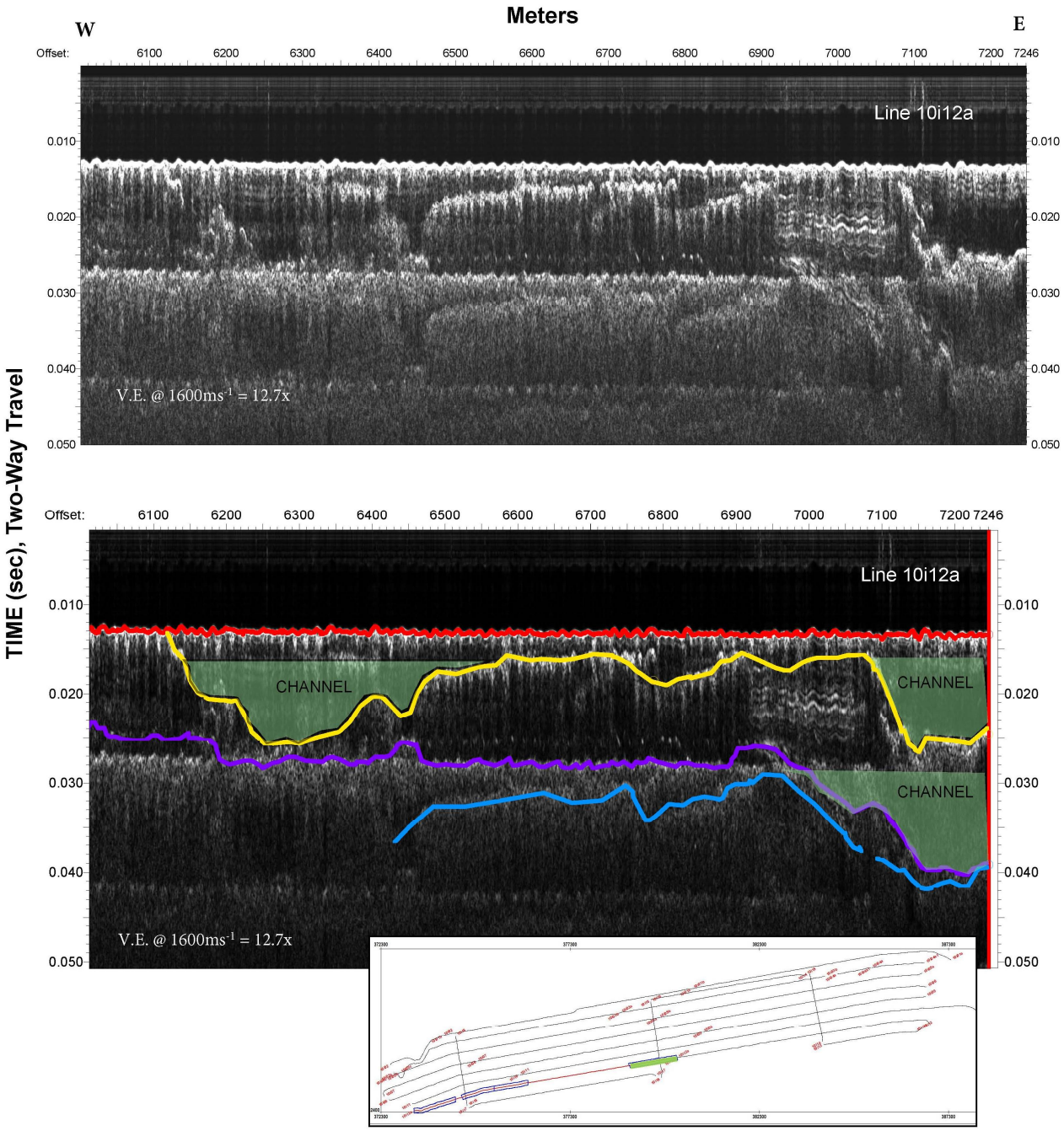

Figure 3.57 Multiple channel-like structures are seen along Horizon A in this segment of line 10i12a with the following measurements: (western structure) 7.2 m deep by 495.1 m wide structure with 4.1° western and 1.6° eastern slopes; (eastern structure) 7.6 m deep by 250.6 m wide structure with a 7.2° western slope. Horizon P includes a channel-like structure that overlaps onto survey 10i12b with measurements of 8.8 m depth by 373 m width with a western 3.6° slope. The interpretation of Horizon B includes a similar channel-like structure as seen in Horizon P, but with measurements of 10.8 m depth by 400.6 m width with a 38.7° western slope.

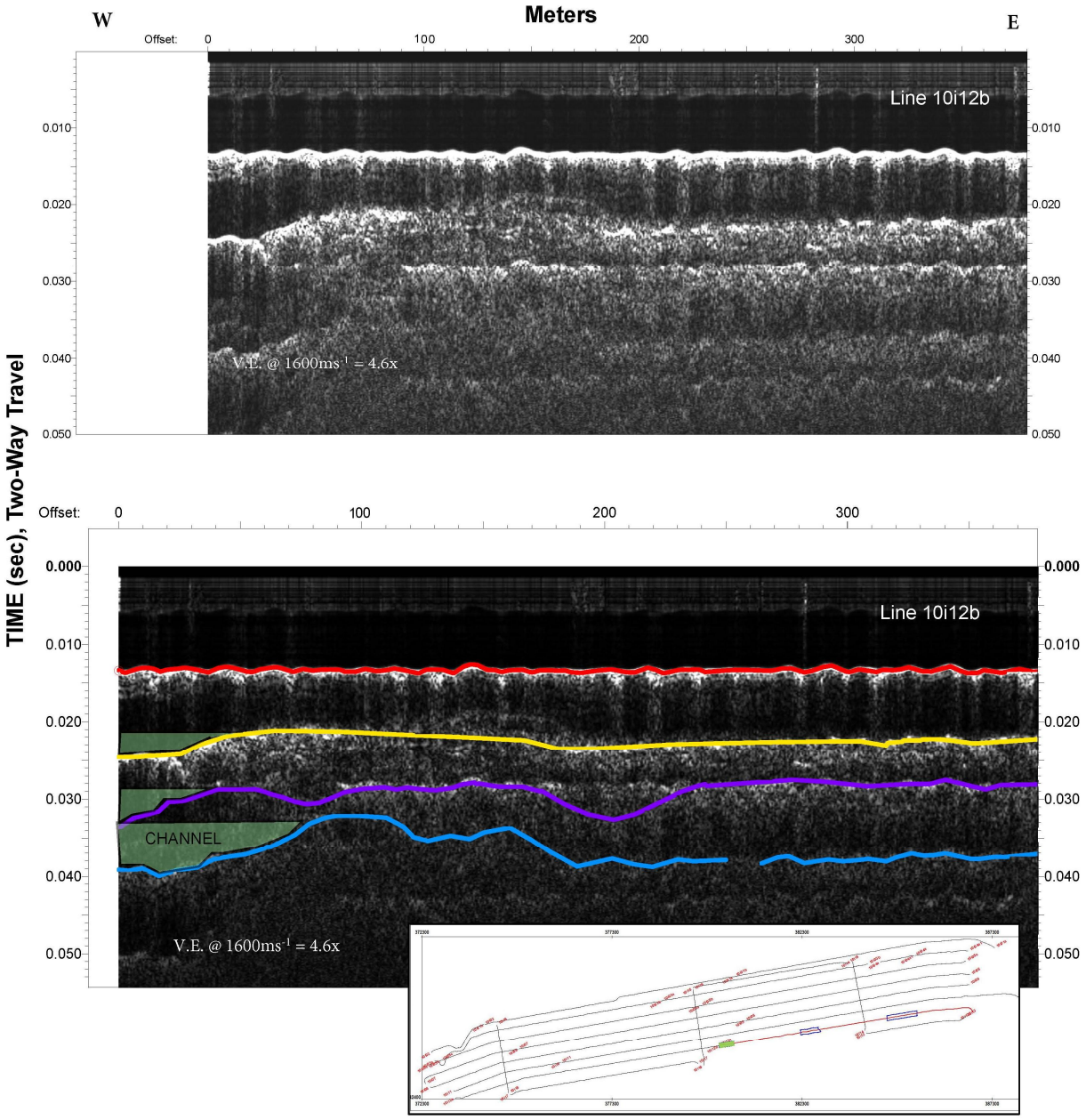

Figure 3.58 The remaining channel structures found in Figure 3.57 are seen along horizons A, P, and B of this segment of line 10i12b.

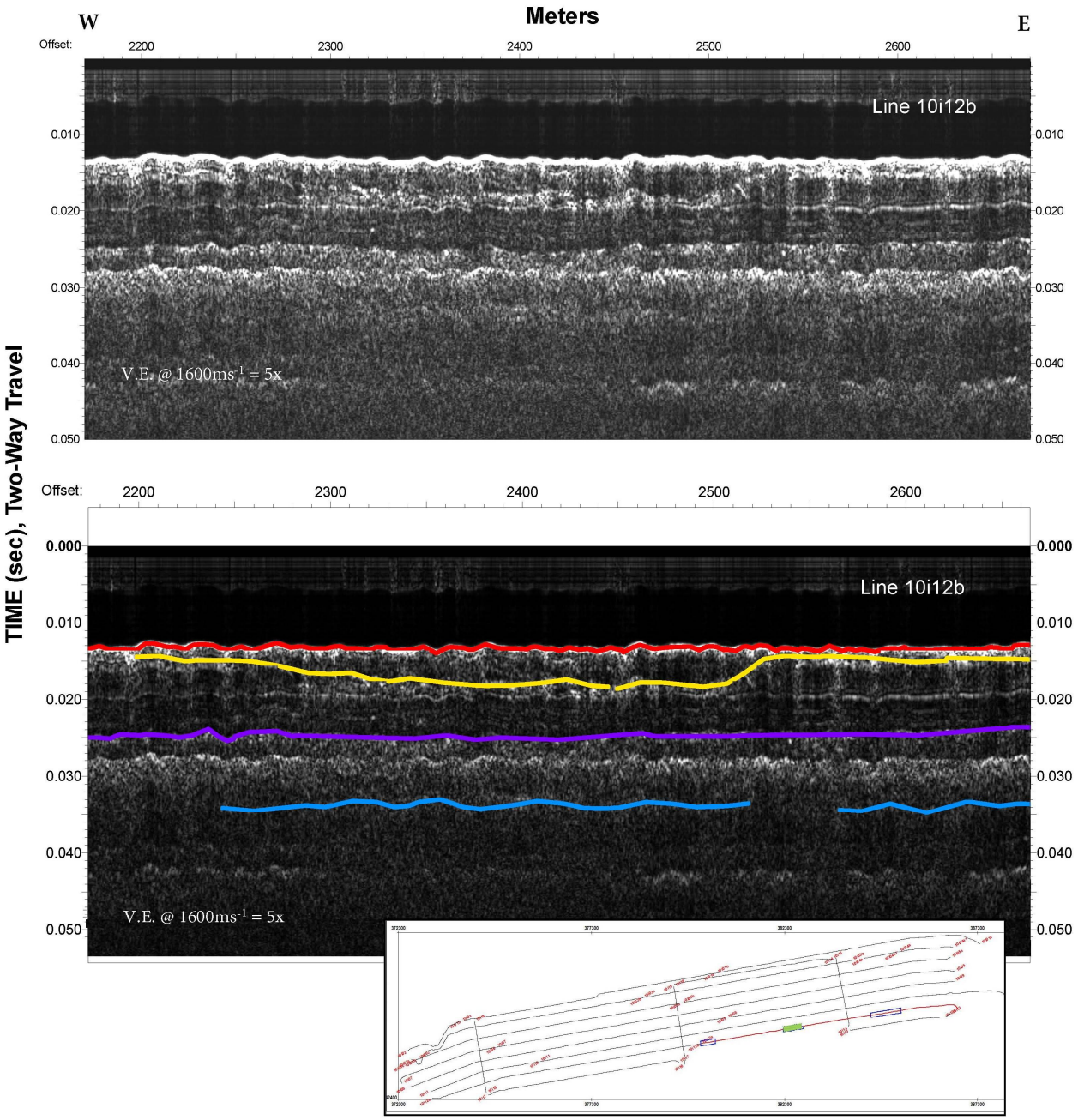

Figure 3.59 Horizon A includes a channel-like structure with a varying depth of 0.9 m to 2.7 m by 240.7 m wide with a 1.5° western slope and an eastern slope of 7.9° in this section of line 10i12b.

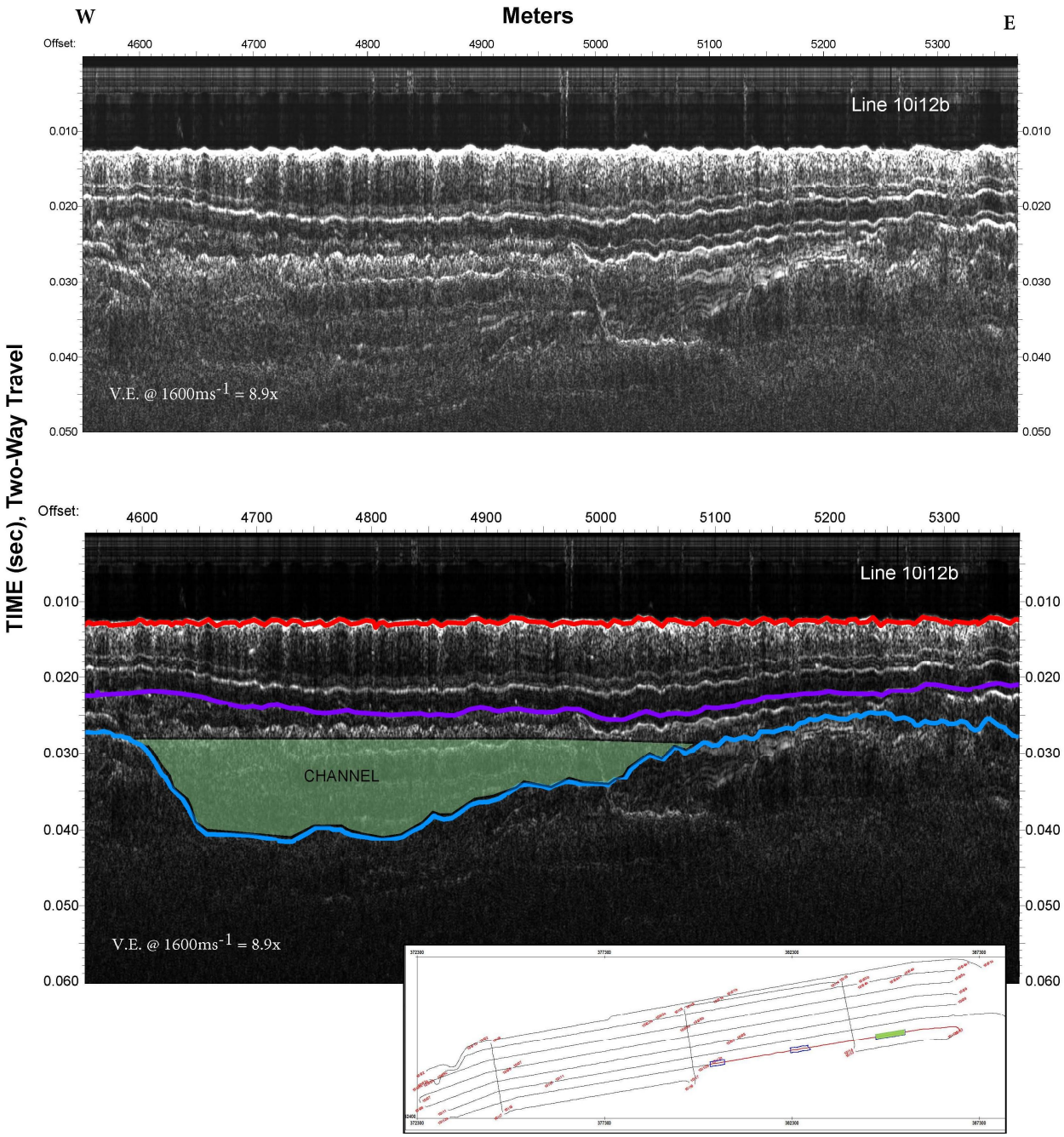

Figure 3.60 A channel structure is seen along Horizon B in this segment of line 10i12b. This channel structure has depths varying from 9.9 m to 4.5 m, is 478.4m wide, and has a 8.9° western slope and a 2.3° eastern slope.

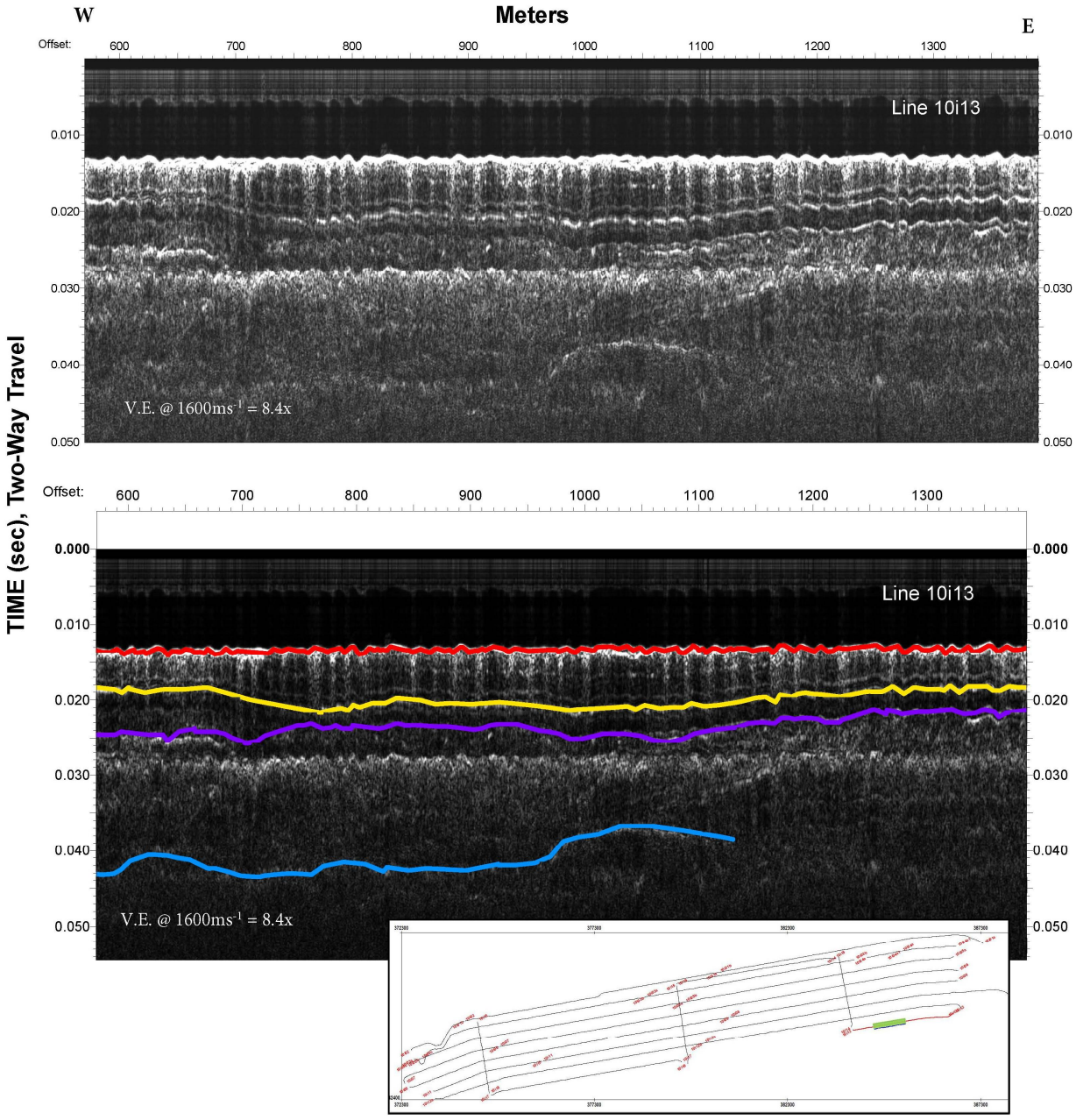

Figure 3.61 The interpretation of this line segment of line 10i13 include horizons A and P as predominantly horizontal. Horizon B includes a slope upward to the east, but poor imaging limits further interpretation.

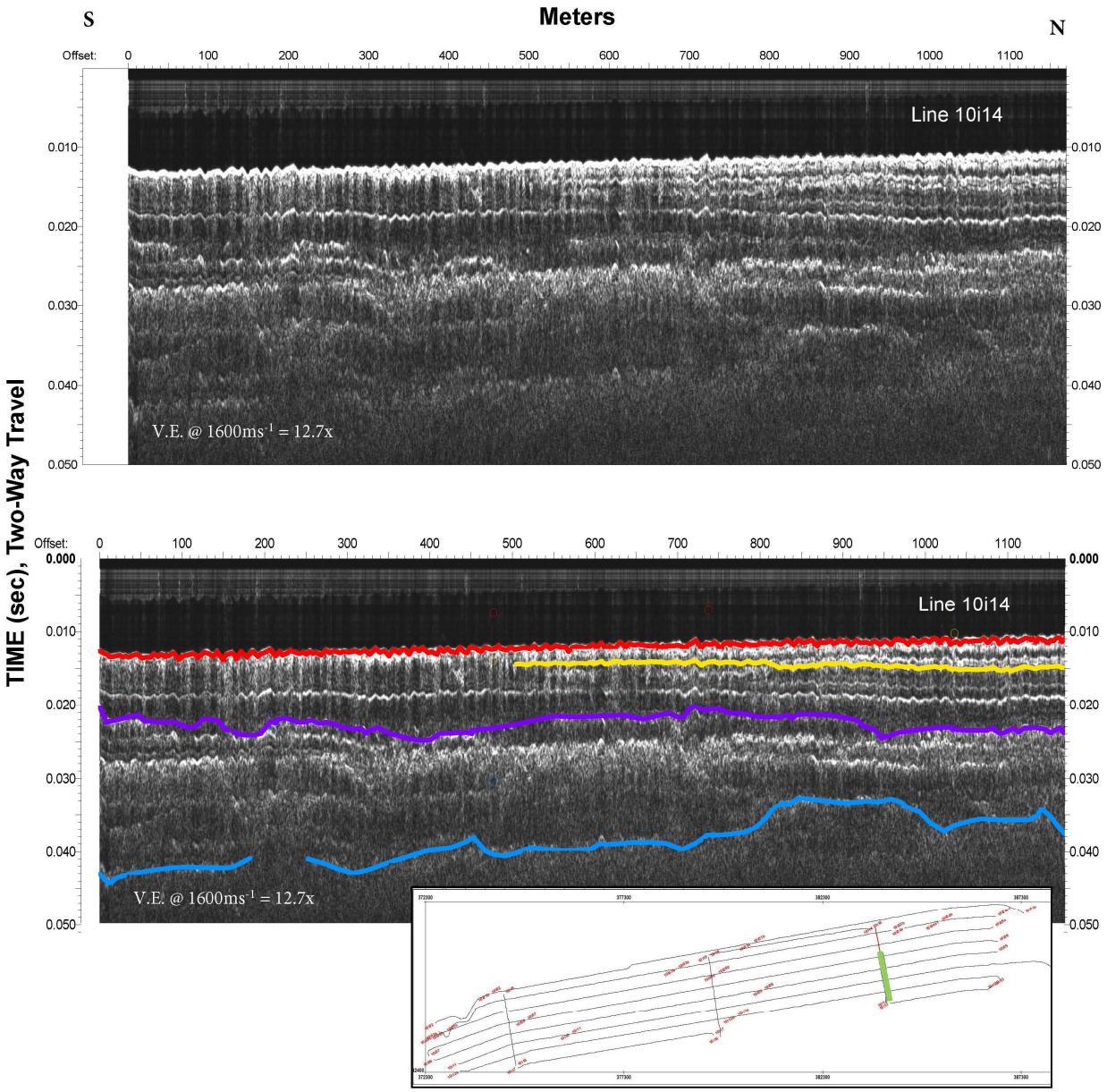

Figure 3.62 This segment of line 10i14 shows an interpretation of Horizon B having slope upwards towards the shore. Line 10i14 runs north-south, perpendicular to Dauphin Island.

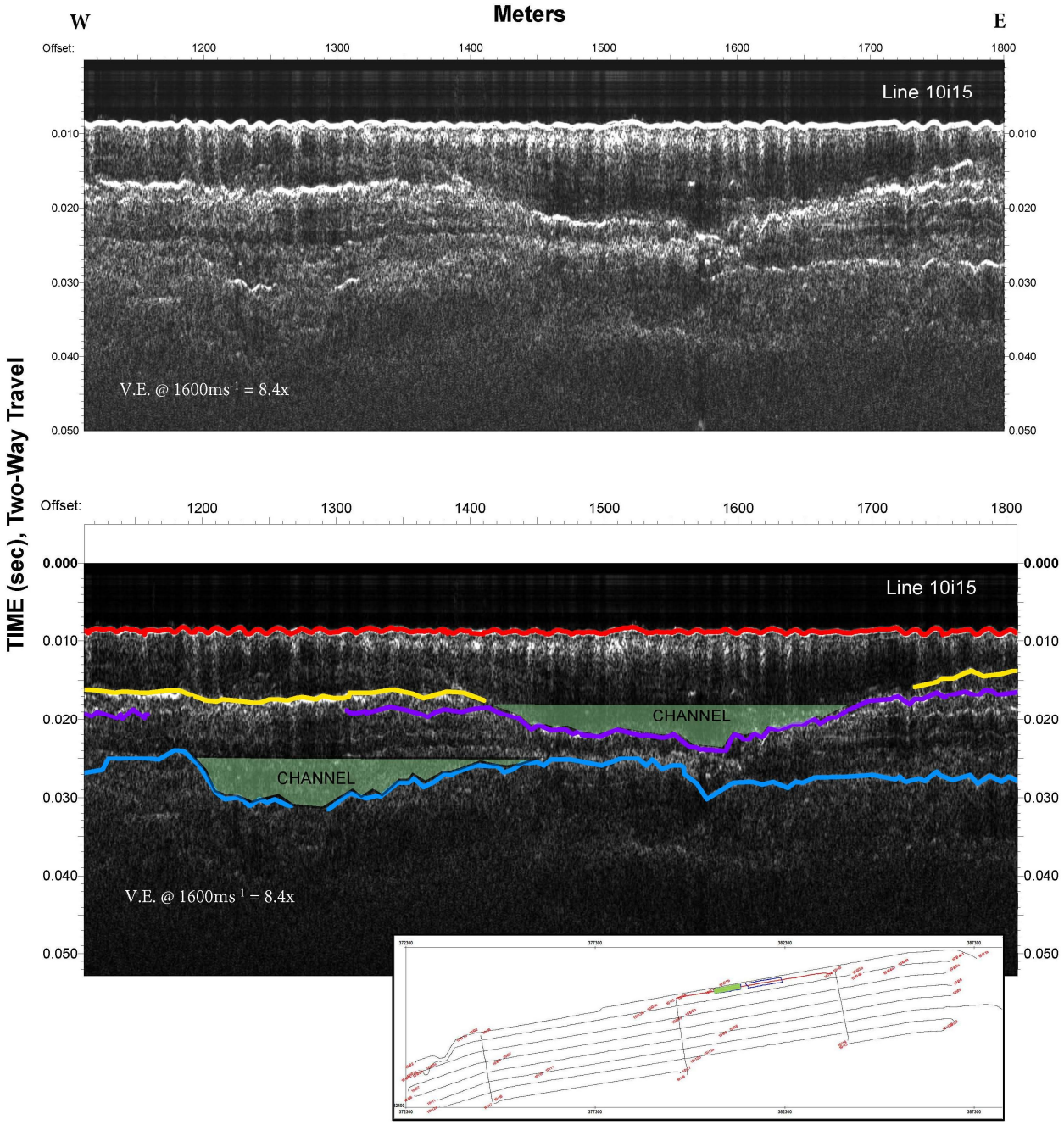

Figure 3.63 The Horizon P interpretation includes a channel-like structure with depths varying from 3.2 m to 4.5 m and a 303.9 m width in this segment of line 10i15. The slopes of this structure are a 2.4° western and a 2.9° eastern slope. Horizon B includes a channel structure with a depth range of 4.1 m to 2.3 m with a 242 m width, 5.3° western, and a 2.1° eastern slope.

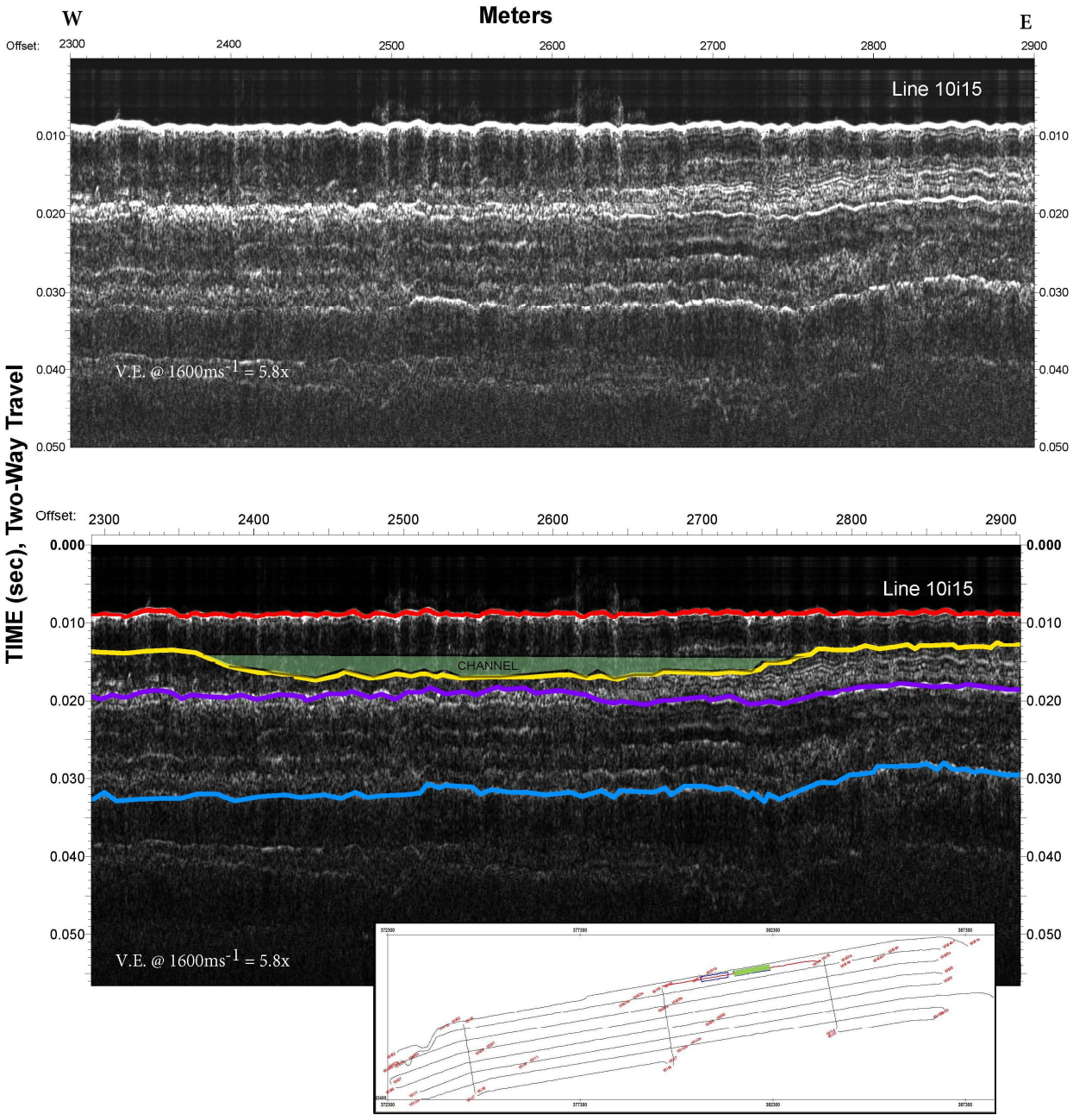

Figure 3.64 The interpretation of Horizon A in this segment of 10i15 includes a channel structure with a depth range of 2.3 m to 1.4 m that is 445.6 m wide with a 1.6° western and a 1.0° eastern slope.

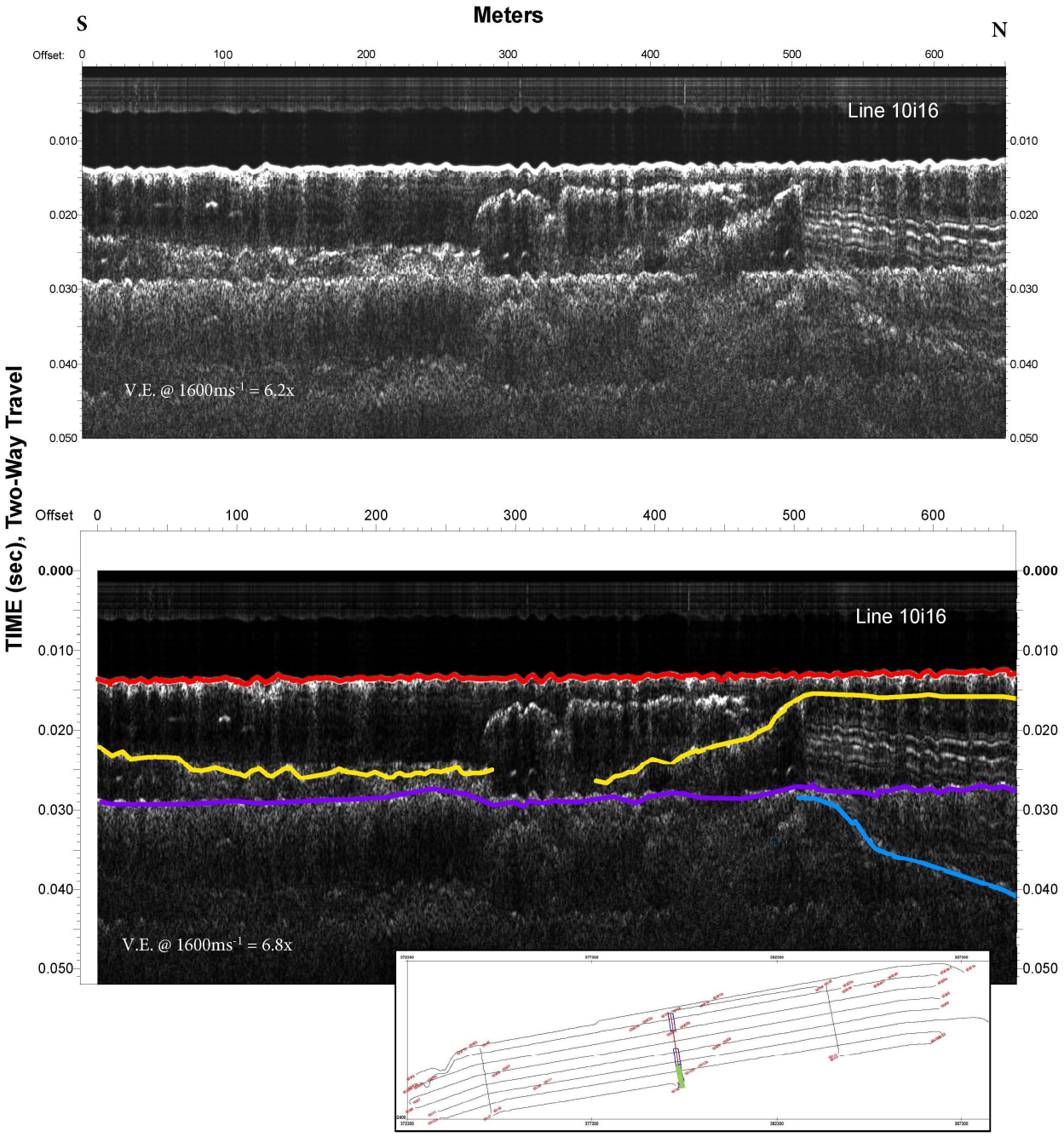

Figure 3.65 Horizon A includes a 3.3° dip to the south in the interpretation of this segment of line 10i16. Line 10i16 runs perpendicular to the island.

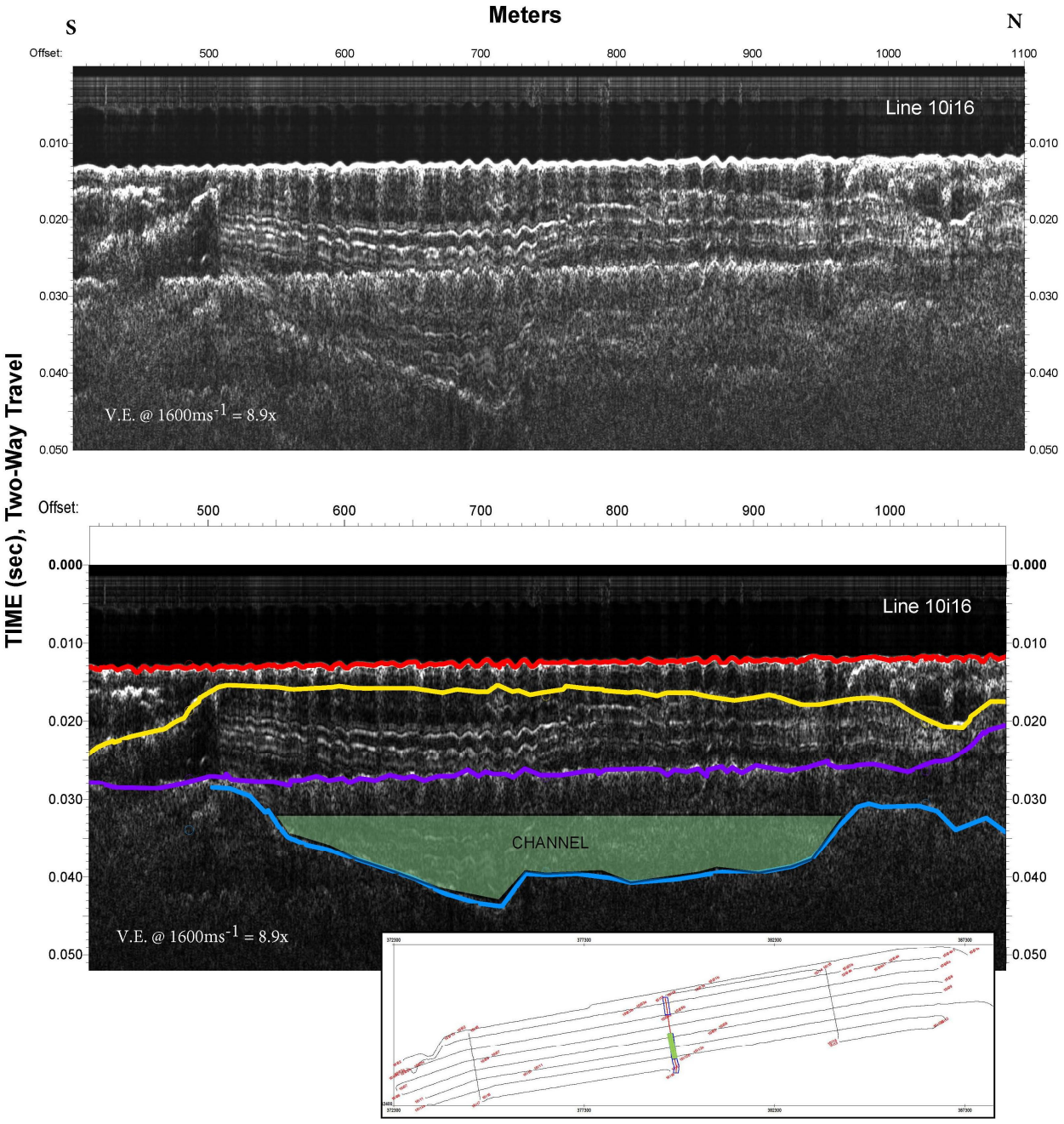

Figure 3.66 A channel structure is seen along Horizon B in this segment of line 10i16. The structure has a depth range of 8 to 10 m and a 450 m width in this northern portion of line 10i16. The channel has a 3.5° western and a 2.8° eastern slope. Horizon A includes a high elevation area which could be a potential shoal.

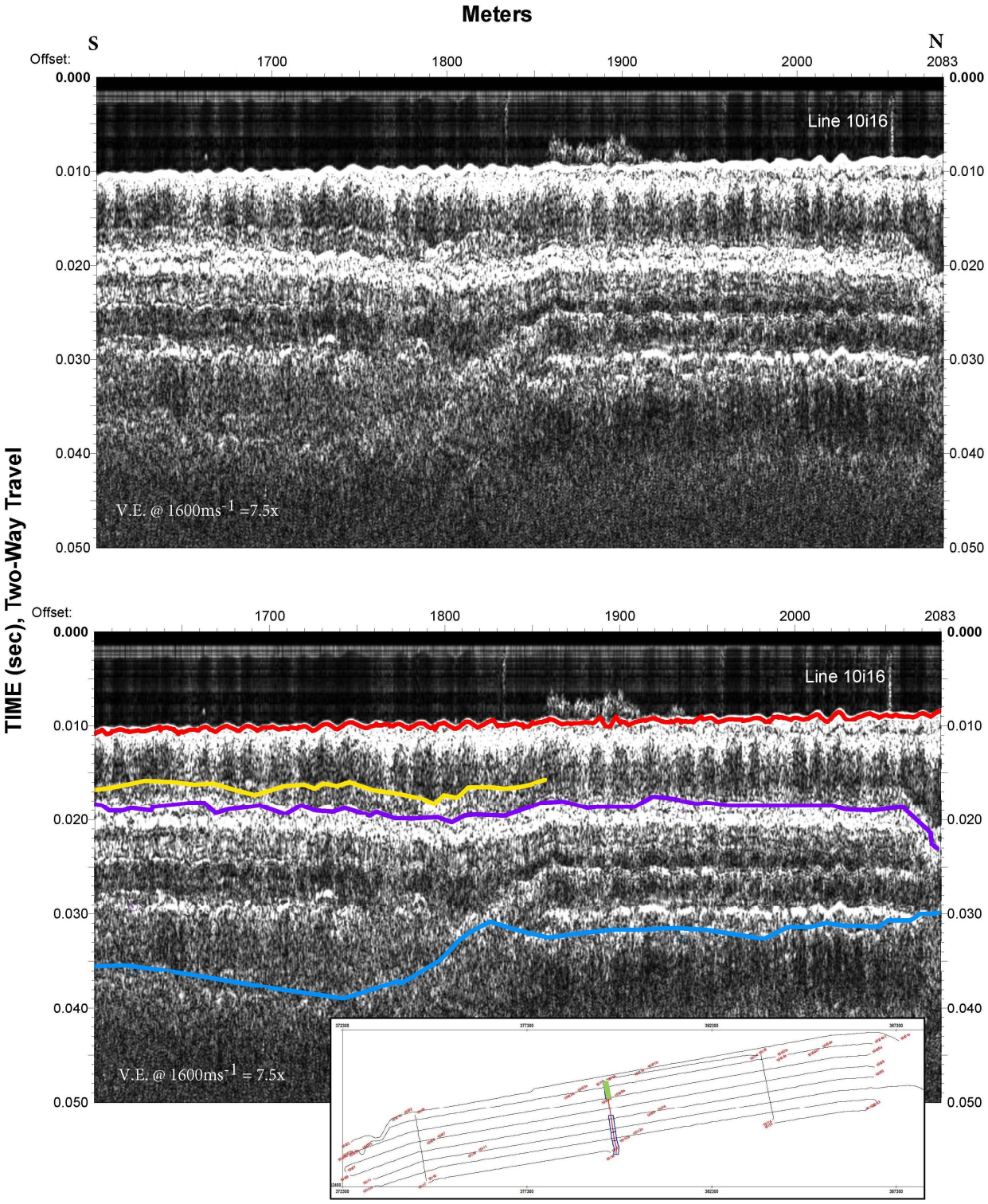

Figure 3.67 This interpretation of this line segment of line 10i16 shows Horizon B with a 5.9° dip to the south.

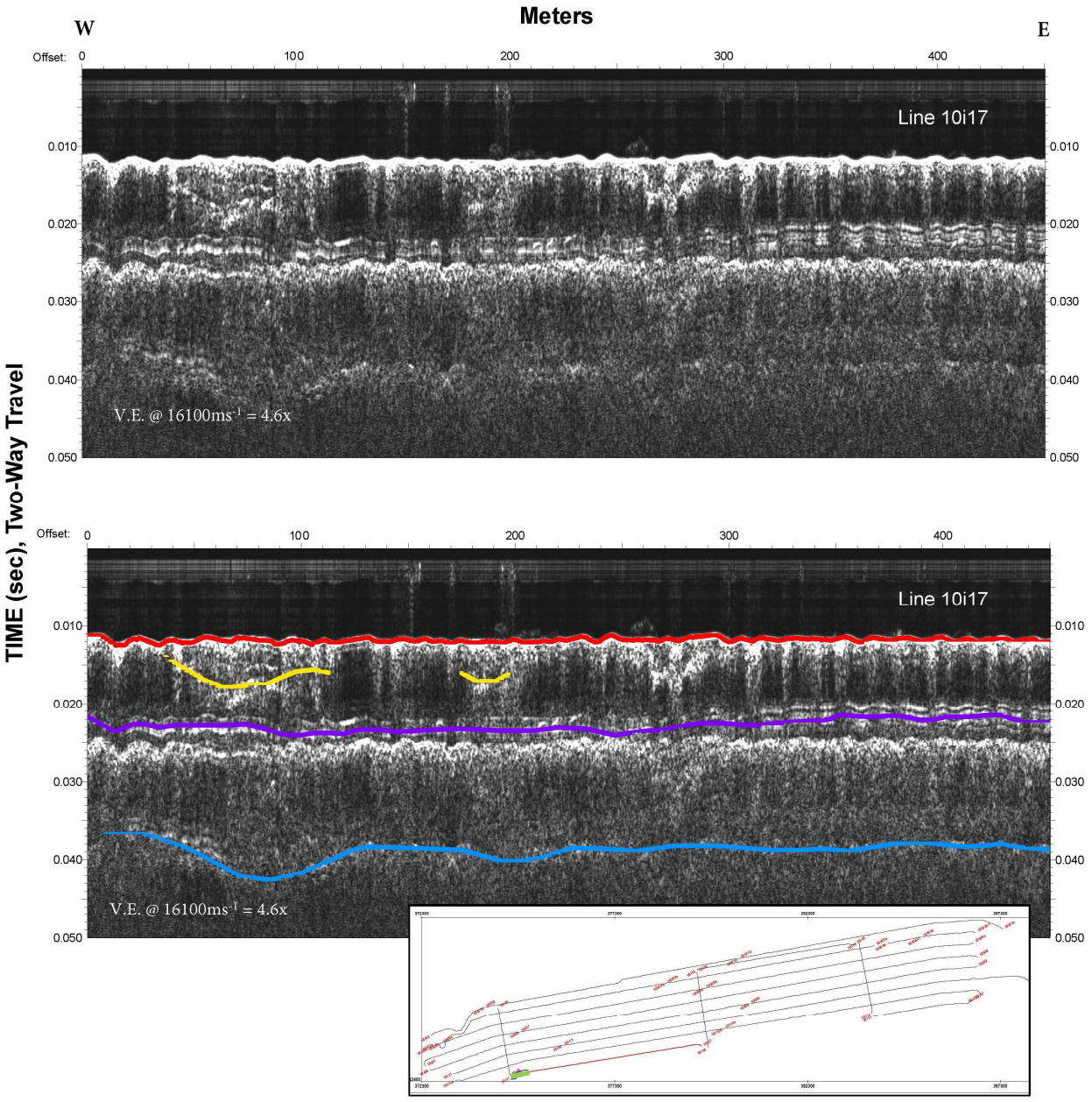

Figure 3.68 Horizon B includes a small channel-like structure in the west of the interpretation of this profile segment of line 10i17.

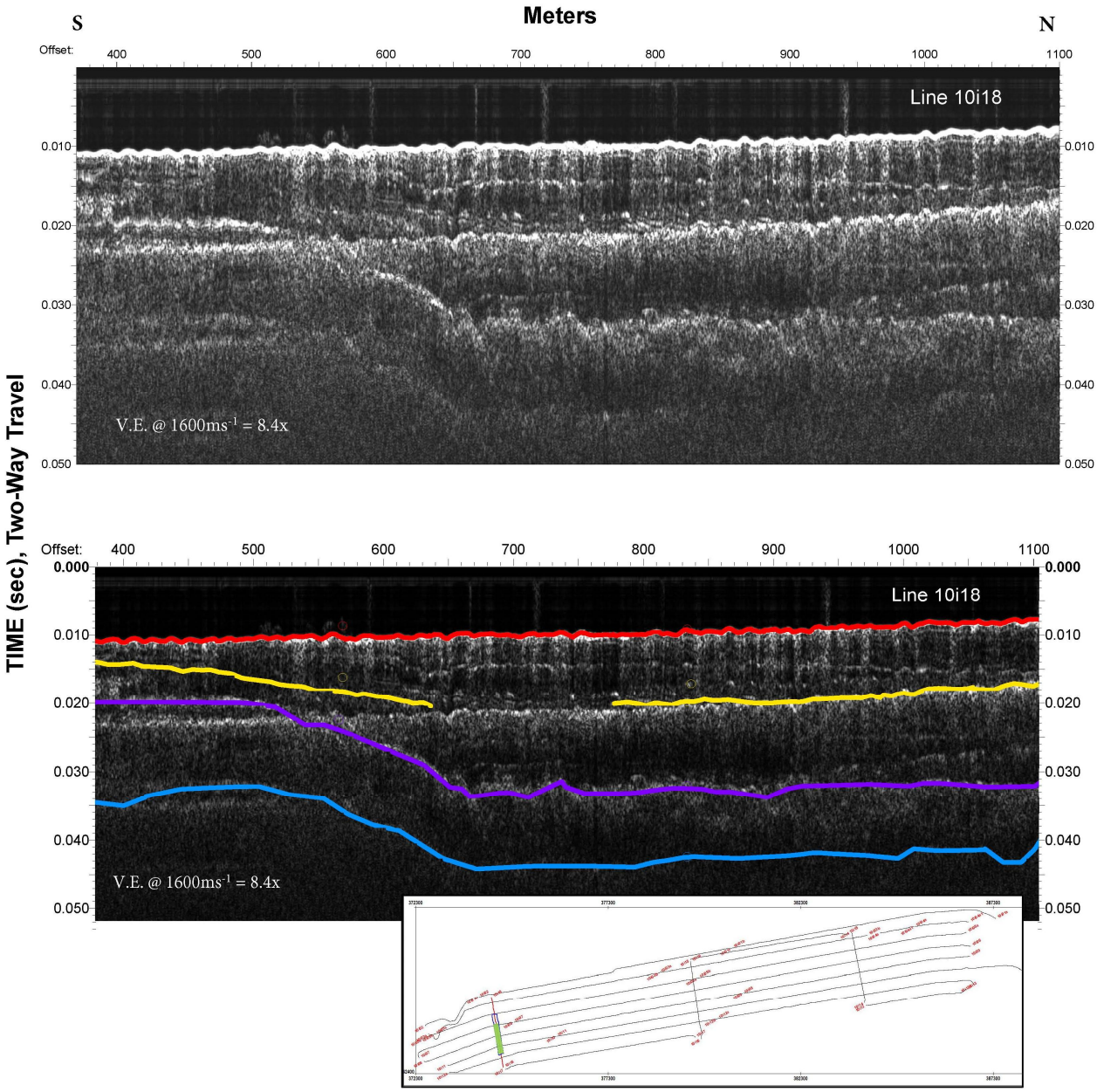

Figure 3.69 In this line segment of line 10i18, dips to the north are seen along Horizons A (1.2°), P (3.6°), and B (3.3°). This is contrary to the southerly dipping seafloor.

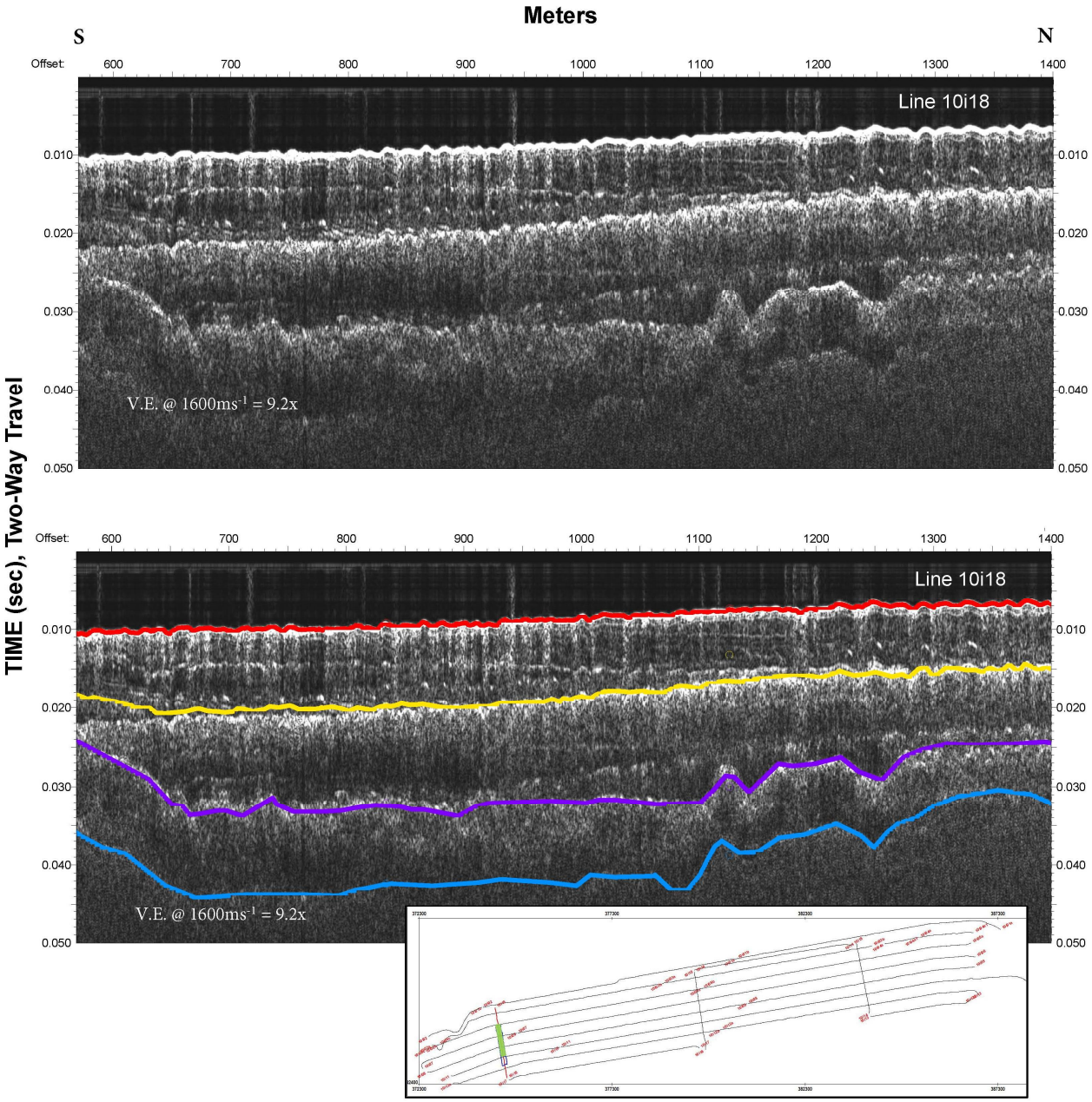

Figure 3.70 The seafloor and Horizon A in this portion of line 10i18 appear to mimic each other, while western dips are seen in Horizons P (5.2°) and B (4.6°).

The interpreted horizons A, P, and B were gridded and contours were generated (Figures 3.71 and 3.72). A grid of the seafloor horizon (Figure 3.71a) was used to validate the gridding algorithm by ensuring that it could faithfully reproduce the known seafloor. The seafloor (Figure 3.71a) dips away from the shoreline within the study area. Horizon A (Figure 3.71b) included shallow features areas that are interpreted as local highs separated by channels or inlets. Figure 3.72 shows Horizons P (3.72a) and B (3.72b). In Horizon P (Figure 3.72a) elongated, E-W shallow structures are interpreted as being cut by inlets and channels. A large shallow area is present in the western part of the survey area. Horizon B (Figure 3.72b) includes large flat areas.

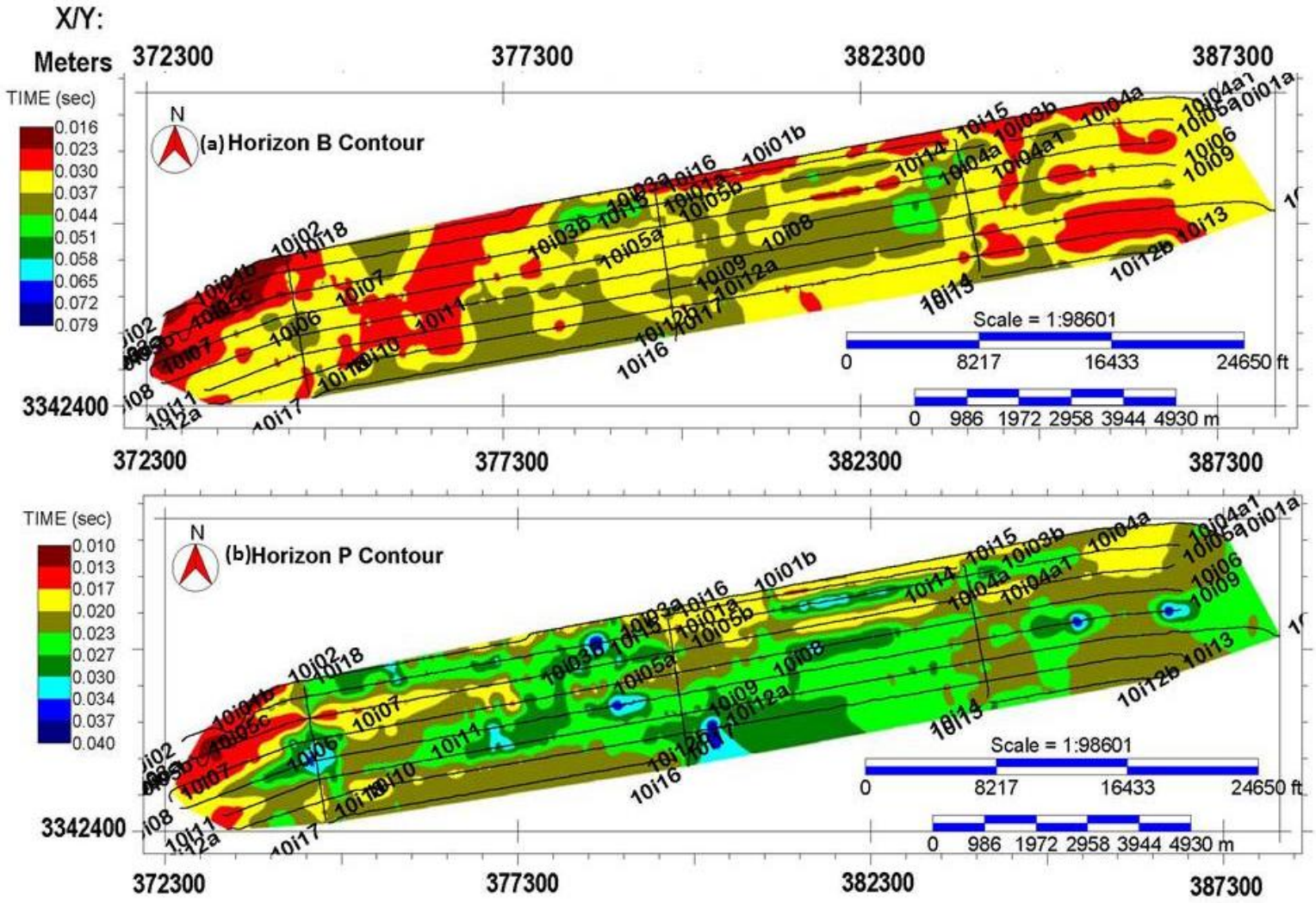

Figure 3.71 Contours for each horizon (seafloor, Horizon A, Horizon P, and Horizon B) were generated to illustrate the terrain at the time when these horizons were deposited. (a) Horizon B (acoustic basement)" is interpreted as largely flat terrain; (b) Sediments below Horizon P (Pleistocene) are interpreted as forming landforms that are elongated in an east-west direction similarly to the present-day island shoreline. There is a suggestion of an inlet passes between high elevation areas.

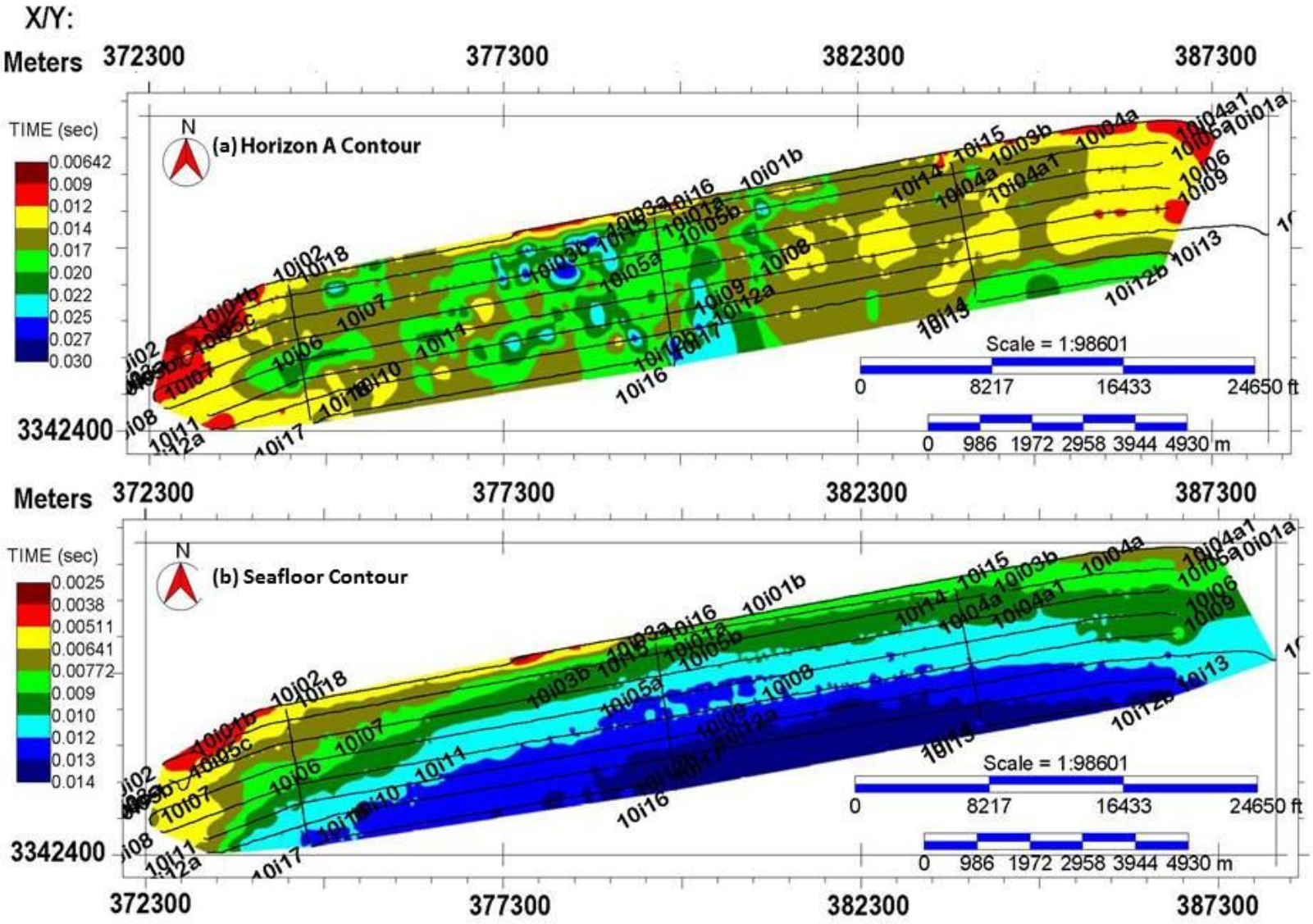

Figure 3.72 (a) Horizon A is interpreted as areas of intermittent high and low relief; (b) Present-day seafloor horizon is seen to gradually dip towards the south.

These findings were compared to aerial imagery to determine the influence of the channels on storm breach location.

3.2 Aerial Imagery

Aerial and satellite imagery were combined with hand-drawn maps to characterize historical breaches and the morphology of Dauphin Island. A 1718 hand drawn French map is the earliest record of Dauphin Island (Figure 3.73) in this study. In 1718 the island was the largest within the NGOM (Byrnes et al., 2010). An 1852 map (Figure 3.74) shows the 1848 breach that created Petit Bois Island. The island was breached again in 1916 by another hurricane system (Figure 3.74). This gap was later closed.

Figure 3.73 A 1718 hand drawn French map of the NGOM when Dauphin Island (Ille Dauphine) was a single entity. The 1848 hurricane separated the western spit into Petit Bois and Dauphin Island.

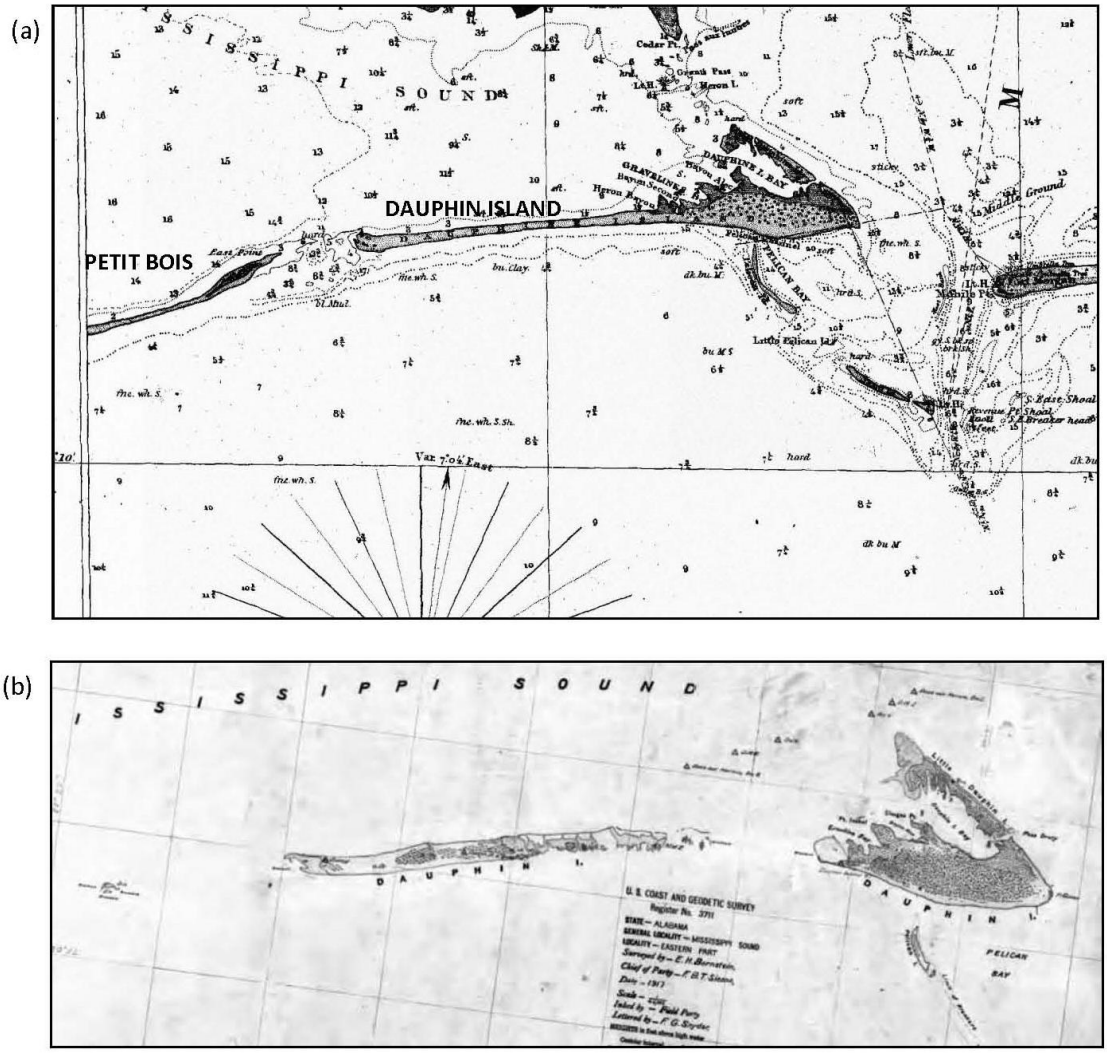

Figure 3.74 (a) 1852 Navigation chart showing the breach created by the 1848 hurricane that separated the western spit of *Ill Dauphine* into two islands, Petit Bois (west) and Dauphin Island; (b) 1916 Navigation chart showing the devastation caused by a 1916 hurricane system. The island replenished the breaches in (b) overtime through longshore transport.

Changes in shoreline and island morphology are clearly seen in different generations of aerial imagery from Google Earth (Figure 3.75). Over the 1992 to 2000 time period the ephemeral Pelican/Sand islands are seen to become more clearly defined as two islands, despite hurricane systems having limited effect during this period.

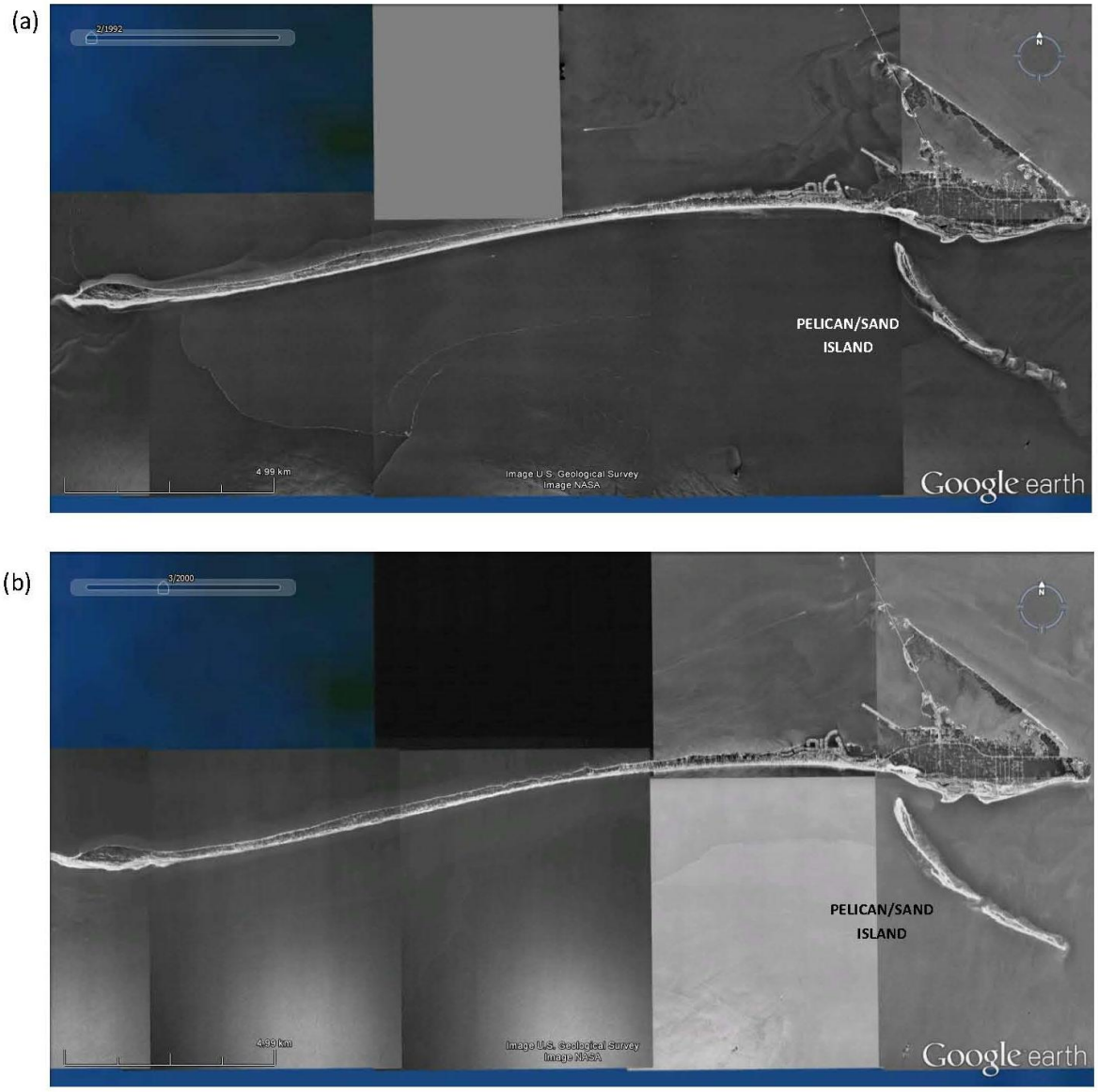

Figure 3.75 (a) A February 1992 Google Earth image shows no inlets or overwash on the northern shore of the island. Pelican/Sand Island displays morphological changes compared to the more elongated portions of Pelican Island towards the southeast in the lower (b) image from March 2000.

Overwash during Hurricane Ivan created inlets in the western spit of Dauphin Island (e.g. Ivan Inlet in Figure 3.76a). This area, weakened by this major hurricane, was not able infill before Hurricane Katrina hit in 2005. Hurricane Katrina exploited the Ivan Inlet area, created a 1.5 mile breach (Katrina Cut; Figure 3.76b). Aerial imagery from 2012 (Figure 3.77) shows Katrina Cut still open and the full amalgamation of Pelican/Sand Island to Dauphin Island. It is clear that

these two major hurricane systems resulted in rapid and major morphological changes over a short period.

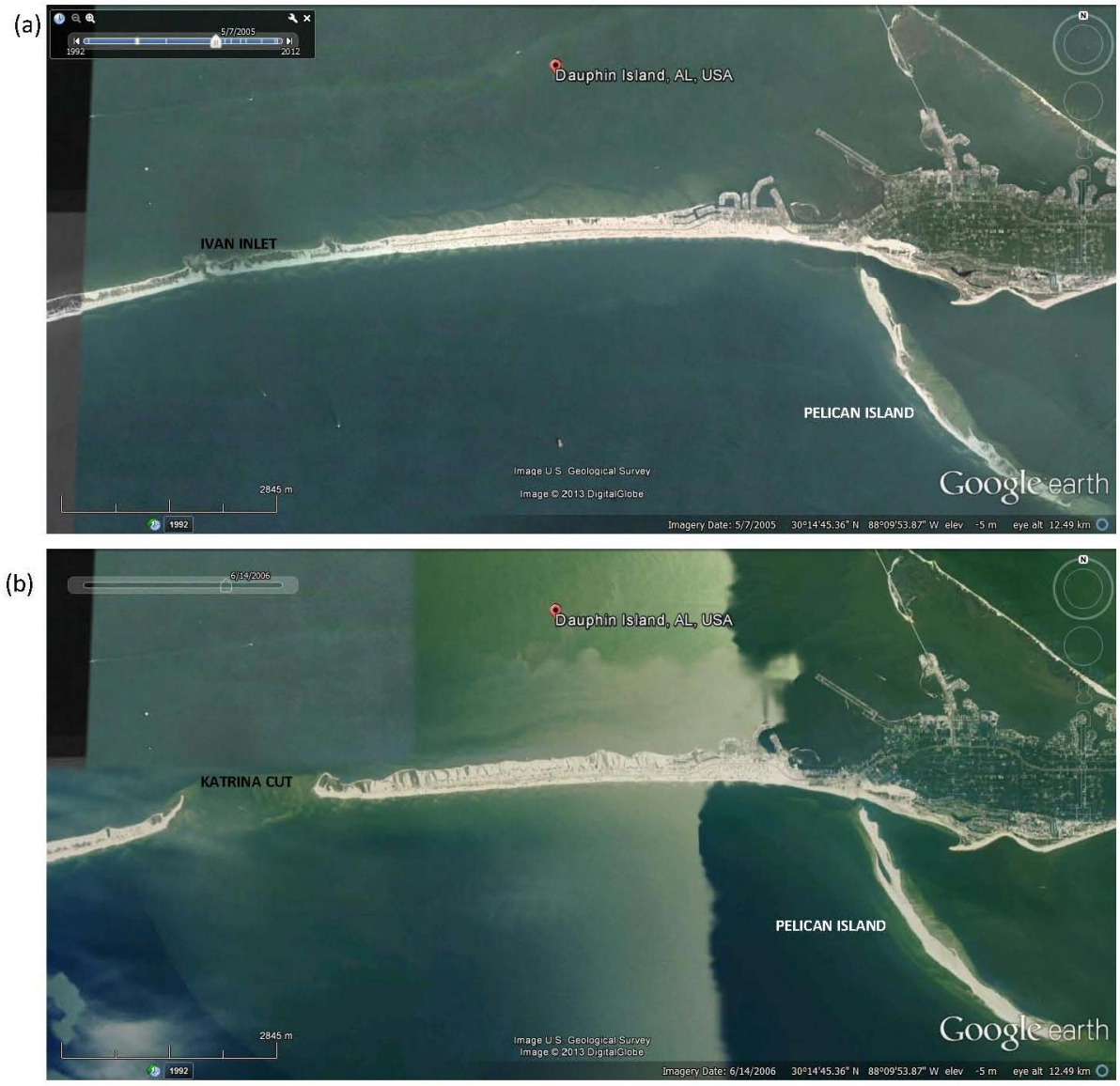

Figure 3.76 (a) May 2005 image displays a partially submerged small breach a few months after Hurricane Ivan but prior to Hurricane Katrina. (b) A June 2006 image following Hurricane Katrina. Both breach locations are in the same vicinity. The ephemeral Pelican Island has migrated north towards Dauphin Island as seen in the 2006 image (b). This migration has limited the amount sediment from littoral drift that traveled through the pass between the Dauphin and Pelican islands. This would slow the rate of recovery from a storm on the island.

Figure 3.77 A Google Earth Satellite Image from January 2012 showing the amalgamation of Pelican Island with Dauphin Island. Katrina Cut remains but the gap is closed artificially with rip-rap connecting the east and west ends of the breach.

3.3 Lidar

The Lidar data were obtained from the NOAA Coastal Services database. Analysis of these data took into account inconsistencies between the data collected by different agencies. As an example, the USGS dataset collections in this study extend along the entire NGOM from Florida to Louisiana. The point clouds are less dense in order to cover the area and contain lower vertical resolutions. In contrast The USACE data cover a smaller area and have a greater density of points and better vertical resolution. Some datasets include buildings and residential areas, while in others these areas have been masked. These inconsistencies must be taken into account when analyzing the data within the figures 3.78 through 3.80.

(a)

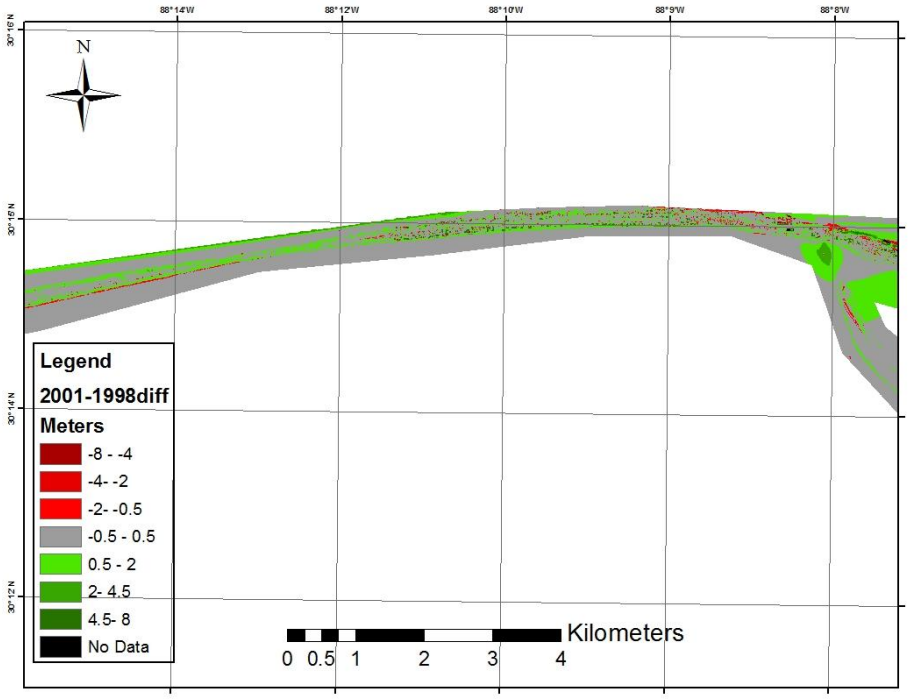

2001 – 1998 Difference Dataset

(b)

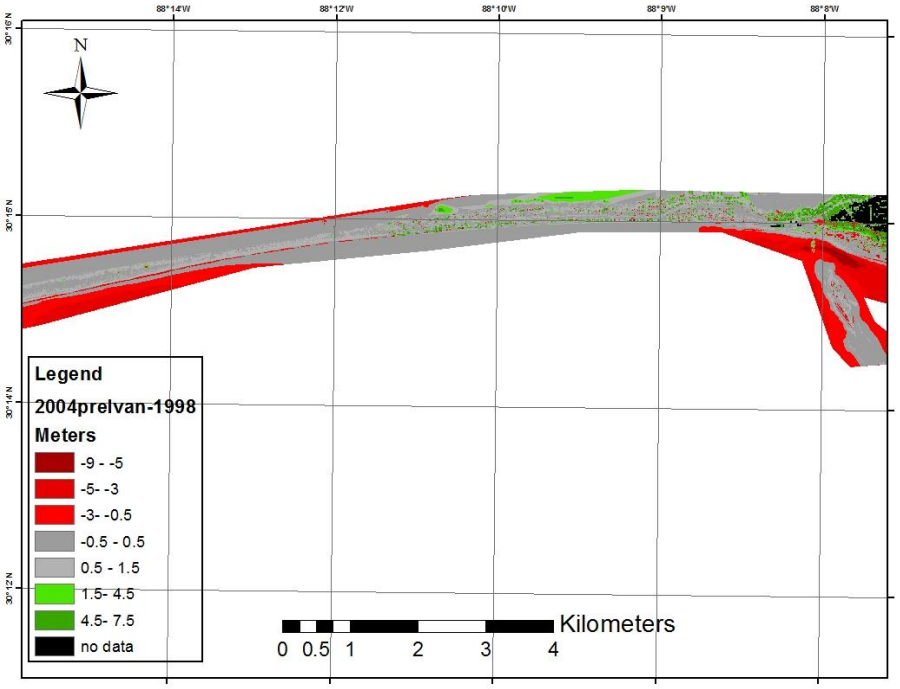

2004 – 1998 Difference Dataset

Figure 3.78 Lidar datasets were interpolated then residuals calculated for different time periods to show deposition and/or erosion on Dauphin Island, AL. The central area of the island was enlarged in these images to show the area of the most recent hurricane breach from Hurricane Katrina in September 2005. (a): A residual between the 1998 and 2001 dataset shows deposition throughout the island, with some erosion along the gulf shoreline. During this time only one storm system, Tropical Storm Allison (2001) impacted the Island. (b) Residual between the 2004 pre-Hurricane Ivan and 1998 shows erosion in the inlet between Pelican Island and central Dauphin Island.

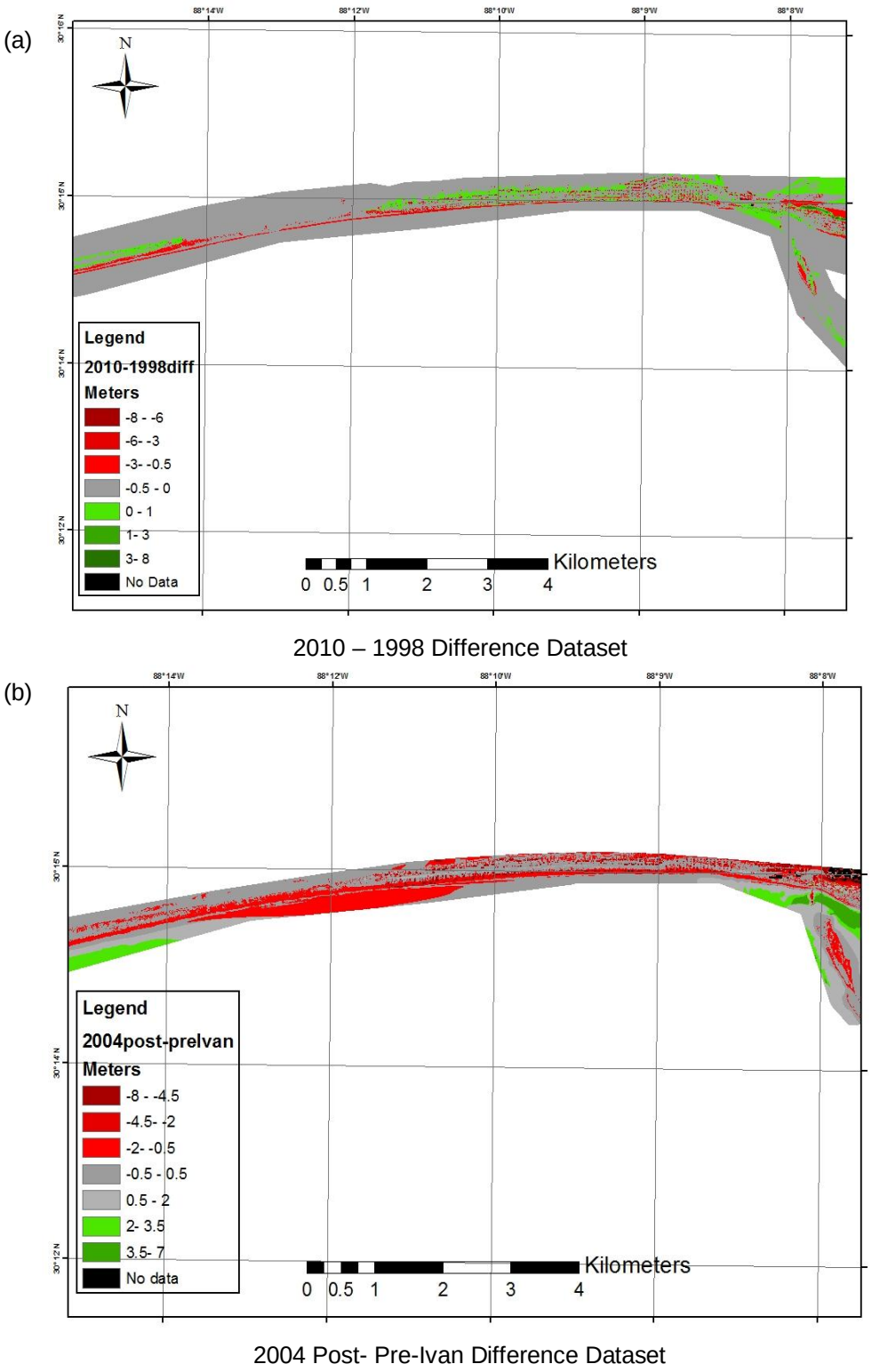

Figure 3.79 (a) Residual for the 2010 and 1998 Lidar data shows the amalgamation of Pelican and Dauphin Island, the hurricane breach area, and deposition from the rollover of the island to the north. (b) Residual for the pre and post hurricane data sets in 2004. The majority of the deposition occurred in the pass between Pelican and Dauphin Island. Erosion is seen in the central portion of the spit.

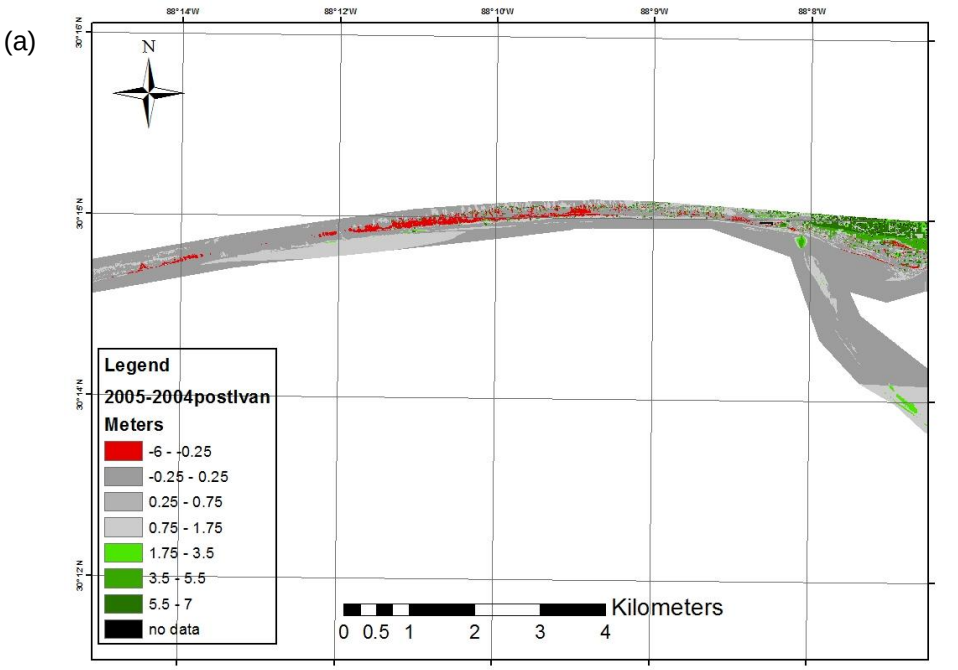

2005 – 2004 Post Ivan Difference Dataset

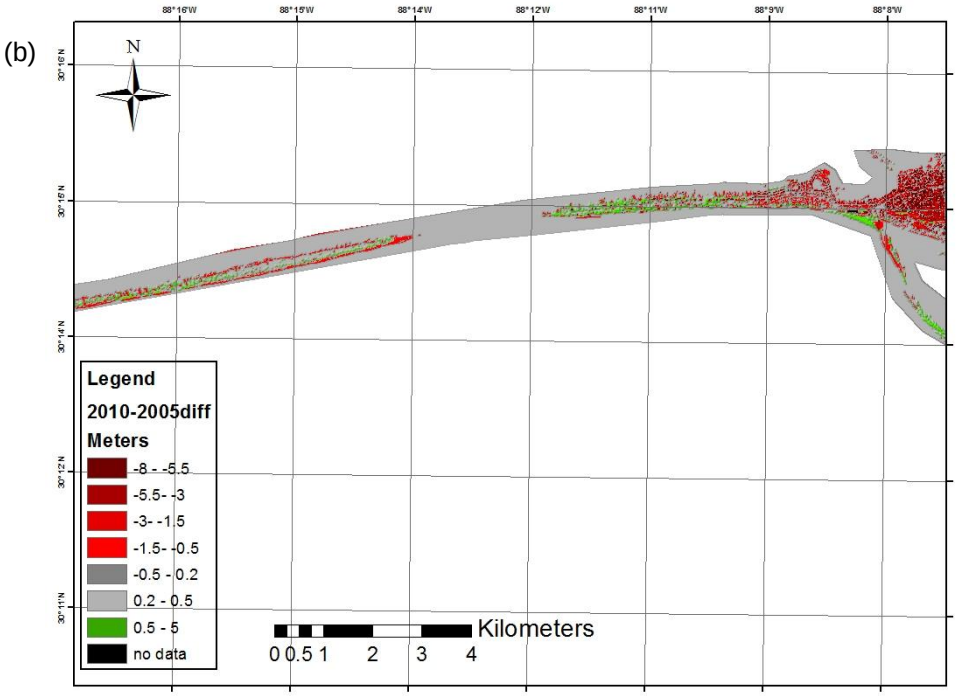

2010 - 2005 Difference Dataset

Figure 3.80 (a): Residual of the 2005 post-Hurricane Katrina and 2004 post-Hurricane Ivan Lidar datasets. Most erosion is seen within the spit of the island where the current storm breach is located. (b) Residual of the 2010 and 2005 post-Hurricane Katrina Lidar datasets. Minimal direct hits from hurricane and strong storm systems occurred within this time period. Little deposition and erosion is seen within the data. The amalgamation of Pelican and Dauphin Island has occurred and is seen as deposition within the inlet between the ephemeral and barrier island.

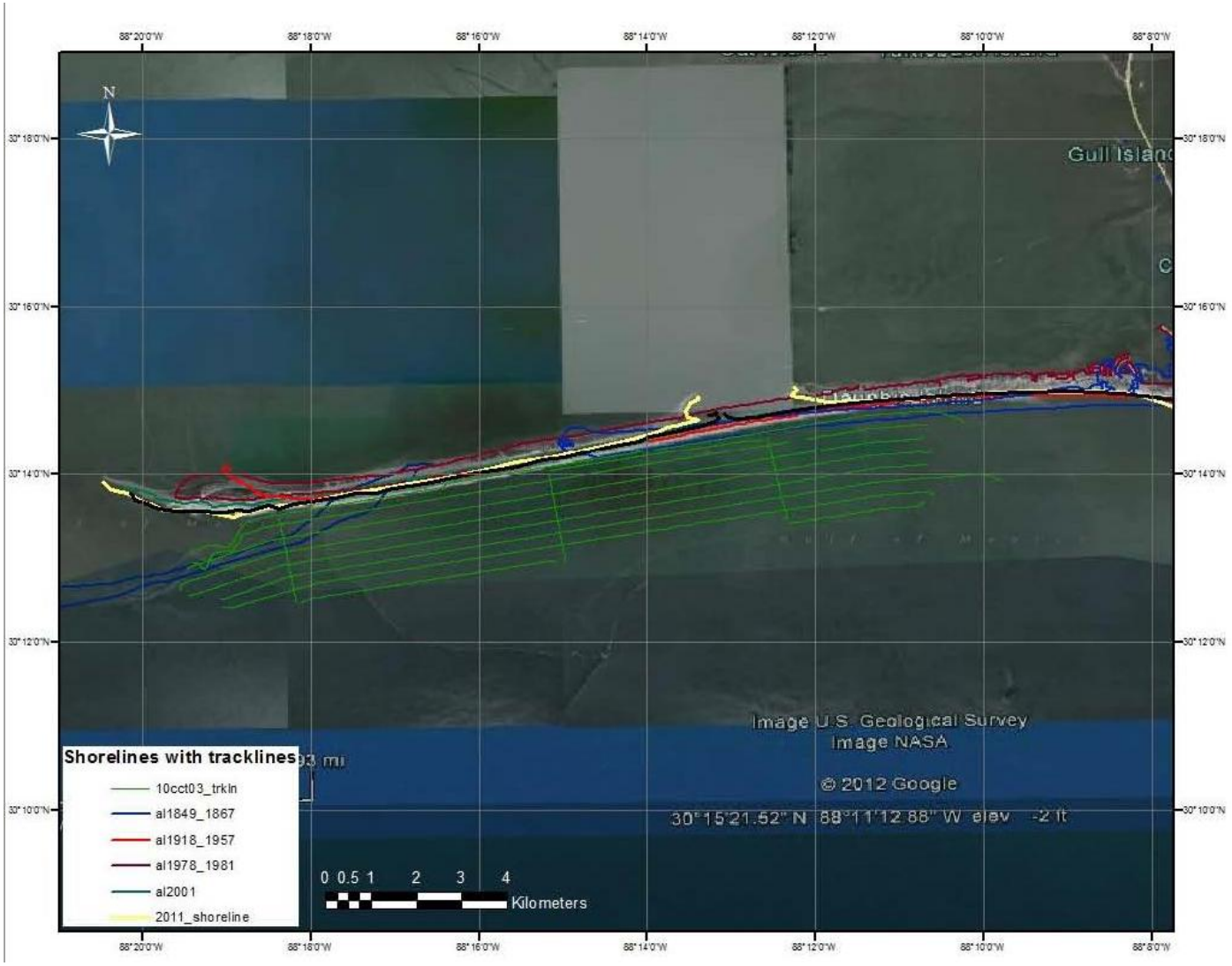

Figure 3.81 CHIRP 2-D seismic reflection survey lines were overlain on an aerial image of the study area. Digitized shorelines (time periods ranging from 1917 to 2011) were used to show shoreline evolution throughout time. This evolution includes progradation to the west, migration to the north/northwest, and the creation of Katrina Cut.

Coastline files were used to locate historical barrier island breaches (Figure 3.81). A calculation of the difference between the 1998 and 2001 Lidar datasets clearly shows erosion of Dauphin Island (Figure 3.82a). During this time period there was little storm activity within the NGOM. Deposition within the Pelican Pass between Dauphin Island and the ephemeral Pelican Island is apparent. Deposition to the north of the island implies island rollover. Much of the remaining area shows little to no deposition or erosion (gray in Figure 3.82). Between 1998 and the spring of 2004 (pre-Hurricane Ivan; Figure 3.83b) there were no hurricane systems in the area. Erosion is seen around Pelican Island, Pelican Pass, and the Gulf of Mexico shoreline of Dauphin Island.

The residual between the 1998 and 2010 datasets (Figure 3.84a) shows deposition within Pelican Pass and the amalgamation of Pelican Island and Dauphin Island. Rollover of the spit to the north is apparent as the Gulf of Mexico shoreline erodes and sediments are deposited on the Mississippi Sound shoreline (Figure 3.84b). The time period spanning Hurricane Ivan in 2004 (Figure 3.85) includes erosion along the Gulf of Mexico side in central Dauphin Island and within the central portion of Pelican Island. Deposition is seen within Pelican Pass, east of Pelican Island, and at the western end of Dauphin Island.

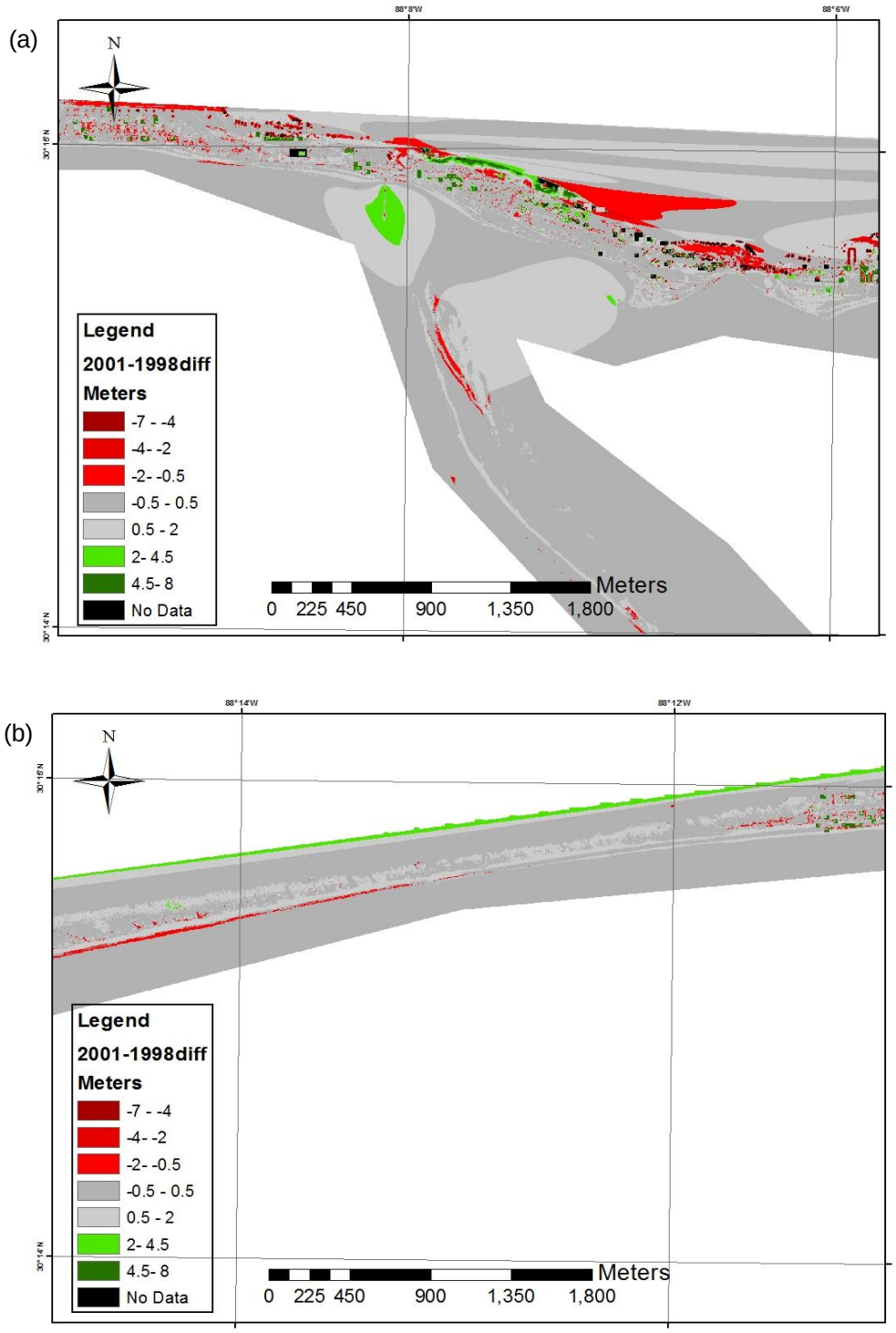

Figure 3.82 (a) The residual between the 1998 and 2001 LIDAR images in the vicinity of Pelican Pass shows deposition (green) within the pass and erosion (red) along the eastern side of Pelican Island. The depositional area seen in this area correlates with the present-day fishing pier and serves as an area for deposits to build and accrete onto. Overall the Pelican Pass area had minimal to no erosion or deposition (gray areas). (b) An enhanced view of Katrina Cut shows primarily erosion along the south shoreline and deposition along the north shoreline. Deposition along the north and erosion along the south implies island rollover and migration to the north.

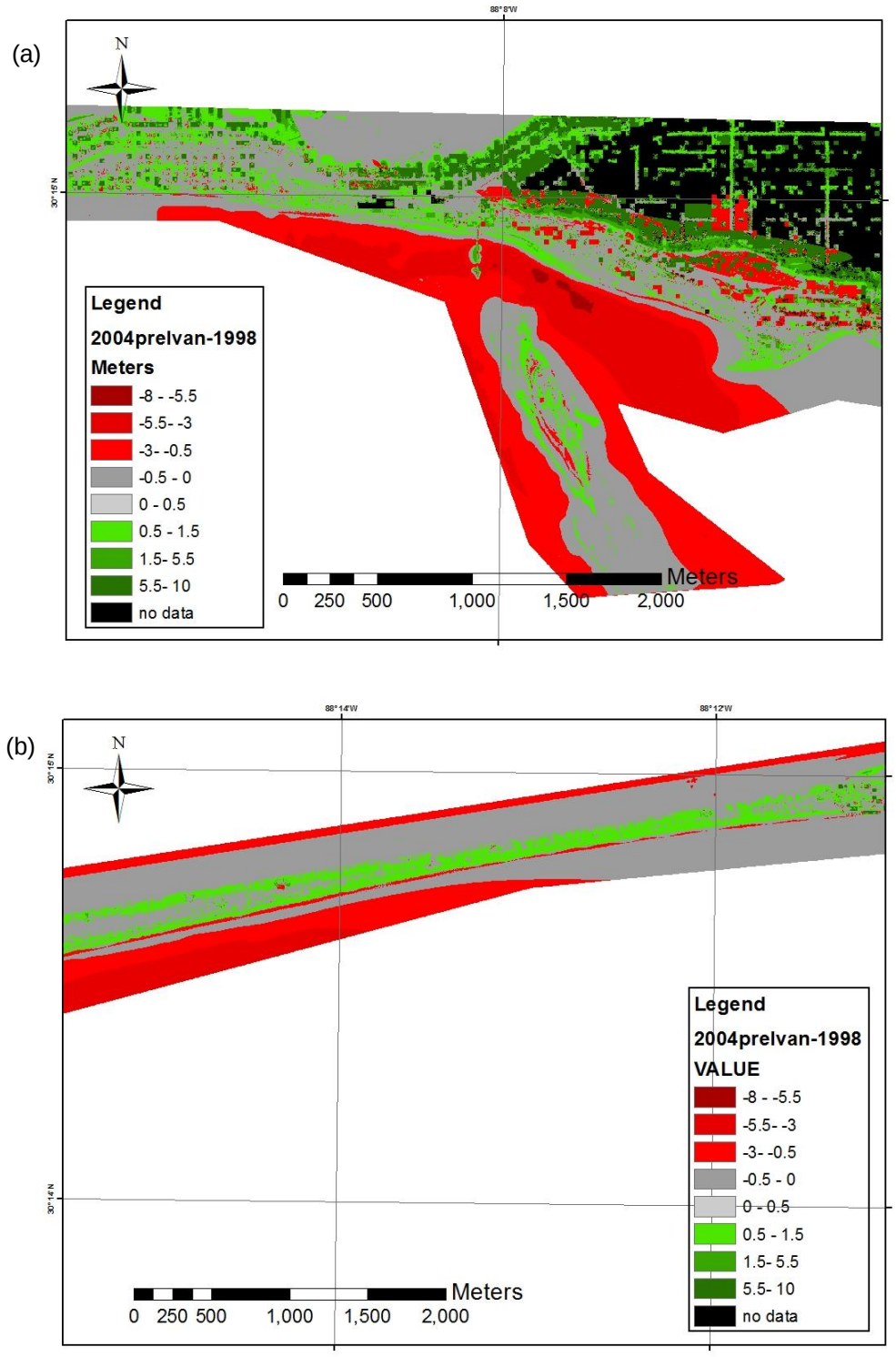

Figure 3.83 (a) The Pelican Pass region in 1998 and pre-Hurricane Ivan residual shows primarily erosion. Depositional or areas of little erosion or deposition are located along the central portions of the island. Although no hurricane systems affected Dauphin Island directly during this time, the dataset could have potential elevation errors from the collection method that created the erosional areas. (b) During this time the Katrina Cut region is characterized by erosion.

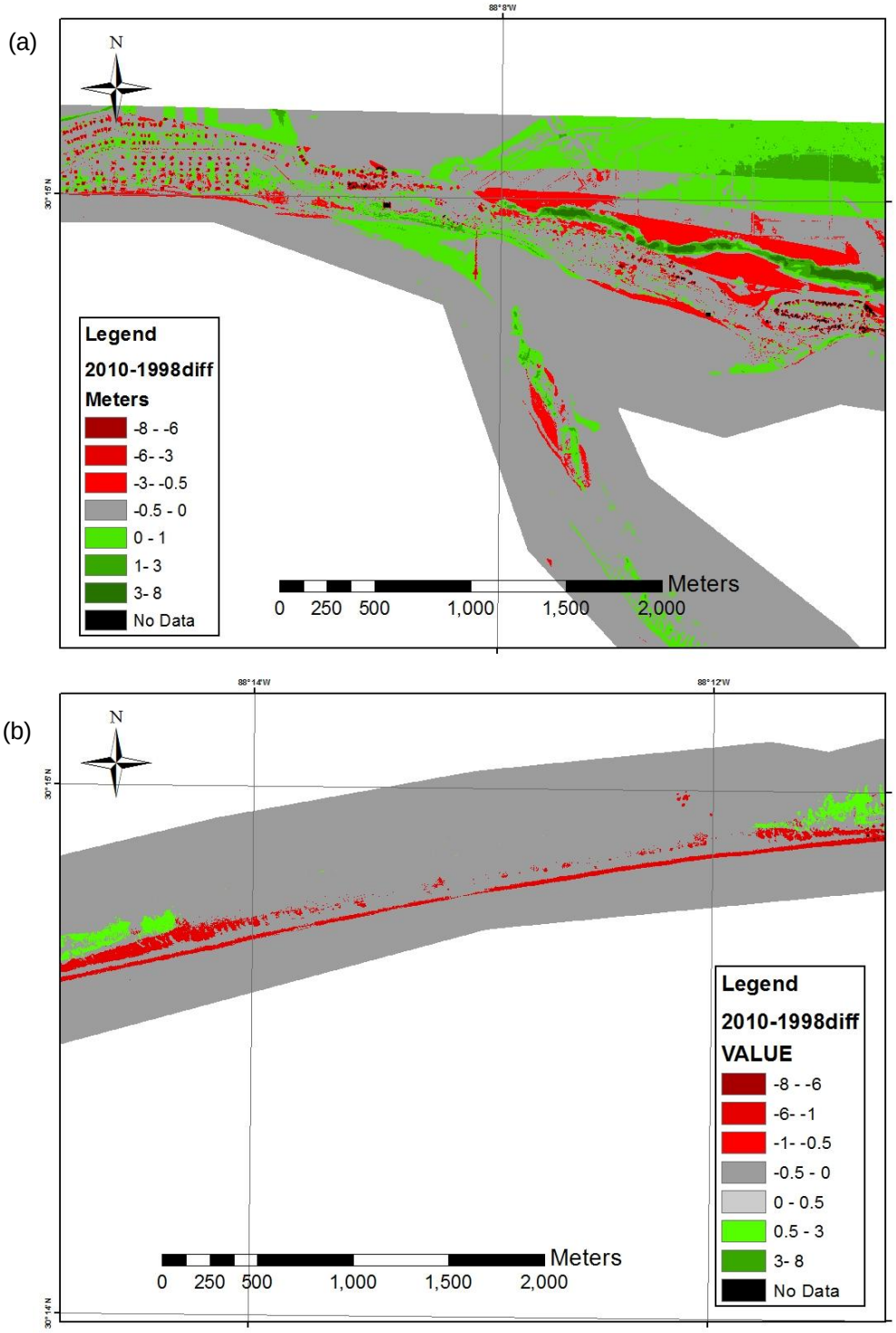

Figure 3.84 The residual between the 1998 and 2010 datasets for (a) Pelican Pass and (b) Katrina Cut. (a) Pelican Pass is characterized by deposition where the amalgamation of Pelican Island has occurred during this time span. (b) The breach from Hurricane Katrina in 2005 is seen in this figure. Hurricane Katrina made landfall in western Mississippi directly to the west of Dauphin Island creating a 2500 m breach.

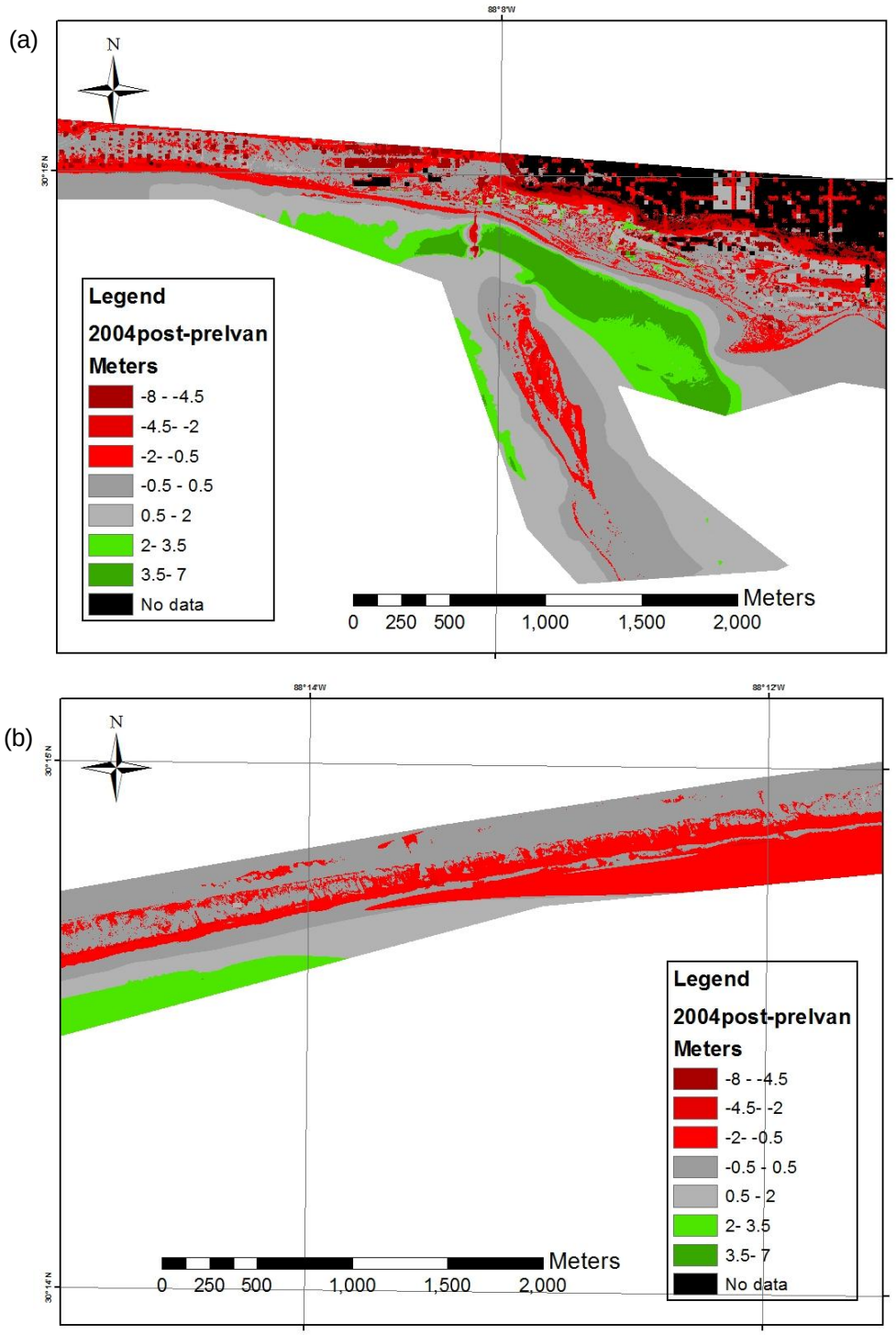

Figure 3.85 The residual between the pre- and post-Hurricane Ivan (2004) dataset shows deposition and erosional in the vicinity of (a) Pelican Pass and (b) Katrina Cut. (a) A large depositional volume is seen in Pelican Pass and along the west side of Pelican Island. The subaerial portion of the island shows erosion. (b) Katrina Cut is an area of high erosion where the breach is located. This area experienced extensive overwash but did not submerge below sea level until it was further eroded by Hurricane Katrina.

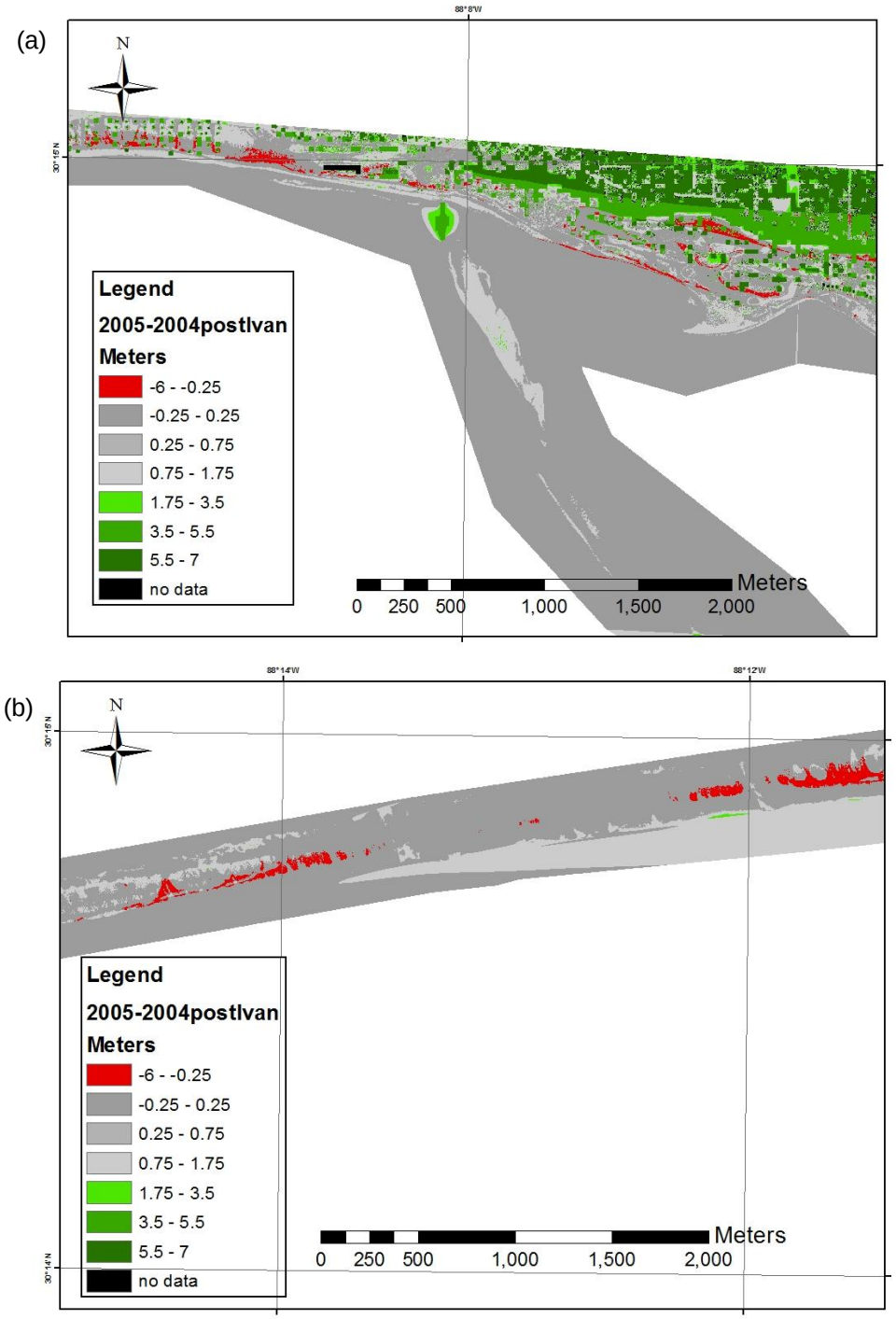

Figure 3.86 (a) The residual between the Hurricane Ivan (2004) and Hurricane Katrina (2005) datasets shows deposition within Pelican Pass and some erosion along the gulf shoreline of Dauphin Island. (b) The residual for Katrina Cut clearly shows erosion and the 2500 m gap created by Hurricane Katrina.

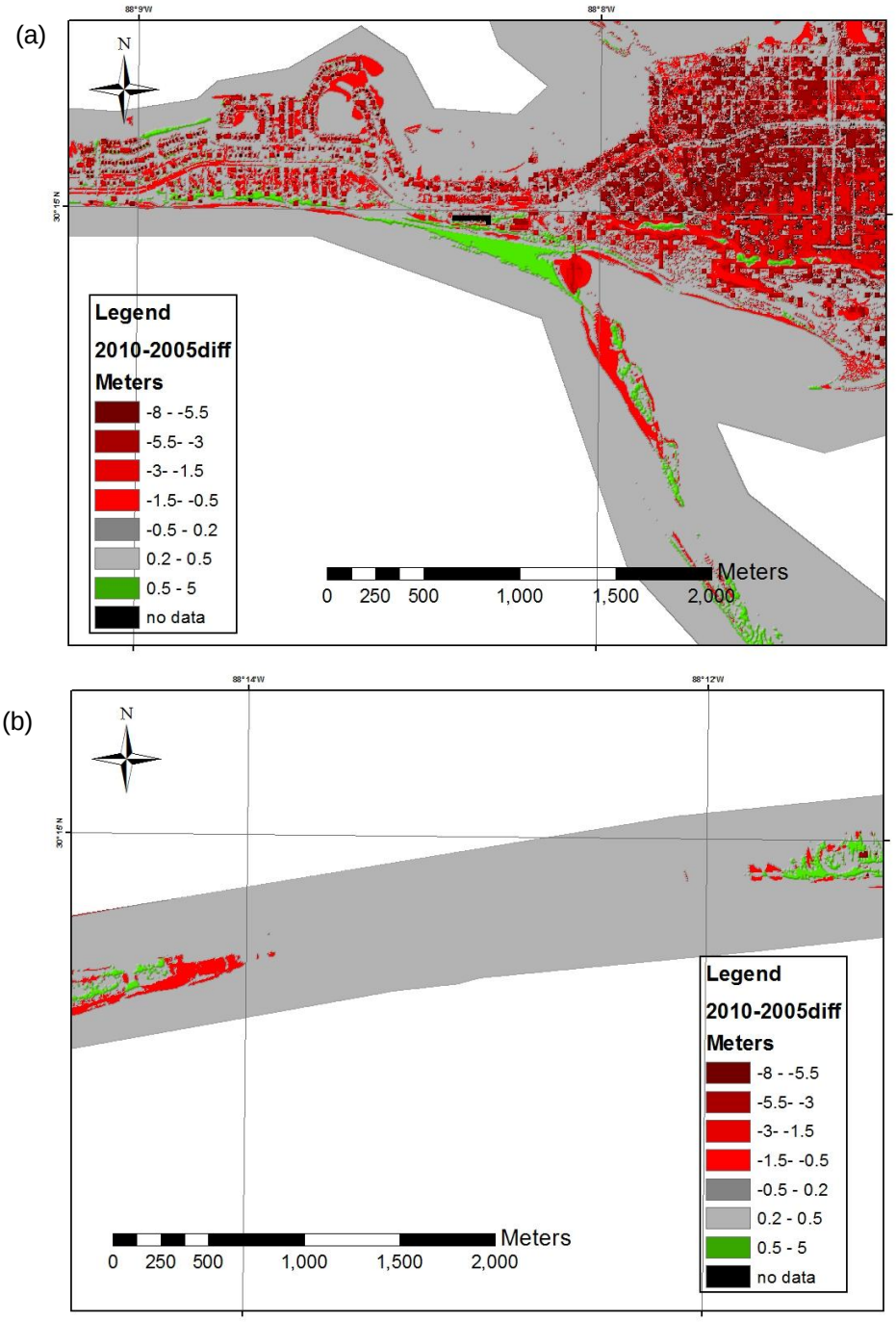

Figure 3.87 The residual between the post-Hurricane Katrina (2005) and 2010 datasets for (a) Pelican Pass and (b) Katrina Cut. (a) Deposition is seen in Pelican Pass. Some area of Pelican Island experienced erosion. These erosional areas may be lagoonal areas that have developed since the amalgamation of Pelican Island. (b) The Katrina Cut area experienced deposition along the north shoreline and erosion along the gulf shoreline due to the migration of the Dauphin Island to the northwest.

The post Hurricane Ivan (2004) to post Hurricane Katrina (2005; Figure 3.86) data show continued erosion along the central Gulf of Mexico coastline of Dauphin Island (Figure 3.86b). This is also the location of Katrina Cut. Little deposition is evident along the elongated spit shoreline. Deposition is seen along the eastern portion of Dauphin Island (Figure 3.86a). The post-Hurricane Katrina time period (2005 to 2010; Figure 3.87) is one of little storm and hurricane activity, with some erosion along the eastern portion of the island. The deposition seen on the north side of the island, and within Pelican Pass, is again evidence of gradual island rollover through natural affects from tidal, current, and wave activity.

4.0 DISCUSSION

Channel structures, formed by river systems present during Late Pleistocene and Early Holocene periods of low sea level when the coastline was further south and closer to the continental shelf break (Otvos, 1970, 1985; Byrnes et al., 2010; Figures 3.71 and 3.72), are clearly seen in the 2-D seismic reflection data profiles. As sea level rose, these river systems were infilled with lagoonal, barrier, and marine deposits (Otvos, 1985; Nordfjord, 2006). As the rate of sea level began to oscillate during the Holocene, (Otvos, 1970; Kindinger, 1988; Parker, 1993; Byrnes et al., 2010) the deposits and incised valleys on the Mississippi-Alabama shelf were buried during high stands and eroded and reworked during low stands. These channel locations are well correlated with historical barrier island breaches (Figures 3.82 through 3.84).

Unlike the eastern portion of the island that has been consistently above sea level during the period of channel formation (Otvos, 1985; Cipriani and Stone, 2001; Byrnes et al., 2010), the lower elevation western spit is more susceptible to breaches, overwash, and rollover (Figure 1.4). Lack of vegetation exacerbates this issue (Morton, 2004). Examination of the locations of the channels identified in the 2-D seismic reflection data and correlation with former shorelines

shows that the channels correlate well with the 1852 Petit Bois breach, the 1917 hurricane breach, and the 2004/2005 Hurricane Ivan and Hurricane Katrina breaches (Figures 3.76 thru 3.79). This is strong evidence that channel locations may have a direct impact on breach location. Though beyond the scope of this study, it is hypothesized that this is due to differential subsidence. In more recent times, this effect may be amplified by anthropogenic effects (e.g. dams, shoreline restoration, beach renourishments, groins, and seawalls) and a change in sediment supply due to the amalgamation of Pelican and Sand islands. Although the littoral drift of the NGOM flows to the west, in the last ten years there has been isolated reversal in drift, separate from the littoral drift, directly to the west of Pelican Island (Cipriani and Stone, 2001). This may also impact the ability of the island to recover today. Along with the longshore drift, deposits from Mobile Bay (silts, clays, and fine sediments; Otvos, 1985; Byrnes et al., 2010) travel west and are deposited within the study area (Hummel, 1999), infilling breaches and the relict structures with very fine to fine grained sediments which would account for subsidence within the valleys. While the western spit is more prone to morphological changes, the eastern portion of Dauphin Island is more stable with vegetated areas and abnormally high dunes (4 to 5 m dunes) compared to the remaining NGOM islands (Byrnes et al., 2010). The stability of east Dauphin Island provides a core for the spit to prograde laterally to the west. As the spit progrades westward due to littoral drift, the channels and breaches are infilled.

The contours created for each horizon describe different geologic settings. Flocks et al. (2009) cores places Pleistocene deposits at 10 to 20 m depths. Horizon P in this study falls within this depth range and is interpreted as a potential Pleistocene horizon. No core samples within the study area were found to establish an estimated time span for Horizons A and B. Horizon B is the deepest interpreted horizon in the CHIRP data. The contours of Horizon B

(figure 3.71a) are interpreted as a low-lying fluvial environment with minimal relief. Meandering streams and rivers within this flow plain are evident from the channel structures interpreted in the seismic profiles. River valleys, interpreted from a compilation of geophysical methods (e.g. Flocks et al., 2009), show river systems reaching farther offshore on the Mississippi-Alabama continental shelf (e.g. Figure 1.2 and Figure 4.1).

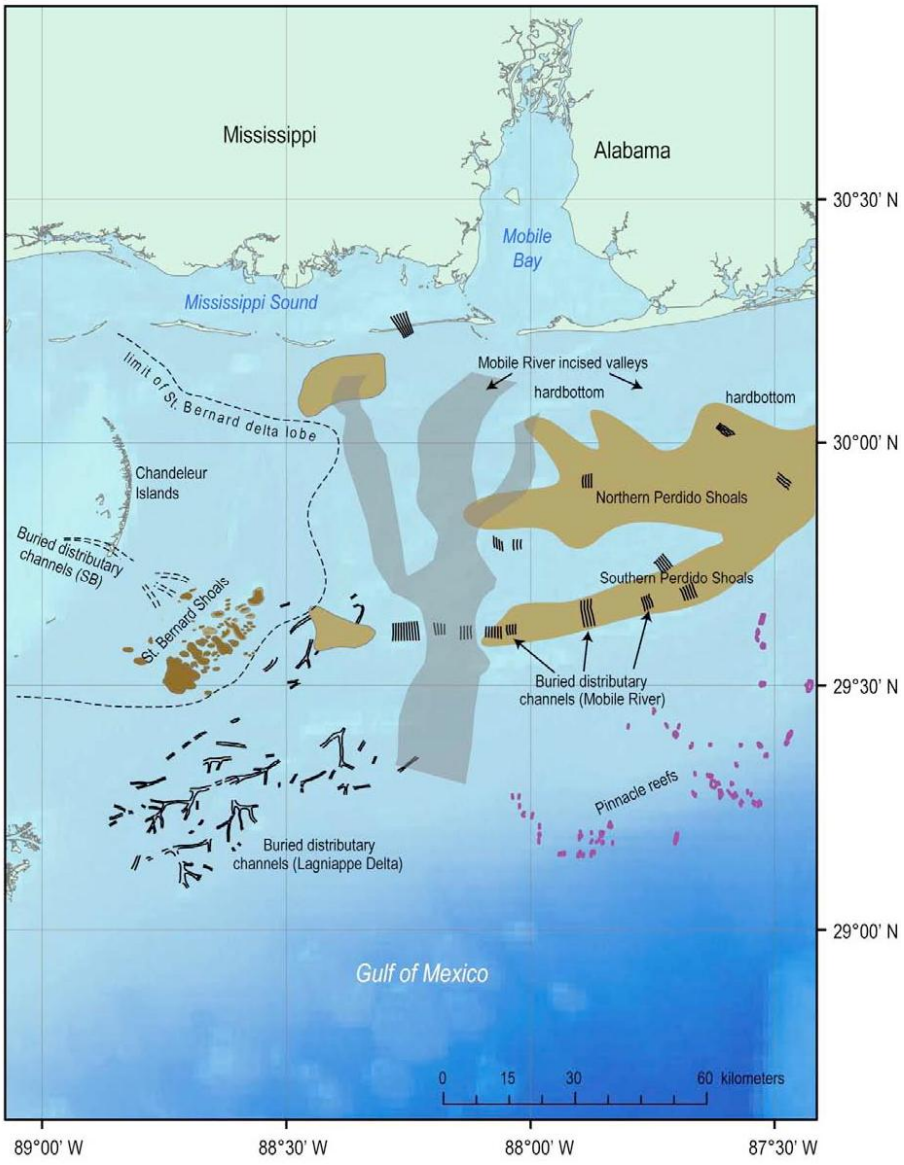

Figure 4.1 The Flocks et al. (2009) study of sand sources for beach nourishment shows river systems, shoals, and distributaries from a compilation of studies of the Gulf of Mexico continental shelf. These structures were created when sea level was approximately 160 m lower than present-day. As sea level rose these structures were flooded. Shoals and sand sheets preserved the valley systems within the subsurface.

Horizon P (Figure 3.71b) is interpreted as the Pleistocene surface (e.g. Flocks et al., 2009). The shoreline during this time was located near todays NGOM shelf edge approximately 120 m below present day sea level (e.g. Figure 1.2; Flocks et al., 2009; Donoghue, 2011). The features interpreted in the contours are elongated high elevations that could be relict lagoonal islands. At this time the Mobile River system had cut through the shelf and coastal-plain environments stretched to the mid-shelf (Figure 4.1; Kindinger et al., 1994). These local highs may have provided the platform for the development and migration of the NGOM islands.

Horizon A (Figure 3.72a) is interpreted as having several high areas at the edges of the survey area with low elevations towards the center. The interpretation of Horizon A is that the higher elevation areas are relict island structures. The time span following Horizon P includes the Early Holocene where the rate of sea level change varied drastically in response to melting ice sheets (Donoghue, 2011). The irregular shapes and locations of the high areas seen in Horizon A could be a result of reworked island structures (Figure 3.71b). The wave and tidal action from the sea level variations could create a high energy environment where deposits would not settle in one area. The barrier islands would develop in a more eustatic environment where the sediments would have time to prograde and develop an island (Kindinger et al., 1994). The higher elevation points at the northwest and northeast portions of the survey in Horizon A could be evidence of the decrease in rate of sea level rise where sediments would deposit and become subaerial. These areas are closer to present day Dauphin Island shoreline.

The seafloor horizon (Figure 3.72b) is interpreted as a steady slope towards the gulf.

The results from the Lidar study clearly quantify the magnitude of erosion and deposition from 1998 to 2010. Even though more intense hurricane systems occurred in the 1800s and the early to mid-1900s (NOAA Hurricane Database), hurricane systems within the last

century have impacted Dauphin Island. Figures 3.78 to 3.80 illustrate the amount of erosion and deposition on the island, while figures 3.81 to 3.87 are focused on the Pelican Pass and Katrina Cut areas. Figure 3.73 shows the difference between the earliest datasets, 1998 and 2001. Minimal erosion and deposition occurred during the two-year span. The residual map for the 1998 to 2004 (pre-Ivan) period shows a total erosion volume of 24,217632 m^3, with the most significant portion in Pelican Pass (Figure 3.81a) and in the westernmost portion of the figure. Deposition volume was a total of 15,006,244 m^3. During this time, few strong storm systems impacted Dauphin Island. It is thus interpreted that the amount of erosion and deposition calculated is primarily a result of littoral drift and longshore transport. The magnitude of this sediment supply has decreased in modern time (Cipriani and Stone, 2001; Morton, 2004; Byrnes et al., 2010), resulting in greater erosion than deposition as seen in the comparison of the volumes. The residual map (Figure 3.79b) spanning Hurricane Ivan shows a large amount of deposition in Pelican Pass (Figure 3.84a), and erosion in the vicinity of Katrina Cut (Figure 3.84b). The same areas affected during the storm surge from Hurricane Ivan were affected during Hurricane Katrina (Figure 3.80a). Although there is only a year time span between the two storms, the areas previously affected by Ivan are further impacted by Hurricane Katrina. The pre- and post-Hurricane Ivan residuals indicated a study area net loss of 9,926,907 m^3. Locally a net gain of 8,615,858 m^3 was calculated within Pelican Pass and a net loss of 6,322,467 m^3 was calculated within the Katrina Cut area. A net gain of 2,926,442 m^3 was calculated along the Gulf of Mexico shoreline. The post-Katrina and Ivan residual dataset show a net loss of 687,464 m^3 within Katrina Cut (Figure 3.85b) and a total gain of 133,292 m^3 along the Gulf of Mexico shoreline, including Pelican Pass (Figure 3.85a). The erosion and deposition from Hurricane Ivan are much greater when compared to the volumes resulted by Hurricane

Katrina. Although Hurricane Katrina resulted in a greater morphological impact, Hurricane Ivan contributed more to the erosion and deposition of Dauphin Island. The location and strength of these two hurricanes impacts the amount of erosion and deposition because of the effects of the tide, wind, and surge intensified by the hurricanes. As Pelican Pass closed, deposition was not as voluminous along the Gulf of Mexico side of the spit. Little to no storm systems occurred or directly affected the area during the five-year time span between 2005 and 2010 (Figure 3.80b). During this time period littoral drift and longshore transport were the dominant factor in natural deposition and erosion.

Byrnes et al. (2010) studied sediment transport and budget for Dauphin Island along the Alabama coastline from the 1917/20 to the 1986/2002 time periods. Mobile Navigation Channel is located between the easternmost point of Dauphin Island and the westernmost point of Morgan Peninsula (labeled as Fort Morgan in Figure 1.1). Net deposition west of the channel and bypassing Pelican Island was calculated to be 144,000 cubic m/yr of sediment. This aided in closure of the 1916 breach (Byrnes et al., 2010). The time span of the model included minimal hurricanes affecting Dauphin Island and concludes before Hurricane Ivan. The study illustrates the natural process of deposition/erosion from longshore transport. Storm systems generally moved sediment from the ebb-tidal delta to the north-northwest before depositing sediments on Dauphin Island producing in the volume necessary to sustain the island and nourish storm breaches, overwash inlets, and potentially progradation to the west.

A comparison between the effects of Hurricanes Ivan and Katrina shows that there was less erosion and deposition from Hurricane Katrina than from Hurricane Ivan. This is despite the qualitatively greater physical morphological change seen in the post-Katrina 2005 lidar (Figure 4.2). Katrina Cut in the post-Hurricane Ivan 2004 dataset (Figure 4.2b) has clearly been impacted

with overwash, reducing relief and creating a small inlet. Hurricane Katrina further eroded this area, creating a 2500 m channel across the island spit (Figure 4.2a). Further, this area is clearly correlated with an ancient river channel as seen in the CHIRP 2-D seismic reflection data.

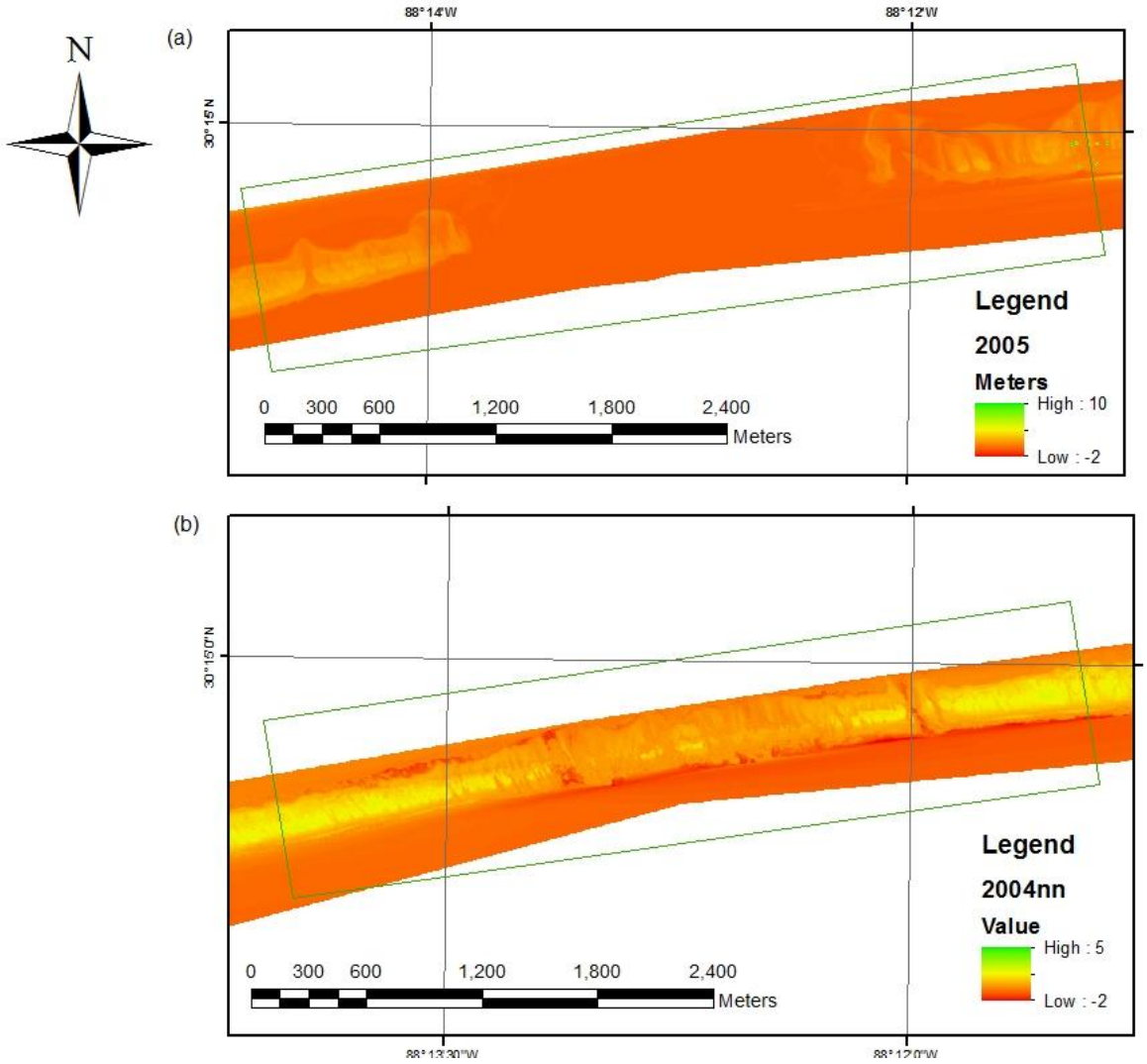

Figure 4.2 Comparison of 2004 post-Hurricane Ivan and 2005 post-Hurricane Katrina images of the Katrina Cut area (green polygon): (a) 2005 post-Hurricane Katrina shows very extensive erosion within Katrina Cut. (b) The 2004 post-Hurricane Ivan data show a large amount of overwash within the area eroded in 2005.

Similarly, the channel systems in Horizon A (Figure 4.3) show a correlation to the 1850 and 2005 hurricane breaches. Horizon P (Figure 4.4) has similar channel systems to Horizon A.

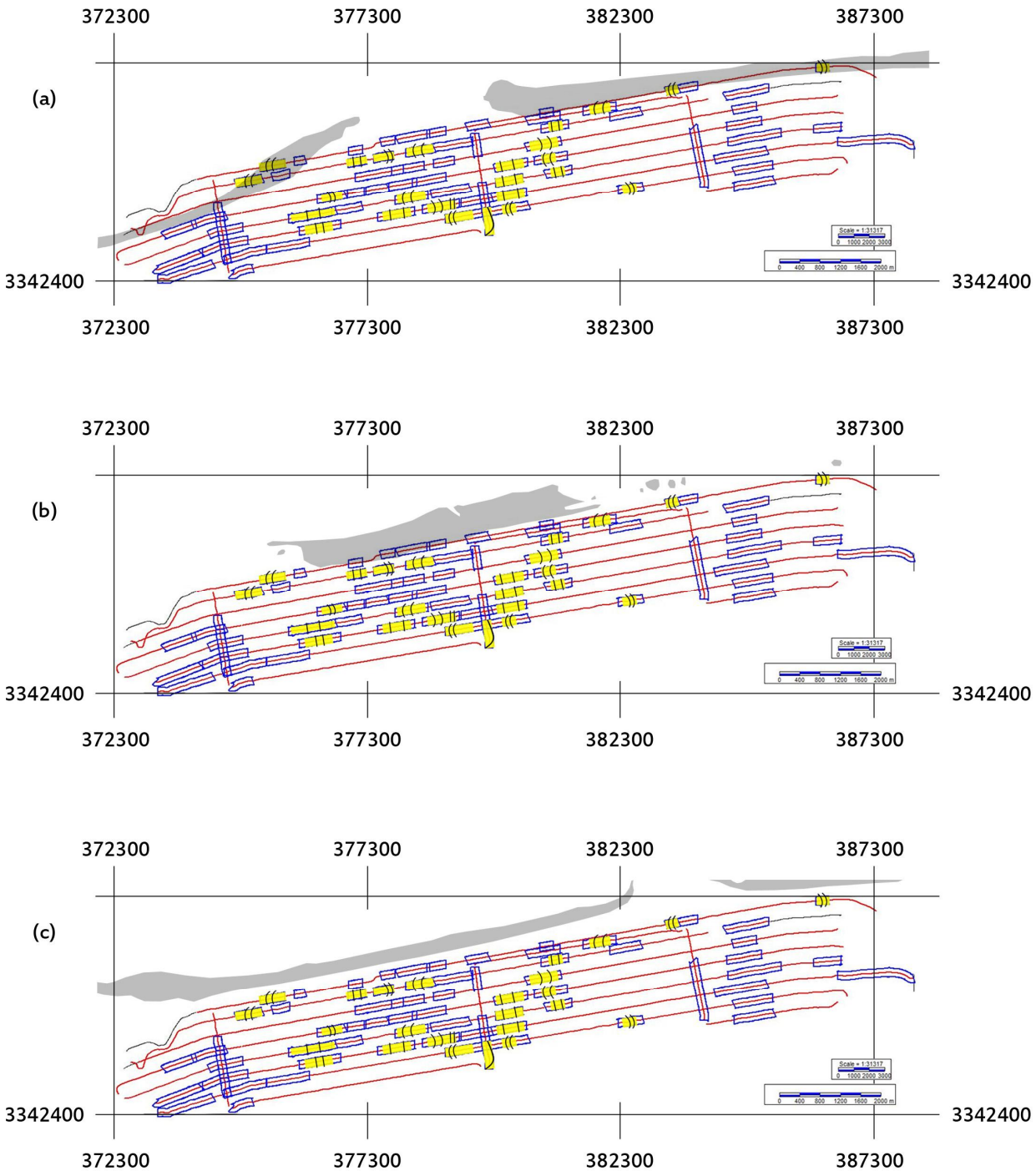

Figure 4.3 Interpreted Horizon A channels. The yellow rectangles indicate channels seen in the seismic profiles within Horizon A. The line marks indicate a bend in the channel and the direction of the bend. (a) Horizon A channels (plotted with the 1850 shoreline) are consistent through the consecutive parallel profiles. The location of the channels appears to correlate to the breach the separated Petit Bois and Dauphin Island. (b) The 1917 shoreline correlates with a few channels on either end of the remaining portion of the island spit. The 2007 shoreline (c) has two small inlets (east) located closest to the shoreline that could correlate to more recent overwash and storm systems events.

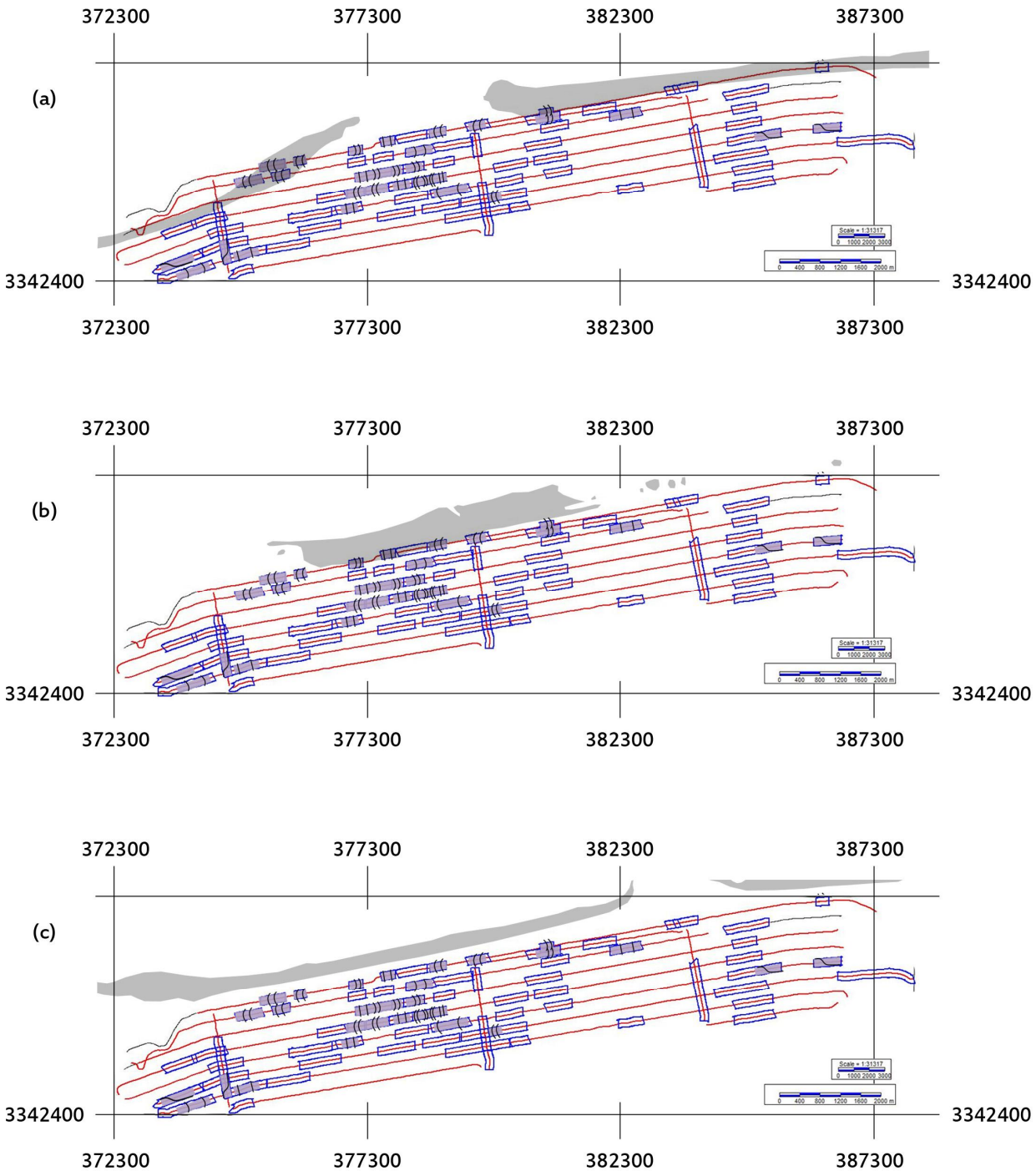

Figure 4.4 Horizon P channels interpreted. The purple rectangles indicate channels seen along Horizon P with direction of channel bends or slopes (a) Horizon P has channels that correlate to the 1850 shoreline. Alternating flow directions indicate potential meandering rivers during the "Pleistocene" time period. (b) The 1917 shoreline show few channels on the west end that indicate eastward bends on the western end of the remaining spit; and 2007 shoreline (c) indicates all the channels have been overlaid by deposition and the westward progradating spit.

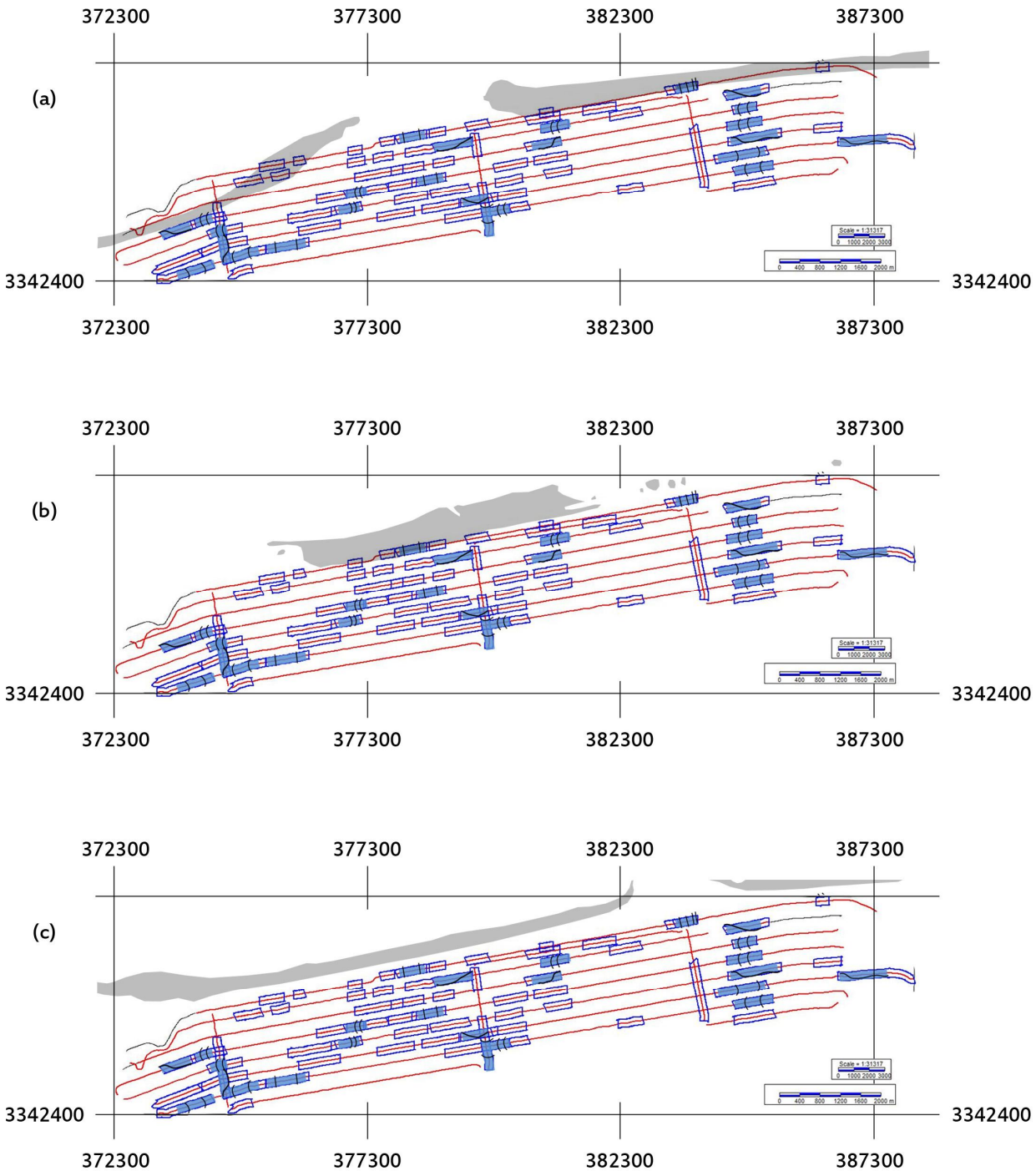

Figure 4.5 Horizon B channels interpreted. The blue rectangles on the survey indicate channels seen along Horizon B within the seismic profiles. The direction of channel bends or slopes are indicated by the line marks in the blue rectangles. Horizon B channels correlate best with 1917(b) and 2007(c) shorelines: (a) 1850 shoreline has few channels that correlate within the breach of the shoreline, while the more consistent channel indications are on either side of the remaining land of 1917(b) shoreline. The most consistent river system in Horizon B is seen at the east portion of the spit and correlates with the 2007 Katrina Cut area. This river system is fairly deep and wide which would allow for a wider breach if subsidence occurred.

The ancient river system seen in Horizon B in the eastern portion of the survey area (Figure 4.5c) is interpreted in the 2-D reflection seismic data (Figures 3.20, 3.22, 3.33, 3.43, 3.50, and 3.60) as having an average depth of 9.6m and average width of 626m. The depth and width of the river would create an extensive area where subsidence may be enhanced and thus the impact of large hurricane systems would be greater. The amount of erosion within this area from both hurricanes is seen in Figure 4.2. An interpretation of the channel systems (Figure 4.6) identified in the area (figures 4.3 through 4.5) along horizons A, P, and B is presented. The cross-hatch area represents the areas of potential enhanced subsidence (Figure 4.6d) and correlates with part of the river system in Horizon B (Figure 4.5). A more detailed result would come from running hydro-bathymetry models of the Pelican and Dauphin Island region to determine the amount of deposition and erosion that occurred during the Lidar dataset time spans. This would add information from below sea level beyond the reach of Lidar.

(a)

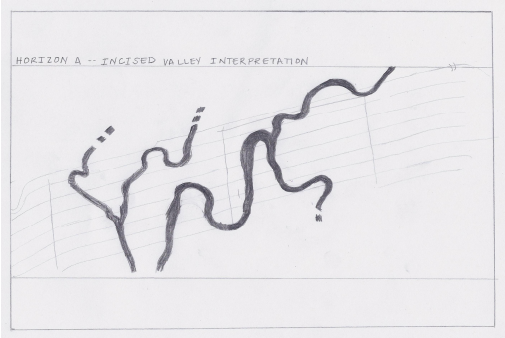

(b)

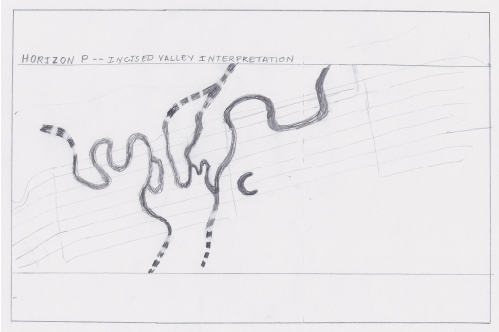

(c)

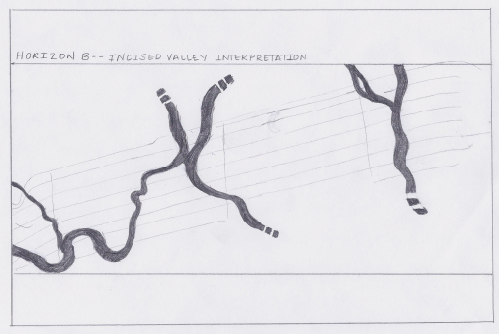

(d)

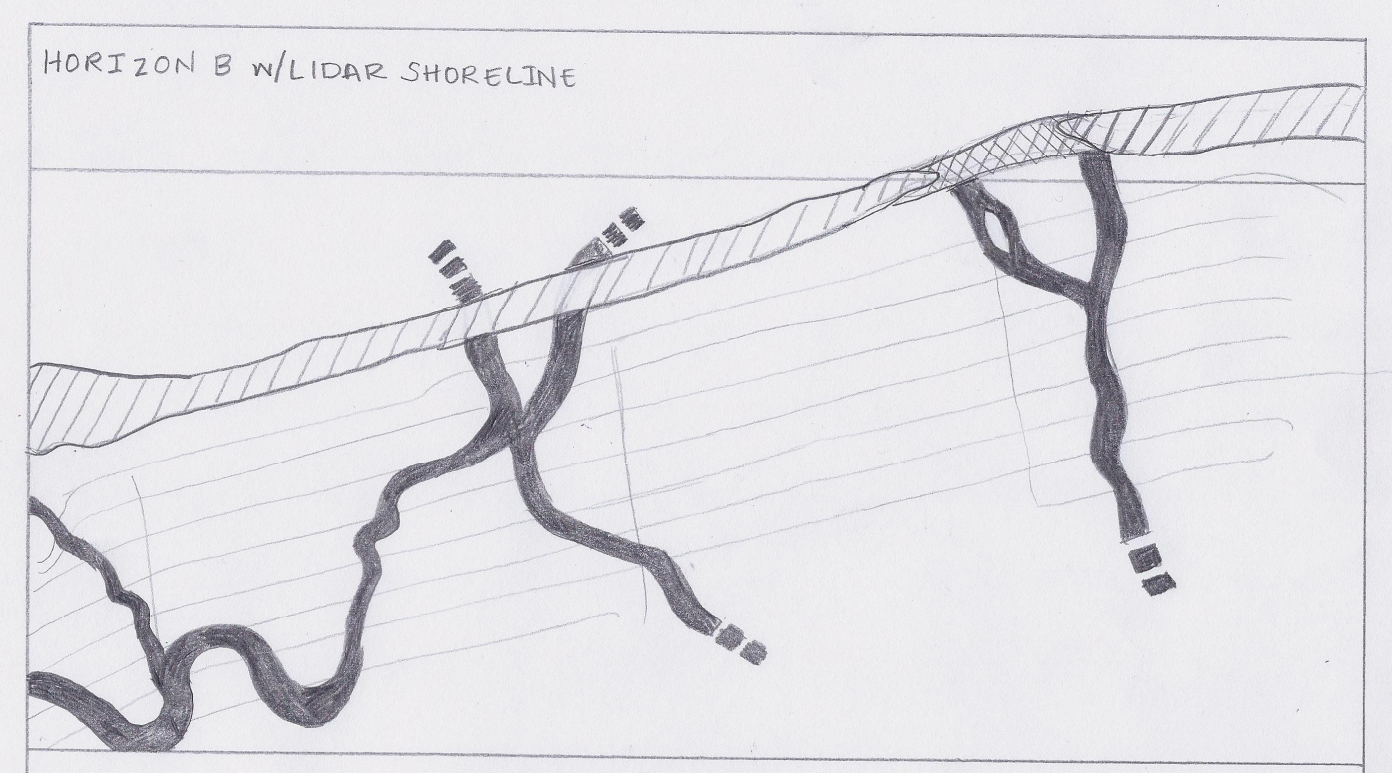

Figure 4.6 (a) The Horizon A river system using channel interpretations from Figure 4.5; the environment shows meandering rivers. The dashed river lines are estimated river paths. (b) Horizon P is characterized with meandering rivers and at least one oxbow. (c) Horizon B is characterized by river systems that are more elongated in a north to south direction. (d) An interpretation of the 2010 and 2005 residual coastline and Horizon B channels shows. The easternmost channel correlates well with the location of Katrina Cut.

Interpreting horizons and gridding horizon contours can better illustrate the river valleys among the channel structures. The interpretation of the channel from the contour maps shows a flood plain or inlet system from a fluvial and proto-barrier island environment. Though beyond the scope of this work, more accurate dating of these channel structures, and therefore their interrelationships and environment of formation, could be derived from the dating of sediments or fossils.

The amalgamation of Pelican Island occurred previously in 1717 (Cipriani and Stone, 2001; Byrnes et al., 2010). As with many ephemeral islands, Pelican and Sand Island consistently change with the tides and wave action. A 1717 hand drawn map shows Pelican Island connected to Dauphin Island with a lagoonal area to the east (Figure 4.7a). Almost three centuries later in January 2012 an aerial image (Figure 4.7b) shows the same configuration. Although there is no record of hurricane systems in 1717, the history of strong hurricane systems in the Atlantic and Gulf areas (NOAA hurricane database) within the last two centuries includes several systems within the NGOM. The island has recovered naturally when affected by these storms. There are no records or images of Pelican Island connecting to Dauphin Island within the last two centuries to compare the effects of this connection on the Dauphin Island's ability to recover from major erosional events. Aerial, satellite, and Lidar images suggests the ephemeral islands migrate northwest during period of little storm activity. The elimination of an additional transport inlet may limit the amount or rate of deposition occurring west of Pelican Island, including the remaining islands in the NGOM island chain.

(a)

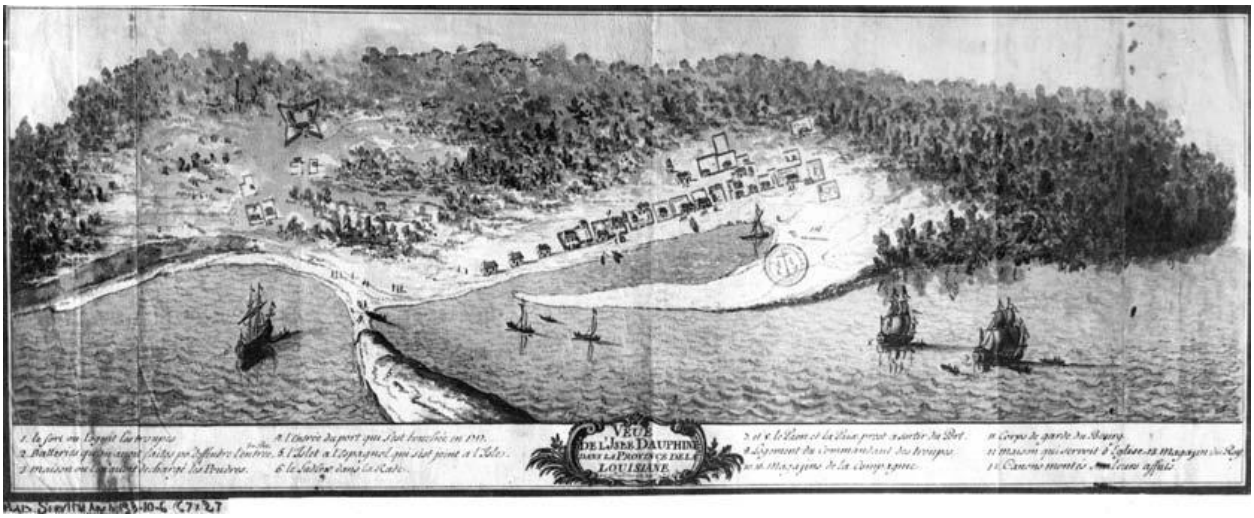

(b)

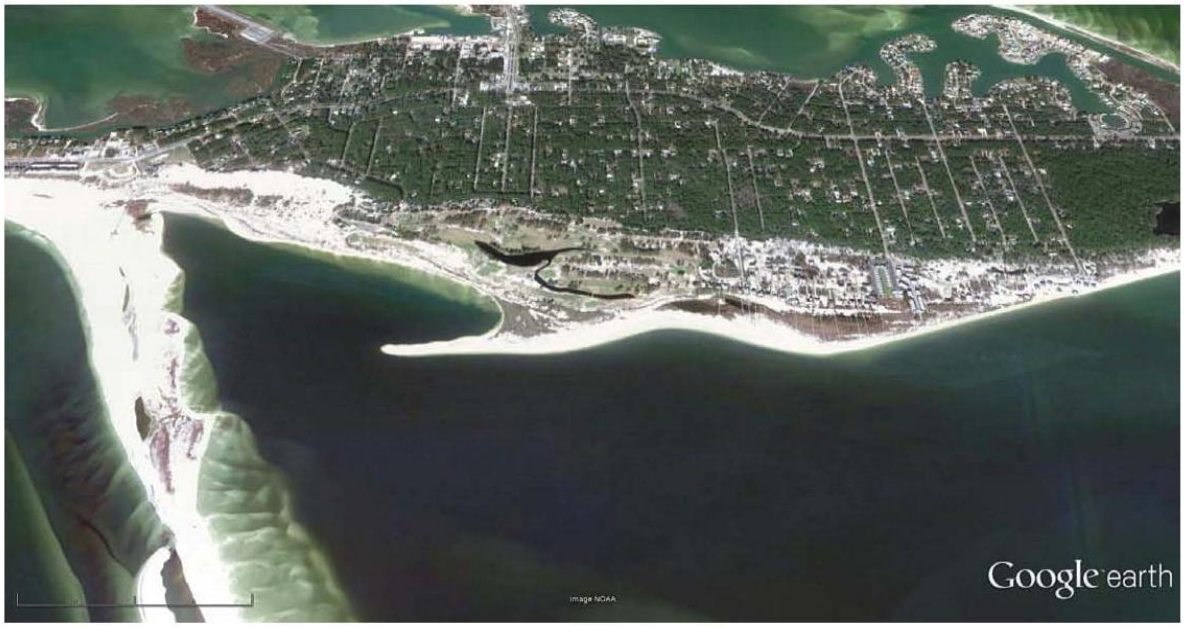

Figure 4.7 (a) A French drawing of Dauphin Island from 1717. This drawing shows the amalgamation of Pelican Island and the lagoonal/port environment created by the connection of the ephemeral island. (Dauphin Island Historical Map archive; Byrnes et al., 2010). (b) A Google Earth image taken in January 2012 shows a very similar environment to the 1717 image.

The data presented in this study are important in the prediction of which areas will be most heavily impacted by large storm events in the future. The future of Dauphin Island and all barrier islands is vital to the ecosystems and economic survival of coastal cities.

5.0 CONCLUSION

A range of geophysical methods were used to determine the affects of relict channels on the susceptibility of breach locations along the western spit of Dauphin Island. Morphological changes to the island from storm systems and natural deposition has been quantified.

1) The data suggest a correlation of buried river channels with historic breach locations. It can be hypothesized that fine grained channel fill may result in the differential subsidence of the overlying island and a greater susceptibility to overwash and breaching during the passage of strong storm systems.

2) Northern migration of Dauphin Island is seen in the Lidar and aerial imagery. Storm overwash creates deposits along the north side of the island. The low-energy environment of the Mississippi Sound includes minimal erosion. Pelican Island migrates north with the island. Lidar results from the 1998/2010 residual (Figure 33.79a) shows deposition along the north side of Dauphin and Pelican islands and erosion mostly along the Gulf of Mexico spit shoreline. Minimal erosion was seen along the north side of the island in all of the Lidar results. The shorelines extracted from aerial imagery (Figure 3.81) show a north to northwest migration. Migration of these islands to the north will continue into the future as a result of sea level rise and storm activity.

3) The process of the accretion of Pelican Island onto Dauphin Island is repeated historically (Figure 4.7). The data show the greatest deposition within Pelican Pass that contributed to the amalgamation of Pelican Island was a result of Hurricane Ivan (Figure 3.85). Minimal deposition was seen in this area from Hurricane Katrina. A difference in storm track could be a contributing factor. Hurricane Ivan fell to the east of Dauphin Island in Florida, while

Hurricane Katrina had landfall west of the island and impacted the western NGOM. Deposition continued in Pelican Pass through littoral drift and longshore transport.

REFERENCES

Boggs, S., Jr., 2006, Principle of Sedimentology and Stratigraphy (Fourth Edition), UpperSaddle River: Pearson Education, Inc., p. 306-316.

Byrnes, M.R., Griffee, S.F., and Osier, M.S., 2010, Channel Dredging and Geomorphic Response at and Adjacent to Mobile Pass, Alabama: Final Report: Applied Coastal Research and Engineering, Mashpee, MA, Prepared for U.S. Army Corps of Engineers Engineering Research and Development Center Coastal and Hydraulics Laboratory, ERDC/CHL TR-10-8

Cipriani, L.E. and Stone, G.W., 2001, Net Longshore Sediment Transport and Textural Changes in Beach Sediments along the Southwest Alabama and Mississippi Barrier Islands, U.S.A.: Journal of Coastal Research, v. 17, no. 2, p. 443-458.

Cooke, C.W., 1968, Barrier Island Formation: Discussion: Geological Society of America Bulletin, v. 79; p. 945

Cooper, J.A.G. et al., 2012, Barrier Islands on Bedrock: A New Landform Type Demonstrating the Role of Antecedent Topography on Barrier Form and Evolution: Geology, v. 40, p. 923-926.

Dean, R.G., 1997, Models for Barrier Island Restoration: Journal of Coastal Research, v. 13, no. 3, p. 694-703.

Donoghue, J.F., 2011, Sea level history of the northern Gulf of Mexico coast and sea level rise scenarios for the near future: Climatic Change, v. 107, p. 17-33.

Dubois, R.N., 1990, Barrier-Beach Erosion and Rising Sea Level: Geology, v. 18, p. 1150-1152.

Field, M.E. and Duane, D.B., 1976, Post-Pleistocene history of the United States inner continental shelf: Significance to origin of barrier islands: Geological Society of America Bulletin, no. 5, p. 691-702

Flocks, J. G., J. M. Sanford, and J. L. Smith., 2010, Sediment distribution on the Mississippi-Alabama Shelf, Northern Gulf of Mexico. Reston, VA USGS Open-File Report 2010–1002.

Forde, A.S., Dadisman, S.V., Flocks, J.G., Wiese, D.S., DeWitt, N.T., Pfeiffer, W.R., Kelso, K.W., and Thompson, P.R., 2011, Archive of digital Chirp subbottom profile data collected during USGS cruises 10CCT01, 10CCT02, and 10CCT03, Mississippi and

Alabama Gulf Islands, March and April 2010: U.S. Geological Data Series 611, 11 DVDs

Forrest-Vandera, B.M., Larenas, M., and Andrews, J.A., 2011. Attachment J: Dauphin Island Coastline Restoration: Sand Search Investigation. Boca Raton, Florida: Coastal Planning & Engineering, Inc. 38p (Prepared for Town of Dauphin Island, Alabama)

Hoyt, J.H., 1967, Barrier Island Formation: Geological Society of America Bulletin, no. 9, p. 1125-1136

Hummell, R.L., 1999, Geologic and Economic Characterization and Near-term Potential of Sand Resources of the East Alabama Inner Continental Shelf Offshore of Morgan Peninsula, Alabama: Prepared by the Geological Survey of Alabama in fulfillment of U.S. Department of the Interior, Minerals Management Service Cooperative Agreement No. 1435-01-98-CA-30935.

Kindinger, J.L., 1988, Seismic Stratigraphy of the Mississippi-Alabama Shelf and Upper Continental Slope: Marine Geology, v. 83, p. 79-94.

Kindinger, J.L., Balson, P.S., and Flocks, J.G., 1994, Stratigraphy of the Mississippi-Alabama shelf and the Mobile River incised valley system, in Dalrymple, R.W., Boyd, R., and Zaitlin, B.A., eds., Incised-Valley Systems: Origin and Sedimentary Sequences: Tulsa, OK, Society for Sedimentary Geology Special Publication 51, p.83-95

Lutgens, F.K. and Tarbuck, E.J., 2003, Essentials of Geology (Eighth Edition), Upper Saddle: Prentice Hall, pgs. 382-384

Matias, A., Ferreira, O., Vila-Concejo, A., Garcia, T., and Dias, J.A., 2008, Classification of Washover Dynamics in Barrier Islands: Geomorphology, v. 97, p. 655-674.

Morton, Robert A., Miller, Tara L., and Moore, Laura J., 2004, National assessment of shoreline change: Part 1: Historical shoreline changes and associated coastal land loss along the U.S. Gulf of Mexico: U.S. Geological Survey Open-file Report 2004-1043.

National Hurricane Center. National Weather Service: National Oceanic and Atmospheric Association, 1870. Web. 20 Dec. 2013.

Nordfjord, S., Goff, J.A., Austin, J.A., JR., and Gulick, S.P.S, 2006, Seismic Facies of Incised-Valley Fills, New Jersey Continental Shelf: Implications for Erosion and Preservation Processes Acting During Latest Pleistocene-Holocene Transgression: Journal of Sedimentary Research, v. 76, p. 1284-1303

Otvos, E.G., Jr., 1970, Development and Migration of Barrier Islands, Northern Gulf of Mexico: Geological Society of America Bulletin, v. 81, p. 241-246

Otvos, E.G., Jr., 1977, Post-Pleistocene history of the United States inner continental shelf: Significance to origin of barrier islands: Discussion and reply: Geological Society of America Bulletin, v. 88, Doc. No. 70512, p. 734-736

Otvos, E.G., 1981, Barrier Island Formation Through Nearshore Aggradation – Stratigraphic and Field Evidence: Marine Geology, v. 43, issue 3-4, p. 195-243

Otvos, E.G., Jr., 1985, Barrier Platforms: Northern Gulf of Mexico: Marine Geology, v. 63, p. 285-305.

Otvos, E.G., Jr., 2001, Assumed Holocene Highstands, Gulf of Mexico: Basic Issues of Sedimentary and Landform Criteria: Discussion: Journal of Sedimentary Research, v. 71, no. 4, p. 645-647.

Otvos, E.G. and Giardino, M.J., 2004, Interlinked Barrier Chain and Delta Lobe Development, Northern Gulf of Mexico: Sedimentary Geology, v. 169, p. 47-73.

Parker, S.J., Davies, D.J., and Smith, W.E., 1993, Geological, Economic, and Environmental Characterization of Selected Near-Term Leasable Offshore Sand Deposits and Competing Onshore Sources for Beach Nourishment: Prepared by the Geological Survey of Alabama in fulfillment of U.S. Department of the Interior Minerals Management Service Cooperative Agreement No. 14-35-0001-30630.

Pe'eri, S. and Long, B., 2011, LIDAR technology applied in coastal studies and management. In: Pe'eri, S. and Long, B. (eds.), Applied LIDAR Techniques, Journal of Coastal Research, Special Issue No. 62, 1–5. West Palm Beach (Florida), ISSN 0749-0208

Pendleton, E.A., Baldwin, W.E., Danforth, W.W., Dewitt, N.T., Forde, A.S., Foster, D.S., Kelso, K.W., Pfeiffer, W.R., Turecek, A.M., Flocks, J.G., and Twichell, D.C, 2011, Geophysical data from offshore of the Gulf Islands National Seashore, Cat Island to Western Horn Island, Mississippi: U.S. Geological Survey Open-File Report 2010-1178, DVD-ROM. (Also available online at http://pubs.usgs.gov/of/2010/1178/.

Quinn, R., Bull, J.M., and Dix, J.K., 1998, Optimal Processing of Marine High-Resolution Seismic Reflection (Chirp) Data: Marine Geophysics Researches v. 20, p. 13-20.

Rosati, J.D. and Stone, G.W., 2009, Geomorphic Evolution of Barrier Islands along the Northern Gulf of Mexico and Implications for Engineering Design in Barrier Restoration: Journal of Coastal Research, v. 25, no. 1, p. 8-22.

Schwartz, M.L., 1971, The Multiple Causality of Barrier Islands: The Journal of Geology, v. 79, no. 1, p. 91-94

Stockdon, H.F., Sallenger Jr., A.H., Listt, J.H., and Hohnan, R.A., 2002. Estimation of Shoreline Position and Change Using Airborne Topographic Lidar Data: Journal of Coastal Research, v. 18, no. 3, p.502-513.

Twichell, D., Pendleton, E., Baldwin, W., Foster, D., Flocks, J., Kelso, K., DeWitt, N., Pfeiffer, W., Forde, A., Krick, J., and Baehr, J., 2011, The shallow stratigraphy and sand resources offshore of the Mississippi Barrier Islands: U. S. Geological Survey Open-File Report 2011-1173, at http://pubs.usgs.gov/of/2011/1173/.

Williams, K., Pinzon, Z.S., Stumpf, R.P., and Raabe, E.A., 1999, Sea-level Rise and Coastal Forests on the Gulf of Mexico: Prepared for the U.S. Geological Survey by the Department of Botany, University of Florida: U.S. Geological Survey Open-File Report 99-441

APPENDIX A

A.1 Longhsore Drift

Longshore drift or current is created when waves approach the shore at an angle and some of the wave is deflected laterally and parallel to the shore (Figure A.1; Boggs, 2006).

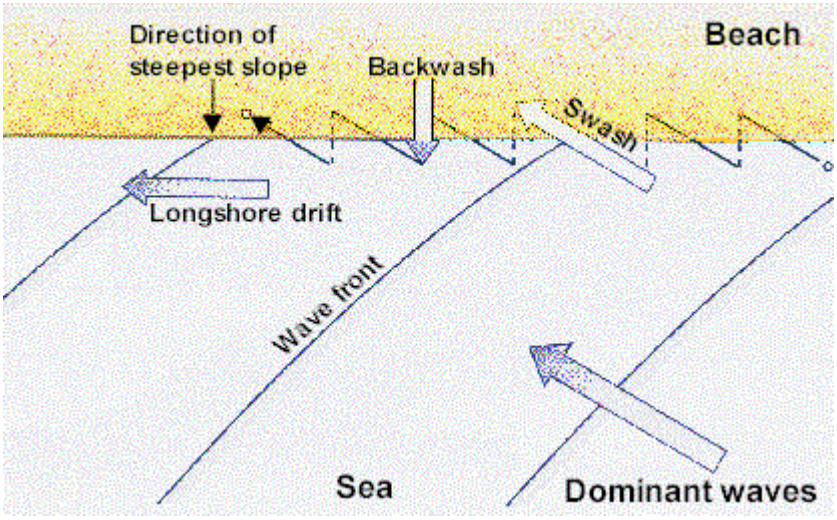

Figure A.1. This illustration demonstrates the movement of longshore drift/current. As the current moves along the shoreline, incoming waves from the sea make contact with the current and beach at an angle causing the waves to deflect within the swash zone. This zig-zag movement creates deposition and erosion as the current continues parallel to the shoreline. Smaller grain sizes are found down-drfit of the current because fine-grained sediments are easily transported. (www.geographyfieldwork.com)

The shape and composition of the shoreline is greatly influenced by longshore drift. Longshore drift is based on prevailing wind direction, swash and back wash, and it deposits, removes and re-deposits sediments along coastlines (NOAA Ocean Service Education). This current is within approximately 10 m offshore from the shoreline called the littoral zone. Shoreline deposition is heavily based on the sediments within the littoral zone. The longshore drift moves up beaches according to the angles of the dominant waves and will pull back out to sea due to gravity. Wave direction is influenced by wind direction. The drift will vary slightly according to sediment type as well, meaning coarse-grain sediment beaches will not be as affected from breaking waves as a

finer-grained sediment that will erode quicker. This natural drift has drastic effects if altered unnaturally.

Figure A.2. This image is an example of shoreline erosion from longshore current. This current was intensified from increased wave activity from storms. Increased swash and backswash movement causes the beach sediment to loosen then move down-drift with the longshore current. (NOAA Ocean Service Education)

Jetties or groynes are coastal engineering structures designed to keep sediments on beaches. Although it may seem to work on one side of these structures, the adjacent beach has negative results. If the longshore current has east to west direction (as in the NGOM) and a manmade structure is blocking the natural flow of the drift, high rate erosion will occur on the western sides of these structures. Even though nature has its own way of rebounding, there are some coastal engineering structures that can provide some aid to lessening shoreline erosion.

The longshore drift and current are crucial to the sustainability of barrier islands. This current maintains a sediment supply for deposition and moves sediments westward along shorelines depositing sediments. Although the sediment supply from inland river systems has been minimized from anthropogenic activity, offshore sands found on the eastern Gulf of Mexico shelf and Florida embankment contribute to the longhsore drift sediment supply.

A.2 Wisconsin glaciations

The latest glacial period of North America, which occurred during the Late Pleistocene (approximately 122 to 11 kya), is known as the Wisconsin glaciation (Kansas Geological Survey). This was the most recent major advance of the North American ice sheet complex which includes the Cordilleran ice sheet, the Innuitian ice sheet, the Greenland ice sheet, and the Laurentide ice sheet (largest of all the ice sheets). At the height of this glaciations period, this complex ice sheet covered most of Canada, the Upper Midwest, and New England (Figure A.3).

Figure A.3 Illustration of the glacial extent in North America of the ice sheet complex that occurred during the Wisconsin Glaciation. (Kansas Geological Survey)

At the height of these ice sheets, Wisconsin Ice sheet extended as far south as Nebraska and Iowa, containing important clues for geologists today into the Pleistocene ecology and

climate (Kansas Geological Survey). The Wisconsin Ice sheet contained much of the world's freshwater and lowered sea level significantly by approximately 85 to 130 m. This ice sheet lowered sea level enough to permit animal and human migration across a land bridge found between North America and Siberia, known as the Bering Strait.

As time moved into the Holocene period, glacial retreat or melting flooded oceans with vast amounts of fresh water causing eustacy and sea level to rise. Sea level rise is also attributed to the continent's isostacy, or elevation changes, in response to effects from sinking by immense weight from ice or rising as ice melts (Kansas Geological Survey; Bloom, 1991). Isostatic adjustment can also occur during glacial retreat (Lutgens and Tarbuck, 2003). This process occurs when a new level of gravitational equilibrium is established, such as when a glacial load creates subsidence. As the glacier melts, the lithosphere slowly rebounds until isostatic equilibrium is achieved. Sea levels are affected as a result of this isostatic adjustment to deglaciation. This activity occurred during the Early to Late Holocene seen and documented throughout surrounding waters, including the NGOM. In rapid response to the vast influx of fresh water from de-glaciation, sea level rose rapidly at approximately 0.25 cm/yr (Williams et al., 1999). At the time of the formation of the NGOM barrier island chain (approximately 4.5 kaya) sea level rates slowed dramatically to average rate of 0.04 cm/yr (Williams et al., 1999 and references therein). Studies have estimated sea level to rise to approximately 0.14-0.17 cm/yr (Davis and Mitrovica, 1996; Willaims et al., 1999). With the oscillating rise in sea level, the migration and rollover of the barrier islands sustained the islands through deposition from offshore sediments. The migration and rollover to the northwest continues today and seen within the results of this study.